In-situ cure monitoring of epoxy resin systems

A thesis submitted for the degree of Doctor of Philosophy

by

Graham Powell

Department of Materials Engineering, Brunel University

April 1998

Acknowledgments

There are a number of people to whom I would like to express my grateful appreciation for their part in this work.

Firstly thanks to my supervisors, Dr. Chris France and Dr. Gerard Fernando for all of their help, advice and support throughout the project, to Prof. Ron Spooncer for his technical insights and suggestions and to the project supervisors from the DRA, Dr. John Barton and Dr. Sally Hitchin.

Many thanks to Dr. Peter Crosby for his support and friendship throughout the project, to all the other students and staff who have shared in my time at Brunel and all who have passed through "057."

Many, many thanks to my parents for their encouragement and support in all I have ever undertaken.

Finally I would like to dedicate this thesis to Kathryn, my wife, who has had more confidence in me than I have had at times, and without whose endless strength and patience I would not have managed.

Table Of Contents

1 Abstract

This thesis describes the work carried out at Brunel University to develop novel optical fibre sensors capable of monitoring the cure state of an epoxy/amine resin system.

The sensors were of simple construction, consisting of an optical fibre from which the silicone cladding layer had been removed over a short length. This stripped length was embedded into the curing resin system. The sensor was successfully used in two ways:

i) as an evanescent absorption sensor to monitor specific absorption bands of the resin system. The absorption of energy from the evanescent wave of the optical fibre by absorbing media allows evanescent absorption spectra to be obtained. Absorption spectra were obtained from sensors embedded in a model curing resin system over narrow wavelength ranges. These wavelength ranges corresponded to positions of known absorptions in the spectra of active components in epoxy/amine systems. By monitoring the change in these absorptions it was possible to obtain information about concentration of the amine hardener functional group throughout cure;

ii) as a refractive index sensor capable of monitoring the changes in the refractive index of the resin system during cure. A laser diode was used to launch light into the sensor and the intensity of light emerging from the other end of the fibre was monitored. Changes in the resin system refractive index caused changes in the guiding properties of this the sensor. This resulted in a significant change in the intensity of light recorded by the detector and allowed the cure process to be followed. This sensor was also embedded into a unidirectional pre-preg system and was able to follow the cure of the system.

The results from the two sensing methods have been compared with data obtained using FTIR spectroscopy and Abbe refractometry during the resin system cure.

A theoretical model of sensor response has been developed and compared with the experimental data obtained. The sensor response has also been compared to predictions made by several models of evanescent sensor systems obtained from the literature. These models have been modified so that they can be applied to a sensor embedded into a curing resin system. An analysis of the correspondence between theory and experiment is presented.

2 Introduction

Advanced fibre reinforced composites are important engineering materials consisting of an arrangement of fibres surrounded by a resin matrix. Thermosets, such as epoxy/amine resin systems, tend to be used extensively for high performance applications. The term "cure" is used to describe the transformation of a resin from a viscous liquid to a glassy solid as a result of applied energy. To achieve this transformation a curing agent, such as an amine, is reacted with the epoxy resin. The transformation is accompanied by changes in the resin's chemical and physical properties and as a result in the mechanical properties of the composite system.

This thesis describes the development of *in-situ* techniques used for cure monitoring which employ an optical fibre as the sensor.

It is difficult to give a definition of a composite material. Many naturally occurring materials derive their properties from a combination of several distinguishable components. For example, many body tissues consist of high stiffness fibres in a lower stiffness matrix. The fibre alignment permits maximum stiffness in the direction of high loads but extreme flexibility. Similarly, wood exhibits a fibrous structure that affords it high stiffness and flexibility. The strength and toughness of metallic alloys and engineering plastics are achieved by combining high strength phases with tough ductile phases.

Three main points can be put forward in an attempt to define a composite[1]:

i) it contains two or more mechanically and physically distinct materials;

ii) it can be made by mixing the separate materials in a controllable way to optimise the material properties;

iii) the properties of the composite are superior to the properties of the individual components.

Fibre reinforced composites (FRCs) consist of fibres, which have a very high strength and modulus, and plastics or resins, which may be ductile or brittle but normally provide good chemical resistance. These are combined to give a material with new and superior properties. The combination can produce a material with the strength and stiffness of the fibres and toughness and chemical resistance of the matrix.

FRC materials have enjoyed a rapid growth of use in engineering applications recently. This has mainly involved the replacement of traditional materials, suggesting they have superior properties for many applications. These advantages are mainly the specific modulus and strength (modulus and strength *per* unit mass) which means that the weight of components can be reduced. The other significant advantage is a flexible design approach. FRCs can be fabricated into complex shapes, and strength and stiffness introduced into a component where it is crucial, by tailoring the fibre arrangement and alignment. These advantages mean that composites have found applications in fields as diverse as the aerospace and car industries, the chemical industry (in pipes and vessels etc.), the electrical and electronic industry (circuit boards, insulators, panels etc.) and the recreational industries (in sports racquets, golf clubs, skis etc.). The matrix materials most widely used in FRCs are epoxy resins.

The extensive research into the properties of FRCs in recent years has mainly concentrated on failure processes in load bearing applications which are, on the whole, dominated by the fibre properties. However,the resin matrix properties such as resin failure strain[2], void content[3], crosslink density[4], and interlaminar shear strength[5] can influence damage development and progression in the composites. Composite structures are often fabricated from layers of fibres pre-impregnated with resin known as "pre-pregs".

Important matrix related issues, which can influence the cure kinetics of a composite, include:

i) the extent of cure and the homogeneity of the cure in large composite structures;

ii) the chemical state of the resin (or pre-preg) prior to cure including the absorbed moisture content of the resin which may arise from repeated freeze/thaw cycles of pre-pregs stored at low temperature to prolong their shelf life;

iii) the chemical composition and stoichiometry of the reagents *i.e.* the relative concentrations of resin and curing agent;

iv) the cure schedule used to process the resin/composite and optimisation of cure schedules, to compensate for the state of the resin.

The effect of the cure schedule on the ultimate mechanical properties of the resin has been examined by several authors [6, 7, 8, 9]. The environmental stability of the composite, *i.e.* its resistance to factors such as the ingression of moisture, can also be influenced by the extent

of cure of the resin[10]. Furthermore, with a large and/or thick structure it is necessary to ensure a uniform rate of cure throughout the composite to avoid a loss in structural integrity. There has, however, been insufficient attention paid to optimising these factors and to the long term health monitoring of resin matrices in composites. Therefore, there is demand for a monitoring technique that is capable of determining the state of cure of a composite *in-situ*, *i.e.* from within the composite matrix, and without affecting the integrity of the finished component.

It can be seen from the above discussion that a study of a system for the monitoring of cure of the resin matrix of a composite, exploiting an optical fibre sensor, is likely to be of value. There is a large body of work describing optical fibre sensors for the measurement of a multitude of parameters and on techniques for the cure monitoring of resins and composite structures. A number of researchers have employed optical fibre techniques for the monitoring of cure of resins or composites (section 3.5).

The novelty of the approach described here lies in the use of an evanescent sensor to monitor the cure of an epoxy resin system by tracking the concentration of specific species within the system at discrete wavelengths. Although models for the response of an evanescent sensor to changes in concentration of an absorber do exist there have been no comparisons between the predictions these model make and experimental results. A comparison of this kind has been performed as part of this study. The sensor has also been used to monitor the refractive index change of a resin and much original work has been carried out relating the refractive index of a curing resin to its state of cure. The results obtained using the sensor have been related to cure state data obtained using more traditional techniques, namely Fourier Transform infra-red spectrscopy (FTIR) and Differential Scanning Calorimetry (DSC).

This project was carried out under the supervision of the Defence Research Agency (DRA) which provided management and supervision for the project. Because the project was procured by a tendering process with the DRA, a comprehensive project plan was in place from the start of the project. Quarterly progress meetings were held with the DRA at which progress reports and a presentation of results for the preceding quarter were given. Owing to its multidisciplinary nature two researchers undertook the project. One researcher (the author) addressed those issues concerned with optoelectronics and instrumentation such as sensor design, equipment design and sensor modelling. The second addressed those issues

that were nominally concerned with chemistry such as resin selection, resin chemistry, cure kinetics and kinetic modelling.

2.1 Aims and objectives

The initial project aim was to investigate and develop novel techniques based on optical fibre evanescent field spectroscopy for the *in-situ* cure monitoring of the chemical processes in FRCs. Correlation was sought between the *in-situ* cure monitoring techniques and the cure kinetics and chemistry *via* DSC, Fourier transform infrared spectroscopy and near infrared (NIR) spectroscopy, dynamic mechanical thermal analysis (DMTA) and rheology. The techniques involving refractive index sensors were investigated at a later stage of the work.

The advantages of the proposed optical evanescent wave sensor system are:

i) that it tracks directly the cure state of epoxy resin in real time throughout the cure cycle. This is much preferred to indirect methods such as the monitoring of acoustic velocity, dielectric properties, magnetic resonance imaging and changes in rheological properties;

ii) that the technique utilises a simple light intensity modulated system using narrow band sources, one for each functional group instead of a dedicated FTIR. This keeps costs down over FTIR or other more indirect methods of cure monitoring;

iii) that the optical fibre network forms an integral part of the composite structure allowing the possibility of the use of the fibres for post-cure condition monitoring;

iv) that during the processing of large FRC structures an on-line *in-situ* cure monitoring facility will provide information on rate of cure at various precise locations within the structure. This could allow optimisation of autoclave parameters to provide more efficient cure regimes;

v) that the sensor has immunity from electromagnetic interference (*e.g.* from autoclave operation) and is connected *via* a dielectric to the instrumentation, eliminating groundloops;

vi) that although the research was based on resin systems cured with amine curing agents, the technique could be applied to other resin systems, providing they had absorptions in the transmission window of the embedded optical fibres.

The original proposal stated the research project objectives as follows.

i) preliminary studies of neat resin/curing agent to establish characteristic absorption frequencies in the wavelength range of fibres/sources;

ii) selection of light sources, optical fibres and detectors. Using results from i) appropriate sources, detectors and fibres to be selected;

iii) correlation with other established cure techniques. Cure characteristics of selected resin systems will be studied using FTIR, NIR, and DSC;

iv) cure monitoring equipment design addressing issues of incorporating sources and detectors with embedded fibres. The original proposal suggested multimode communications fibres with wavelength tuneable laser diodes, standard telecommunications connectors and InGaAs detectors;

v) evaluation of cure monitoring equipment performance;

vi) correlation of results and modelling both kinetic chemical models and sensor response model;

vii) fabrication and cure monitoring of unidirectional composites incorporating fibres;

viii) correlation with conventional techniques;

ix) preparation of final report in the form of two PhD theses.

This thesis contains details of the work conducted by the author towards the fulfillment of the above targets. The basic principle of evanescent absorption spectroscopy is based on the characteristic infrared and NIR absorption frequencies for the epoxy resin system being used as the matrix of an FRC. It was proposed that changes in these during the cure process could be detected using commercial telecommunications fibres and laser diode sources. Changes in the magnitude of characteristic absorption bands of epoxy systems are greater at longer wavelengths, however the proposal outlined the use of the shorter wavelengths at which telecommunications fibres are transparent and telecommunications sources operate as a way of reducing costs and increasing reliability and signal to noise ratios.

Spectroscopy is a useful tool, which can be used to monitor the depletion of a chemically active functional group (e.g. epoxy or amine), in a curing resin system as a function of processing time and temperature. Light, consisting of wavelengths corresponding to the

absorption frequencies of the epoxy or amine active species, was launched into previously, locally stripped optical fibres. As will be shown in section 3.3 some of the light energy carried by an optical fibre is contained within the cladding material. This is known as the evanescent wave. In the stripped region of the proposed fibre sensor the epoxy resin acts as the cladding, hence selective absorption of the energy in the evanescent wave takes place as a function of changing chemical composition of the resin.

2.2 Thesis outline

The main reasons why it is desirable to have a method of monitoring the cure of an epoxy resin system have been outlined in the preceding section.

This thesis continues in the next chapter with a review of the literature which was relevant to the work which was carried out. This includes literature covering the general background knowledge which was needed to perform the work. It also includes the literature which set the context of the work described here, in relation to the cure monitoring methods which have been utilised in the past, including those employing optical fibres as the sensing elements. The topics covered in the literature review are as follows:

i) optical fibres and optical fibres sensors; giving a brief description of how optical fibres work, what constitutes an optical fibre sensor and the advantages of optical fibre sensors over their electrical counterparts;

ii) the epoxy amine cure reaction; covering the basics of the mechanisms of the epoxy amine cure reaction;

iii) the evanescent wave and attenuated total reflection spectroscopy. How the evanescent wave arises and how it can be put to use in spectroscopy techniques;

iv) cure monitoring techniques covering methods that have been used to monitor the cure of resin systems by other researchers in the past;

v) optical fibre cure monitoring discussing cure monitoring techniques which use optical fibres as their sensing elements.

The thesis then proceeds with a general experimental section covering aspects of the experimental procedure which is relevant to both the evanescent absorption sensor and the refractive index sensor.

Since two very different sensing techniques were investigated in this study the experimental procedure, results and discussion pertaining to the two sensors have been split into separate chapters for clarity. Chapter 5 contains the experimental procedure, results and discussion pertaining to the evanescent absorption sensor, whilst chapter 6 covers that pertaining to the refractive index sensor. The work contained in chapters 5 and 6 has been published widely and a listing of these publications can be seen in Appendix 3.

The final chapter contains a summary of the work undertaken, conclusions which were drawn from the experimental work and suggestions for future work to be carried out on the sensing techniques.

Appendices are included at the end of the thesis containing the listings of the computer programs written and used during the study, the author's publications and references from the literature.

3 Literature Review

This Chapter is a review of the literature applicable to this project. It outlines many of the methods that are used to establish the degree of cure of epoxy resin based materials concentrating on those methods which are capable of monitoring cure *in-situ*. The following topics are discussed:

i) optical fibres and optical fibre sensors;

ii) the epoxy/amine cure reaction;

iii) the evanescent wave and attenuated total reflection;

iv) traditional Cure monitoring techniques;

v) cure monitoring using optical fibres;

3.1 Optical fibres and optical fibre sensors

3.1.1 Optical fibres

All light guides, including optical fibres are based on the principle of total internal reflection. A ray of light passing through a boundary between two dielectrics of differing refractive indices is refracted through an angle which is dictated by Snell's law (Figure 3-1 a) and equation - 3.1.

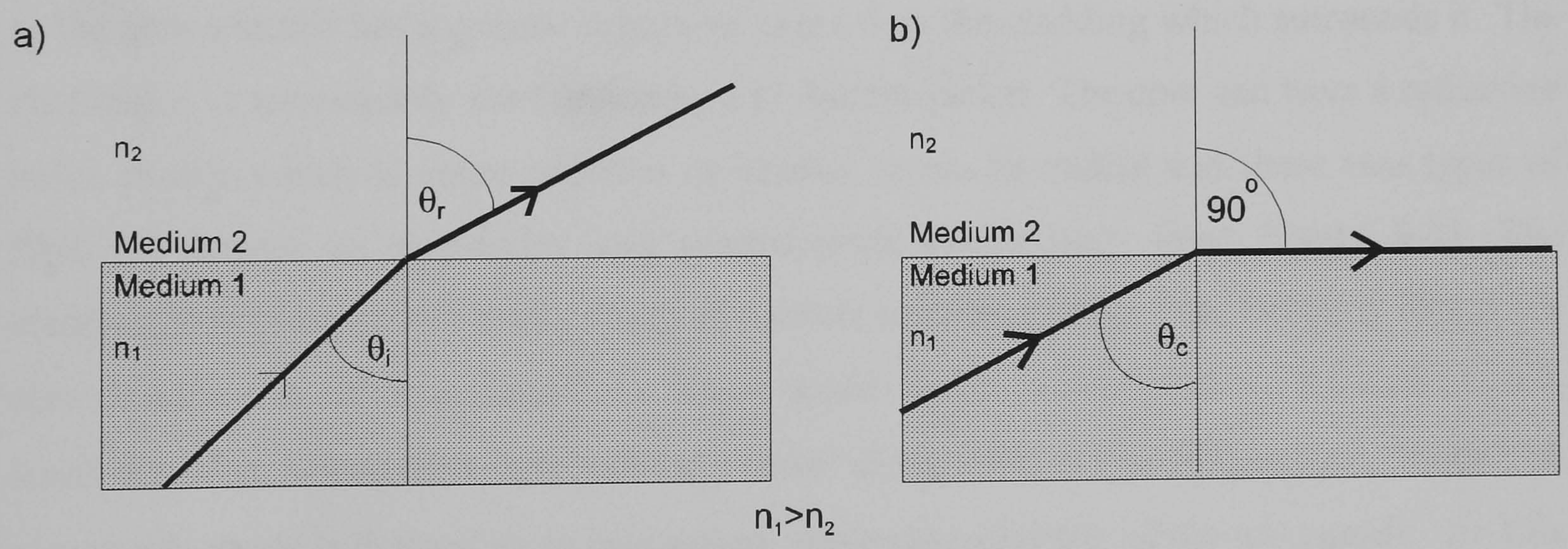

Figure 3-1 a) refraction at a dielectric surface and b)light refracted at the critical angle

$$\frac{\sin\theta_i}{\sin\theta_r} = \frac{n_2}{n_1}$$

- 3.1

θ_i is the incident angle of the ray with respect to the normal of the boundary and θ_i is the refracted angle; n_2 and n_1 are the refractive indices of the two media. The refractive index of a medium is defined as the ratio of the speed of light in a vacuum to its speed in that medium. Water, for example, has a refractive index of about 1.3. At the point where θ_i becomes 90° the refracted beam passes along the boundary and any increase in θ_i after this point will cause the refracted beam to be totally reflected within medium 1 (Figure 3-1b). θ_i at this point is called the critical angle θ_c.

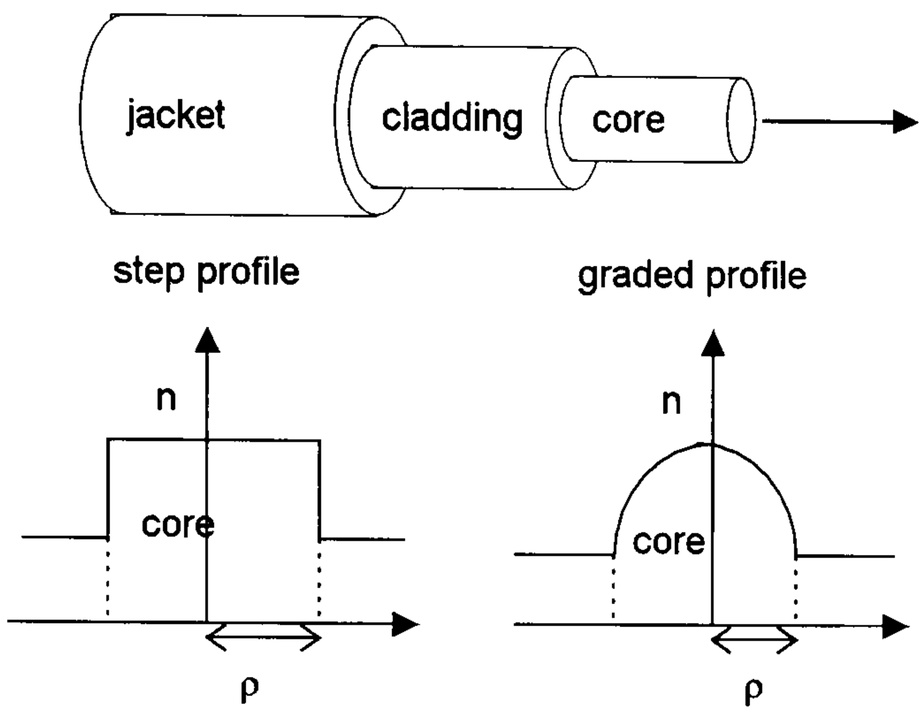

Figure 3-2 Construction and typical profiles of optical fibres

An optical fibre is a dielectric structure composed of nearly transparent dielectric materials that transports energy at wavelengths in the infrared or visible portions of the electromagnetic spectrum. The diameter of these fibres is generally small, typically 125-1000μm, and made up of three layers as shown in Figure 3-2. The central region is known as the core and this has a greater refractive index than the cladding which surrounds it. The cladding is in turn usually surrounded by a protective jacket. The core can have a refractive index profile which is either uniform or graded across its radius and these two types of fibre are known as step-index and graded-index respectively (also Figure 3-2). The cladding index is typically uniform and of a lower refractive index than the core. Fibres are also classified as either multimode or single mode. Single mode fibres have a core of such small diameter, ≈5μm, that light will only travel along them in one propagation "mode". A waveguide mode is defined as an elementary wave characteristic of the waveguide[11] (in this case the fibre). A mode propagates with characteristic phase and group velocities cross-sectional intensity distribution and polarisation. Multimode fibre will, due to the larger dimensions of its core, carry many more propagation modes (typically several thousand).

Optical fibres are electromagnetic waveguides working at optical frequencies. To understand the basic principles of light propagation it is easiest to start with a geometrical

optics approach. Classical geometric optics provides a reasonable description of light propagation in regions where the refractive index varies only slightly over a distance comparable to the wavelength of the light. This is typical of the multimode optical fibres used in this study.

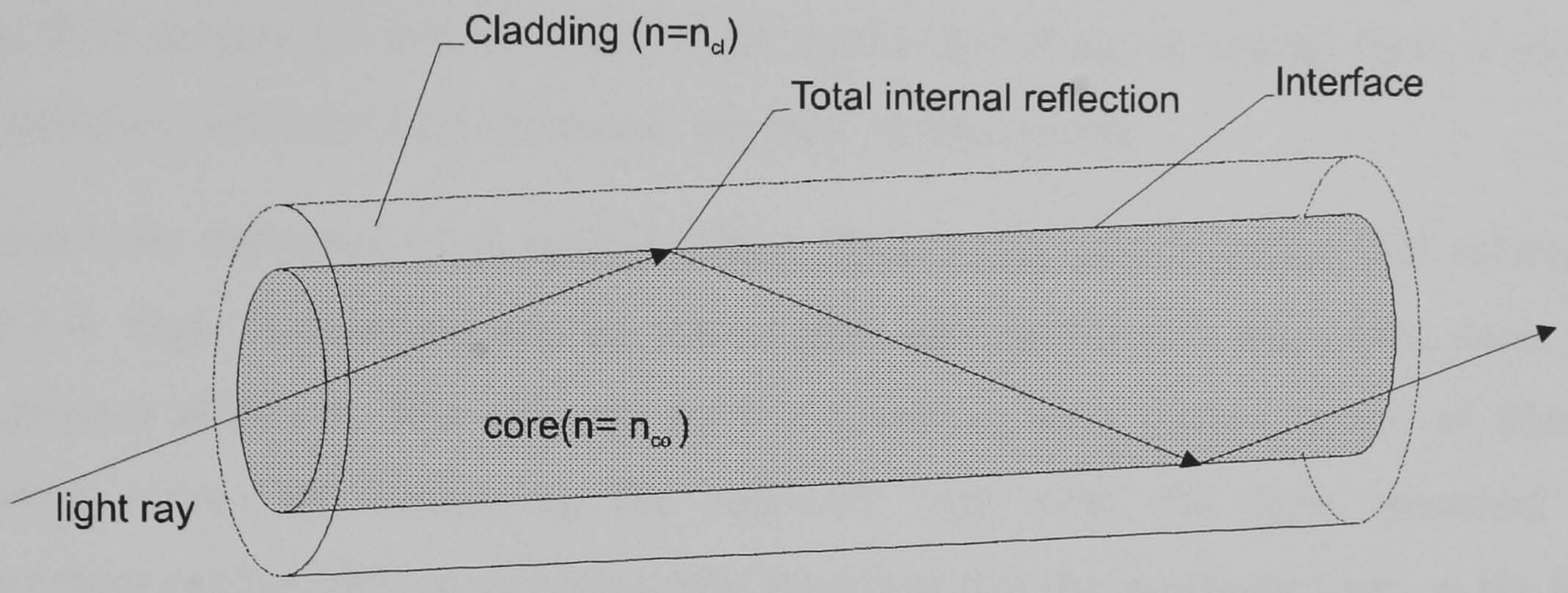

Figure 3-3 Propagation of light in fibre

An optical fibre effectively creates a continuous circular dielectric interface between two dielectrics and it is easy to see that light entering the fibre at greater than the critical angle for the two media will pass along the fibre in a series of reflections from the interface (Figure 3-3). Combining the important fibre parameters with the free space wavelength of the light, λ propagating in the fibre, it is possible to form a single dimensionless parameter *V*, known as the normalised frequency of the waveguide. This is defined as

$$V = \frac{2\pi\rho}{\lambda}\left(n_{co}^2 - {n_{cl}}^2\right)^{1/2}$$

- 3.2

where ρ is the core radius and n_{co} and n_{cl} are the core and cladding refractive indices respectively. The quantity $(n^2_{co}-n^2_{cl})^{1/2}$ is often referred to as the numerical aperture of the fibre and is a guide to the range of incident angles the fibre will accept. Ray theory is valid for cases where $V \gg 1$, because in this domain diffraction at the core/cladding interface plays an insignificant part in the propagation of light in the fibre[12]. The theory for the refractive index sensor described in this thesis is based on the geometrical optics approach since *V* was greater than 200 for the fibres used in this study.

An exhaustive treatment of optical fibres and their theory can be found in Snyder and Love (1983)[12]. An early, and much referenced paper, on the basic theory of optical fibres, which

includes some information useful for the calculation of modes in multimode fibres (as will be seen later) is by Gloge[13]. This paper concentrates on the mode parameters and propagation constants for singlemode and fibres with several modes, but contains a useful treatment of multimode fibres also.

3.1.2 Optical fibre sensors

Optical fibre sensors are devices where light, transmitted along an optical fibre, is modified by an external parameter (*e.g.* chemical, physical or biological).

The most basic definition of an optical sensor fibre sensor can be given with reference to Figure 3-4. Light is launched into an optical fibre and guided to a measuring point where some process affects it. The affected light is conveyed by a further length of fibre to a measuring point. By comparing the received light with the light launched some measurement can be inferred providing that the effect that the measurand has on the light is reproducible and not subject to interference from other parameters.

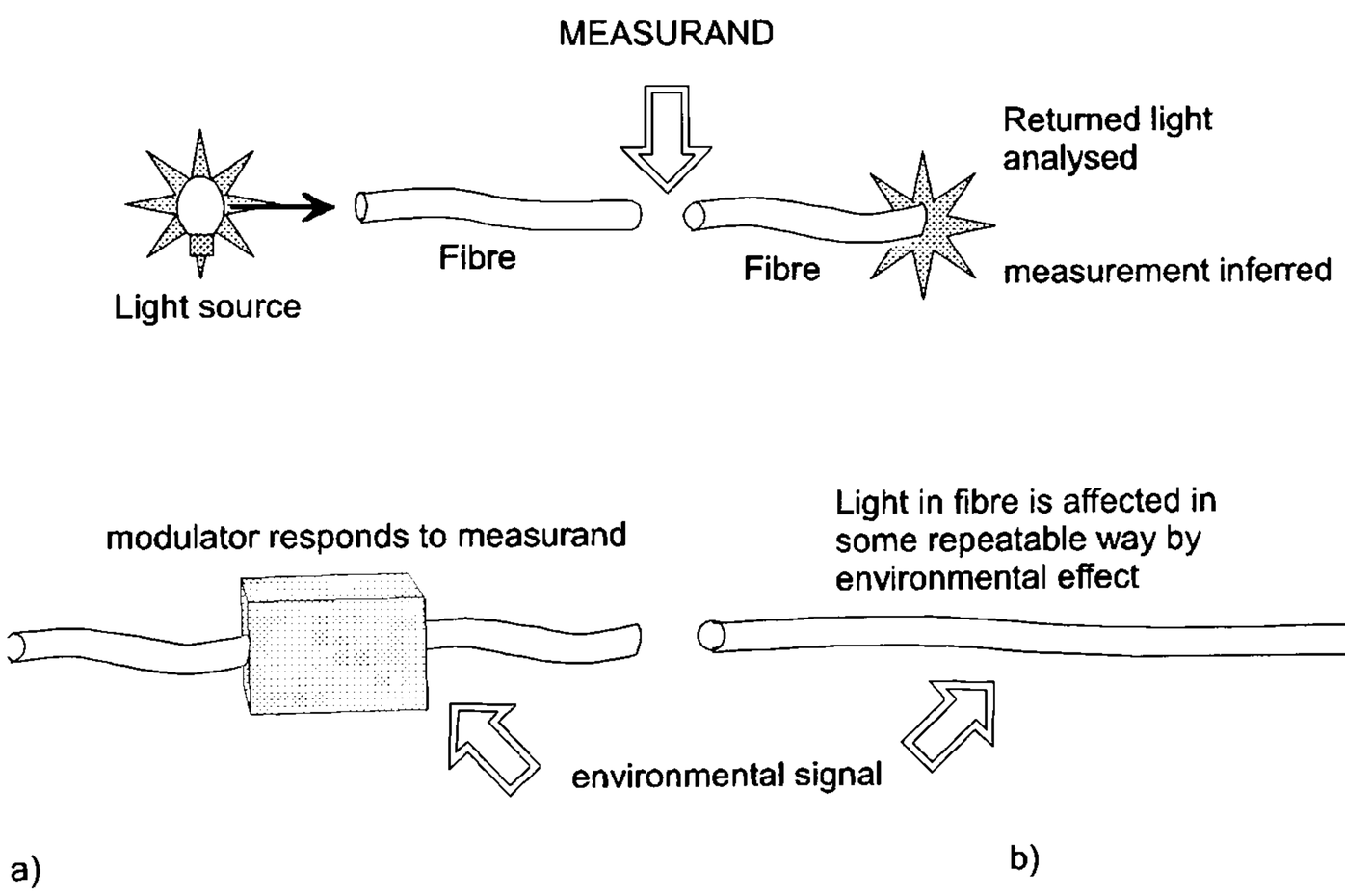

Figure 3-4 Basic optical fibre sensor configurations, a) extrinsic sensor and b)intrinsic sensor

There are two basic classes of optical fibre sensors. These are known as intrinsic and extrinsic. In extrinsic sensors the fibres are used as light guides, taking light to a modulator which impresses information onto the light in response to some environmental stimulus. The light is then taken either by the same, or a second fibre to a detector. The modulator may contain one or more devices for generation, modification or transformation of the light such as mirrors, or a gas or liquid cell. *i.e.* the sensing or modification of the photonic signal takes place outside of the fibre.

The second type of sensor relies on some property of the fibre itself to respond to an environmental change and convert it into a modulation of the light passing through it. These are known as intrinsic sensors and may further be divided into subclasses depending on the mechanism by which the light has information impressed upon it, such as phase, intensity or polarisation modulation. Intrinsic sensors are more suitable for composite embedment since they generally have the smallest dimensions and so present the smallest perturbation to the composite matrix.

Optical fibre sensors can be used to sense a wide variety of parameters. The reader is directed to the excellent introduction to the field of optical fibre sensors in the books by Dakin and Culshaw[14,15] which will not be repeated here. The first of these presents a summary of the technology associated with fibre sensors, some essential theory and a review of the components which are integral to fibre sensors. The second volume contains essays on most sensor types, extrinsic and intrinsic, mono- and multimode. Together, these volumes form a good introduction to fibre sensor technology and give an indication of the vast array of parameters which fibre sensors have been employed to measure.

3.1.3 The advantages of optical fibre sensors

Optical fibres sensors are eminently suitable for use in composite structures and the interest shown in them in recent years is, in the main, due to the advantages optical systems have over their electrical counterparts[16]. The main advantages optical fibre sensors have over electrical sensors for many measurements are listed below:

i) probably the most important advantages in composite materials are the inert nature of optical fibre composition and their small cross section. The fibres used in composites are often glass of a similar composition to optical fibres. This means that they are more compatible with a composite matrix than an electrical sensor would be and can be embedded in a composite structure without perturbing that structure to the degree that a comparable electrical sensor would;

ii) optical fibres can carry signals with immunity to electromagnetic interference ensuring that data on an optical fibre cannot be corrupted. This is of particular importance in industries using heavy electrical switching gear and the aerospace industry which is becoming ever more reliant on the integrity of signal to prevent the failure of aircraft in flight. Since a cure sensor is likely to be used in an electrically

noisy environment (*e.g.* power to an autoclave being switched for temperature control) this is a distinct advantage;

iii) being insulators, optical fibres are useful for linking apparatus at different electrical potentials. This property can be exploited in high voltage systems, medical equipment and lightning protection.

iv) optical fibres are considered to be safer than electrical systems owing to the small power levels of the light in the fibre. This has obvious benefits in explosive atmospheres where a spark may trigger an explosion.

v) the low loss characteristics of optical fibres present the possibility of having large distances between the sensor head and the instrumentation without the need for amplification *i.e.* measurements can be made remotely.

vi) an optical fibre is, in general, lighter and less costly than the equivalent length of copper cable having a similar bandwidth. This allows more information to be transmitted along a single fibre than a single wire of similar dimensions. This property has been exploited to great effect by the communications industry;

vii) an optical fibre can itself be used as a sensing element, particularly to parameters such as temperature and pressure;

viii) multiple optical fibre sensors can be placed along the same length of fibre creating a multiplexed system of discrete sensors. It is possible to interrogate each sensor separately hence obtaining spatial information on a particular measurand. Dakin[17] & Kersey[18] have written review papers covering a selection of some of the more interesting theoretical concepts employed in multiplexing optical fibre sensors onto a single fibre length.

Sensing techniques that utilise monomode fibres offer high resolution and a wider range of transduction methodologies. However, because singlemode sensors usually use phase-based optical techniques to exploit these advantages it is necessary to use coherent laser sources and to construct the sensor to mechanical tolerances of the order of the wavelength of the light being used. The interferometric methods used to interrogate such sensors lead to incremental rather than absolute outputs, *i.e.* the signal repeats for every 2π change in phase. This causes problems on power-up and at any other time the power is interrupted.

For a system to be practical it is appropriate to use multimode fibres since they can be made more rugged because tolerances are not so tight and have a correspondingly lower cost. Multimode optical fibre sensors are usually based on either:

i) intensity modulation, employing modulation of the transmitted light amplitude in the sensing region;

ii) wavelength filtering, which employs a simple method of wavelength detection methods and a stable wavelength source; or

iii) rate-modulation hybrid techniques, where electronics with low power consumption are incorporated into the measuring heads.

More examples of optical fibres sensor technology can be found in the text by Eric Udd (1991)[19]. This book covers the basic principles of optical fibre sensing and also gives examples of a large selection of the applications where optical fibres have found uses as sensing elements.

This section has explained what an optical fibre is and shown the advantages of such fibres when used as sensors over electrical sensing techniques. The next section describes the main features of the reactions which occur during the epoxy/amine cure reaction.

3.2 The epoxy/amine cure reaction

A basic understanding of the mechanisms of cure was needed for this work so that the degree of cure of the epoxy system being monitored could be related to the concentrations of reactants detected with the sensing method being used. The chapter starts with a simple explanation of how an epoxy resin is defined and what a curing agent is and the purpose it performs. The chapter then gives an outline of the basic chemical reactions which are generally thought to occur during the cure of epoxy resins such as those used here.

The mechanism and kinetics of the cure schedule determine the network structure of the cured resin and this in turn determines its mechanical and physical properties.

For most applications, epoxy resins are converted from a liquid to a three dimensional, infusible solid held together with covalent bonds. This process is called curing or hardening and is initiated using chemical hardeners or curing agents. Curing agents can either be:

i) catalytic, in which case they serve as initiators for homopolymerisation. Homopolymerisation involves molecules joining with like molecules to form a network;

ii) multifunctional, functioning as reactants in the polymerisation reaction. This is a co-polymerisation or polyaddition reaction; *i.e.* two or more molecule types are involved.

Co-polymerisation reactions result in the formation of a three dimensional network of resin molecules crosslinked *via* the curing agents. For aerospace composite applications this sort of reaction is desirable since the highly crosslinked reaction product has increased mechanical strength and chemical resistance. Typical curing agents for such systems include amines, amides and acid anhydrides.

3.2.1 The chemical structure of cure components

Epoxide or epoxy resins contain the epoxide group, also called the epoxy, oxirane or ethoxyline group which is a three membered oxide ring (see Figure 3-5).

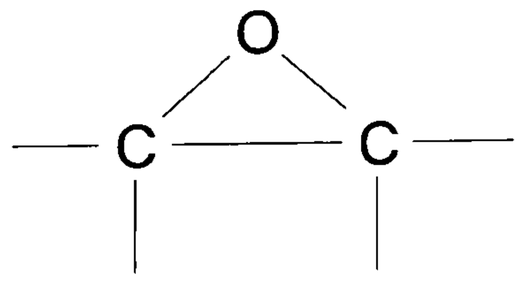

Figure 3-5 An epoxide group

Epoxy resins can generally be regarded as compounds containing more than a single epoxy group *per* molecule. The resins polymerise *via* these epoxy groups with the use of a cross-linking agent (or hardener) to form a tough three dimensional network. Epoxy compounds will generally react with a compound containing active hydrogen atoms *e.g.* phenols, primary and secondary amines and carboxylic acids. In these reactions the epoxy ring opens up to form a primary or secondary alcohol in combination with hardener molecule.

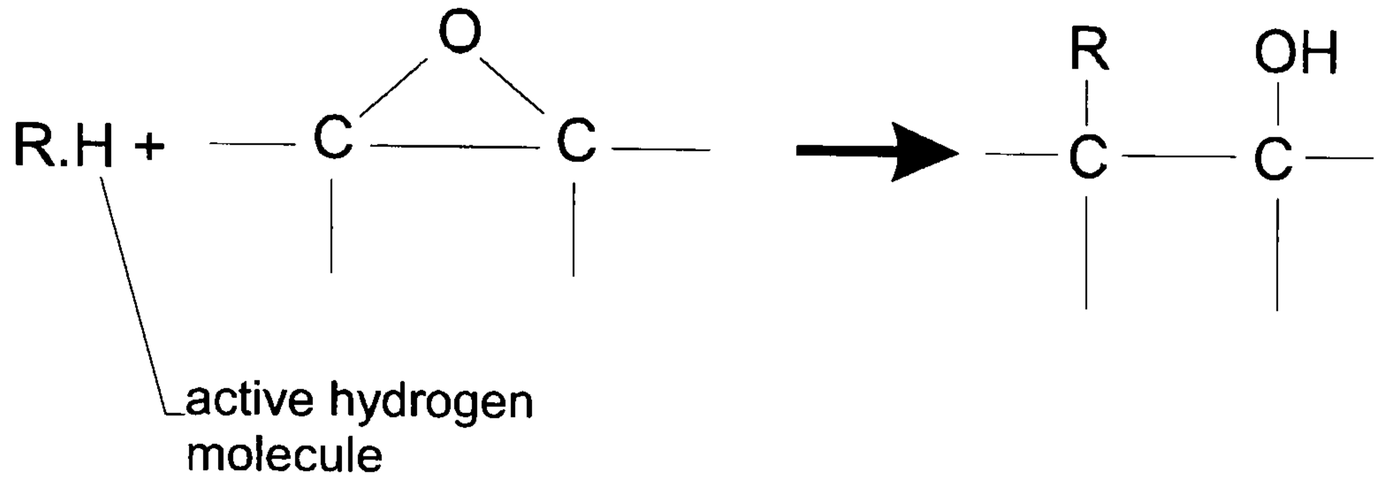

Figure 3-6 Reaction of epoxy ring with active hydrogen

Many molecules become joined as this reaction repeats and in this way a crosslinked structure can be produced. The next section will discuss the mechanisms of the epoxy/amine cure reaction in more detail since this is the reaction of interest in this study.

3.2.2 The cure reaction

It is generally accepted that during the amine-epoxide cure reaction two main processes occur. These can be seen in Figure 3-7. Primary amines present in the mixture at the start of the reaction react with an epoxide ring forming a secondary hydroxyl group and a secondary amine. The secondary amine can then undergo further reaction with another epoxide group to form a further secondary hydroxyl and a tertiary amine. This tertiary amine could then act as a catalyst for epoxide homopolymerisation, depending on its mobility within the resin hardener mixture. The hydroxyl groups formed by these reactions can also act as catalysts and so it can be seen that autocatalysis occurs during the early stages of cure.

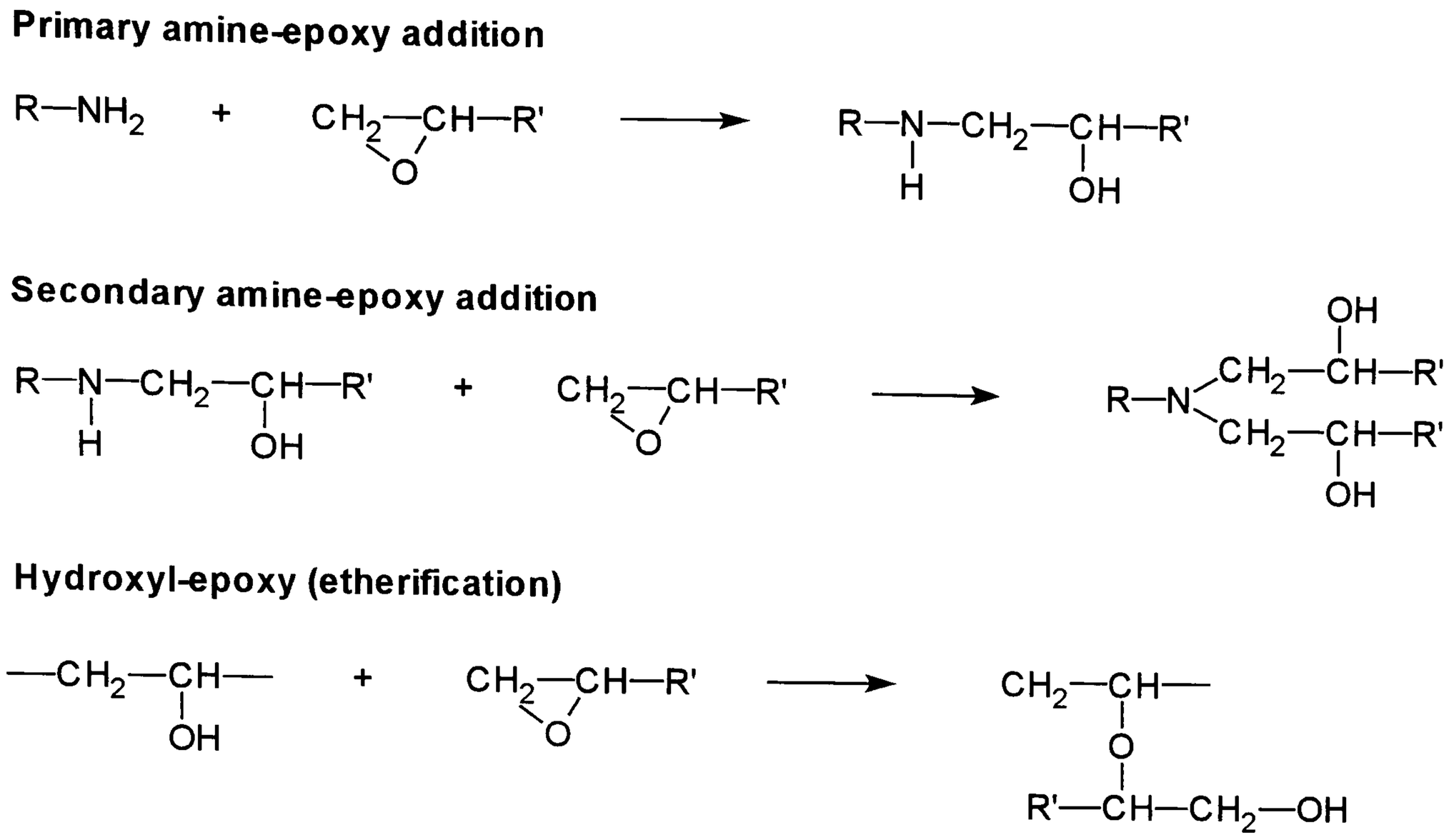

Figure 3-7 Generalised reaction scheme of epoxy-amine systems.

When the curing agent is an aliphatic amine Rozenberg[20] states that it is possible for the tertiary amine formed in the secondary amine-epoxy reaction also to catalyse the epoxy group polymerization. He goes on to say, however, that when aromatic amines are used as curing agents such reactions do not take place.

Shechter *et al.*[21] and Dusek *et al.*[22] showed that only when epoxide groups were present in excess did the hydroxyl groups formed in the amine-epoxy addition reactions add to the epoxide ring. This reaction is known as etherification (see Figure 3-7).

3.2.3 Reaction mechanism of epoxy-amine cure

Because of their importance as engineering materials, epoxies and their cure mechanisms have been the focus of a great deal of research over the past fifteen years. To characterise the reaction mechanisms of epoxy resins it has been common practice to use the epoxy resin phenyl glycdyl ether (PGE) because it is a monofunctional epoxy (*i.e.* it contains only one epoxy ring.). This simplifies the analysis of the reaction since it is not accompanied by the large changes in viscosity and other physical properties associated with the cure of multifunctional resins. An early paper using this technique is that by Schecter *et al.*[21]. Here the authors examine the cure of PGE with diethylamine. They found that certain solvents such as IPA (iso-propyl alcohol), water and phenol, catalysed the reaction and attributed this to the solvents' hydrogen bond donor properties. Smith[23] extended this work, suggesting that the reaction proceeds as follows:

the epoxy group forms a hydrogen bonded molecule in the presence of certain species. This weakens the C-O bond in the epoxy and the H-X (where X the rest of the amine or hydroxyl reactant) making reaction with a nucleophilic (positive attracted) reagent more likely than with the normal epoxy molecule.

The following mechanism for the amine-epoxy reaction was proposed by Mijovic *et al.* [24]:

It is required for a hydrogen bond between an epoxy group or an amine group to be formed as above. They suggest that three types of hydrogen bond complex are possible which may participate in the reaction:

i) Epoxy-hydroxyl: Rozenberg[25] states that the epoxy hydroxyl reaction is the most likely route *via* which the epoxy ring is opened. This reaction represents an autocatalytic reaction since hydroxyl groups are accumulated (see Figure 3-7). The amine hydroxyl reaction can be seen in Figure 3-8. The hydrogen bonded complex formed makes the carbon in the epoxy ring vulnerable to nucleophilic attack by amine molecules *via* a trimolecular complex.

ii) Epoxy-amine: The non-catalytic reaction path is represented by the epoxy amine reaction. This reaction is important when the number of hydroxyl groups available to take part in reaction 1 above is low for example at the beginning of the reaction. The amine reacts with the epoxy to form a hydrogen bond complex[24,25], again making the carbon in the epoxy ring more vulnerable to nucleophilic attack. Primary or secondary amines present in the system act as the nucleophiles forming the trimolecular complex which as in reaction 1 breaks down to form either a secondary or tertiary amine. This reaction can be seen in Figure 3-9. Rozenberg[25] observes that even small amounts of moisture decrease this reaction rate since the hydroxyl groups are much better proton donors (*i.e.* electrophilic species) than amines. The observed rate constant of the catalytic reaction is higher by a factor of 40 to 50 times than that of the non-catalytic reaction meaning the concentration of proton-donor molecules is very important when considering possible crosslinking reaction routes.

iii) Amine-hydroxyl: This hydrogen bond reaction path is stated by Mijovic [24] only to be present when the hydroxyl concentration has reached a certain threshold level. Beyond this threshold the hydroxyl-amine complexes formed react with epoxy hydroxyl complexes to produce secondary or tertiary amines *via* a transition complex.

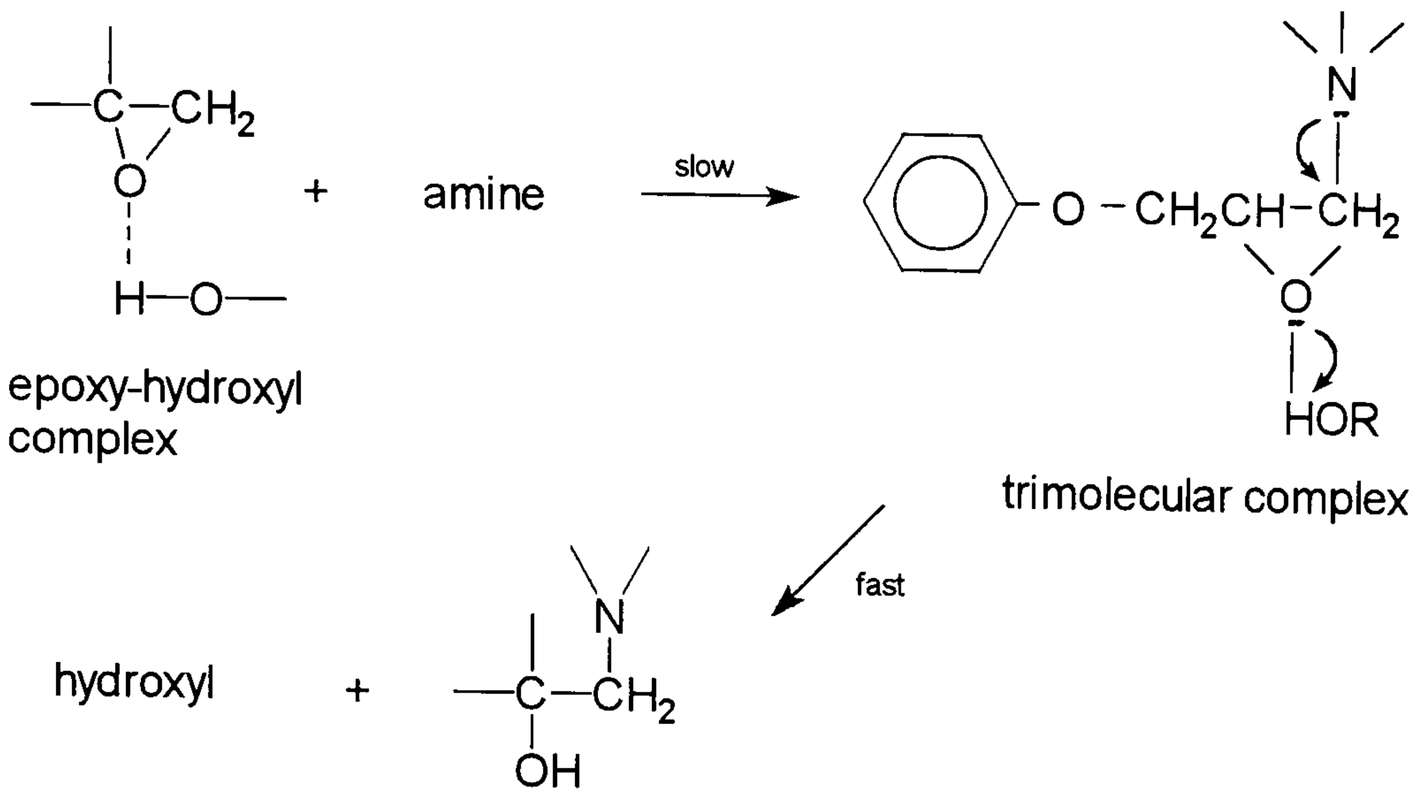

Figure 3-8 Mechanism of amine addition to an epoxy-hydroxyl complex.

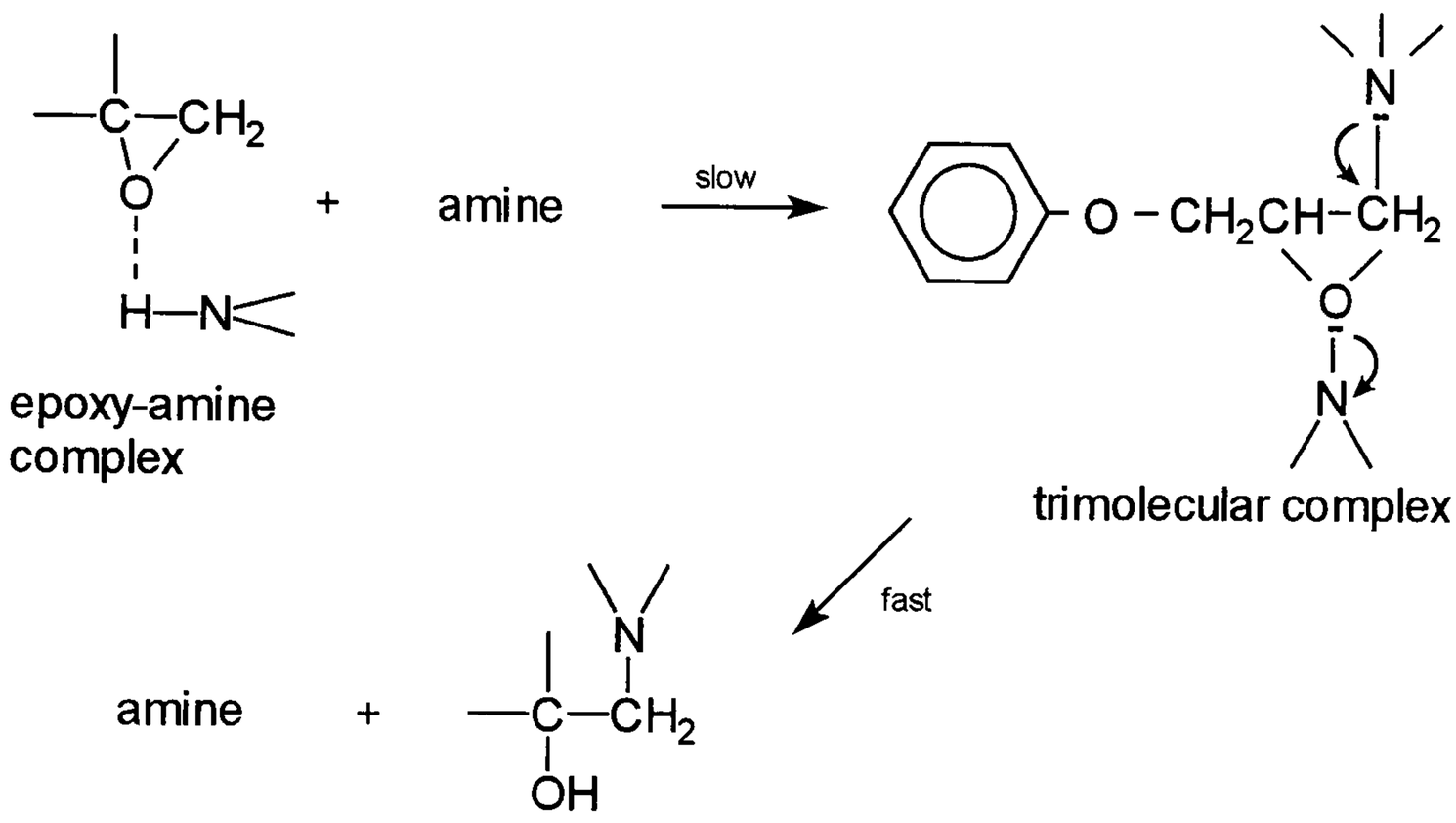

Figure 3-9 Mechanism of amine addition to an epoxy-amine complex.

The above reaction path has not been widely reported in studies of epoxy-amine kinetics[24]. However, the author's colleague has found excellent agreement between predicted and experimental results when this scheme was included in a mathematical model.

The mechanism of all three of these reactions routes can be summarised as follows:

[hydrogen-bond complex]+amine ➔ [transition complex] ➔ secondary or tertiary amine.

The rate controlling step for all three is the ring opening step (as shown in Figure 3-8 & Figure 3-9).

Thermodynamic parameters for the formation of model complexes, presented by Rozenberg[25], suggest a temperature dependence for the formation of proton-donor-acceptor complexes. For a model system of phenyl glycidyl ether, aniline and cyclohexanol, at temperatures below 60-70°C the order of complex bond strength is as follows:

HIGHEST STRENGTH OH---OH > E---OH > A_1---OH > A_2---OH > A_3---OH

where OH = hydroxyl containing species, E = epoxy group, A1, A2, and A3 are primary, secondary and tertiary amine respectively.

However,at higher temperatures the series A_i---OH becomes reversed so that the relative concentrations of complexes produced from hydroxyl groups and secondary and tertiary amines increases. This, therefore, shows that there is a chemical effect for the retardation in rate during the latter stages of cure as well as a retardation in rate due to diffusion effects as the viscosity increases[25].

Sections 3.1 and 3.2 have dealt with the fundamentals of optical fibres and with the basics of resin cure chemistry. The next section will examine the origin of the evanescent wave which is the phenomenon by which the sensor investigated in this study operates.

3.3 The evanescent wave and attenuated total reflection spectroscopy

The evanescent wave is utilised in the technique of attenuated total reflection (ATR) spectroscopy. ATR is generally carried out using an ATR attachment for a conventional transmission spectrometer. This attachment consists of a crystal in contact with the analyte. Light is launched from the spectrometer into the crystal and is totally internally reflected a number of times. The light emerging from the detector is detected and a spectrum of the analyte obtained. This is covered in more detail in section 3.3.2. The principle of ATR can be extended to fibres, replacing the ATR element with an optical fibre. This is described in section 3.3.3. Section 3.3.1, examines the evanescent wave, including how it arises, the depth to which it penetrates into the secondary medium and some experiments which have been performed to demonstrate its existence. It is possible using conventional theory to predict the amount of energy present in the evanescent field and hence obtain an indication of the potential sensitivity of the evanescent optical fibre sensor.

3.3.1 The evanescent wave

Total internal reflection is a phenomena predicted by Snell's law (section 3.1.1) whereby light is completely reflected from a dielectric interface. Although electromagnetic theory and total internal reflection have been studied since the time of Newton, as recently as 1947 a new phenomenon associated with total internal reflection was discovered. Goos and Hänchen showed that there was a slight displacement of a light beam upon reflection[26].

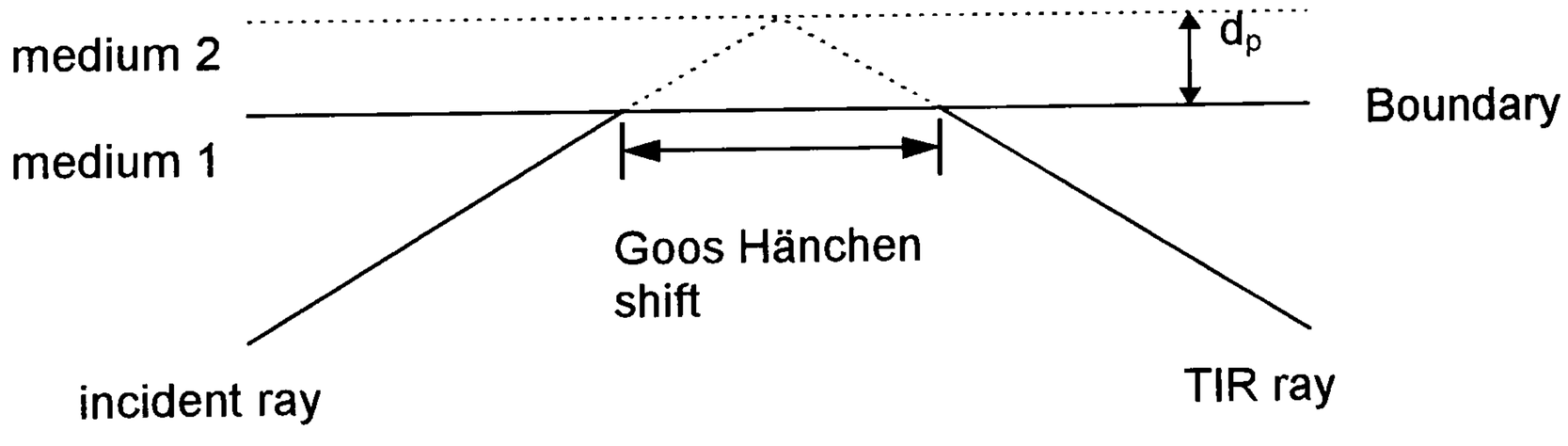

Figure 3-10 Goos-Hänchen shift for total internal reflection

This is consistent with the incident ray being reflected from a parallel plane which lies a short distance, d_p, within the second material. This is also consistent with the phase shift which is seen in the reflected ray. This phase shift is seen as due to the extra optical path travelled by the ray. It is therefore evident that Snell's law does not entirely describe total internal reflection. What actually occurs is that a standing wave, which is normal to the interface of the two media, is set up in the denser medium and in the rarer medium an

evanescent, non-propagating electric field is set up. This field decays exponentially with distance from the interface. A more sophisticated description involves analysis of the resultant interference pattern set up as the reflected light wave interferes with the light incident on the interface. This can be analysed mathematically by using a wave-based picture of the reflection at the dielectric interface.

Consider a plane boundary between two dielectrics and let this boundary be in the *xy* plane so that the *z* axis is normal to the boundary. A plane electromagnetic wave with frequency ω and wave vector $\underline{\boldsymbol{k}}$ in a dielectric medium is given by[27]:

$$\underline{E} = E_0 \exp i(\omega t - \underline{k}.\underline{r})$$

- 3.3

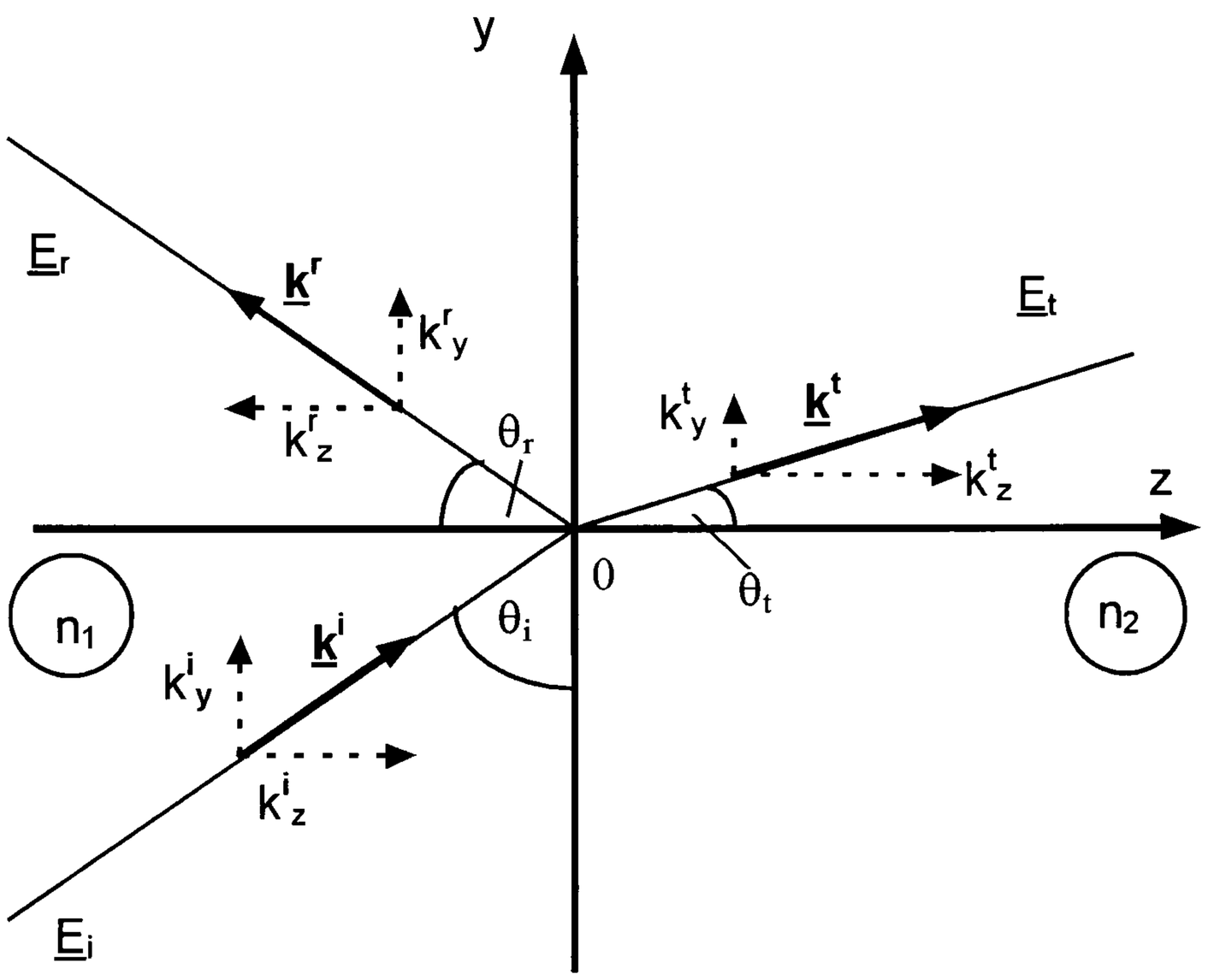

Figure 3-11 an electromagnetic wave incident at an angle θ_i in the yz *plane to an interface in the* xy *plane separating two dielectric media of refractive indices n_1 and n_2 produces a reflected wave at angle θ_r and a transmitted wave at angle θ_t*

Where ***E*** is the electric vector of the plane wave at a distance ***r*** from the origin. Following its interaction with the interface the reflected wave is :

$$\underline{E}_r = E_{ro} \exp i(\omega_r t - \underline{k}^r .\underline{r})$$

- 3.4

and the transmitted wave is:

$$\underline{E}_t = E_{to} \exp i(\omega_t t - \underline{k}^t . \underline{r})$$

- 3.5

since $\underline{k}^i$ is in the *yz* plane $\underline{k}^i.\underline{r}=k^i{}_y+k^i{}_z$

At the interface (z=0) the sum of the incident and the sum of the reflected electric fields must equal the transmitted field *i.e.* the sum of equations - 3.3 & - 3.4 must equal equation - 3.5. For this to be true at all times t and for all points on the interface:

$$\omega = \omega_r = \omega_t$$

- 3.6

so that there can be no frequency change occurring. The incident and reflected waves are in the same medium with refractive index n_1 so that that their velocities must be the same, say v_1, so:

$$\underline{k}^i . \underline{k}^i = k_i{}^2 = \frac{\omega^2}{v_1{}^2} = k_r{}^2$$

- 3.7

and

$$k^{t2} = \frac{v_1{}^2 k^2}{v_2{}^2} = \frac{n_2{}^2 k^2}{n_1{}^2}$$

- 3.8

but for the sum of incident and reflected waves to be equal to the transmitted wave for all y *i.e.*:

$$k_y{}^i = k_y{}^r = k_y{}^t$$

- 3.9

for the transmitted wave the last two equations give :

$$(k_z{}^t)^2 = \left(\frac{n_2{}^2}{n_1{}^2}\right) k_i{}^2 - k^i{}_y{}^2$$

- 3.10

now since $k^2=\omega^2/v^2_1$, $k^i_y=k^i sin\theta$, and $v_1^2/v_2^2=n_2^2/n_1^2$

$$k^t{}_z{}^2 = \frac{\omega^2}{v^2}\left(1-\frac{n_1{}^2}{n_2{}^2}\sin^2\theta_i\right)$$

- 3.11

now for total internal reflection (section 3.1.1), where $n_2<n_1$, when $\theta>\theta_c$, $n_1\sin\theta_i$ will be greater than 1 so k^t_z will be a complex number, say $\pm i\beta$. The transmitted wave equation becomes:

$$\underline{E}_t = \underline{E}_{0t}\exp(\pm i\beta)\exp i(\omega t - k_y y)$$

- 3.12

A positive exponential for the first term is obviously unrealistic since it represents a field which increases with distance into the second medium and becomes infinite. The negative term describes the wave amplitude which falls away exponentially with distance from the interface. The second term describes how the wave travels along the boundary as a surface or *evanescent* wave having the same frequency as the incident wave. Thus, we have an equation which describes the disturbance in the second medium and demonstrates the origin of the evanescent wave.

The evanescent field can be characterised by its *penetration depth,* d_p. This is the distance from the interface where the electric field drops to 1/e of its intensity at the interface. The penetration depth is referred to as the skin depth in some texts.

The electric field in the z-direction is given by:

$$\underline{E}_{tz} = \underline{E}_{tz0}\exp-\beta z$$

- 3.13

Therefore, $d_p=1/\beta$ will be the point at which $\underline{E}_{tz}$ falls to 1/e of its interface value.

From equation –3.11

$$k^t{}_z = -ik\left(\frac{n_1{}^2}{n_2{}^2}\sin^2\theta_i - 1\right)^{1/2} = -i\frac{2\pi}{\lambda_i}\left(n_{12}{}^2\sin^2\theta_i - 1\right)^{1/2} = -i\frac{2\pi}{\lambda_t}\left(\sin^2\theta_i - n_{21}{}^2\right)^{1/2} = -i\beta$$

- 3.14

since λ_t, the wavelength in the second medium $=n_{12}.\lambda_i$ where $n_{21}=n_2/n_1$ and $n_{12}=n_1/n_2$.. So:

$$\beta = \frac{2\pi}{\lambda_t}\left(\sin^2\theta_i - {n_{21}}^2\right)^{1/2}$$

- 3.15

Therefore :

$$d_p = \frac{\lambda_t}{2\pi(\sin^2\theta_i - {n_{21}}^2)^{1/2}}$$

- 3.16

From this equation it can be seen that the penetration depth is proportional to wavelength and that it becomes larger as $n_{21} \Rightarrow 1$ *i.e.* as the two refractive indices become better matched.

A demonstration of the effect is seen in Figure 3-12. This demonstration arises from Newton as part of his *Opticks* and was studied by Hall[28] in great detail. Light incident on the prism at greater than the critical angle will be totally reflected. If a lens of large radius of curvature is placed in contact with a the prism the light will pass through it at the point of contact. If the area of the spot is measured it can be seen to be greater than the area of contact showing that some light is transmitted through the lens even where no contact is made. If the angle of incidence is increased the size of the spot decreases in accordance with equation- 3.16. In addition if white light is used the edge of the transmitted spot is found to be red and the edge of the reflected "hole" is seen to be blue. This verifies the wavelength dependence of the penetration, the longer red light being transmitted whereas the shorter blue light is reflected.

There are two different methods which can be employed to couple energy from the evanescent wave and thus demonstrate its existence by making the reflection at above the critical angle less than total. These two methods are:

i) frustrated total reflection (FTR) where some or all of the evanescent wave energy is redirected and there is no overall energy loss;

ii) attenuated total reflection (ATR) where energy is absorbed and there is a loss.

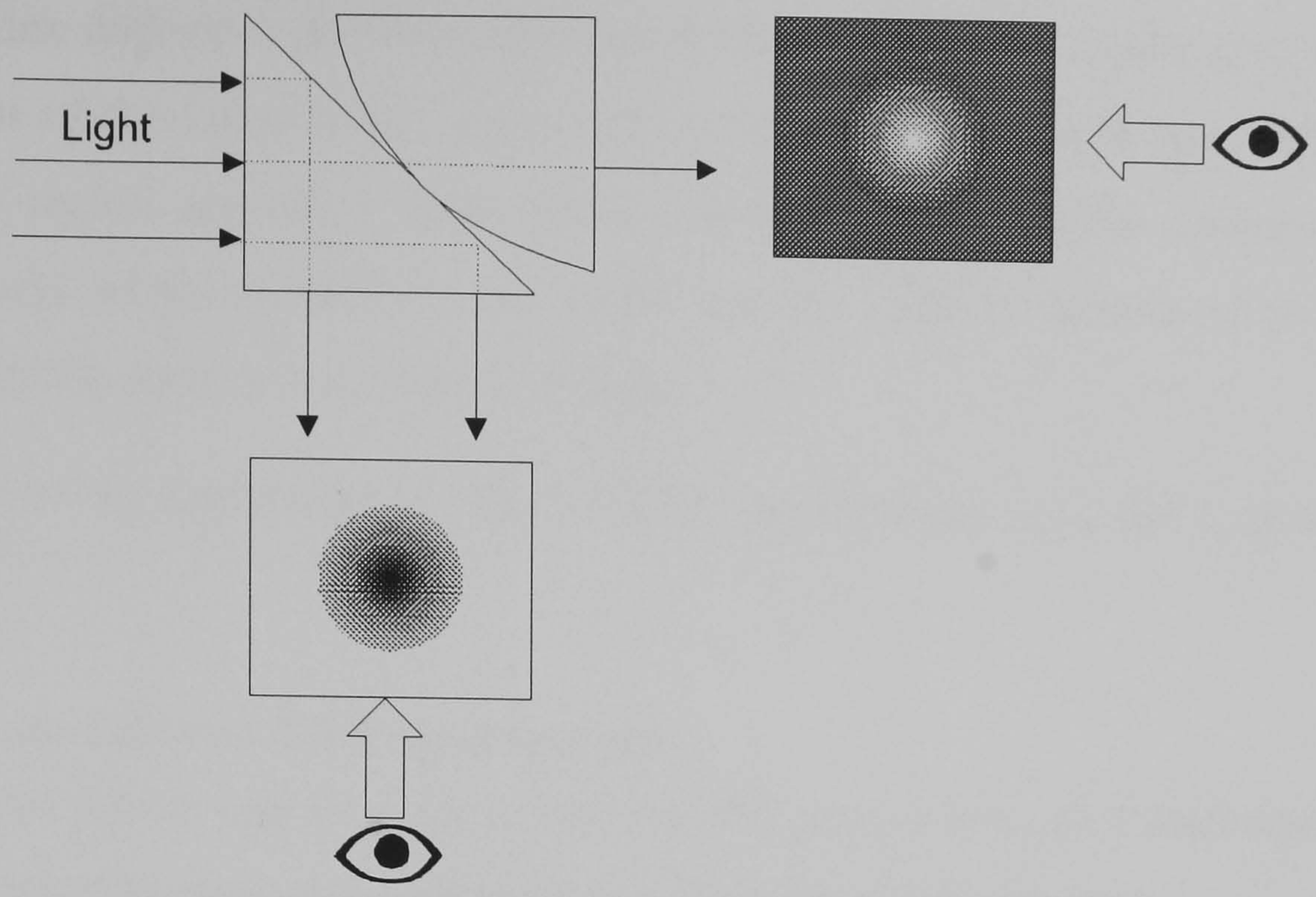

Figure 3-12 Experiment to demonstrate penetration of evanescent field into rarer medium and its dependence on wavelength and angle of incidence.

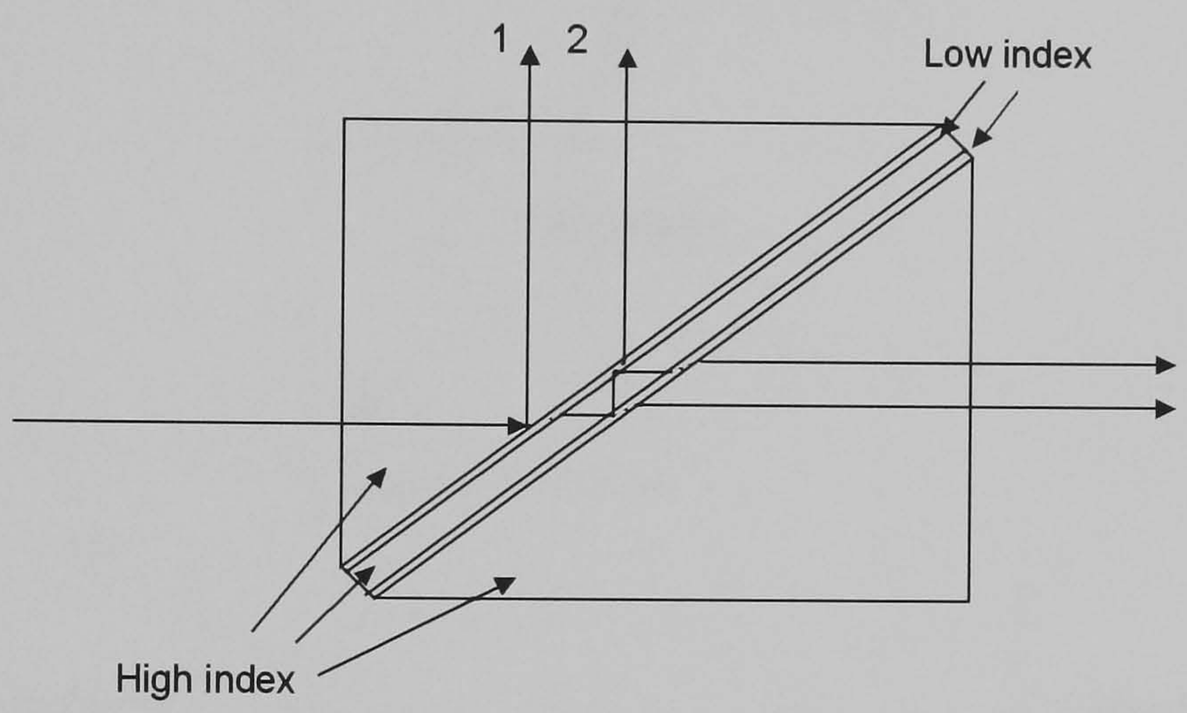

Figure 3-13 The frustrated total reflection filter.

It occurs when the evanescent field has sufficient energy to extend through the lower index region and into a nearby region with a higher index. ATR is the evanescent equivalent of bulk absorption whereby the energy of the field is reduced by giving up some of its energy to the medium through which it is travelling. FTR is theoretically a lossless coupling, but, can be accompanied by ATR and/or scattering losses that result in a loss of energy. FTR is employed in the manufacture of optical beamsplitters and filters. Beamsplitters are often cubic in shape, being made up of two 45° prisms with their hypotenuse faces placed close to each other. By adjusting the gap between the two prisms and the refractive index of the medium between them the cube can be made to transmit or reflect any proportion of the incoming light. An extension of this is the *frustrated total reflection filter*[29]. This is, in effect, an almost ideal Fabry-Perot filter and is similar in construction to the adjustable beamsplitter being made up of two prisms. However, the two are separated by a high

refractive index dielectric sandwiched between two lower index layers (see Figure 3-13). The thickness of the lower index layers determines how much light enters the high index region. This region acts as a Fabry-Perot cavity and, by careful choice of the layer thicknesses and refractive indices, the cavity can be made to behave as an interference filter for a specific narrow wavelength of light.

The most important application of ATR is ATR spectroscopy. And this is described in the next section.

3.3.2 Conventional ATR spectroscopy.

In conventional optical spectroscopy a light beam is passed through a thickness of a sample material and its transmission is measured as a function of wavelength.

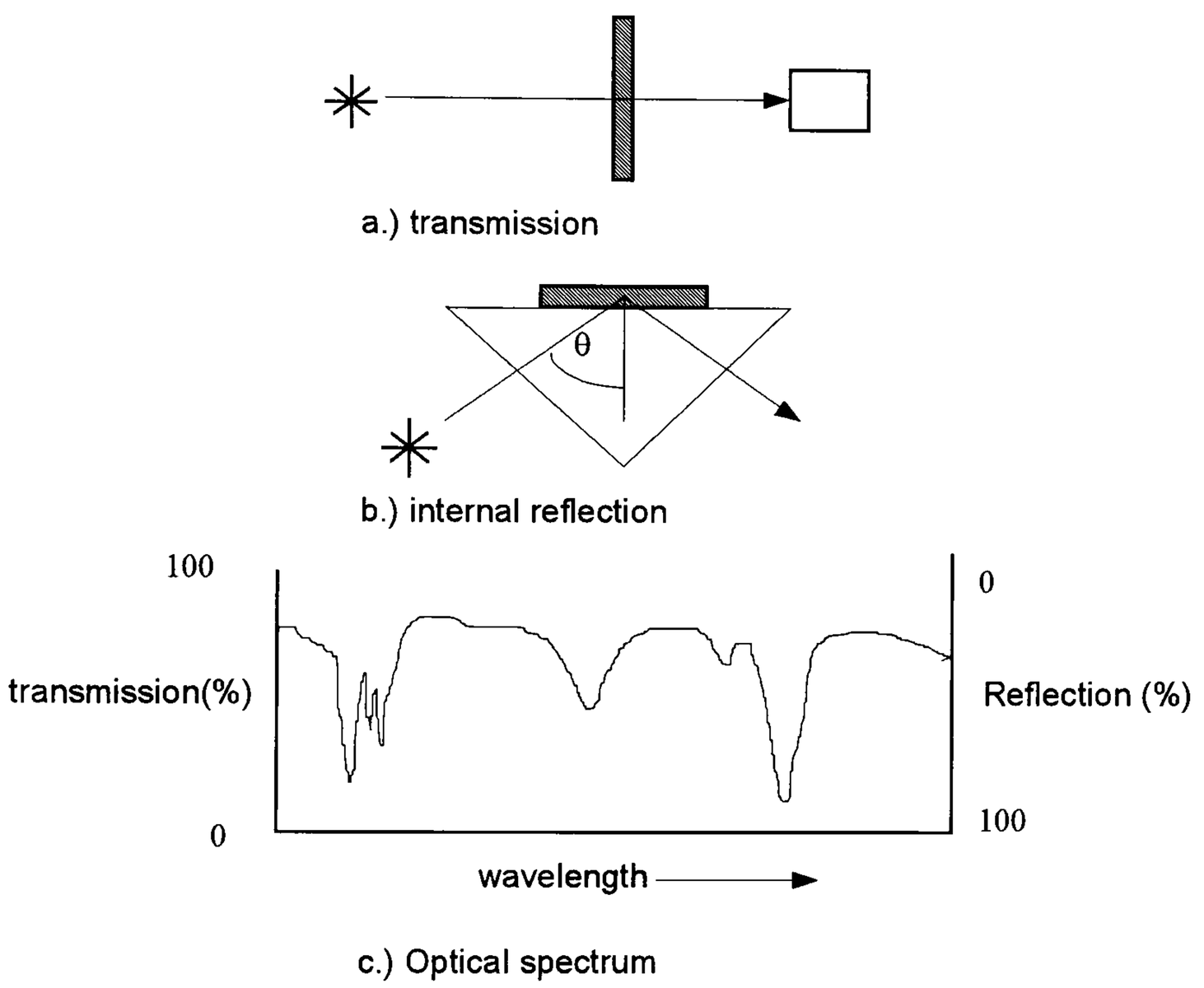

Figure 3-14 comparison of conventional transmission and internal reflection spectroscopy (after Harrick[33].)

This gives the characteristic transmission spectrum of the sample material (Figure 3-14, a) and c.)). Transmission spectra have become useful for identification purposes although they are a complex amalgamation of all of the optical properties of the material. However the spectra are very reproducible and there are vast libraries of spectra for comparisons to be made with. Internal reflection spectroscopy is a method where an optical spectrum is recorded by placing a sample in optical contact with a transparent medium which is optically denser. This is known as the internal reflection element (IRE). Light is launched into the IRE at an angle greater than or equal to the critical angle so that total internal reflection occurs. The wavelength dependence of the reflectivity of the sample is then

measured (Figure 3-14 b)). The reflectivity is affected by the absorption of the evanescent wave which penetrates a short distance into the sample medium. Internal reflection spectroscopy, using a single reflection, was developed by Fahrenfort[30] who demonstrated that strong absorption bands could be obtained for certain materials using a single reflection. He later employed the technique using 3 to 5 reflections. His name for this technique was attenuated total reflection (ATR). Increasing the number of reflections is analogous to increasing the pathlength in transmission spectroscopy.

The technique was extended by Harrick[31,32], for studying surfaces and thin films, and Harrick's text[33] remains the definitive work on attenuated total reflection spectroscopy. ATR has a number of advantages over transmission spectroscopy in certain instances. These are for sample materials that are:

i) highly absorbing or nearly opaque (and would require very thin sample films in transmission spectroscopy);

ii) difficult to cast into a film of uniform thickness;

iii) possess specific surface properties which differ from the bulk material. These can be probed by the small, defined penetration depth of the evanescent wave;

iv) in the liquid or gas phase.

However, ATR does have its shortcomings, not least, that it is difficult to relate an ATR spectrum to actual concentrations of species present. The method, therefore, has long been used as a qualitative analysis technique. The main problem arises because of the change in refractive index of the analyte medium. However, it will be shown later that the technique can be utilised in a qualitative way for the monitoring of cure of an epoxy resin system.

The refractive index of an absorbing substance can be considered to be composed of a real and a complex part, *i.e.*:

$$\hat{\mathbf{n}} = n + i\kappa$$

- 3.17

where n is the conventional index of refraction equal to the ratio of the speed of light in a vacuum to the speed of light in the medium and κ is the complex part of the refractive index and which is equal to $\alpha\lambda/4\pi$ where α is the bulk absorption coefficient of the medium. κ is sometimes known as the extinction coefficient. This arises from substitution

of a complex expression for a harmonic light wave being substituted into Maxwell's wave equation (*i.e.* substituting k, the wave vector, with a complex wave vector given by $\omega/c\,\hat{\mathbf{n}} = \omega/c(n+i\kappa)$.)

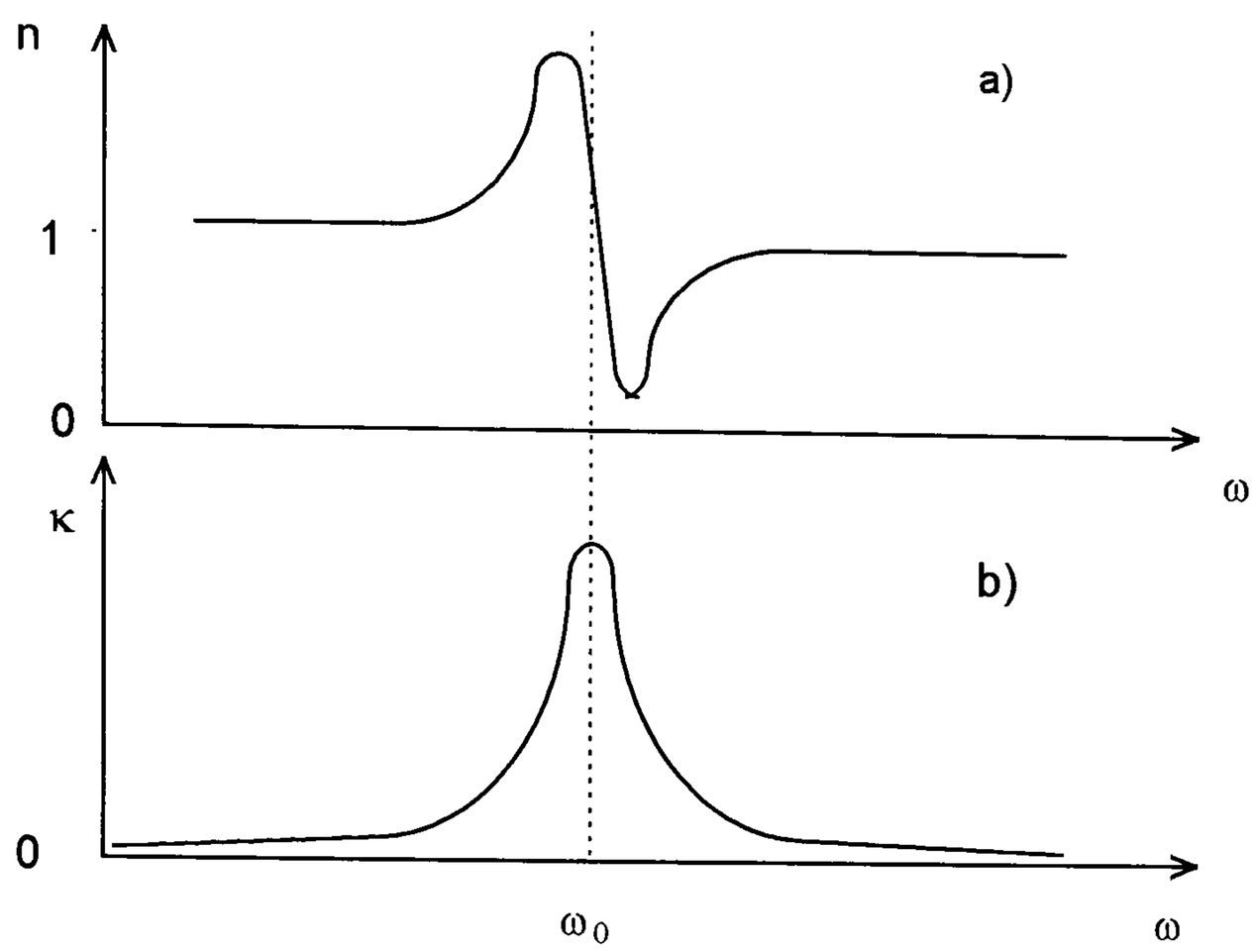

Figure 3-15 Graphs of a) the index of refraction and b) the extinction coefficient as a function of frequency near a single absorption band.

Figure 3-15 shows the general way in which n and κ depend on frequency. There are resonance frequencies present which are dependent on the resonant frequencies of the electrons in the medium. The index of refraction is greater than unity for small frequencies (longer wavelengths) and increases with frequency as a resonance frequency is approached. This is the case of "normal dispersion", which is exhibited by most transparent materials over the visible range of the spectrum. At or near a resonant frequency however the refraction becomes "anomalous", that is the refractive index decreases with increasing frequency. To take into account the fact that individual electrons will be bound differently it is common to assume that a certain fraction, f_1 of the electrons in a medium have an associated resonant frequency ω_1, a fraction f_2 a resonant frequency ω_2, and so on. The square of the complex refractive index of a medium is then commonly expressed in the form[34]:

$$\hat{n}^2 = 1 + \frac{Ne^2}{m\varepsilon_0}\sum_j \left(\frac{f_j}{\omega_j^2 - \omega^2 - i\gamma_j\omega} \right)$$

- 3.18

which is a summation, extending over all the electron states, indicated by the subscript j. Here e is the electron charge, N the number of electrons *per* unit volume and m the electron

mass. The fractions f_j are known as oscillator strengths. The damping constants associated with various frequencies are denoted by γ_j . Anomalous dispersion can be observed experimentally if the absorption is not too strong at the resonant frequency.

The equations describing the proportion of light reflected at a dielectric interface, with the introduction of this complex refractive index, require significant calculation effort. Therefore in the early days of ATR spectroscopy methods of transformation were developed so that ATR could be made analogous to transmission spectroscopy. The most prevalent of these is the effective thickness method that was proposed by Harrick *et al.*[35]. The effective thickness is defined as the thickness of material required to give a spectrum of the same contrast in a transmission experiment as that obtained *via* internal reflection. This approach has it problems however as illustrated by Müller *et al.*[36]. They present a treatment of the problems that it is necessary to deal with when measuring the concentration of a component of a system from the ATR spectrum of the system. They redefine the effective thickness for the lossy case, which deviates from the lossless case on which Harrick's calculation for effective thickness is based. The lossy case is the case where the reflecting medium is absorbing *i.e.* the case with ATR spectroscopy. One of the most important findings of this paper is the statement that it is not sufficient to equate a concentration change in an analyte to a change in the absorption index of the substance, κ, in calculations for sensitivity. They stated that it is also necessary to take into account the medium refractive index change as a result of the concentration change. This has a large effect in the case of resin cure monitoring as will be discussed later. In this paper the concentration of an absorbing species is not actually dealt with and they only calculate the concentration of a non-absorbing solute, using ATR. The complications of determination of the true absorption spectra of liquids is discussed by Hawranek and Jones[37] who emphasis the necessity of a standard for the calibration of ATR spectra against standard transmission spectra.

Because of these inherent difficulties ATR was until recently essentially a method for qualitative analysis with quantitative analysis being confined to the evaluation of optical constants [38, 39, 40] . Hansen[41] presented a treatment of the equations for reflectivities at a plane boundary to obtain absorption rules for single and multiple ATR spectrometer cells. Equations are given for all types of incident polarisation and the findings are that if the ATR parameters are selected carefully and the complex part of the refractive index, κ, is not to large, *i.e.* 0.3 or smaller, absorbance is linear with κ and with concentration of

absorbing species if Beer's law holds. However,calculations are again limited to optical constants. There have been many trials in the direction of quantitative analysis but not really any systematic approach to the problem. Müller *et al.*[36] attempted this in the paper mentioned above, concluding only how the concentration of non-absorbing samples can be measured. More recent attempts have used a Kramers-Kronig transformation[42] on the ATR spectrum to estimate the spectrum of the absorption index, κ, which is then used to correct the absorption spectrum. This process is used iteratively to obtain a good estimate of the true absorption and refractive index spectrum. The procedure was used quite successfully by Hawranek and Jones [37, 43]. Bertie and Eysel[44] use this iterative procedure to determine the optical constants of several organic liquids. They describe a use of the optical constants thus measured, to calculate traditional infrared intensities but present no results of this kind. The method is described in a paper by Huang and Urban[45] which compares two methods of performing the iteration. The paper finds that the method proposed by Bertie and Eysel [44] is more suited to weak bands whereas that proposed by Dignam and Mamiche-Afara[46] is applicable to a wider range of absorption intensity although less accurate for weak bands. A new device known as a "circle" cell, essentially a multiple reflection cylindrical ATR cell, has been used by several authors to obtain quantitative measurements. Sperline *et al.*[47] present a way of calibrating a circle cell in such a way that general quantitative spectroscopic measurements are simplified. They use a standardising solution to measure the average reflectance angle in the cell and the number of reflections and mathematically fit measured ATR absorbances using the number of reflections as a parameter. The use of the circle cell in ATR is more akin to the use of fibre optics for evanescent wave spectroscopy, being of the same cylindrical geometry, and this will be dealt with in the next section.

An alternative way of looking at the absorption of the evanescent wave is presented in Carniglia *et al.*[48]. This paper treats the interaction of evanescent photons with molecular dipoles and gives an insight into interactions at a microscopic level with ATR. This paper also covers the possibility of fluorescence. This is effectively the inverse process to evanescent absorption whereby molecules in the external medium are excited by the evanescent wave as in the absorption case but then re-emit a photon, perhaps of a different wavelength. The photons thus emitted would have a homogenous distribution and be detected external to the sample or by measuring the proportion reflected back into the ATR element.

A review of the literature has highlighted that measuring actual concentrations of species using ATR spectroscopy is still problematic. It remains however a very useful and frequently used technique for the measurement of parameters such as surface reactions[49,50], and diffusion. ATR's application to cure monitoring has been restricted due to the problems introduced by the large refractive index change which occurs during cure. An example of ATR being used for this purpose, however, was undertaken by Snyder and Fuerniss [51]. This describes a method for the qualitative monitoring of a photo resist cure reaction.

3.3.3 Optical fibre, evanescent wave absorption spectroscopy.

Optical fibres guide light *via* total internal reflection and therefore will possess an evanescent field at the interface between core and cladding where the reflection occurs. It is normal for a fibre to have a cladding much thicker than the depth to which the evanescent wave penetrates so that the reflected light is not frustrated or coupled into adjacent fibres causing crosstalk. If this cladding is removed or thinned, and replaced with an analyte substance, the evanescent wave can interact with the analyte, *via* ATR, and so be observed spectroscopically.

It is only recently that optical fibres have begun to be used in the field of chemical sensing using the evanescent field. This is maybe because of some inherent difficulties that optical fibres present when used as internal reflection elements (IREs). These difficulties are outlined by Harrick[33] who pays little attention to the use of fibres as internal reflection spectroscopy elements. He warns however that cylindrical rods and fibres in internal reflection spectroscopy "...may have advantages because of their simplicity in preparation.." but "..should be used with caution." This he says is "..because of the complicated optical paths, calculations of angles of incidence and hence of effective thickness cannot easily be made." It has already been shown that the calculations associated with ATR are complex. However,when a fibre is used, the associated calculations become much more complicated. Bends in the fibre further complicate matters and so calibrations are required.

Despite these difficulties, numerous researchers have employed optical fibres as ATR elements. Sensor of this kind are more commonly known as fibre optic evanescent wave absorption sensors or evanescent field absorption sensors. Many experimenters have made use of infra-red transmitting optical fibres made of materials such as silver halide[52],

sapphire[53], heavy metal fluoride[54,55] or chalcogenide[56,57] glass. Conventional silica fibres[58] have also been used as have silica fibres modified for use in the infra-red[59] by reducing their hydrogen content. A brief survey of infra-red fibre types for use in evanescent wave spectroscopy, giving typical characteristics can be seen in Table 3-1.

Fibre	Core diameter (μm)	Coating thickness (μm)	Cladding thickness (μm)	Wavelength range (μm)	Attenuation (dBm^{-1})	Refractive index	Operating temperature (°C)
Chalcogenide glass	250	45	30	3-10	0.5 @ 6 μm	2.9	300
Fluoride glass	250	45	40	0.5-4.3	.02@ 2.6μm	1.51	250
Sapphire	250	none	core only	0.2-4	20@ 3μm	1.7	>1500
silver halide	250	none	core only	303-15	0.7@ 10.6μm	2.0	400

Table 3-1. Typical characteristics of infra-red fibres [57].

The most common method used by these researchers is to launch light from a spectrometer, usually an FTIR, into the infrared fibre. The light passes through the sensing region where it is detected by either the spectrometer's detector or an external detector. In this way an evanescent absorption spectrum is obtained.

Fibre evanescent wave sensors do have several attractive features *e.g.*:

i) remote sensing capability[60];

ii) geometric flexibility and possibility of examining small amounts of material[52];

iii) its intrinsic construction which allows multiplexing [61];

iv) relative low cost and ruggedness over conventional ATR.[62]

The launching of the light from spectrometer to fibre in experiments carried out to date has often involved a complicated optical arrangement of mirrors of lenses such as that seen in George *et al.*[63]. It has been suggested that a more compact and low cost method would to be use a compact tuneable source such as a laser diode. Schnitzer *et al.* [64] present such a system in which they use silver halide fibre and a tuneable, lead salt, diode laser. A water absorption spectrum was obtained in this paper. Difficulties are presented by the use of such lasers due to their poor beam quality and the need for them to be cooled cryogenically which make them difficult to use with optical fibres. Systems utilising tuneable sources

will become more viable with the emergence of more compact tuneable laser sources at longer wavelengths.

Fibre optic evanescent wave sensors have been employed to measure many different parameters *e.g.*:

i) solids (aluminium corrosion[65]);

ii) liquids (water[52, 64] , dye solutions[77], gas solutions[66], iso propyl alcohol[67], organic solutions[68, 69,70]);

iii) biological specimens (antigens/antibodies[71,72,73], urea/plasma[56], drugs[74]);

iv) gaseous specimens[75] (ammonia[76] and oxygen[77], CO_2[78], methane[79],);

v) physical parameters (temperature[80], pH[81]);

vi) cure of composites [82,83,84].

The sensors utilised for composite cure monitoring are of greatest interest for this research and will be covered in more detail in section 3.5.2.

3.3.3.1 Biosensors

Biosensing is a field in which evanescent sensors are used extensively. It is therefore instructive to look briefly at the configurations used in the detection and measurement of many biological stimuli. Biosensors tend not to be strictly intrinsic in nature because they use additional molecules incorporated into the sensor to detect stimuli and it is the reaction to the stimuli which are then detected by the evanescent sensor.

Fibre evanescent wave absorption sensors are used for biological sensing because of their potential for remote and continuous sensing, small size, freedom from electrical interference and relative biocompatibilty for use in the body. Biological sensors are almost unique amongst optical fibre sensors in having made the transition from laboratory to commercial application. Most fibre optic biosensors employ either fluorescence or absorbance spectroscopic techniques to quantify the analyte. Fluorescence is the more frequently used technique because of its higher sensitivity. These sensors usually employ one of two different optical configurations at the sensing region[85]:

i) excitation, by the evanescent wave, of a fluorescent recognition molecule coated onto the fibre surface which binds to the analyte; or

ii) distal-cuvet configuration where fluorescent detector molecules are immobilised at the fibre-end in a porous matrix.

The evanescent configuration is most important in biosensors and of greatest interest here. Hirschfield[86] and Harrick and Loeb [87] were the first to show that fluorescing species near an interface could be excited by the evanescent wave. The principle of total internal reflection of fluorescence was employed by Kronick and Little[88]. The principle was adapted for use in optical fibres by Andrade *et al.*[89] The use of the evanescent field geometry requires attention to detail from the designer to assure good sensitivity since for the large (≈500μm) multimode fibres commonly used, only a small fraction (<0.01%) of the power entering the waveguide appears in the evanescent field. Also the light coupled back into the fibre for detection is much smaller than for a typical fluorometer. These immunosensors have the advantage of operating at only one wavelength; that at which the fluorescent molecules are excited. Yoshida *et al.*[90] examined the effect of the excitation wavelength on the sensitivity of a fluoro-immunosensor and obtained an order of magnitude higher sensitivity over conventional systems by using excitation light of wavelength 650nm with a fluorescent label called allophycocyanin.

Many biosensors use only small sections of fibre which are immersed in a flow cell or the absorbent medium and have light endfire launched into them with an IR source, see for example, Eenik *et al.*[71] and Carome *et al.*[73]. Much of the published work concentrates on the chemical reactions responsible for identification of specific molecules by fluorescence. Thompson and Ligler[85] present an overview of the basic principles employed in these "recognition molecule" processes. A method of binding the recognition molecules to the silica surface of the fibre is given by Bhatia *et al.*[91]. Golden *et al.*[72] focus on the development of several aspects of the sensing system including sensor tapering for increased sensitivity (see section 3.3.3.2), and the ability of probes to regenerate for repeated use. Love and Button[92] discussed the physical problems associated with evanescent sensing. They present a treatment of the optical characteristics of an evanescent wave fluorescence biosensor. A semi-classical model was compared with results obtained by systematically varying the optical launch conditions and cladding refractive index with good agreement. Love was also co-author on a paper where the sensitivity limits to a particular immunoassay experiment is calculated and the kinetics of the fluorescence process modelled using a calculation of the number of moles of a dye can be sensed over a $1mm^2$ area of sensor[93]. Glass *et al.*[94] examine the effect of the numerical aperture of the

fibre used on the signal level observed in evanescent fluorosensors. They showed that the signal level is a highly sensitive function of the numerical aperture. This has important ramifications in the field of evanescent sensing as will be shown in the next section.

3.3.3.2 Sensor enhancement

The proportion of power in the evanescent field for a multimode fibre with core diameter 200μm, n_{co}=1.46 and n_{cl}=1.41 at 1500nm, according to Gloge's[13] estimation (given by $4V/(3\sqrt{2})$), is approximately 1.2%. This is obviously a small proportion of the fibre launch light which actually has an opportunity to interact with the analyte. The remaining light in the fibre is unmodulated and therefore constitutes a large "noise" signal. Therefore various researchers have sought ways to increase the proportion of light in the evanescent field or the penetration depth of the field so increasing sensitivity. Equation - 3.16 shows that the evanescent wave penetration depth is greatest for total internal reflection at angles corresponding to higher order modes. The lower order modes penetrate less deeply, and so exhibit less absorption and produce a reduction in the signal to noise ratio of the measurement being made. As a result a way of increasing sensitivity is to populate the higher order modes preferentially. Several methods have been proposed to achieve this. Ruddy *et al.*[60] used an annular optical mask to suppress lower order modes and to launch light into the cladding modes of the fibre. The size of the mask however would seem to be difficult to optimise and there is no proof in this paper of an actual improvement in sensitivity over a system not employing a mask.

Higher order modes may be generated at the sensing region by tapering. Gupta & Singh[95,96] give a theoretical explanation of the increase in sensitivity. They do this for several taper profiles, linear, exponential and parabolic and conclude that the exponential taper profile theoretically produces the greatest enhancement. Presumably, owing to the difficulty of fabricating sensors with such profiles there is no experimental evidence to confirm this theoretical prediction. In simple terms a tapered sensor increases the angle at which light travelling along the fibre meets the interface between core and interface. A ray tracing determination of the penetration depth of the evanescent wave for a tapered sensor can be seen in a paper by Golden *et al.*[97]. A commercially available internal reflection spectroscopy cell employs a short length of chalcogenide fibre which has been tapered. The cell is known as the "FiberCell" and is described in a paper by researchers at Nicolet instruments[98]. The advantages of this cell are described as being its ability to acquire

spectra of extremely small sample volumes (<10μl) and high sensitivity. Its disadvantages are the difficulty in making quantitative measurement, as discussed above, the delicate nature of the tapered fibre and the ease with which the cell becomes contaminated beyond the point where it is useful.

Bending or coiling the fibre should also increase the sensitivity of the sensor, not only by allowing more sensor to be contained in a smaller sample but by increasing the angle at which rays strike the core/analyte interface. Many researchers have taken this approach, for example Bürke and co-workers [70,99] and Degrandpre & Burgess [61, 100]. These authors do not present any treatment of the effect of the curvature of their fibre however a brief examination of the effect can be seen in the paper by Takeo and Hattori[101].

Stewart *et al.* [102] show how the sensitivity of an evanescent sensor for monitoring gas can be improved by using a D-fibre (a fibre with a D cladding cross-section[103]) with a thin high index overlay and calculate that the sensitivity of the sensor can be enhanced by up by 2-3 orders of magnitude. The overlay increases the interaction of the evanescent wave with the absorbing medium. These workers also suggest using a porous coating, of a similar refractive index to the fibre cladding, into which the gas can penetrate to enhance sensitivity. This technique has been employed by several other groups. For example Macraith[104] uses a sol-gel derived porous glass coating to enhance both absorption and fluorescence evanescent sensors. A low numerical aperture is achieved, by replacing the cladding with a porous coating of similar refractive index, the proportion of energy in the evanescent field is increased (see equation- 3.16). The analyte is still able to come into contact with the evanescent wave due to the porous nature of the glass. One disadvantage of these porous coatings is the ease with which they can be contaminated.

Further papers by Macraith and colleagues [105, 55] and by Blyler *et al.* [106]show the use of a dye doped sol-gel in an oxygen sensor. This is actually a fluorescence sensor however it shows the use of porous cladding to bring analyte and fibre core close together without compromising fibre guiding properties.

Yet another method of enhancement is to coat the sensor region of a fibre with a compound which attracts the substance which is to be detected. For example, Bürck *et al.*[107,70] use an "extracting membrane" which is hydrophobic and enriches the organic compounds which are to be detected. Of course this is fine for the detection of the presence of materials

however again the diffusion kinetics into the polymer coating limits the quantitative measurements which can be made.

The preceding sections have dealt with the background to optical fibre sensing and resin cure. It has been shown that, although complicated, optical fibre evanescent absorption spectroscopy shows promise as a method for determining the state of cure of an epoxy resin system. The following sections will cover the methods which are currently used to determine the state of cure of a curing resin or composite (section 3.4) and optical fibre methods of determining the same(section 3.5.). Included in section 3.5. are references to the author's publications which cover refractive index and evanescent wave optical fibre cure sensing.

3.4 Cure Monitoring techniques

3.4.1 General sensing techniques for cure monitoring

It is very difficult to measure directly the viscosity and extent of cure of the resin matrix for a composite material. Traditionally the methods employed have been based on thermal and dynamic analysis. A variety of methods have been used in the past to monitor the important parameters in the epoxide cure reaction. The most important methods are covered below.

3.4.1.1 Tracking of heat of reaction

Heat fluxes into and out of the composite mass are followed to determine factors such as the onset of the exotherm reaction. This yields important information on the state of cure of the system. Many papers have been published by Barton [108,109,110] on the DSC analysis of various resin systems and the relation of results to cure. Perry *et al.* [111] monitored the cure of an epoxy graphite composite using a dual heat flux sensor designed from a pile of three thermocouples to provide on-line estimation of thermal diffusivity and to measure the change in heat flux for calculating the Damkohler number. The results were verified using DSC. The Damkohler number, D_a is defined as the rate of heat generation over the rate of heat conduction and can be used to represent three cure characteristics:

i) onset of reaction exotherm is when D_a becomes non-zero;

ii) accelerated reaction exotherm beginning when D_a exceeds 1;

iii) the end of the reaction can be seen when D_a returns to 0.

The heat fluxes were measured by spacing thermocouples within a composite close enough that there is a linear temperature gradient between them but far enough apart that there is a discernible temperature difference. The main drawback of this technique was noise corruption which introduced at the thermocouple which required a high degree of filtering and reduced the accuracy. Prime [112] presents a good review on methods for studying cure kinetics of thermoset resins.

3.4.1.2 Dielectrometry

Other techniques which have been successfully used to follow the viscosity changes in the resin during cure are based on dielectric analysis methods. Kim and Lee [113] used a simple electronic circuit, two comparators and an oscilloscope to monitor a resins dielectric

constants during cure. In the dielectrometry measurement, dielectric constants, such as the electric loss factor of the resin, were measured as a function of time. Two electrodes were embedded in the composite and an electric field applied between them. Since the resin is a dielectric this was, in effect, an electric capacitor. The charge that this capacitor could store depended on the ability of the dipoles and ions present in the resin to follow an electric field oscillating between the electrodes. The loss factor of the resin represents the energy expended by the field in aligning the dipoles in the resin. This method was considered one of the most promising before optical fibres were applied to the problem. The dielectric method has none of the advantages of optical fibres and is susceptible to electromagnetic interference in its measurement. The technique is also susceptible to being rendered inaccurate by impurities in the resin which themselves act as dipoles and hence can introduce inaccuracies.

The relationship between viscosity and dielectric properties is also complex and a function of delivery and storage time and composition of the resins. Martin[114], Mopsik *et al.* [115] & Kranbuel *et al.*[116] have used dielectric methods also to study cure. Mopsik tracked the cure of a DGEBA (diglycidyl ether of bisphenol A) resin using AC-conductance measurements. Martin used resistance measurements and dielectric analysis techniques. Typically these sensors occupied an area of about $20mm^2$ whereas initially the whole composite was sandwiched between two layers of aluminium foil. A review of dielectric cure monitoring techniques presented by Ciriscioli and Springer can be found in reference [117].

3.4.1.3 Ultrasonic techniques

The application of ultrasound as a method of monitoring composite cure was first published by Sofer and Hauser in 1952[118]. They noticed that as a resin gels and cures the properties of the propagation (velocity and attenuation) of ultrasonic acoustical waves within the solid change. This is quantified in the paper by Lindrose[119]. An account of a more recent attempt by Yoon *et al.* can be found in reference [120]. Harrold and Sanjana[121] embedded acoustical waveguides, made of materials such as nichrome and polyester fibre-glass, into composites and showed that these systems responded to changes in the viscosity and acoustic impedance of the resin .

Most of the above methods are bulk methods *i.e.* they measure the properties of the composite as a whole. It is desirable, as mentioned before, to make measurements at point locations throughout the sample so as to get an idea of the homogeneity of the cure.

Because of their small dimensions fibre optics are ideal for this since they can be placed throughout the composite without appreciable disturbance of the material structure and properties.

3.4.2 Cure monitoring of epoxy resin systems by near-infrared spectroscopy

The optical fibres sensor being researched by the author uses optical fibres to monitor the cure of epoxy resin systems in the NIR region of the spectrum. There therefore follows a summary of researchers who have monitored cure in the near infra-red. These techniques are usually carried out using FTIR spectroscopy.

The near-infrared (NIR) spectral region can be defined as the wavelength range from 700nm to about 2500nm. Absorption bands in this region are due to overtones and combinations of the fundamental mid-IR molecular vibration bands. Overtone bands (harmonics) appear as approximate integer multiples of fundamental vibrations. For example a strong absorption at 4μm will give rise to a weaker absorption at 2μm. The most prominent observed overtones are those of O-H, C-H and N-H groups although all fundamental vibrations can exhibit overtones in the NIR. Combination bands can also occur in the NIR. These result from simultaneous excitation of two different fundamental frequencies to give sum or difference "beats". There are several reviews on NIR spectroscopy and its application to quantitative and qualitative analysis[122,123,124]. These are useful references for theory and peak assignments. For quantitative analysis the NIR region has advantages over the mid-infrared as many of the bands in the mid-infrared region overlap. This makes quantitative analysis difficult. On the other hand, NIR spectra are simpler and bands are well resolved allowing more accurate quantitative measurements. For epoxy-amine systems, the bands of primary importance are due to vibrations of N-H, O-H, and C-H. Table 3-2 below lists the bands present in a diglycidyl ether of bisphenol-A resin together with their assignments[125,126,127,128,129].

GROUP	ASSIGNMENT	WAVELENGTH	COMMENTS
Epoxy	2nd overtone of the C-H stretching vibration.	1159 nm (8627 cm^{-1})	Weak band[1]
	1st overtone of C-H stretch in epoxy group	1650 nm (6060 cm^{-1})	Can be overlapped by adjacent bands.
	Combination of the C-H stretching fundamental at 3050cm^{-1} with the C-H_2 deformation band at 1460cm^{-1}.	2206 nm (4532 cm^{-1})	Most suitable for quantitative analysis
Hydroxyl	Combination of O-H stretching and deformation vibrations	2090 nm (4785 cm^{-1}), 2050 nm (4878 cm^{-1})	
	1st overtone of the O-H stretching fundamental	1432 nm (6983 cm^{-1})	Hydrogen bonded peak. (Hydrogen bonding causes a shift to longer wavelengths).
C-H (aromatic)	1st overtone of C-H stretching vibration	1668 nm (5995 cm^{-1})	Internal calibration peak.
	Combination band of the aromatic conjugated C=C stretch (1625cm^{-1}) with the aromatic C-H fundamental stretch (3050cm^{-1})	2137 nm (4680 cm^{-1}), 2164 nm (4622 cm^{-1})	Used as an internal standard by Min *et al.* who do not say which peak was used (quotes peak at 2165-2136nm).
C-H (aliphatic)	-CH overtones of -CH_2, -CH_3	1700 nm (5882 cm^{-1})	The series of bands at 1770nm, 1734nm, 1670nm and 1690nm can all be attributed to aliphatic C-H groups.
	2nd harmonic of a C-H stretch of the methyl group[15]	1188 nm (5232 cm^{-1})	
	-CH_3 combination band[6,19]	2300 nm (4350 cm^{-1})	
	-CH_2 combination band of methylene group[5,19]	2400 nm (4170 cm^{-1})	
	Terminal methylene band due to unsaturation[6]	2100 μm (4760 cm^{-1})	

Table 3-2 Absorption bands of diglycidylether of bisphenol-A epoxy resin in the near-infrared region

Strehmel *et al.*[128] used NIR spectroscopy to investigate the effects of different amounts of imidazole on the cure of a diglycidyl ether of bisphenol-A, DGEBA, with 4,4-diaminodiphenylmethane (DDM). The samples were each cured under the same conditions and the product spectra were compared. All spectra were normalised to the aromatic C-H combination band at 1670nm. The residual epoxy content was calculated by the authors from the intensity of the epoxy group at 2205nm relative to the aromatic C-H overtone (1670nm) using the unreacted mixture of DGEBA and DDM as the value for 100% epoxide.

Schiering *et al.*[130] describe the cure of a diglycidyl ether of bisphenol-A with *meta*-phenylenediamine. Samples were cured using different cure schedules and the products were analysed by near-IR spectroscopy. The bands analysed post-cure were the primary amine band at 1980nm and the -NH overtone at 1503nm. Both of these bands were ratioed to the aromatic C-H combination to account for path length differences. The primary amine band at 1980nm was not observed for any of the cured films and therefore the band at 1503nm was taken as being directly proportional to the secondary amine concentration.

Min *et al.*[131] describe a similar technique to analyse the cure of DGEBA + DDS (diaminodiphenylsulphone) both with and without thermoplastic polysulfone modifier. Samples were mixed at 120°C and cast into discs. These were then placed in an air oven at two different temperatures, 130°C and 205°C for various time intervals so that different cure degrees of cure were achieved. The authors also discuss the use of two different bands for use as internal standards. The peaks were described as the combined CH_2, -CH band at 1691-1669nm and the phenyl group band at 2165-2136nm. However, the band at 1691-1669nm does not correspond with other near-IR literature obtained for DGEBA resin systems since this range covers two absorption peaks

Dannenberg[127] used NIR spectroscopy to follow the cure of a diglycidyl ether of bisphenol-A resin with ethylenediamine at room temperature. A glass cell of 10mm pathlength was used and the cure was followed using a grating spectrometer collecting spectra over a period of 12 hours. The epoxy peak height at 2205nm was used to determine the epoxy value after ratioing to the non-ratioing absorbance band at 1668nm and reference to previously obtained calibration curves. The data presented for the epoxy value were seen to drop quite steeply from the first to the second data point. After this initial epoxy value decrease the shape of the epoxy value against time curve showed a typical "s-shape" typical of these systems.

Chike *et al.*[129] used an NIR spectroscopy method to investigate the reaction between diglycidyl ether of bisphenol-A and diethylamine at room temperature. Only the epoxy band at 2210nm was analysed using a corrected peak height method and the results were compared with those obtained for Raman studies over the range 600-1350cm^{-1}. An excellent correlation was seen for quantitative data obtained by the two methods.

NIR spectroscopy of tetraglycidyl 4,4'diaminodiphenylmethane (TGDDM) + DDS reactions have been reported in several papers by George, St John and co-workers [63,

[132,133,134]. The reaction kinetics of a stoichiometric system at 160°C were discussed by St John *et al.*[132]. Spectra were recorded for the isothermal cure by placing the resin sample in a quartz tube inside a heating block in the spectrometer. Spectra were then obtained up to a cure time of 300 minutes. A further discussion on the kinetics of the reaction occurs in a later section. In a further paper, DeBakker *et al.* [135] discuss the use of FT-Raman spectroscopy to follow the cure of TGDDM+DDS. Raman spectra were obtained by curing samples for different lengths of time in a heating block at 160°C remote from the spectrometer. After various time intervals samples were removed from the heating block and scanned by Raman spectroscopy. The results were compared with *in-situ* near-IR spectroscopy and a good correlation was seen for the limited data set.

DeBakker *et al.*[133] describe a novel technique for simultaneous DSC and NIR spectroscopy of a TGDDM+DDS system. An external tungsten lamp was collimated and focused into a DSC microscopy cell. A sample of resin was placed in a glass pan on the DSC sensor and radiation from the lamp source was set-up to pass through the resin and glass pan. After the radiation had passed through the sample, a mirror directed the light towards the sample compartment of the spectrometer. The spectrometer was configured for emission measurements and the internal lamp was switched off to prevent interference. Two isothermal temperatures were used for cure monitoring; 150 and 170°C. By obtaining instantaneous reaction rates for primary amine, tertiary amine and ether groups from near-IR spectroscopy together with DSC heat flow data, reaction enthalpies were calculated for each of the reactions taking place during cure.

The next section covers the work of authors who have extended these techniques and employed optical fibres in measuring the cure parameters.

3.5 Optical fibre cure monitoring

3.5.1 Acoustic wave monitoring.

Davis et al. have demonstrated a variation on the acoustic method of monitoring composite cure[136]. They used interferometric optical fibre sensors to detect propagating ultrasonic elastic waves generated by the laser ablative method (pulses generated by the localised heating effect of a fast pulsed laser) and by using piezo-electric actuators. The laser/ultrasound pulses can be delivered by a fibre bundle facilitating remote operation (Liu *et al.*[137]). The response of the optical fibre to the propagating elastic waves is determined by the propagation direction and polarisation direction of the waves with respect to the

orientation of the fibre and the state of polarisation of the beam in the fibre. The transit time of the waves, from surface to sensor location, was shown to decrease as the cure process progresses. The fibre sensor works using an all fibre interferometer which has one arm embedded in the curing composite. A schematic of their equipment is shown in Figure 3-16

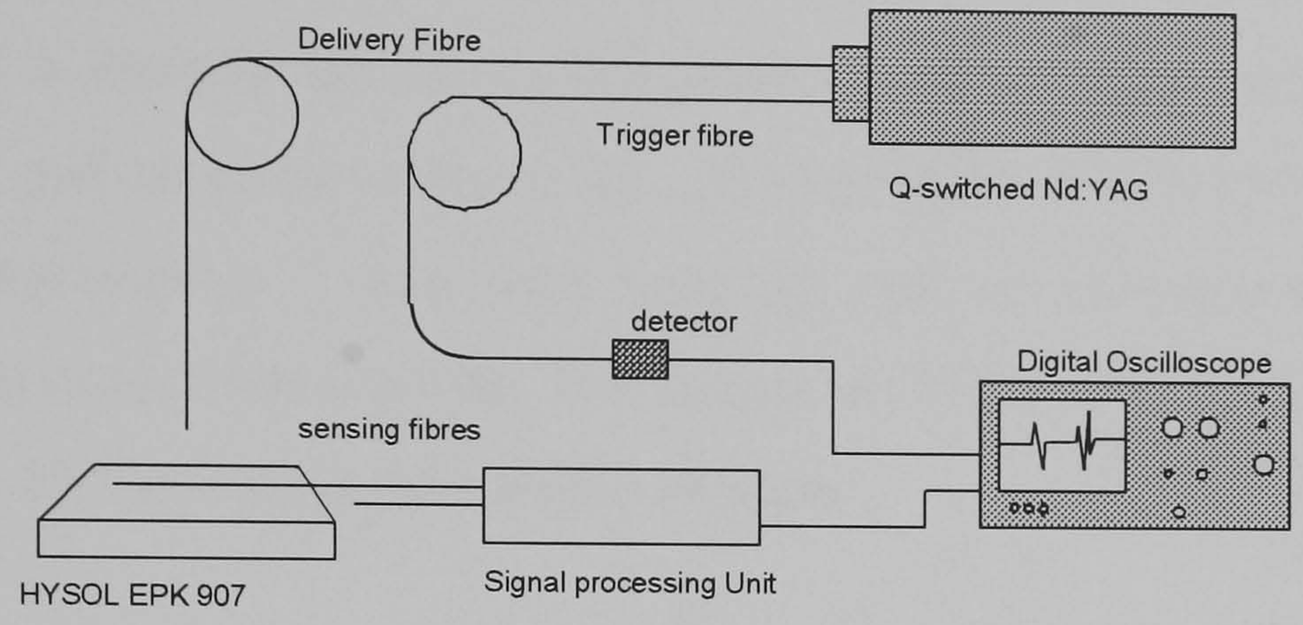

Figure 3-16 Schematic of fibre optic detection of laser generated ultrasound in a curing epoxy specimen

They produce plots of the relative time delay of the ultrasound signals as a function of cure time but, do not take these as far as processing the signal to obtain measurements of phase velocity and hence the bulk and shear moduli of the epoxy. An improved version of the apparatus is presented by the same authors the following year[138].

3.5.2 Refractive index cure monitoring

The change of refractive index that an epoxy resin undergoes during its cure cycle is characteristic of the crosslinking process and so can be used to monitor cure. Presented below is a review of some papers covering methods for cure monitoring by refractive index monitoring.

Hans Dannenberg's paper[139] outlines a method for testing the cure performance of epoxy resins and curing agents. This paper describes how an Abbe type refractometer, was used to monitor the refractive index of an epoxy. The Abbe is a prismatic device working on the measurement of a critical angle between a prism of known refractive index coated with a substance of unknown refractive index. A polymer film is used to prevent resin adhering to the prism of the instrument and the cure rate of the resin determined by taking a measurement of the resin refractive index at regular intervals. All measurements were taken at 590nm (the sodium D line). This is a standard wavelength at which refractive indices of any material are measured. Dannenberg was able to track the cure rate and determine the gel point (the point at which the resin an incipient crosslinked and insoluble

network has formed). He did not draw any conclusions as to the relationship between refractive index and chemical conversion of the resin components, but mentioned the similarity in shape between the refractive index curves and the curves obtained by tracking chemical conversion using a spectrometer. The paper compares curves obtained with different combinations of resin and curing agents and contains detailed methodology and suggestions as to refractive index change mechanisms.

Cooper[140] presents a method for the measurement of the refractive index of paraffin, a silicone elastomer and an epoxy resin in the spectral range of 500-1500nm. To do this a Hilger-Chance refractometer [141] was used together with an infra-red viewer. This brief paper describes the experimental set-up. His measured results were used to extrapolate the refractive index to 1600nm using the Cauchy formula:

$$n = A + \frac{B}{\lambda^2} + \frac{C}{\lambda^4}$$

- 3.19

where λ=the wavelength and A, B and C are determined by solving simultaneous equations at three wavelengths where the refractive index is known. The fit to this was found to be typically better than 2×10^{-4} (refractive index units).

Jones *et al.*[142] describe a refractive index sensor which uses the light cone produced at the end of a fibre (see Figure 3-17) which has a half angle, θ. If the gap is then filled with a medium having an index greater than one the cone angle is diminished and the light coupled into the other fibre increases. The ratio of the coupled power with the liquid to a reference system with an air gap is a function of the medium's refractive index.

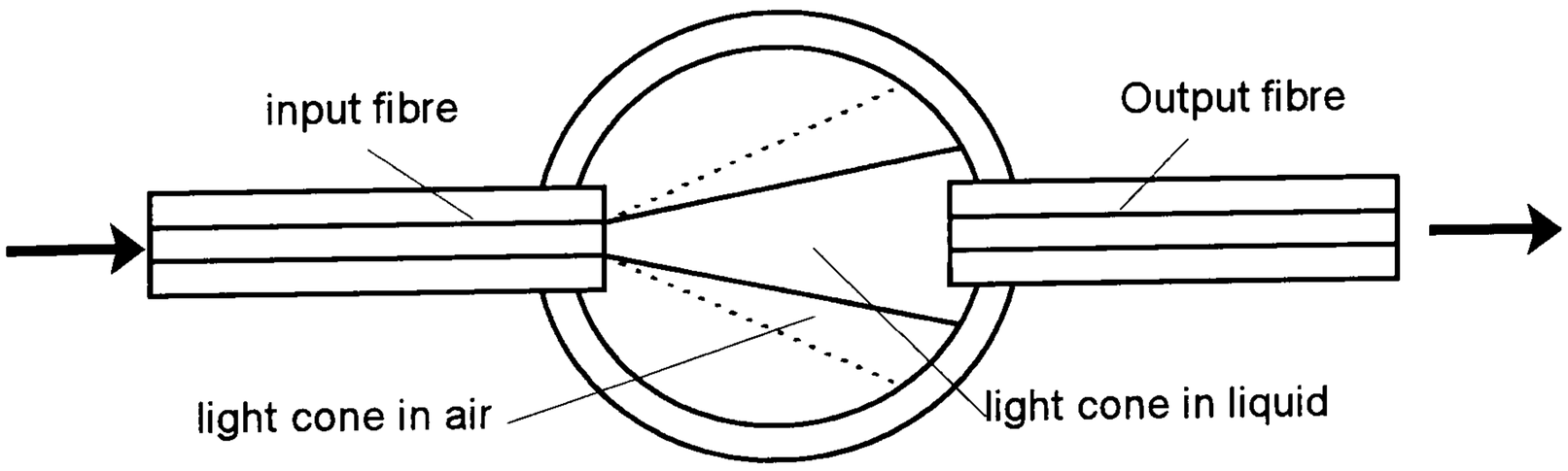

Figure 3-17 Numerical aperture refractive index sensor

Harmer [143] describes a sensor using integrated optics in the form of a Mach Zender interferometer. One arm of the interferometer is protected from its surroundings, the other is exposed (Figure 3-18). Because the optical field is not totally restricted by the

waveguide but some of the field is travelling as an evanescent wave at the guide-surface interface, any change in the surrounding medium will influence the guided modes. In this manner chemicals can be identified through their refractive indices although absolute measurements are said to be difficult.

An early work by Kapany and Pike [144] describes a straight fibre with an unclad region which is used to couple light between input and output fibres. The effective numerical aperture and, hence, the light transmission is a function of the refractive indices of the liquid. This method has achieved a sensitivity of 1×10^{-5} refractive index units.

A fibre can be bent into a curve, typically a simple bend or continuous helix (Karrer and Orr [145]). This has the effect of presenting a larger angle of incidence to the incident rays over the outside of the bend and so increasing sensitivity. Sensitivity to six decimal places has been achieved with this sensor.

Kapany and Pontarelli [146] extend the work in reference 144 by using a tapered glass cone for the photorefractometer. This has a similar effect to a curved fibre in enabling more of the launched rays to be affected by the change in refractive index of the external medium.

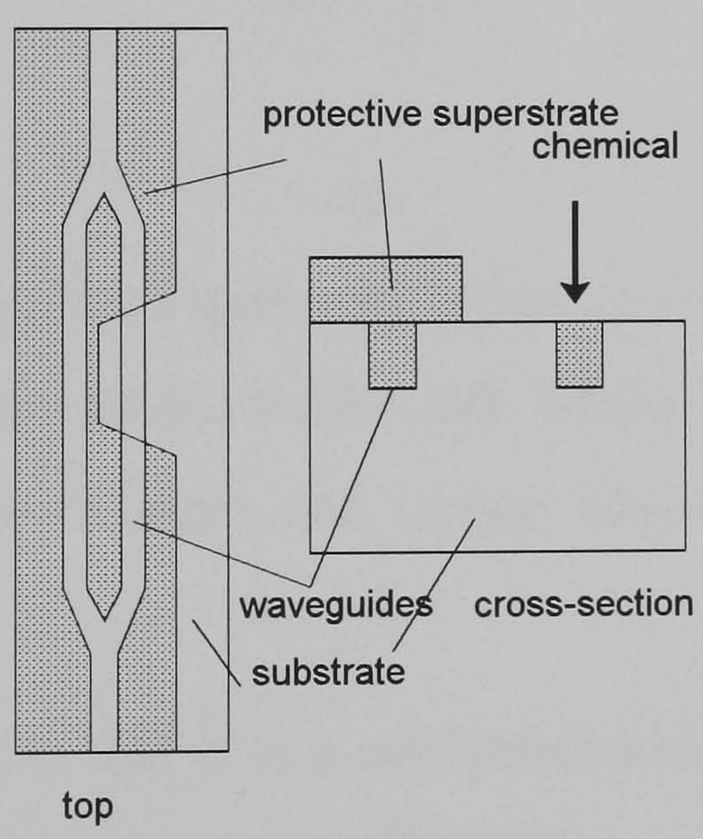

Figure 3-18 *Mach-Zender refractive index sensor.*

Podoleanu *et al.*[147] describe a sensor which provides information on the refractive index of a liquid by interfering two halves of the beam from a laser diode. One half is passed through a liquid cell containing the liquid to be analysed whilst the other half passes through an equivalent distance of air. Thus, a simple two-beam interferometer is set up and from the spectral features of the interference pattern (here measured with a grating and a CCD) the optical path imbalance, and hence the refractive index of the liquid, can be calculated. Accuracies better than 0.1% have been obtained with this system.

Afromowitz[148] presented a further method of composite cure monitoring which sensed the refractive index change as the polymer matrix cures. This took advantage of the increase in refractive index (named optical density here) of a polymer of approximately 1% that occurs when it cures. A short length of pre-cured "polymer fibre" was butt-jointed to some conventional optical fibre and this assembly was then embedded in the composite. Light was launched into the fibre at one end and detected at the other. The curing process was initiated and as the composite cured the refractive index of the polymer surrounding the sensor increased to match that of the sensor. The consequence was that the fibre was unable to confine as much light and when the resin had completely cured nearly all of the light in the fibre was radiated into the resin. When the sensor fibre was initially exposed to the uncured resin there was a 10% drop in transmission, however this fell further after the resin had cured.

Afromowitz explained the effect simply by considering a cured sensor fibre with refractive index n_1 and radius a, embedded in a resin medium, refractive index n_2 ($n_1 > n_2$). The number of guided modes, M, in the sensor can be taken roughly as:

$$M = \frac{V^2}{2} \qquad \textit{- 3.20}$$

Where V, is the normalised frequency given by equation - 3.2. *Thus,* as n_1 approaches n_2, M tends to zero and there are no guided modes left. There will be some residual light left however due to the alignment of input and output fibres and the transmission of the medium.

The strength of this technique is that it is a self-referencing differential technique rather than an absolute technique *i.e.* it requires no calibration.

Afromowitz extended this work using the sensor to monitor the cure of a graphite/EPON 828 (DGEBA) system[149]. The results were essentially the same as before but transient increases in the sensor signals were observed and these were attributed to temperature effects. In a later paper Afromowitz[150] presents a more detailed study of this system. He studied the change in refractive index of a typical aerospace thermoset resin during cure at several elevated temperatures using a fibre-optic Fresnel reflection technique. The refractive index of a curing resin (EPON828) was measured and compared with data from a sample under identical conditions within a DSC. This enabled the extent of cure as a

function of time to be determined and hence the refractive index change as a function of cure was found. This was shown to be non-linear and they have begun to look at the applicability of the Lorentz-Lorenz equation as a model for the cure process.

A rigorous discussion of the behaviour of the refractive index of a typical epoxy-aromatic diamine system is presented in a further paper by Lam and Afromowitz[151]. Models are derived to describe the refractive index dependence on temperature and extent of cure. The model used is an empirical one but predicts the sensor signal up to the resin gel point (conversion of about 0.57) An important point is made that the linear relationship between the refractive index and extent of cure of the resin does not extend beyond the point at which the resin reaches its gel-point. Part II of this paper[152] discusses the performance of the previously proposed cure sensor. A model which describes the performance of the sensor is derived and the sensor is used to predict the gel-point and monitor the resin cure. Although the refractive index/cure relationship is not linear after the gel-point these researchers say that the end of cure is detected with this sensor without calibration.

Zimmerman *et al.*[153] use a similar sensor, this time in typical composite resins and in pre-preg laminates, (the papers discussed so far use only industrial grade, fast cure epoxies). The technique is shown to be valid for these materials. Also the cure state of the composite could be determined from the normalised transmitted power through the resin fibre waveguide.

Several authors have described an optical fibre refractive index sensor based on a fibre with its cladding removed over a small region[154]. In a series of papers by the author and co-workers [155,156,157,158], experiments that were carried out to track the cure of a DGEBA resin with hexanediamine hardener using a high refractive index optical fibre (n = 1.65) with a 20 mm portion of its cladding removed are described.

Kassamakov and Kafedjiev suggest an improvement on the Fresnel reflectometer[159]. They suggest using a spherical reflecting surface at the fibre distal end which has the effect of changing the divergency of the light cone at the end of the fibre. The paper includes calculations on the sensitivity increase although it does not include a quantitative measure of this. The experimental work reported produces two 's' shaped curves which demonstrate that the sensor with a curved end does indeed have greater sensitivity than the sensor where the end has no curvature. The relationship between refractive index and resin

structure can be found in the paper by Fridman and Shchurov[160]. Here, the authors show how it is possible to use the Lorentz-Lorenz equation to obtain such a relationship:

$$R = (\frac{n^2 - 1}{n^2 + 2})(\frac{M}{\rho})$$

- 3.21

where R is known as the molar refraction, n the refractive index, M is the molecular weight and ρ is the density. R is expected to be independent of temperature or physical state for a particular material, and thus $(n^2-1)/(n^2+2)$ should be proportional to density and dependent on the chemistry of the mixture. In the case of a curing epoxy both the density and the chemistry of the epoxy change as a function of cure extent and temperature. Confirmation of the applicability of the Lorenz-Lorentz equation must wait until more detailed measurements of a curing epoxy as a function of cure extent and temperature. Similar material is covered in Askadskii *et al.*[161] although this paper is not directly involved with resins.

3.5.3 Near infra red spectroscopy cure sensors

Near infra-red spectroscopy has already been discussed as a method of monitoring epoxy resin system cure. Standard telecommunication grade optical fibres transmit light in the NIR well and so are of interest to spectroscopists because they allow collection of spectra at a point remote from the spectrometer. Optical fibre sensor configurations based on both transmission [63, 162,163,164] and reflection[165] configurations have been reported in the literature.

One of the most important works detailing remote FTIR spectroscopy is that by George *et al.*[63]. In this work a sample of TGDDM epoxy resin with DDS hardener was placed between two plastic-clad silica fibres aligned in a glass capillary approximately 1mm apart. One fibre had light from a FTIR spectrometer coupled into it and this light was returned to the spectrometer detector *via* the second fibre after passing through the resin sample. The resin spectrum was compared to that obtained *via* conventional FTIR spectroscopy. The remote spectrum was found to be marred by a large absorption band at 1408nm which was due to evanescent absorption by the silicone cladding of the optical fibre .

Mijovic *et al.*[162] have, more recently used a similar configuration to monitor the cure of several epoxy resin systems. This technique is of little use for composite cure monitoring

because of the larger dimensions of fibre and capillary used which would seriously interfere with the composite material properties.

3.5.4 Evanescent wave absorption cure monitoring

Few researchers have investigated the use of evanescent wave spectroscopy for the monitoring of cure. This is probably due to the large refractive index change that occurs during resin cure and the associated problems this causes in the quantitative measurement of resin components as discussed above. Xu and Schlup[166] examined the feasibility of using NIR ATR as a sensor for monitoring epoxy resin cure. They demonstrate the use of NIR ATR for *in-situ* cure monitoring by following the reaction between phenyl glycidyl ether and butylamine curing on an ATR crystal. Various cure spectra are presented but they report that the absorption bands values are approximate and show that since bands for the epoxy and amine groups are well isolated from interference in the spectra that the NIR is more suited to *in-situ* cure monitoring than the mid-IR region. There is however no treatment of the refractive index effect to allow quantitative measurement of these bands. This paper follows from a previous paper by the same authors [167] where the cure of a resin system is monitored using FTIR and the mechanism described by a two-parameter model.

Recently Zhengfang *et al.*[168] have demonstrated the use of an chalcogenide fibre evanescent sensor to monitor the cure of a pre-preg in an autoclave. The sensor was excited using an FTIR spectrometer and the light from the sensor coupled into an external mercury-cadmium-telluride (MCT) detector. Evanescent spectra were taken every 15 minutes. Again, only qualitative analysis of the spectra obtained are given identifying starting reactants, intermediates and final products which it is said can be used to identify polymerisation yields.

The paper that comes closest to the technique proposed here is by Bunimovich *et al.*[169]. This is actually a fiberoptic evanescent wave spectroscopy paper, but contains details of how a tuneable lead salt laser and a tuneable CO_2 laser are used to monitor specific absorption bands in a spectrum during a reaction to determine the state of that reaction. A number of applications are described using fibre evanescent wave spectroscopy (FEWS); the monitoring of liquids and mixtures of liquids to determine mixture composition, gas monitoring, solids, thin films, chemical reactions and pollution in water. The fibres used were silver halide so that the system could work in the mid-IR. The different idea here is the monitoring of single wavelength band by tuning a source to that band although most of

the work presented in this paper was in fact still done using a spectrometer. In this wavelength range, sources and detectors *etc.* need cryogenic cooling and become more costly

Cossins and co-workers[170,171] describe an evanescent sensor manufactured from standard fused silica core optical fibre from which its glass cladding was etched away over a length of 1cm. This sensor was used to track the cure of speciality, low refractive index resins. These resin types are generally of poor mechanical strength and not used in engineering applications. These researchers used such resins to overcome the problems of satisfying the optical fibre guiding conditions (*i.e.* higher core than cladding indices).

Two papers by the author and coworkers [155,156] describe the use of an optical fibre with a high refractive index core (n=1.65) with a portion of its cladding removed to monitor the cure of a DGEBA/hexanediamine system using evanescent wave spectroscopy. In contrast to the work of Cossin *et al.*, it is the use of this specialist fibre that allows the monitoring of the cure of more standard resin systems.

Druy[172] *et al.* give an account of using fibre optics in monitoring composites during cure in an autoclave again by using a composite containing optical fibres interfaced with an FTIR machine. In this work a short length of sapphire optical fibre was used as the sensor since this type of fibre can withstand high temperatures. They fed the signal from FTIR to an autoclave environment *via* zirconium fluoride fibres. Monitoring the spectral changes due to the reaction of the epoxide ring with the amine functionality and the breaking of aliphatic C-H bonds, in a Fiberite 934 (toughened epoxy) laminate, they were able to track the cure of the composite. They also found that the sapphire fibre exhibited superior sensing qualities to the heavy metal doped fluoride glass (HMFG) type. A review of optical fibre cure monitoring techniques can be seen in the paper by Roberts and Davidson[173]

The technique proposed can thus be seen to have a good degree of novelty. What is needed is a good model to allow the refractive index effect to be accounted for in terms of its effect on the specific absorption bands being observed. This will allow quantitative measurements of the components of the resin which change during cure. If this is combined with a kinetic model for the cure reaction then an extremely useful tool for the monitoring of composite or epoxy resin cure will be obtained.

3.6 Summary

In order that an epoxy/amine resin system can be cured to provide optimum performance it is necessary to obtain an understanding of the chemical and physical properties of the system during its cure. Many studies have been undertaken with an aim to obtaining a greater understanding of the cure process of these systems resulting in a higher reliablity process and materials with enhanced physical properties.

In-situ techniques have received much attention in recent years since they allow the cure process to be monitored "on-line" and individual cure processes to be tailored to a particular specimen. Optical fibre sensors have attracted a significant portion of this research effort since their relatively small size and compatibility with the resin matrix causes little perturbation to the material. In addition the use of optical fibre sensor, together with spectroscopic methods, enables the chemical reaction to be investigated during the cure cycle. Many spectroscopy sensors have focused on the mid IR region which necessitates the use of expensive specialty fibres such as chalcogenides. The NIR region, however has possibilities as a region for cure monitoring and in addition allows the use of more conventional silica fibres, reducing costs significantly.

It will be seen later that the way in which absorption and refractive index are intrinsically linked as described in the ATR section (section 3.3.2) had significant ramifications for the study described in this thesis. Epoxy resins undergo a large change in refractive index as cross-linking occurs during the cure process. It was therefore extremely important that this was taken into account when processing the data for any meaningful conclusions to be drawn. The experimental programme thus approached the sensing of cure from two directions;

i) the spectral monitoring of cure using evanescent absorption; and

ii) a study of the change in resin refractive index during cure.

The qualitative and quantitative results presented in this thesis (Chapters 5 and 6) represent a significant contribution to the study of evanescent wave sensors.

A good cure monitoring system offers potential financial savings from better control and lower rejection rate of completed components. These facts show that a market for a "smart" composite cure system exists. It is believed that the technique described in this thesis can offer such a technique effectively, at a low price and in a compact package.

4 Experimental

4.1 Introduction

The preceding sections have laid out the background knowledge which was required to undertake the study described in this thesis. This chapter contains a discussion of the general experimental issues which were considered and which are relevant to both the evanescent absorption sensor and the refractive index sensor. The chapter begins with a description of the process of selecting a resin system to model those systems commonly found in composite pre-pregs. This is followed by a discussion of the sensor design, the selection of an optical fibre type for use as the raw material for the sensor the methods used to fabricate the sensors. Chapters 5 and 6 describe the evanescent absorption sensor and the refractive index sensor respectively and contain their own experimental sections, specific to the experiments performed with each sensor. The work contained in these chapters has been published extensively and a list of these publications can be seen in Appendix 3.

The original project proposal for the project stated that the technique would use "a simple, intensity-modulated system using narrow band sources for each functional group monitored instead of a dedicated FTIR spectrometer". The least expensive narrow band sources operate in the visible and NIR spectral regions. This is because they have been developed for the telecommunications market and are manufactured in large volumes. This also means that they can be very stable, both in terms of wavelength and intensity. The NIR spectral region contains the prominent absorption bands due to C-H, O-H and N-H bonds, which are present in all epoxy/amine resin systems, and therefore this region is ideal for monitoring the cure of such systems.

Two sensors were developed and evaluated as part of this study. Although almost identical in construction the two sensors tracked the cure of a resin system using two very different physical phenomena:

i) the refractive index of the curing resin system; and

ii) the depletion of specific absorption bands in the system corresponding to functional groups such as the epoxy or hardener.

In order to evaluate both sensors it was necessary to select a model resin system and determine the position of absorption bands corresponding to species taking part in the cure reaction. To achieve this the following steps were taken:

i) several commercial epoxy resins were assessed by near IR spectroscopy to identify absorption bands;

ii) a representative resin system was selected which could be used in subsequent investigations.

4.2 Resin system selection

Analysis of the epoxy resin systems evaluated were carried out on a Nicolet 710 FTIR spectrometer configured with a KBr beam-splitter and DTGS detector (range 7800-300 cm^{-1} or 1282-33,000 nm) by the author's co-researcher. For each spectrum 16 scans were collected at a resolution of 2 cm^{-1}.

The system chosen was Shell Chemicals Epikote 828 resin with a hexane-1,6-diamine curing agent. Epikote 828 is a diglycidyl ether of bisphenol -A type epoxy resin[174]. This is a high purity commercial form of DGEBA, which is sometimes employed in aerospace composite systems. An aliphatic amine, hexane-1,6- diamine (Aldrich chemicals 98%), was selected as the curing agent because of:

i) the position of its absorbance band at 1545nm corresponded to commonly available 1550 nm laser sources used for telecommunications (see below section 4.4);

ii) its low volatility compared to similar amines such as ethylenediamine meant that the concentration of reactants would not change during the mixing process and

iii) its low temperature cure properties which allowed refractive index monitoring to be undertaken by Abbe refractometry which had a maximum operating temperature of 80°C.

4.3 Sensor construction

For the evanescent wave to penetrate from an optical fibre into the medium to be analysed it is necessary to either thin or remove the cladding layer of the sensor in some way (see Figure 4-1). The first issue to be addressed was the fabrication of the sensor and, generally speaking, the type of fibre used dictated the method of cladding removal. Fibre selection was thus an extremely important factor and the next section details the rationale behind the

selection of optical fibre, initially for the preliminary experiments which used optical fibre as a chemical sensor, and ultimately for use as a resin cure sensor.

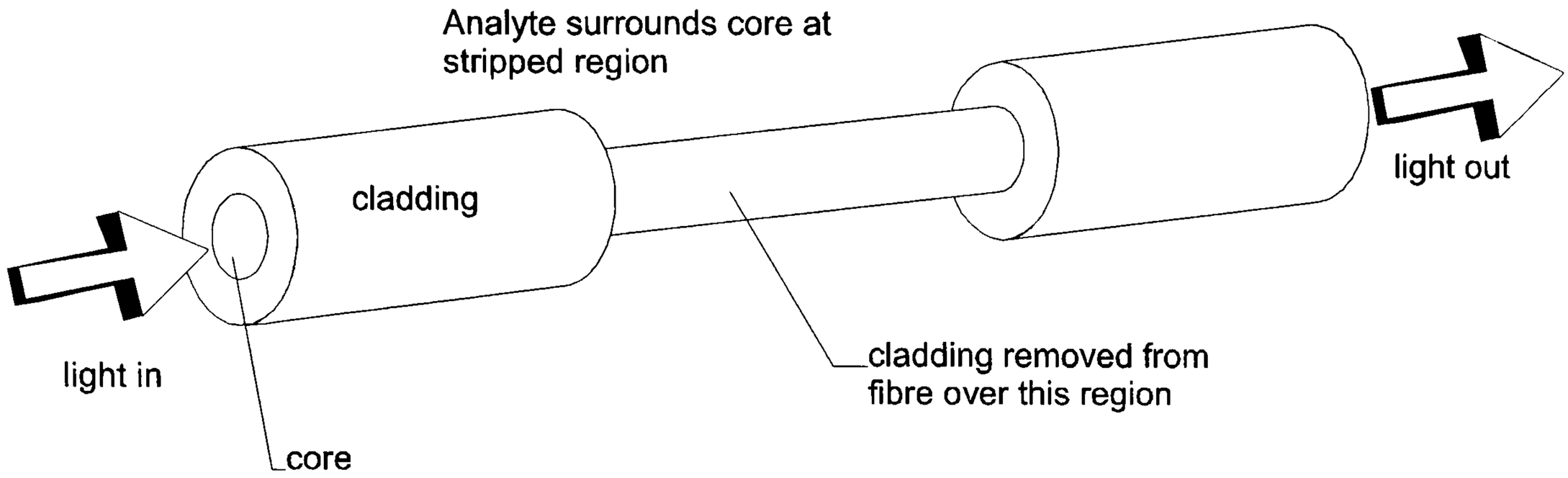

Figure 4-1 Schematic diagram of basic sensor construction (all longitudinal dimensions greatly reduced).

4.3.1 Optical fibre selection

The three criteria on which the fibre selection was made were:

i) the spectral transmission characteristics of the fibre. The fibre would have to be transparent to the spectral regions of interest ;

ii) the core refractive index ;

iii) and the ease with which the fibre could be treated to create a sensor.

As well as these criteria, the side issues of cost and ease of handling also had to be taken into consideration. Table 4-1 contains a summary of some of the fibre types which were considered.

Fibre type.	Transmission window.(μm)	Refractive index of core.	Comments.	Approximate cost m^{-1}
Silica/Silica.	0.4-2.2	1.46	Easily available.	few pence
Polymer clad silica	0.4-1.8	1.46	cladding damaged easily, easy cladding removal.	10-20p
Hard clad silica	0.4 -2.2	1.46	More durable and easily stripped of cladding	40p
High index borosilicate	0.4-2.0	1.6-1.8		10p
Chalcogenide	1.0-6.0	2.2-2.9	Available without cladding	£162
Sapphire	0.2-4.0	1.7	very expensive (single crystal)	£400-500
Silver Halide	3.0-15.0	2.0	degrades rapidly.	£300

Table 4-1 Summary of optical fibre types

The selection criteria for the final fibre which was used are discussed below.

Transmission:

The fibre chosen had to be reasonably transparent, *i.e.* better than 0.5dB m^{-1} in the wavelengths being monitored. Sapphire, silver halide and chalcogenide fibres were considered because they transmit infra-red wavelengths well. However, as can be seen from Table 4-1, these fibre types are very expensive and are also very difficult to work with. Silver halide fibre degrades in visible light, has a high loss (because of the polycrystalline nature of its construction) and is not capable of withstanding the elevated temperatures at which resin cure takes place. It is also opaque in the NIR. Chalcogenide glass fibre has the advantage for this application of being available without cladding. However, its temperature characteristics were not known, and again it is difficult to handle and very expensive. Sapphire fibre is also expensive and only available in short lengths. It does possess excellent temperature characteristics and transmission range and would be a possible sensor candidate if its price were to fall. Most fibre types have a reasonably low-loss characteristic over the range 1-2μm. Figure 4-2 shows the transmission characteristics of four types of fibre made using a fibre monochromator (for details of instrumentation see section 4.4.4). These measurements were all made using 3 metre lengths of the fibres in question. The dip in transmission seen at 2000nm is an artifact of the change in gratings in the monochromator and is normally referenced out in the conversion to absorbance units.

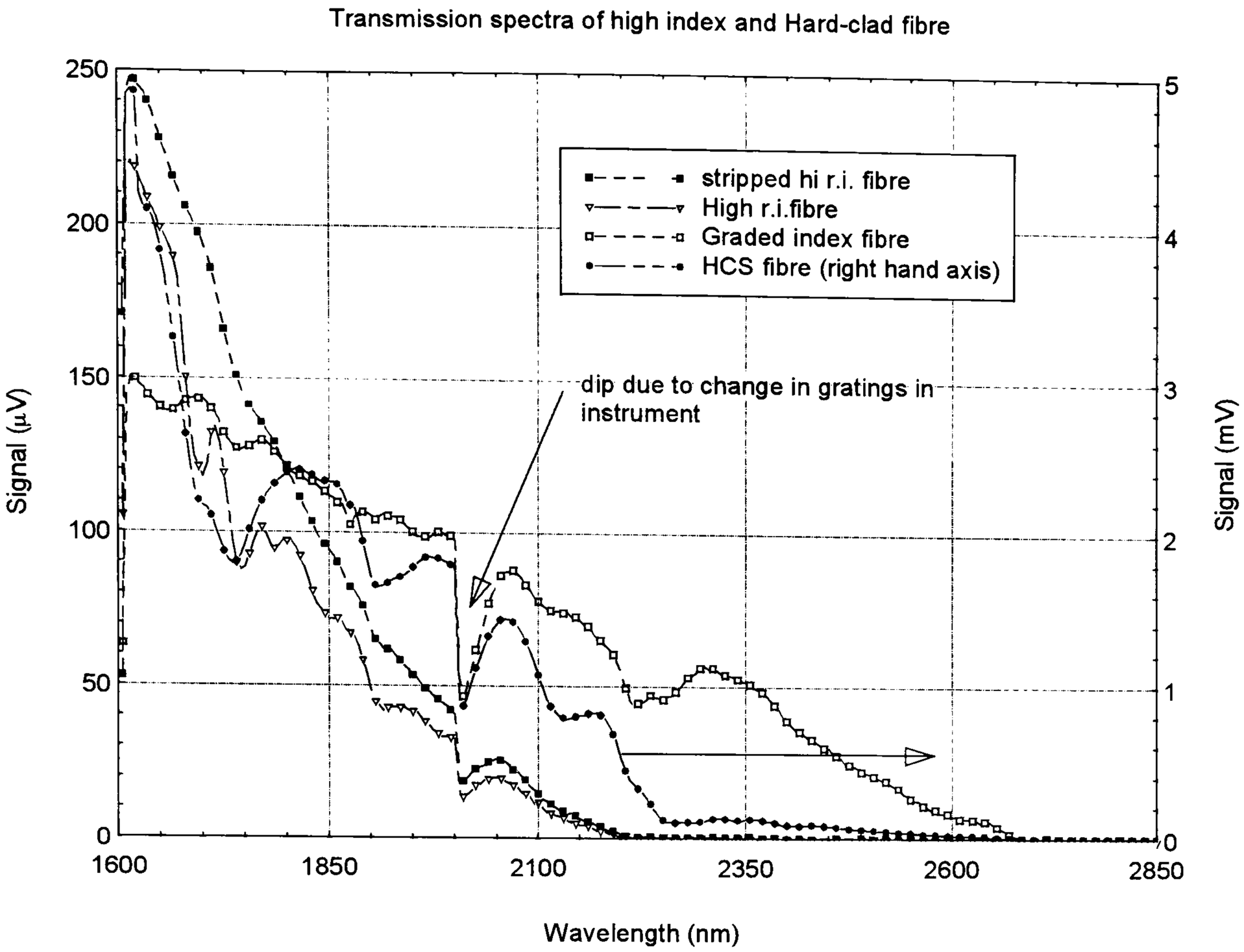

Figure 4-2 Measured transmission characteristics of four fibre types.

The transmission characteristics of all these fibre types can be seen to decrease in this wavelength range for all fibre types. The high index fibre and the polymer clad hard clad silica fibre can be seen to have little transmission above 2.2μm the high index fibre cutting off entirely at this wavelength. The hard clad silica fibre, has a transmittance too small to be of any use for a sensor signal, up to about 2.6μm. This is because this fibre type is polymer clad and the strong polymer absorption bands contributes to the overall transmission characteristics of the fibre (ironically *via* evanescent interaction). The overall intensity difference between this fibre type and the others is due to its larger diameter. The graded index silica fibre can be seen to have a transmittance out to above 2.6μm.

Refractive index:

For use in a resin or composite the use of a fairly special fibre would be unavoidable. This was due to the refractive index of the resin. Pure silica has a refractive index of 1.458. For the guiding conditions of a fibre to be satisfied the cladding of the fibre must have a refractive index lower than that of the core. In the case of hard clad silica fibre the polymer cladding has a refractive index of 1.41. If a silica fibre, with part or all of its cladding removed, is placed in a resin of composite material (which typically have a refractive

index, before cure, of around 1.55) the guiding conditions will not be met and the optical fibre will cease to transmit light. After making inquiries with several manufacturers a source for a specialist high refractive index fibre was found. The manufacturers quoted the core refractive index as being 1.65, satisfying the condition for fibre guidance in a resin system. The core was made from silica doped with lead oxide to increase its index. The fibre was clad with a silicone resin (n_d=1.41) and had an additional acrylate layer which protected the cladding layer. This meant that although the cladding was easy to remove from the core, it was more robust than plastic clad silica fibres. This fibre was used for the bulk of the investigations described in this thesis including all resin and composite cure monitoring investigations. Hard polymer clad fibre was used in a number of experiments where the solution to be analysed was of lower refractive index than silica. For example, some preliminary experiments on curing agent concentrations in solvents were performed using this fibre.

Cladding removal (sensor construction):

The cladding (and core) of standard telecommunications fibre are made from silica and so to remove or thin the cladding from these it is necessary to etch it away. This can be done with glass etchants such as hydrofluoric acid. Owing to the hazardous nature of this substance it was decided to look for an alternative fibre which had a cladding which was easier to remove while being widely available or an alternative etchant. Plastic clad silica (PCS) fibres consist of a silica core surrounded by a polymer cladding. This polymer is extremely soft and so easily removed using a solvent such as acetone to swell and soften it after which it can be removed simply by wiping with an optical tissue. The softness of the polymer also has the disadvantage that it is easily damaged and so is not robust enough to survive handling in the ways encountered when embedding sensors in resin or composite. Hard clad silica fibre consists of a harder polymer (a proprietary fluorinated acrylate) cladding surrounding the usual silica core. This has the advantage of still being simple to remove while being more robust than the PCS equivalent. It was for these reasons that hard clad silica was selected as the fibre for use in the experiments conducted using silica optical fibres. In addition to the cladding layer the hard clad silica fibres also possessed a Nylon buffer layer which acted as a protective sheath.

The stripping methodology is discussed in the next section.

4.3.2 Cladding removal methodology

A method was required, of removing the cladding from the fibres, for all the fibre types, cleanly and consistently and so a number of tests were performed to determine methods of doing this. By consulting the fibre manufacturers it became apparent that there were two approaches:

i) heat stripping; heating or burning off the cladding in a furnace or flame;
ii) chemical stripping; using a solvent or some other chemical to dissolve the cladding.

The cladding was removed from the hard clad silica fibre by burning it off. The fibre was passed through a clean bunsen flame at a speed which allowed the polymer cladding to be burnt away without allowing the silica core to become too hot and degrade (so becoming brittle). Typically a 50mm section of fibre was passed through the flame in 2 seconds. After removal of the cladding the exposed core section was cleaned, first in methanol and then in acetone with gentle wiping with a clean optical tissue.

The best method of stripping the high index fibre was found to be chemical stripping since the doped silica core did not survive exposure to a bunsen flame. Tests were carried out by immersing sections of fibre in a selection of solvents: chloroform, dichloromethane, acetone, hexane and sulphuric acid. This was also performed at a series of temperatures to determine the best conditions. The most effective stripping method was found to be the use of warm concentrated sulphuric acid. The other solvents did swell the polymer cladding, but did not actually remove it. The acid was warmed to 60°C and the fibre immersed in it over the length to be stripped. The cladding removal was visible and took approximately 20 seconds at this temperature. The fibre section was then rinsed, firstly in water, then with methanol and finally with acetone to ensure a clean surface.

Since the evanescent wave penetrates such a short distance from the core surface (of the order of the propagating wavelength) it was important to ensure that the core surface is absolutely clean. Any residue left by the stripping process will interact with the evanescent wave and produce a loss on sensitivity of the sensor. To achieve this the surface of the stripped fibre core was examined using optical microscopy, scanning electron microscopy (SEM) and X-ray photoelectron spectroscopy (XPS). XPS is a technique which can resolve individual chemical elements on a surface.

Optical microscopy showed the fibre surface to be free from any visible contamination as did SEM. XPS analysis showed that there was a lead peak present on the stripped region. Since the fibre core was silica doped with lead oxide this is thought to be the origin of this peak.

4.4 Light source selection and instrumentation issues

In the search for a suitable light source many options were considered although diode lasers were paid the most attention because of their price and availability. A tuneable source of some kind which would be able to cover a wide range of wavelengths would have been the ideal case, however, this proved impractical. Table 4-2 is a coverage of the lasers that were examined and their wavelengths together with a guide to their price.

Wavelength	*Type*	*Material*	*Power*	*Line width*	*Operation*	*Fibre compat.*	*Approx. price*	*Manufacturer.*
266nm	laser	NdYAG	140W	-	pulsed	yes	£ks	Adlas
523nm	laser	NdYLF	1kW	-	pulsed	yes	-	spectra-physics
532nm	laser	NdYAG	140mW	-	CW	yes	£k	PMS electro-optics
670nm	laser	GaAlAs	1mW	1nm	CW	yes	<£100	Toshiba
825nm	LED or laser	GaAlAs	1mW	5nm/ 1nm	CW/pulsed	yes	<£100	EG&G/ Toshiba
1060nm	LED	InGaAs	200μW	5-10nm	CW/Pulsed	yes	≈£300	EG&G
1152nm	laser	HeNe	10mW	-	CW	yes	£5460	Polytec
1310nm	laser	AlGaAs	1mW	-	CW	yes	£600	Laser diode inc.
1550nm	laser	AlGaAs	1mW	-	CW	yes	£750	Laser diode inc.
1650nm	LED	GaInAs/ InP	26μW	50nm	CW	yes	£50	GMMT
1800nm	LED	GaSb	100μW	350nm	pulsed	no	£35	LMS
3300-6300nm	laser	Pb Salts	1-3mW	-	CW/ pulsed	no	≈$3000	Laser Photonics

Table 4-2 Summary of sources considered as possibly suitable for cure monitoring

Lead-salt lasers, which operate in the near to mid infra-red region and show a high degree of tuneability (several tens of nanometres) were thought to be interesting. They have the disadvantage, however, of needing to be cryogenically cooled, an expensive and inconvenient process, and are not very fibre compatible due to the quality of their beam profile and the bulkiness of the cryogenic cooling apparatus. These were decided to be

beyond the project budget and would compromise the aim of trying to build a self contained cure-monitoring system. Other alternatives for tuneable lasers include dye lasers, CO_2 TEA lasers and tuneable, solid state lasers (such as optical parametric oscillators, OPOs). These have a wide range of output wavelengths but again are expensive and, if not bulky themselves, require a bulky pump laser.

It was proposed that telecommunications sources, detectors and fibre would be used since they are cheap, easily handled and readily available so it was necessary to conduct a market survey to discover which wavelength semiconductor sources were available "off the shelf". It was decided that semiconductor lasers were probably the best choice again because of their price and also because of their narrow wavelength linewidth and their power. More power in the fibre would mean a better signal-to-noise ratio in the final signal. They also have a certain degree of tuneability (a few nm) controlled by altering their temperature and current. Semiconductor lasers are also eminently compatible with optical fibres and can be pigtailed and joined using telecommunications connectors, to make launching light simpler. Because of their small size (package dimensions of a few mm) it would be easy to incorporate them into a self-contained instrument. By coupling an adjustable external Fabry-Perot cavity to a diode laser is possible to increase the amount of tuning that can be obtained from one to several tens of nanometres. There are several commercial tuneable diode lasers of this sort available, (eg. Laser Max inc.) centred around the telecommunications wavelengths (1310, 1550nm) and these were also investigated, but at around £6000 each it was decided they were beyond the project budget again.

4.4.1 Laser and Light Emitting Diodes

As mentioned above the original proposal stated that discrete sources were to be used to monitor specific absorption bands. *Thus,* a survey of available optical sources compatible with fibre optics was undertaken to find sources of suitable wavelengths.

The most convenient type of source is the laser diode or light emitting diode (LED) due to their small dimensions and low power consumption. These are most commonly available at wavelengths dictated by the electronics and telecommunications industries. The electronics industry makes use of visible (400-700nm) LEDs and laser diodes for indicators and displays etc. NIR laser diodes (700-900nm) are employed in devices such as compact disc players and CD ROM players and in some local area, fibre optic communication networks. The telecommunication industry uses laser diodes of around 1310nm and 1550nm in their

communications networks. These two wavelengths correspond to the wavelengths of minimum dispersion and minimum loss respectively in standard silica optical fibres meaning signals at these wavelengths can be transmitted with the largest bandwidth and with the least loss. The devices at these wavelengths are therefore mass produced and therefore comparatively cheap. Conveniently the primary and secondary amine band (band 1 in Figure 4-7) lies with its peak maximum at 1535nm. This was sufficiently close to the 1550nm that laser diodes at this wavelength were selected as suitable sources for monitoring this band. A specialist LED, made by GEC Marconi, emitting with a centre wavelength of 1650nm (FWHM $\Delta\lambda\approx$25nm) was chosen to monitor the C-H band at 1647nm (Figure 4-7, peak 2) for internal reference purposes.

With reference to Figure 4-7, it can be seen that at around 1310nm there are no absorption bands. Therefore, for the refractive index monitoring experiments described in Chapter 6 some laser diodes were also purchased at 1310nm so that there would be no interference from nearby absorptions.

It is well known that laser diodes can be wavelength "tuned" to a certain degree by altering the injection current and temperature at which they operate[175]. A series of calibration experiments were therefore carried out on the 1550nm diode lasers to determine their degree of tuneability and wavelength stability.

4.4.2 Diode laser control

For stable wavelength and intensity control of the laser diodes some controller electronics were required. Several systems were examined but the eventual system chosen was an ILX Inc., modular laser diode controller. This unit has four channels, each of which can support either a temperature or diode current controller, the read-out of these parameters being given on a single display.

4.4.3 Diode laser calibration

In order to monitor the wavelength response of the diode lasers to temperature and drive current a method of accurately controlling these two factors was needed. A temperature controlled laser diode mount was designed and constructed incorporating a thermistor for temperature measurement, all the electrical connections for the diode laser and a semiconductor, Peltier heat pump.

Peltier heat pumps are thermoelectric devices that work on the Peltier principle. When an electrical current is applied to the device one side becomes cool and the other warmer. The device does not create or absorb heat but moves it from one of its faces to the other. A device of this type was incorporated into the mount with one side in contact with a copper block containing the laser diode and the other in contact with a heat sink. The laser and Peltier current was controlled by an ILX laser diode controller which also monitored the laser diode temperature *via* a thermistor. The controller would then adjust the current to the cooler in order to maintain the laser diode at the temperature set by the user on its front panel. In this way the temperature of the diode could be controlled with an accuracy of ±0.05°C. The laser diode controller also supplied the laser current and this could be adjusted to ±0.01 mA.

First thoughts were to conduct the calibration of the laser diodes using a spectrum analyser. The spectrum analyser available in the University was found to have an operating range which did not coincide with the wavelengths chosen for use on this project. Problems were encountered in that the detector of the first spectrometer used, a λ-19 Perkin Elmer UV/VIS/NIR, became saturated at the light levels created by the laser and the machine compensated automatically by turning its gain down to almost zero.

Emission spectra were eventually obtained using an FTIR spectrometer with a Raman attachment which enabled it to measure emission spectra directly. This was configured to measure the emission spectrum of light incident into its sample compartment. A fibre was fed into the sample compartment and the light emitted from the fibre end attenuated by a chromatically-neutral filter between it and the detector opening so that the detector in the spectrometer was not saturated. The temperature and current of the laser were adjusted using the laser controller and mount and was left to stabilise thermally for at least 3 minutes before a measurement was taken. This length of time has been observed as adequate for allowing the control system to settle on the set temperature. The laser was then stabilised at another temperature/current and the measurement repeated.

In year 2 of the project a fibre monochromator was acquired (see next section). This was used in later experiments to measure the laser emission spectra. The use of the monochromator was found to give more repeatable results than the spectrometer because it was designed to facilitate easy launch of light into optical fibres. The light from the laser was launched, *via* an optical fibre, into the spectrometer or monochromator. In the case of

the monochromator the input light was chopped and the signal from the detector measured using a phase-sensitive detector, the output of which was then fed into a computer. The operation of the monochromator, as one of the most important pieces of equipment used in this study, is detailed later in this chapter. Figure 4-3 shows the experimental configuration for measurement of the laser diode wavelength using the fibre monochromator. The temperature of the laser diode was varied in 0.1°C increments whilst the current was held constant at the diode manufacturer's recommended drive current. Runs were also conducted holding the diode temperature constant while varying the current in 0.1mA steps.

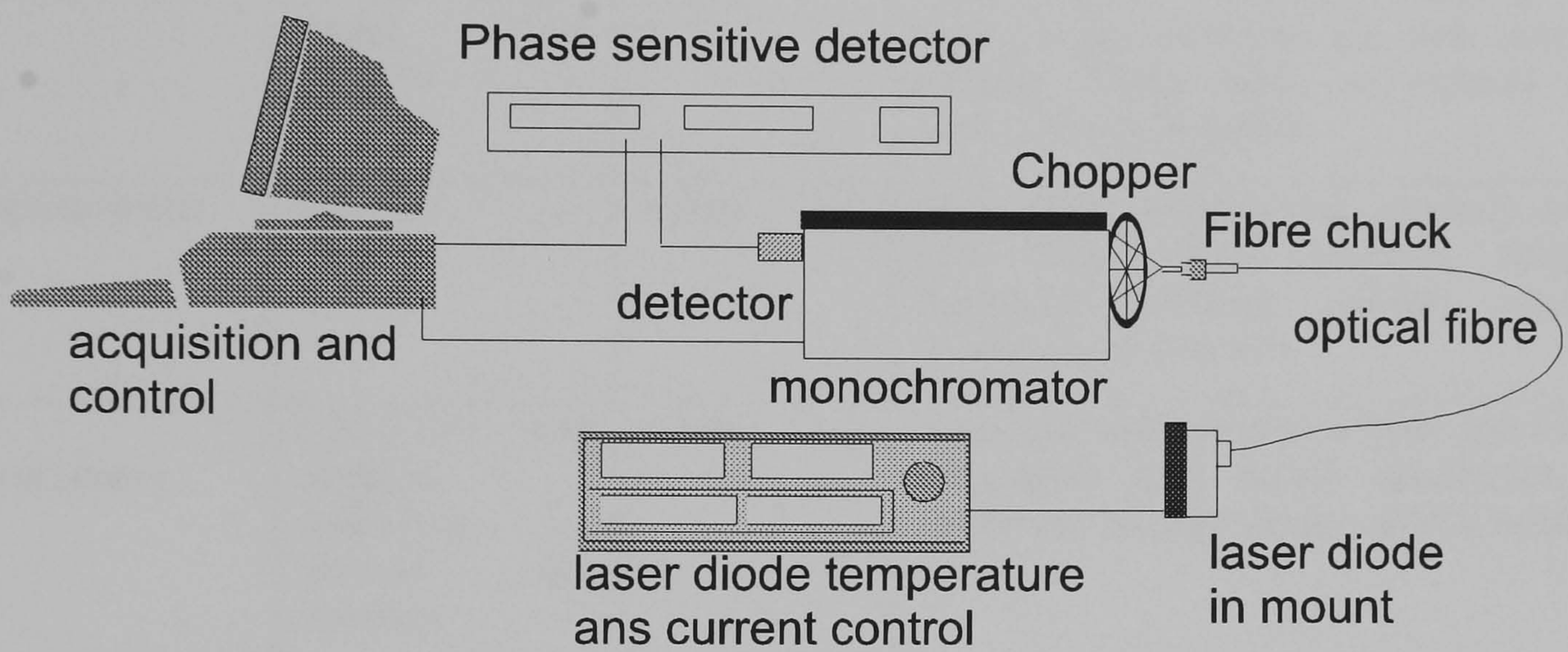

Figure 4-3 Schematic diagram of experimental setup for laser diode wavelength measurement using fibre monochromator

Five repeat temperature and current cycles for two of the lasers having wavelengths specified closest to the spectral region of interest. A further two cycles were conducted on the other two lasers. This constituted over 1500 individual measurements of laser wavelength in total.

4.4.4 Fibre monochromator

It was decided that in addition to the diode laser sources a light source was needed which could provide a spectral picture of the output of the evanescent sensor when immersed in an analyte. These data could then be used to pinpoint the wavelength to which the monochromatic sources would have to be tuned. The light source would need to be tuneable over the range of interest (1-2.5 μm) and be fibre compatible, *i.e.* have a facility for launch into fibre optics. Several candidates were examined, initially tuneable lasers were thought to be most suitable however it soon became clear that a more cost effective and flexible option would be a fibre spectrometer or monochromator. Table 4-3 is a summary of the tuneable light sources that were considered with their advantages and

disadvantages. The system finally selected was a Bentham Instruments fibre monochromator which consisted of a white light source

Source type.	Tuning range (μm)	Resolution	Comments
Dye laser	0.25-0.85	-	Complicated and messy, not tuneable to NIR. Several dyes needed for total tuning range
Optical Parametric Oscillator (OPO)	0.3-3.0	-	Needs pump laser (eg. Ar^+ laser). High maintenance, poor fibre compatibilty
Lead salt laser	1.5-5	-	Require cryogenic cooling. Poor beam quality and fibre compatibility
Tuneable diode laser	1.0-1.8 (100nm tuning *per* module)	0.1nm	Doubts about wavelength stability. Small tuning range (≈100nm) for each laser diode module. Works using an external optical cavity. Fibre compatible
Fibre spectrometer	0.4-0.85	0.5nm	Very quick sampling rate, currently available only with silicon detector wavelength sensitivity although longer wavelength versions soon available
Fibre Monochromator	0.35-3.0+ with multiple diffraction gratings and detectors	0.1nm	Bulky and quite slow to acquire spectra. Fibre compatible with launch attachment, good resolution. Modular design adds to versatility.

Table 4-3 Summary of tuneable light sources considered

which is incident into a monochromator consisting of a set of order sorting filters and diffraction gratings. The gratings were attached to a stepper motor, the controller of which could be interfaced to a computer to allow the wavelengths of interest to be specified. The light source was chopped to allow phase-sensitive detection to be used on the signal, increasing sensitivity. Light was launched into the fibre using a standard microscope objective. This allowed the numerical aperture of the launch light to be adjusted to match the type of fibre being used. This system was considered the best option because of its flexibility, its wavelength range would be capable of extension by insertion of a new grating and order sorting filter. It could also be used with standard photodiodes, in the experiments described below a standard InGaAs photodiode was used which would operate between 1000-1700nm but for longer wavelengths an alternative detector could be used. Driver and acquisition software was written using Data Translation DTVee software which is a derivative of HPVee, the Hewlett Packard modular instrumentation programming software. The program communicates, *via* an RS232 connection, with the stepper motor controller and the phase-sensitive detector to synchronise the scanning of the

monochromator with the acquisition of each point on a spectrum. Each point on a spectrum is sent automatically to the computer *via* the RS232 link and the stepper motor is then instructed to move sequentially onto the next point.

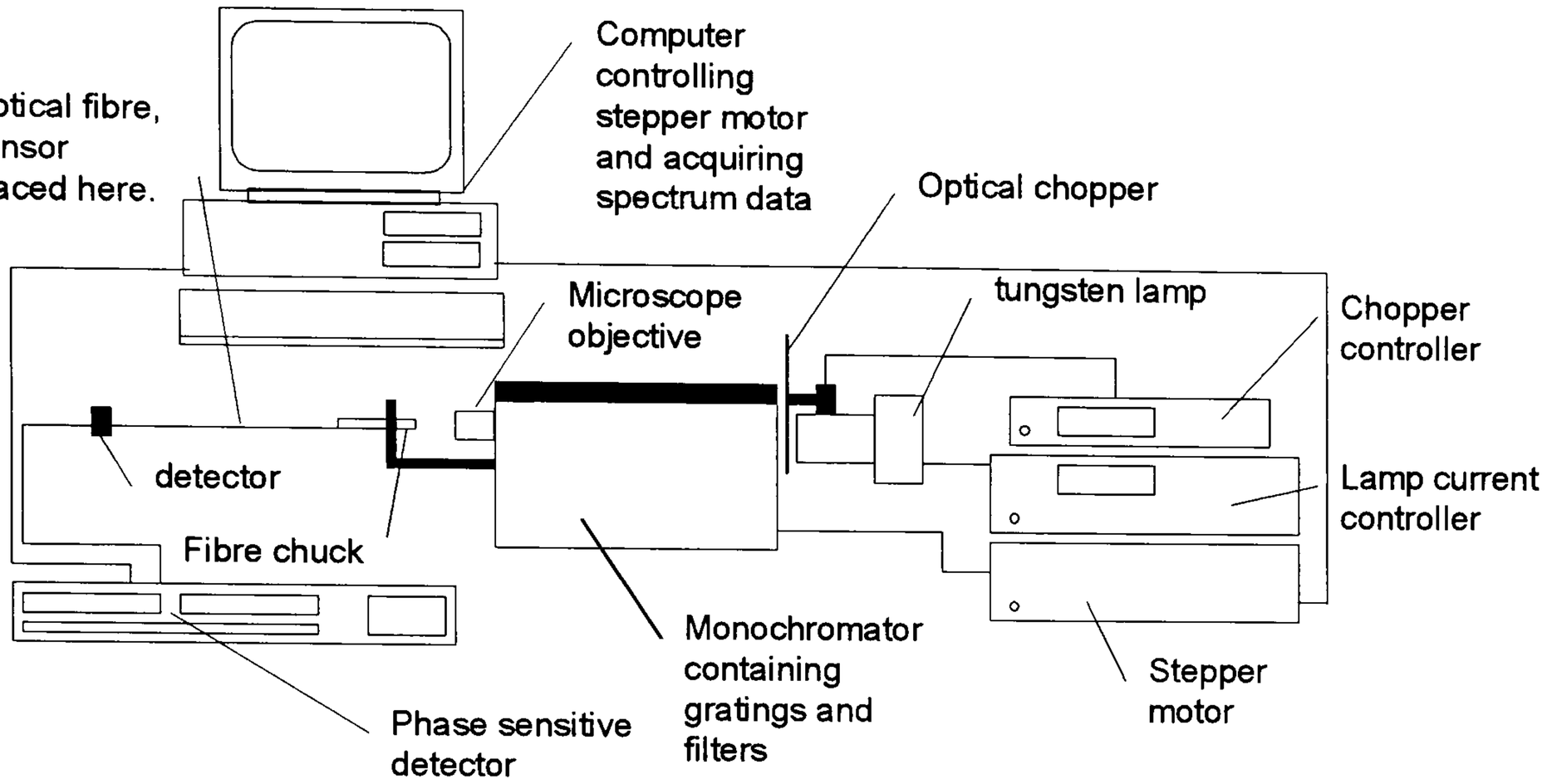

Figure 4-4 Schematic diagram of fibre optic monochromator system showing all system components

A suitable alternative to this system was thought to be a fibre spectrometer, a much more compact, solid state device which simply plugs straight into a PC. It makes use of a static diffraction grating and CCD array to measure spectra. However, when the market survey was being undertaken, these were only available with sensitivity in the visible and very NIR (400-850nm) limited by the CCD which is fabricated using silicon. At the time of writing the company which manufacture these devices have announced a version is under development which is sensitive much further into the NIR. If the *in-situ* cure monitoring work is continued then this device will be a preferable option to the slower and more bulky monochromator used in most of the experiments in this project.

4.4.5 Detector selection

Detector selection was a simple task since there was no requirement for high speeds or extreme sensitivity. The only criterion was a good level of sensitivity in the NIR in areas corresponding to the absorption bands of interest (*i.e.* ≈1.5μm and 2.2μm).

The PIN (positive-intrinsic-negative) photodiode is one of the simplest structures in semiconductor devices. It is also one of the most widely used in long wavelength telecommunications applications because of its reliability and low cost. The structure of an InGaAs (indium gallium arsenide) PIN photodiode can be seen in Figure 4-5.

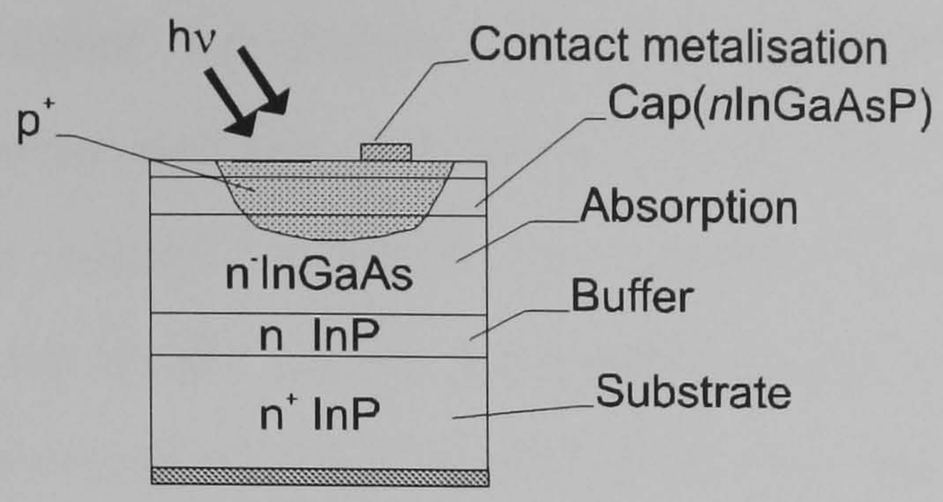

Figure 4-5 PIN diode structure. This is a p-n junction sandwiching an intrinsic, photon absorbing layer.

The PIN diode is basically a *p-n* junction sandwiching a photon-absorbing layer in which electron-hole pairs are created by incoming light. The electrons drift towards the n type material and the hole towards the p-type each contributing a charge of *e* to the current flow in the external circuit. The tiny current that this process produces is amplified to a useful voltage level using a photodiode amplifier. Two, Profile-Instruments, transimpedance amplifiers were bought for this purpose .

Figure 4-6 shows some typical sensitivity curves for two of the most common types of photodiode, silicon and InGaAs taken from suppliers' datasheets.

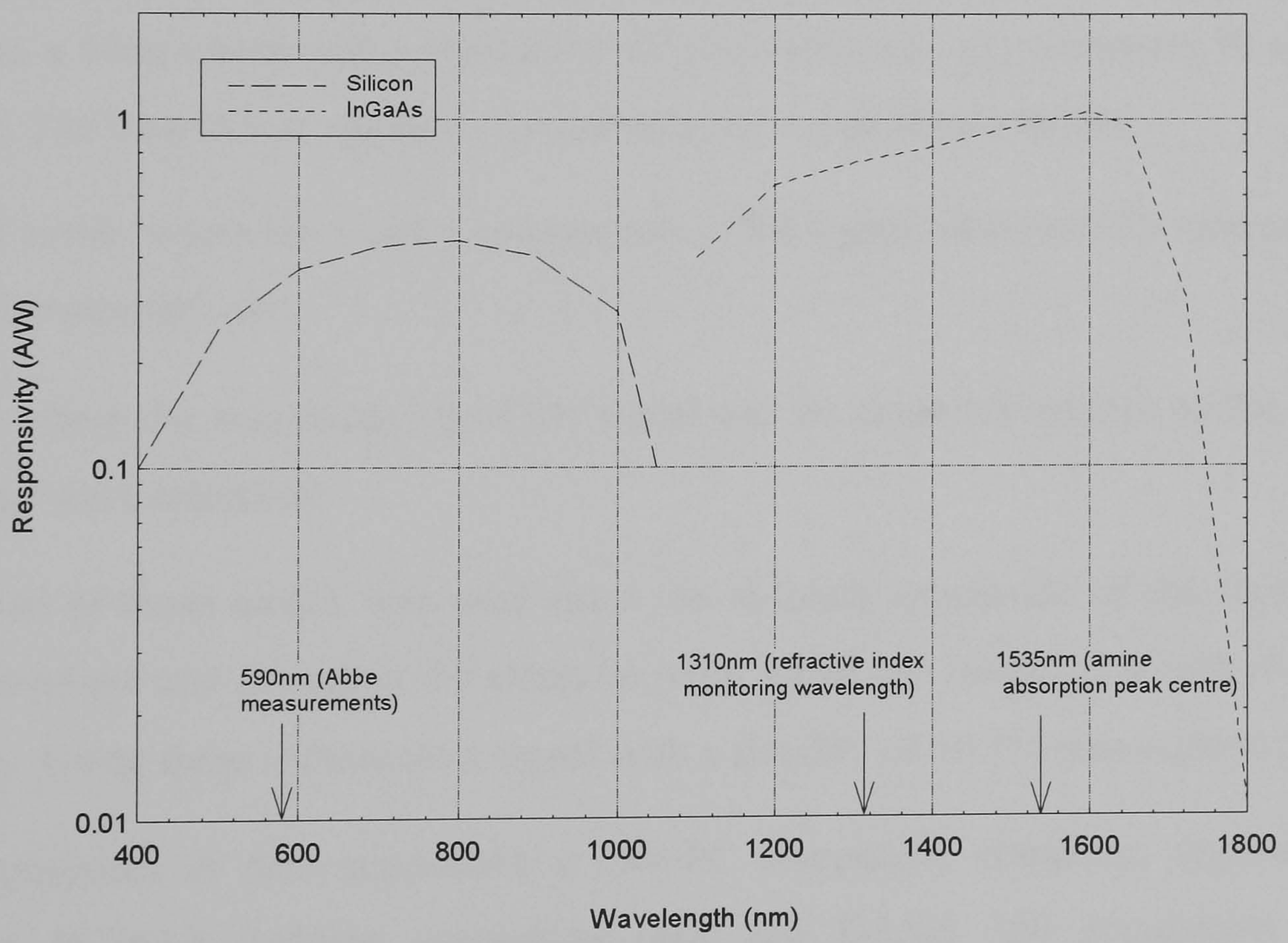

Figure 4-6 Typical relative sensitivities of a silicon and an InGaAs PIN photodiode (from suppliers datasheets)

InGaAs detectors are the obvious choice for the monitoring of the absorption band at 1535nm since detectors of this type have their peak responsivity at around this wavelength. The actual responsivity of the InGaAs photodiodes used in this study was quoted as 0.99 AW^{-1}.

For absorption bands at higher wavelengths an additional PbSe detector was purchased. This is a pyroelectric detector and has a sensitivity from 1.05μm to more than 5μm, but required a thermoelectric cooler to reduce the thermal noise which occurs at room temperature. For work done in the visible wavelength range (*i.e.* some of the refractive index work, section 6) a standard silicon PIN photodiode was used

4.4.6 Signal processing

All spectral signals obtained in the experiments outlined below were obtained from an InGaAs or silicon PIN photodiode. As mentioned above (section 4.4.4) the light into the monochromator was chopped to allow phase-sensitive detection of the output signal and so increase the signal-to-noise ratio of the spectra. The photodiode was connected to the current input of an EG&G lock-in amplifier (model 4510). The current input of this instrument drops the current produced by the diode across either a 1MΩ or a 100MΩ impedance to produce a gain of either 10^6 or 10^8 and convert the signal to a voltage. The majority of signals measured here were taken using the 10^6 gain setting. A time constant of 300ms was used which corresponded to the time taken for the monochromator to scan one step. Thus, a 100nm scan with a resolution of 1nm would take approximately 70 seconds to complete. The lock-in was capable of measuring the signal in two modes:

i) X-Y mode, where the x and y components of the signal relative to the reference signal were measured; and

ii) r-θ, where the magnitude (r) of the signal and its angle (θ) relative to the reference signal were measured.

The second of these modes was used since the absolute magnitude of the signal was of interest to us and any change in the phase between signal and reference would cause a drift in x and y. Using these techniques a signal with a stability of ±0.1% was achieved.

For the purposes of data acquisition a 486 PC compatible computer, together with a Amplicon PC26AT 16MHz acquisition card and DASH 300 acquisition software compatible with the windows environment was used.

4.5 Results of FTIR analysis of model epoxy system

FTIR Cure spectra were taken of the model Epikote 828/hexanediamine resin mixture at isothermal temperatures of 30, 40 50 and 60°C.

For this system, the most important peaks for cure monitoring are at the following wavelengths: O-H (1430 nm), N-H (1538 and 2024 nm), epoxy (1648 and 2208 nm), aromatic C-H (1670, 2136 and 2163 nm).

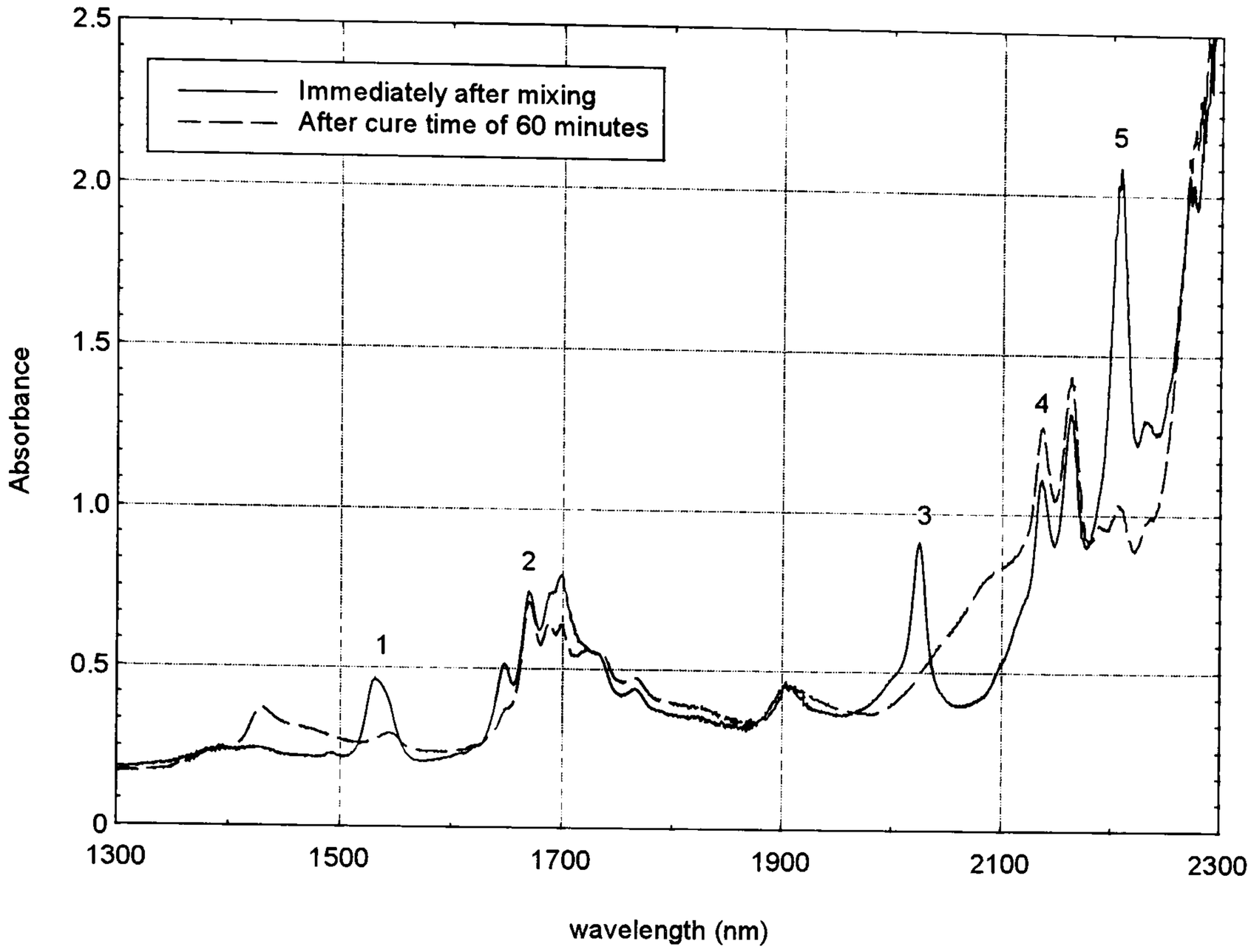

Figure 4-7 Near infra-red spectrum of Epikote 828 and hexanediamine. See Table 4-4 for numbered peak assignments

Figure 4-7 shows the spectra for the resin system before and after cure at 50°C over the range 1300-2300nm. The peaks numbered in the diagram correspond to the band assignments shown in Table 4-4. The bands can be seen to be well resolved allowing accurate quantitative measurements to be made from them.

Peak Number	**Wavelength (nm)**	**Assignment**
1	1535	Overtone of N-H stretch (shown by primary and secondary amine[176])
2	1647	1st overtone of C-H stretching vibration (internal reference)
3	2024	N-H combination (amine)[176]
4	2163	Combination of aromatic conjugated C=C stretch with aromatic C=H fundamental stretch[177,178]
5	2207	Combination of the C-H stretching fundamental with the C-H deformation band (Epoxy absorption) [179]

Table 4-4 Assignments of resin system absorption bands compiled from references 175-179

This graph gives an indication as to which peaks, visible in this spectral region, play a part in the cure process and therefore are suitable for use as an indication of cure state. The peaks numbered 1, 3 and 5 correspond to primary and secondary amine, primary amine and epoxy respectively. The epoxy peak appears in all epoxy amine systems whereas the position of the amine peaks is specific to the curing agent being used. All of these peaks are depleted during cure, making them suitable for cure monitoring. It is a standard spectroscopic technique to employ an internal reference against which all other measurements are compared in order to account for spectra baseline changes due to refractive index or pathlength changes in the sample. Peaks 2 and 4 are due to an aromatic C-H bond and band 2 appears not to deplete during cure . This band is therefore a possible candidate for use as an internal standard. The next task was to select sources which corresponded in wavelength to these absorption bands, in order that light launched into the sensor from these sources would have part of their power absorbed from the evanescent wave.

4.6 Results of laser diode calibration

Three laser diodes were selected from the four which were purchased having nominal wavelengths closest to the 1545 nm peak maximum of the amine absorption band. These were described as following:

i) serial number 30615: quoted wavelength =1554nm;

ii) serial number 30654: quoted wavelength =1550nm;

iii) serial number 30672: quoted wavelength =1549nm.

These lasers were mounted in turn into the temperature-controlled mount, connected to an optical fibre, which was pointed at the detector in the Raman compartment of an FTIR spectrometer. The drive current to the laser was varied at isothermal temperature and also the temperature was varied at a stable current (this was set at the manufacturers recommended drive current of 21mA). This was in order to determine the variation in wavelength with temperature at constant current and with current at constant temperature. The laser was left to stablilise for at least 3 minutes after a temperature adjustment was made. Over 300 spectra were recorded for each laser.

Figure 4-8 and Figure 4-9 are three dimensional plots for one of the lasers (30615) and are typical of those seen for all three.

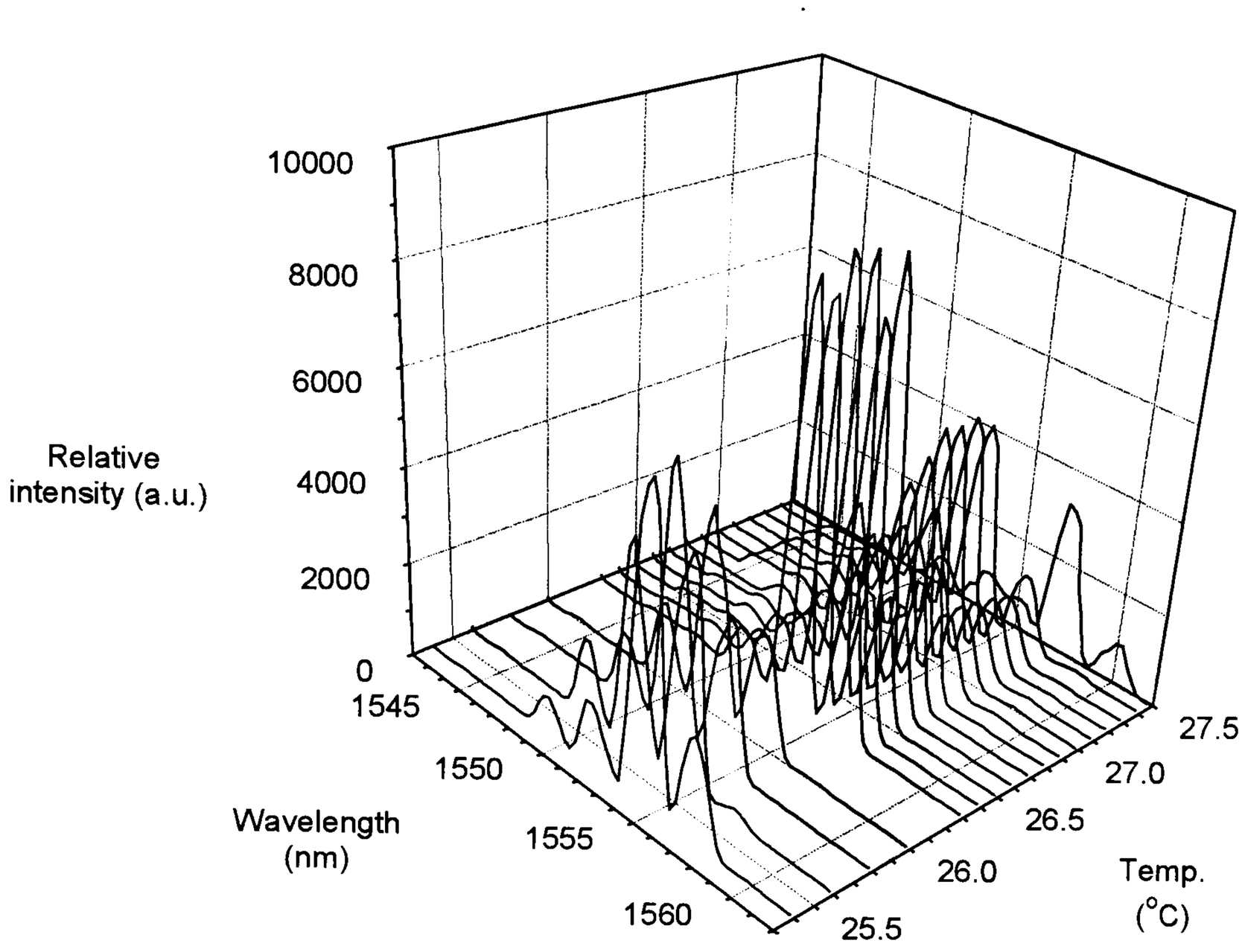

Figure 4-8 Variation in wavelength with temperature for semiconductor laser diode at constant current of 21mA

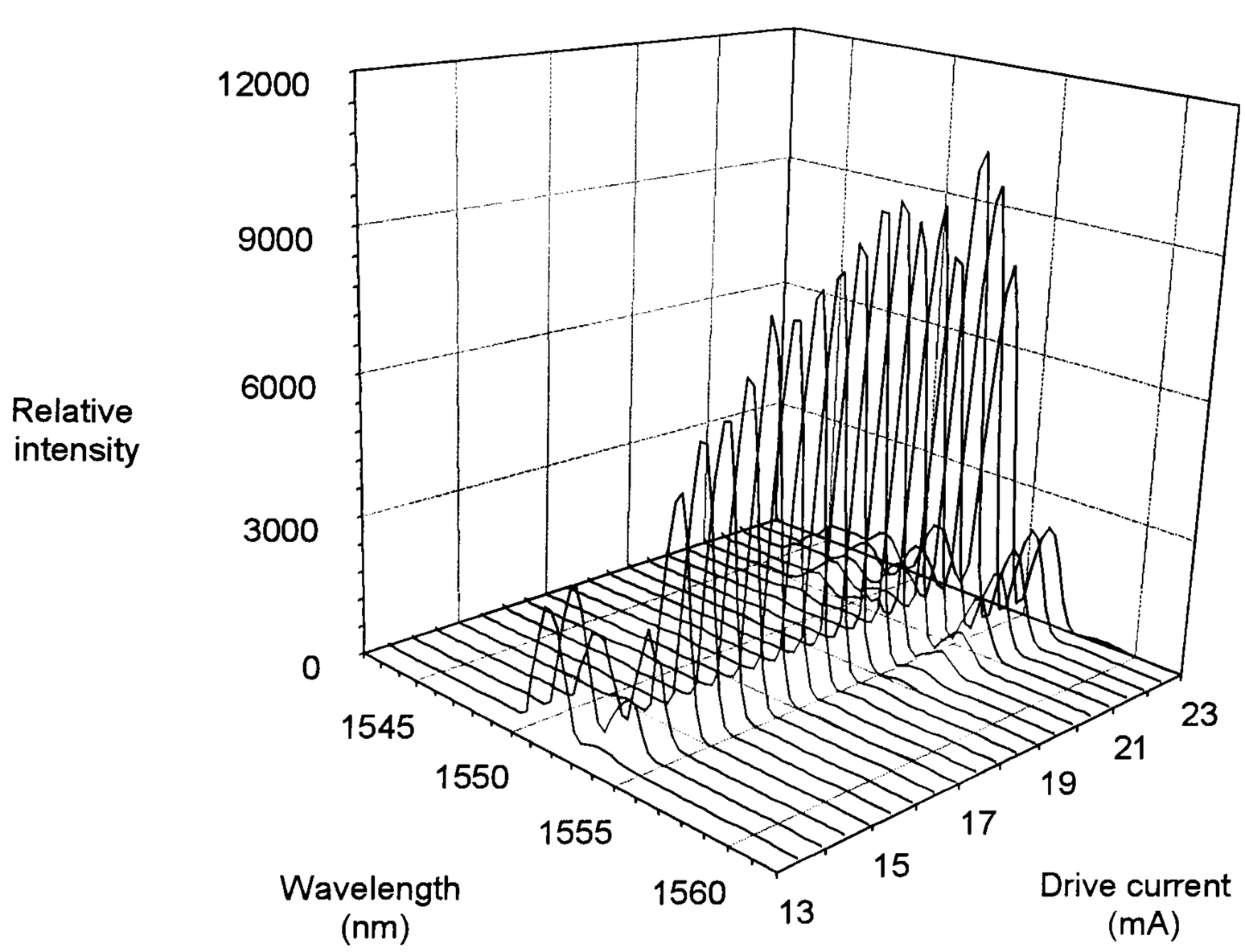

Figure 4-9 Variation of wavelength with changing drive current for semiconductor laser diode (constant temperature 25°C)

The variation in wavelength with temperature (Figure 4-8) can be seen to be unpredictable in nature with the various lasing modes becoming dominant as the temperature changes. The results showed that it was not possible to tune the lasers with temperature controllably and predictably, possibly because the temperature control was not stable enough to keep the cavity length constant.

A similar variation of the drive current at constant temperature (Figure 4-9) showed little promise for laser tuning. Although the change in the lasing modes is more stable and predictable over the useable drive currents there is no steady variation in wavelength. The effect seen is the coupling of power into the laser side modes as the lasing characteristics change.

The wavelength at which a laser emits is dependent on a number of factors, the two main ones being the gain profile and the cavity mode structure. The gain profile of a laser is dependent on the energy levels over which electrons make transitions when they are stimulated by a photon into emitting light. A laser cavity can support oscillations at various frequencies determined by the cavity length and separated by :

$$\Delta\nu = \frac{c}{2nL}$$

- 4.1

where c is the speed of light *in vacuo*, L the cavity length and n the refractive index of the lasing medium. A superposition of the two determines which modes within the laser are amplified.

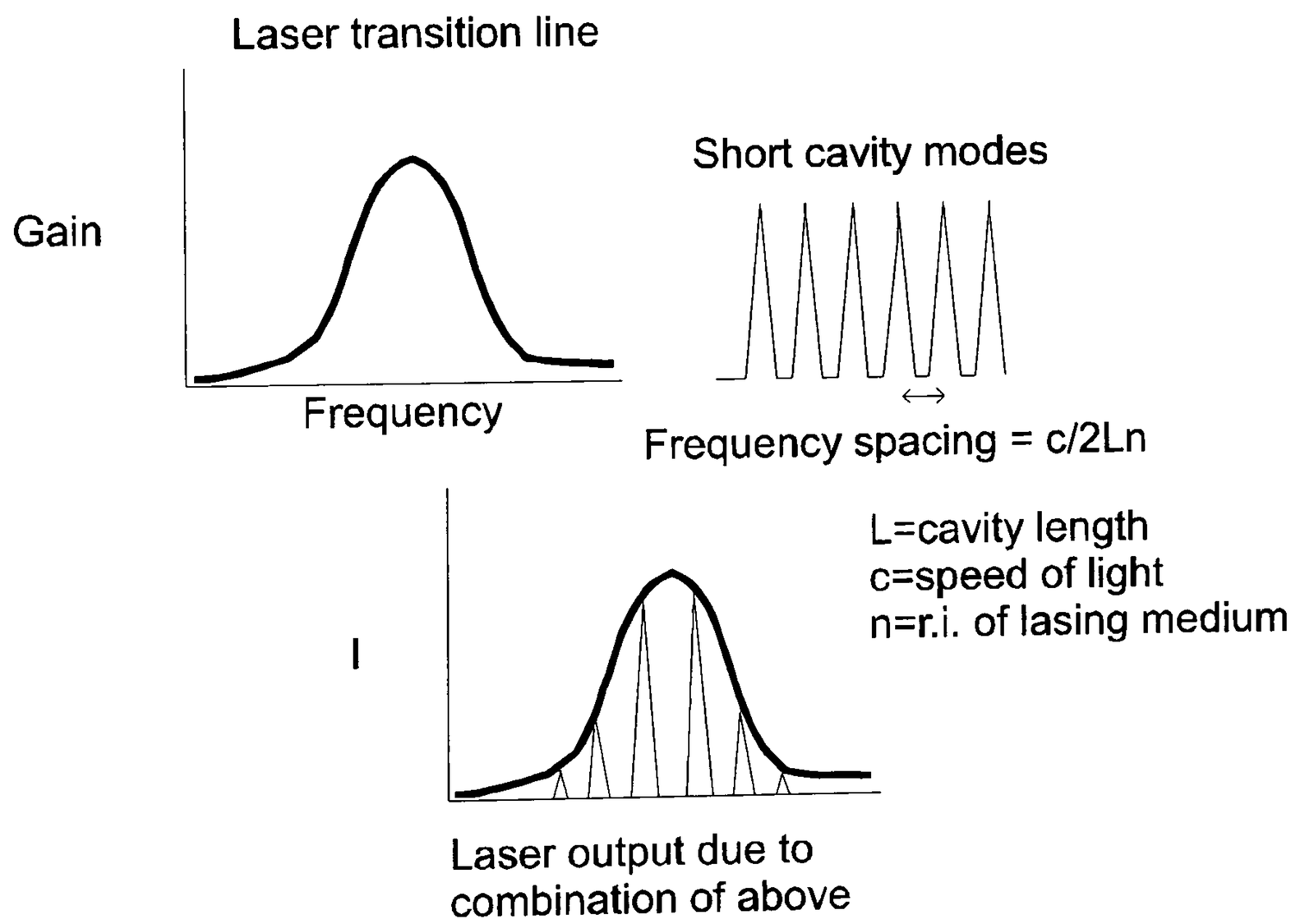

Figure 4-10 Factors affecting laser output wavelength.

Figure 4-10 is a diagram showing the superposition of these two factors. It can be seen that if the gain line is narrow enough and/or the cavity short enough then only a single frequency will be supported. In the case of a diode laser, the gain linewidth can be affected

by drive current and temperature and this will alter the diode's band structure. The cavity modes are also altered due to thermally induced changes in cavity length and this will change the diode's band structure.

5 The evanescent absorption sensor for tracking resin cure

5.1 Introduction

This chapter details the work carried out to investigate an optical fibre cure sensor based on evanescent absorption. The sensor was designed to monitor the cure of an epoxy resin by tracking the change in specific absorption bands that change during the cure reaction. The sensor, being similar in construction to the refractive index sensor, was fabricated from high refractive index optical fibre (n=1.65). The silicone resin cladding was removed from this fibre over a length of approximately 18cm and this portion of the fibre was then embedded in the resin mixture to be cured. Absorption of the evanescent wave penetrating into the resin meant that the strength of absorptions due to specific species (*e.g.* the amine and epoxy groups) in the resin mixture could be observed and hence the concentrations of these species determined. This chapter details the following investigations carried out into the sensor:

i) the theoretical background to the sensor;

ii) preliminary experiments to evaluate the concept of the evanescent sensor by using it to sense chemicals with strong absorbances;

iii) use of the sensor to detect amine solutions such as those used in the cure of epoxy resin systems;

iv) experiments to determine whether the amine solutions bond preferentially to the optical fibre surface;

v) calibration of the semiconductor lasers for use in cure monitoring system;

vi) cure monitoring of epoxy resin systems using the evanescent absorption sensor;

vii) a survey of the goodness of fit of several published models and a model constructed by the author to the evanescent sensor cure data;

viii) comparison to other cure monitoring techniques;

ix) sensor enhancement experiments.

5.2 Theory of operation

Modelling the signal from an evanescent absorption optical fibre sensor in response to a concentration or refractive index change in an analyte is important in order that quantitative data can be obtained from the sensor. The problem is relatively simple when the fibre being used is either single mode or possesses only several well-defined optical modes. In these cases an accurate calculation of the proportion of launch power in the evanescent field can be made[180,181] and from this an accurate prediction of the sensor response. An example of such a calculation can be seen in the paper by Colin *et al.*[182] who consider a theoretical fibre with only two propagation modes. The effect of the length and diameter of the fibre on signal-to-noise ratio is calculated. However, a fibre having just two modes would have a core diameter of a few micrometers. This would make such a sensor impractical in any real application because a silica fibre of these dimensions would not be very robust. It is for these reasons that practically all researchers use multimode fibres for evanescent sensors. These have core diameters of at least 100μm and it is much easier to launch light into a multimode fibre since alignment of source and fibre has a larger tolerance than the same operation in singlemode fibres. Fibres of these dimensions possess hundreds, if not thousands, of propagation modes and so a different approach is required in calculating their sensitivity. A macroscopic approach is normally taken which considers all modes at once by considering the light distribution in the fibre.

5.2.1 Models from literature

Several approaches have been taken to the problem. Many revolve around finding an attenuation coefficient, γ, which fits the equation

$$P(L) = P(0)\exp[-\gamma L]$$

- 5.1

where L is the length of the unclad region of the fibre, P(L) the power transmitted at length L, P(0) the power launched into the fibre and γ is the evanescent absorbance *per* unit length. This equation alone has been used to determine the rate of a chemical reaction[183] by making γ time dependent.

For absolute calculations of concentrations from evanescent sensor signals an explicit expression for γ is needed. The derivation for an expression of γ for a single ray incident at

an angle θ measured normal to the fibre analyte interface is presented below. This equation is derived Ruddy[184] and Gupta and Singh[185], the derivation proceeding as follows:

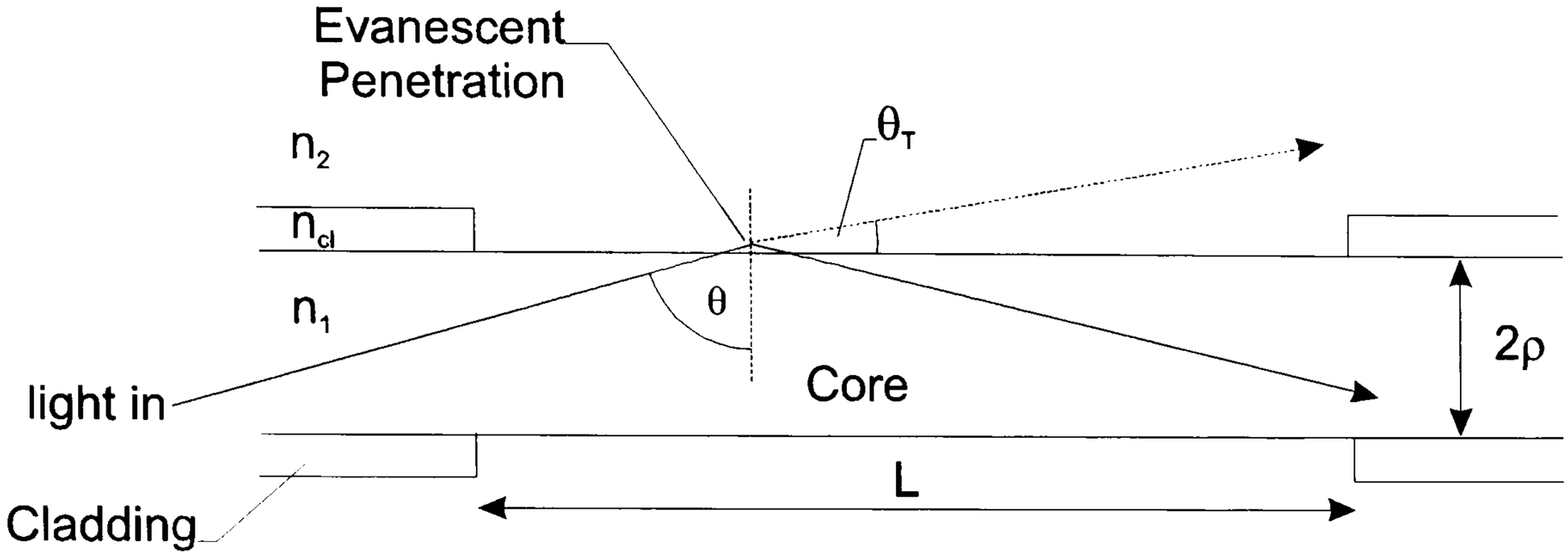

Figure 5-1 propagation of light in optical fibre

γ, the attenuation due to evanescent absorption *per* unit length, can be written $\gamma=NT$ where N is the number of reflections *per* unit length of fibre and T is the transmission coefficient of the light on penetrating the cladding. From simple trigonometry it can be seen that for a fibre, core radius ρ, $N=cot\theta/2\rho$ where θ is the angle at which the light strikes the interface (see Section 3.1). The transmission coefficient T can be derived by considering the analyte refractive index to be complex *i.e.* $\boldsymbol{n_2}=n_2-jn_2^*$ and using the well-known Fresnel coefficients for reflection at a dielectric interface. The complex refracted angle θ_T can be calculated as [186]

$$\cos\theta_T = -j\sqrt{n_{12}^2 \sin^2\theta - 1}$$

- 5.2

Where $j=\sqrt{-1}$ and $n_{12}=n_1/n_2$. For the weakly guided case ($n_1 \approx n_2$), T is the same for both polarisations (TE and TM). This case is treated by Snyder and Love[187]. For the strongly guided case ($n_1 >> n_2$ as is usual for evanescent sensors) the penetration depth of the TM mode varies by a factor varying from n_{12}^2 at the critical angle to n_{21}^2 at $\theta=\pi/2$. Considering the TE modes (which contain the majority of energy in a fibre)

$$T = \frac{4n_1 n_2 \cos\theta \cos\theta_T}{\left|n_1 \cos\theta + n_2 \cos\theta_T\right|^2}$$

- 5.3

Substituting in equation - 5.1, T can be seen to be real and given by:

$$\frac{4n_1^2\cos\theta\,\mathrm{Im}(\sin^2\theta - n_{21}^2)^{\frac{1}{2}}}{n_1^2 - n_2^2}$$

- 5.4

The imaginary part of $(\sin^2\theta - n^2_{21})^{1/2}$ is

$$\frac{n_2 n_2}{n_1^2\sqrt{\sin^2\theta - n_{21}^2}}j$$

- 5.5

using equation - 5.3 and the complex refractive index $n_2 - jn^*_2$,

$$T = \frac{\alpha\lambda n_2\cos\theta}{\pi(n_1^2 - n_2^2)\sqrt{\sin^2\theta - n_{21}^2}}$$

- 5.6

since $n^* = \alpha\lambda/4\pi$ where α is the bulk absorption coefficient of the medium and λ the light wavelength. This expression for n^* comes from a solution of Maxwell's equations for a complex n.[188] Since $\gamma = NT$, an expression can be obtained for $\gamma(\theta)$

$$\gamma(\theta) = \frac{\alpha\lambda n_2\cos^2\theta}{2\pi\rho(n_1^2 - n_2^2)\sin\theta(\sin^2\theta - n_{21}^2)^{\frac{1}{2}}}$$

- 5.7

This is the absorption coefficient for a single ray incident on the sensing region at an angle θ. To be of real use this equation has to be summed over all rays entering the sensing region of the fibre, over all angles θ. The upper limit of θ is always $\pi/2$ for fibre optics (*i.e.* rays travelling straight down the fibre). Using this as the upper limit to θ the following expression is obtained:

$$\gamma\left(\frac{\pi}{2},\theta\right) = \frac{\alpha\lambda n_2}{\pi\rho(n_1^2 - n_2^2)}\left[\tan^{-1}\left(\frac{\cos\theta}{\sqrt{\frac{\sin^2\theta}{\sin^2\theta_c} - 1}}\right) + \sin\theta_c\sin^{-1}\left(\frac{\cos\theta}{\cos\theta_c}\right)\right]$$

- 5.8

Typically, evanescent wave sensors are used to monitor the concentration of an absorbing substance in a non-absorbing solvent. In this case, the refractive index n_2 of the absorbing medium effectively remains constant and the sensitivity of the sensor can be shown to be proportional to $L\gamma/\theta$ [189]. Also for constant n_2 and $\theta=\theta_c$, (the critical angle of the lead in fibre of the sensor), equation - 5.7 can be reduced to [184]:

$$\gamma(\frac{\pi}{2},\theta)=\frac{\alpha\lambda}{2\pi\rho n_1(1+\sin\theta_c)}$$

- 5.9

However, for a curing resin system, the refractive index changes throughout cure by a substantial amount and so the sensitivity expression retains a term which is dependent on n_2. From - 5.7 it can be seen that the change in n_2 also makes a large contribution to γ. An increase in absorbance should be seen at all wavelengths due to the rise in n_2. This can be used to advantage, to sense refractive index at a wavelength away from an absorption band (see §6.3.2) but for quantitative measurements of absorption bands this effect must be accounted for. When used for monitoring an epoxy cure reaction the lower limit of θ is a function of the resin refractive index and hence dependent on cure time expressed as:

$$\theta(t)=\sin^{-1}\frac{n_2(t)}{n_1}$$

- 5.10

i.e. the critical angle of the sensing region at time t. This cure time dependence needs to be incorporated into the model. Gupta and Singh [185,189] also extend their theoretical model for fibres with core diameters which decrease along the length of the sensor region (*i.e.* tapered fibres) with several taper profiles (see §5.4.8)

The second most frequently encountered model in the literature makes allowances for the refractive index effect by including a term based on the numerical aperture change in the sensing region brought about by the refractive index change of the analyte.

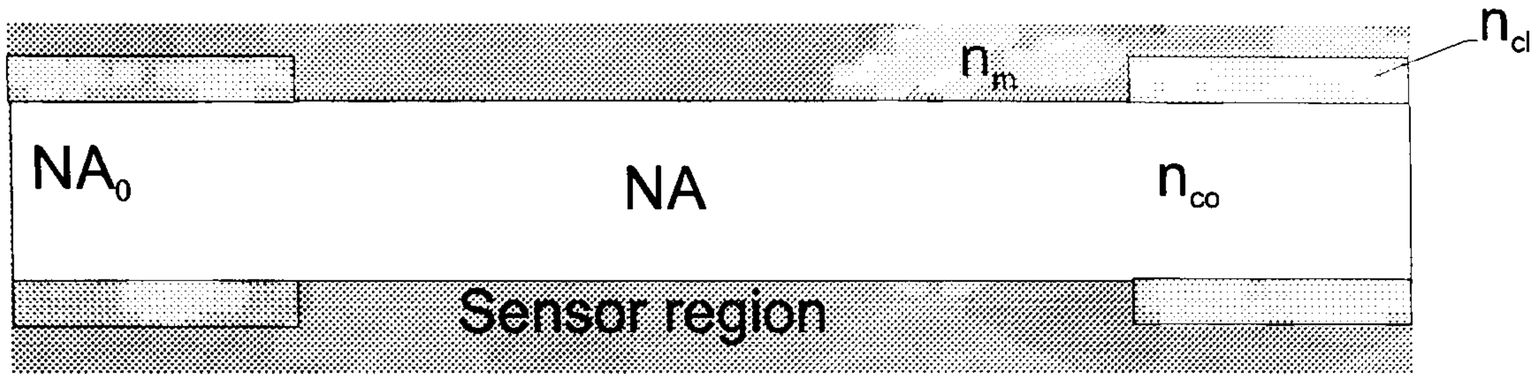

Figure 5-2: definition of terms for the Degrandpre and Burgess model

Bobb *et al.*[190] describe the light attenuation at a non-absorbing wavelength by accounting for the change in numerical aperture of the core/analyte region:

$$I = I_0\left(NA^2 / NA_0^2\right)$$

- 5.11

where $NA=(n^2_{co}-n^2_m)^{1/2}$ and $NA_o=(n^2_{co}-n^2_{cl})^{1/2}$. Here n_{co} is the core refractive index, n_{cl} the fibre cladding refractive index and n_m the analyte medium refractive index. I is the intensity transmitted by the sensor when immersed in the analyte and I_o is the intensity transmitted when the sensor is in air. Equation - 5.11 is derived from the normalised frequency V, defined in section 3.1

$$V = \frac{2\pi\rho}{\lambda}\left(n_{co}^2 - n_{cl}{}^2\right)^{1/2}$$

- 5.12

where n can be either n_m or n_{cl}, ρ is the fibre radius and λ the wavelength of light in free space [111]. In physical terms - 5.11 just accounts for the change in the number of modes the sensor region can support. In a multimode fibre the total number of modes a fibre can support is given by

$$N = \frac{1}{2}V^2$$

- 5.13

It does not take into account re-excitation of modes which occurs if a fibre is bent. Calculations do exist which take into account the modal distribution within the fibre and

the light propagation in a bend[191, 192] However, this equation is useful for qualitatively predicting the response of the sensor.

The light attenuation at an absorbing wavelength can be described by[193,79]

$$-\log\left(\frac{I}{I_0}\right) = \alpha_e Lc + \log\left(\frac{NA_0^2}{NA^2}\right)$$

- 5.14

where $\alpha_e = r\alpha_c$, L is the sensor length, c is the concentration of the analyte, α_c is the analyte bulk absorbtivity and the fraction of the total light intensity contained in the evanescent field, r is given by[13]

$$r = \frac{k}{V} = \frac{k\lambda}{2\pi\rho NA}$$

- 5.15

Here k is a proportionality constant. The refractive index dependence of the sensor response appears in both the second term and also in the effective absorptivity terms in equation - 5.14 since r (equation - 5.15) has a dependence on refractive index. The second term accounts for the light lost at the sensor from guided modes being converted to radiated modes due to the numerical aperture change. At identical wavelengths for fibres of the same radius the power distribution depends on the numerical aperture of the fibre so if the analyte refractive index changes a change in the effective absorbtivity, α_e, is observed. The attenuation of light in the fibre increases with analyte absorbtivity, refractive index, wavelength, sensor length, fibre radius and bend radius [70].

Although extremely important for an accurate calculation of the sensitivity of an evanescent sensor few papers which use the constant k in their theoretical discussions actually put forward a value for it. The most quoted value of the proportionality constant k has been calculated by Gloge[194] from a consideration of the power distribution in a multimode fibre as $(4\sqrt{2})/3 \approx 1.89$. This paper is one of the most referenced fibre optic papers in the literature. However, it has only a sparse treatment of multimode fibres and many assumptions based on the limit of weakly guiding fibres *i.e.* $\Delta = (n_{co}-n_{cl})/n_{cl} << 1$. This is patently not the case for evanescent sensors since in the sensing region n_{cl} is usually much smaller than n_{co}. An improved estimate of r such as that derived by Ruddy[184] may improve the accuracy of this theory. Ruddy's expression for r is as follows:

$$r(\pi/2,\theta) = \frac{1}{V}\frac{\sin^{-1}(\cos\theta/\cos\theta_c)\sin(\pi/2-\theta_c)}{\pi/2-\theta}$$

- 5.16

It can be seen that this expression retains a dependency on the critical angle of the sensor region θ. The incorporation of this expression and the dynamic nature of refractive index of a curing resin form part of the study being undertaken by the author.

The non-linear nature of the observed absorbance with sample concentration and pathlength is discussed by Ruddy[195]. This paper also contains a further evanescent absorbance model that is explained briefly here.

The allowed propagation modes in an optical fibre are characterised by discrete values of the propagation constant β or the component of the wave vector along the fibre axis. For light of wavelength λ and wave number $k=(2\pi/\lambda)$, $\beta=n_{co}k\cos\theta$.

When an optical fibre's cladding material is absorbing or replaced by an absorbing medium, the total power of a mode is reduced. The attenuation may be quantified in terms of an evanescent wave absorption coefficient γ given by [10]:

$$\gamma = \frac{n_{cl}\alpha k U^2}{\beta V^2 W}$$

- 5.17

where α is the bulk attenuation coefficient of the absorbing cladding , n_{cl} is the real part of its refractive index, V is the normalised frequency defined in equation -3.2 and U and W are the Bessel function parameters for the core and cladding E-fields respectively and are related to V by the equation[10]:

$$U^2 + W^2 = V^2$$

- 5.18

The magnitude of α is directly related to the bulk absorbance (the Beer-Lambert absorbance) of the absorbing cladding or to the product of its absorptivity and concentration for direct transmission through it. It is also related to the imaginary part of the cladding index by $\alpha=2k\kappa^*_{cl}$ (see equation -5.15). Equation - 5.17 is derived from is derived from the fractional loss in power of a wave internally reflected at an interface with

a medium of complex (or lossy) refractive index ($n_{cl}+i\kappa_{cl}$) using an analysis based on Fresnel reflections at a dielectric interface as in Ruddy's previous model.

If the absorber is in contact with the evanescent wave over a length of fibre L then the mode transmittance is given by :

$$T = \exp(-\gamma L)$$

- 5.19

and a mode of incident power P_0 is reduced to a power P_T is after a length L of fibre where:

$$P_T = P_0 \exp\left\{-\frac{n_{cl}\alpha L}{n_{co}V}\frac{x^2}{\left[\left(1-x^2\right)\left(1-2\Delta x^2\right)\right]^{1/2}}\right\}$$

- 5.20

where $x=M/N'$, M being the mode index and N' its upper limit ($=V/\sqrt{2}$) and Δ is the refractive index profile height given by:

$$\Delta = (n_{co}^2 - n_{cl}^2) / 2n_{co}^2$$

- 5.21

For a multimode fibre with a large V number (and larger number of modes, see - 5.13) this expression can be integrated over all modes using x as a continuous variable. Converted to absorbance ($A=-log_{10}(P_T/P_0)$) this integral is expressed as follows.

$$A = -\log_{10}\int_0^1 \exp\left[\frac{-n_2\alpha L}{n_1 V}.\frac{x^2}{\left(\left(1-x^2\right)\left(1-2\Delta x^2\right)\right)^{\frac{1}{2}}}\right].dx$$

- 5.22

The integral represents a summation of the fraction of power lost by all modes over a distance L and can be used to predict the absorbance of an evanescent sensor in a n absorbing medium.

The literature sources from which these models were taken make no comparison of their predictions with experimental data. For a proper analysis such a comparison is needed in order to select the model which gives the most accurate prediction of the sensor response. A comparison of the accuracy of these models compared to evanescent absorption data is

presented in sections 5.4.4 and 5.4.7. In the first of these sections the models are compared to sensor absorbance data from solutions of known concentration and the second from the sensor when embedded in a curing resin.

5.2.2 Penetration depth model

From a comparison of the models from the literature with experimental data it was seen that several gave a very poor prediction of the evanescent absorption of the optical fibre sensor (see section 5.4.4). Therefore, a further model was developed by the author during the course of the project based on the penetration depth equation. The approach taken in this model is as follows.

The penetration depth of the evanescent wave, created by a totally internally reflected ray, from an optically dense medium into a rarer medium is given by equation 16) (section 5.1):

$$d_p = \frac{\lambda_t}{2\pi(\sin^2\theta_i - {n_{21}}^2)^{1/2}}$$

- 5.23

where λ is the wavelength of the incident light, θ_i the angle of incidence of the ray normal to the medium interface, n_{21} The ratio of the refractive indixes of the rarer medium to the optically denser medium. d_p is the depth at which the evanescent wave reaches e^{-1} of its interface value and takes into account a single reflection at the interface at a specific angle of incidence θ_i. In a fibre there are many such bounces over a range of angles between the critical angle and the limiting angle of glancing incidence, 90° to the interface. The number of reflections *per* unit length for a ray at an angle θ is given by the equation:

$$N(\theta) = \frac{\cot\theta}{2\rho}$$

- 5.24

Where ρ is the radius of the fibre core. The penetration depth equation can be extended to produce an expression for the *effective thickness (*see section *3.3.2)*. This is an expression for the effective sampling thickness of the evanescent wave from a single reflection and is a measure of the strength of coupling to the sample medium. It is useful in comparing internal reflection spectra to transmission spectra. This can be approximated for small absorptions by the equation [11]

$$d_e = \frac{n_{21} d_p E_0^2}{2\cos\theta}$$

- 5.25

Where E_o is the incident electric field strength.

To produce a prediction of the effective pathlength for an evanescent absorption sensor, it is necessary to take into account all incident angles for all rays. This was done by integrating the product of the number of reflections and the effective thickness over all angles present in the fibre *i.e.*:

$$D = L\int_{\theta_c}^{\frac{\pi}{2}} N(\theta) d_e(\theta) d\theta$$

- 5.26

where D is the effective pathlength and θ_c is the critical angle at the fibre/medium interface.

The prediction of absorption at wavelength λ for a sample of absorptivity α can then be calculated in an analogous way to transmission spectroscopy *i.e.*:

$$A = -\log\frac{I}{I_0} = \alpha D$$

- 5.27

This model, although relatively simple in nature was shown to give good predictions of the evanescent fibre absorbance (see section 5.3.4). The predictions of this model and a comparison with that given by those from the literature can be seen in section 5.4.7.

5.3 Experimental procedure

An initial set of experiments were undertaken to explore the concept of the evanescent sensor and to prove that it could be used as a chemical sensor.

The experiments proceeded as follows:

i) the detection of cuprous chloride using an LED operating at 830nm using an evanescent sensor. This was a proof of concept experiment to ensure that the optical fibre signal could be affected by an analyte in contact with its core;

ii) the detection of amines similar in structure to those used as resin hardeners. This was done first using a transmission cell and then with the evanescent sensor.

5.3.1 Chemical detection- cuprous chloride

Very early experiments involved the immersion of sensors in a one molar solution of cuprous chloride in methanol. Cuprous chloride has a broad, strong absorption centred on 800nm. Light from a 830nm LED source was launched into the sensor and the signal from the sensor monitored. The sensor was moved from air, to methanol and to the 1.0 molar $CuCl_2$ solution. It was then returned to the methanol to be washed and finally left to dry in air to establish whether the process had in any way affected the guiding properties of the fibre. The results from these experiments can be seen in section 5.4.1.

5.3.2 Amine sensing: transmission cell

A fibre transmission cell was constructed and used to determine the extent of the absorption of the light from a laser diode at 1550nm by an amine hardener solution.

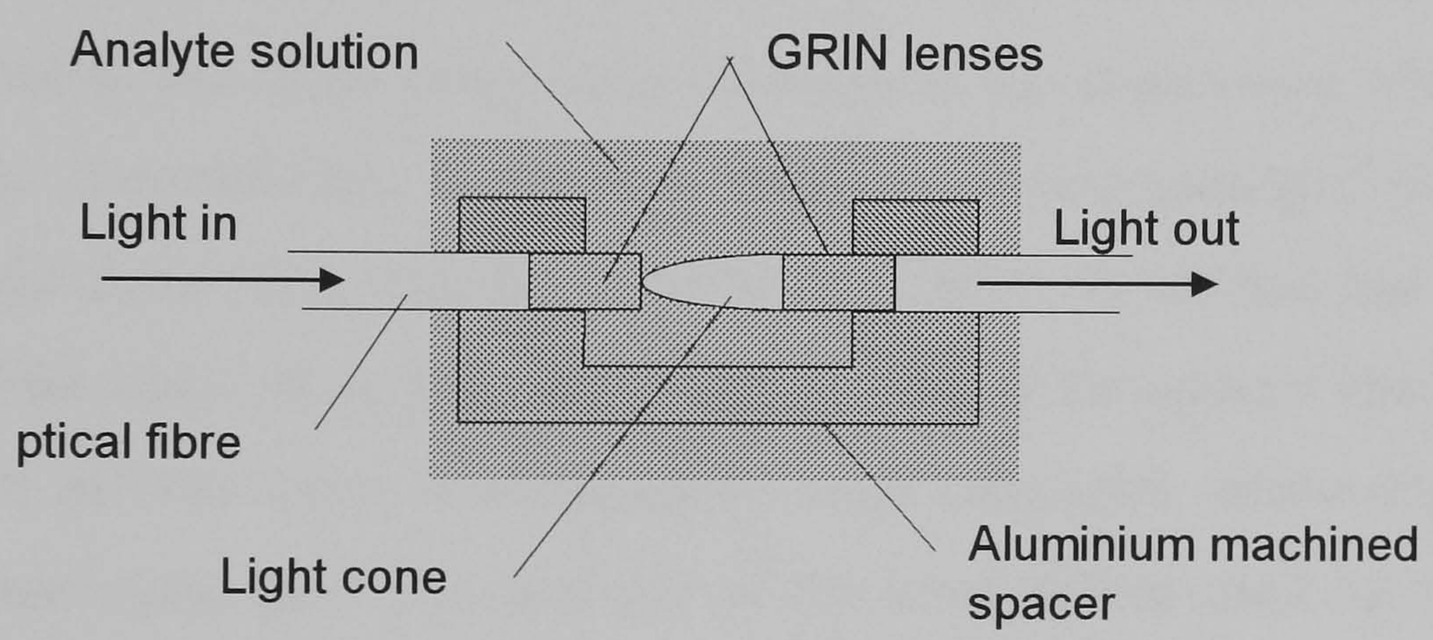

Figure 5-3 Design of fibre optic transmission cell used to determine absorption of laser light by amine solution

A small transmission cell was set up the design of which can be seen in Figure 5-3. Five solutions of dibutylamine in hexane of concentration 0 (pure hexane), 0.294, 0.622, 1.135, 1.737 and 2.151 mol dm^{-3} were made up and the transmission cell was immersed into each of these solutions in turn. The cell was washed in hexane and dried between each immersion. Finally the cell was immersed in pure hexane again, to verify that there was no build up of the amine on the graded index (grin) lenses which could have affected the signal.

Similar experiments were performed using potential amine curing agents and solvents to determine whether the sensor was capable of detecting changes in concentration of these substances analogous to those occurring in a curing resin system. Hard clad silica fibre was

used for the sensor in these experiments the cladding being removed using a clean bunsen flame. Laser diode sources with wavelengths of 1551nm corresponding to the amine absorption peak centred on 1547nm were used (this absorption positioned was determined using FTIR spectroscopy). The experiments were performed in two ways:

i) several amine-in-solvent solutions of known concentration were made up prior to the experiment starting. The sensor was immersed sequentially in each of these being washed thoroughly in solvent between each immersion. The sensor signal was read directly from the photodiode amplifier at each concentration;

ii) the prepared sensor was immersed in a suitable solvent and the amine added 1ml at a time using a burette at 1 minute intervals. The solvents used were chloroform, IPA or dichloromethane which were determined to have no absorptions in the spectral range of interest *via* FTIR and a lower refractive index than the fibre core to satisfy guiding conditions. The solvent was placed in a vessel containing a magnetic stirrer so that the amine was dispersed throughout the solvent upon addition. The solvent was also cooled in ice to minimise evaporation throughout the experiment which would alter the solution concentration. The laser diode sources were packaged in ST connectors and the light from them was launched into the fibre which had had ST connectors attached. The signal from the sensor was monitored throughout the addition of the amine. The amine/solvent concentrations were calculated afterwards to produce a concentration/signal plot. A schematic of the arrangement used for this experiment can be seen in Figure 5-4.

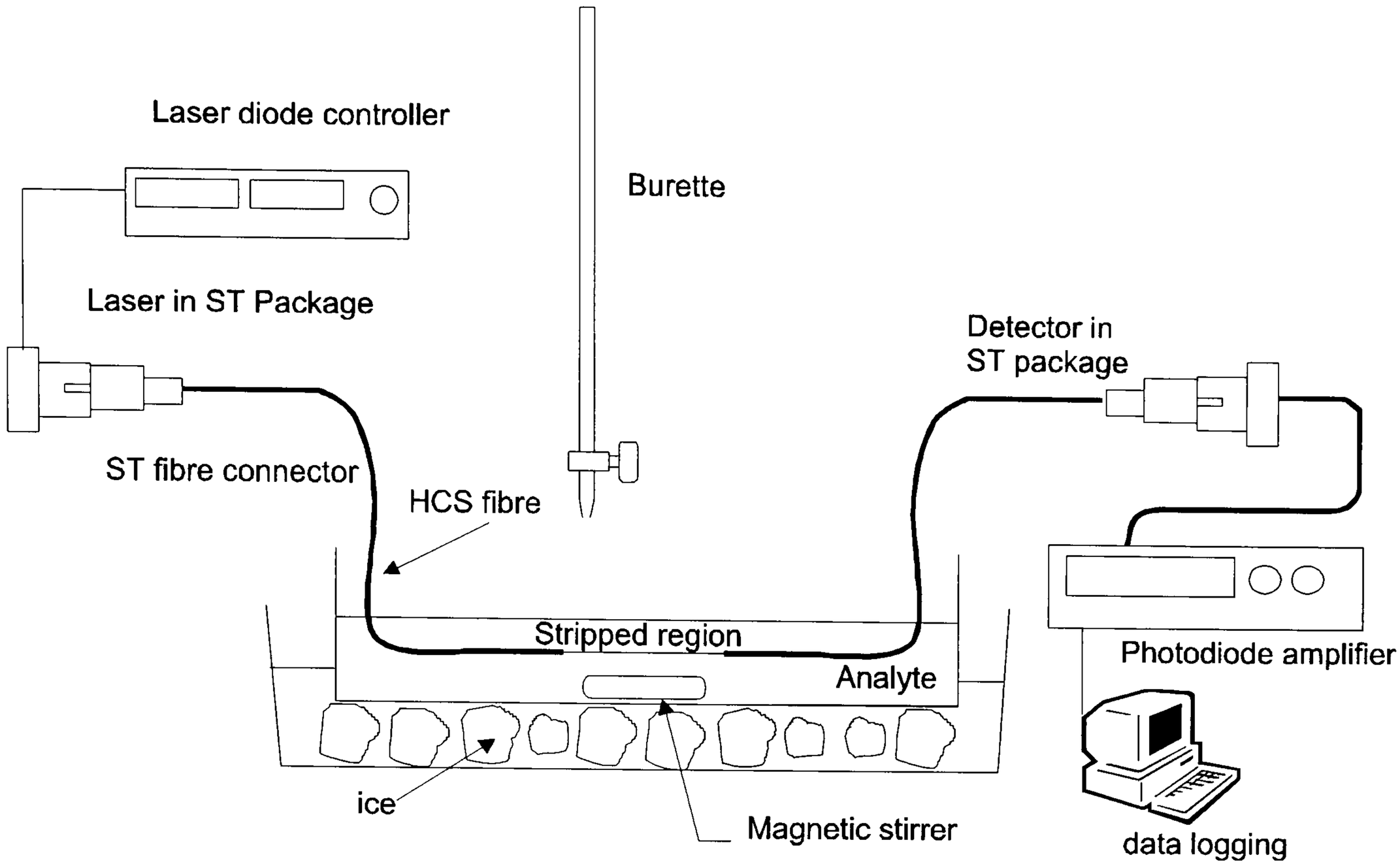

Figure 5-4 Experimental arrangement for amine sensing

5.3.3 Fibre surface effects

There was some concern that the fibre sensor itself could be modifying the behaviour of the solution or mixture in which it was embedded. This arose when it was noticed that the absorption peaks from sensors, which had been left to soak in amine solution, had become more intense. Several experiments were carried out to determine whether amine molecules were being preferentially adsorbed onto the cores of the fibres being used to fabricate the sensors.

Five 200mm sensors were fabricated from hard clad silica fibre using the method described above. These were in each laid, in turn in a vessel containing a 50% ethylene diamine solution in IPA (isopropyl alcohol). The vessel was chilled and sealed to minimise solvent evaporation from the solution. The volume of solution was verified to be the same at the end of the experiment as at the beginning, eliminating the possibility that any changes in the absorption seen by the sensor were due to a change in concentration *via* evaporation of solvent. Ethlyene diamine was used since it has a similar chemical structure and properties to hexanediamine, the amine used in the majority of the cure experiments, and was readily soluble at room temperature in a variety of available solvents. It also possesses a similar primary/secondary amine absorption band centred on approximately 1545nm. Spectra were acquired, over the wavelength range 1450-1550nm, from the sensors using the fibre

monochromator at 10 minute intervals for the first five hours of immersion and at hourly intervals for a further 17 hours. The data were examined to determine whether there was any change in the absorbance seen by the sensor during the immersion time. After this time the sensors were removed from the amine solution and thoroughly washed in pure IPA. A further scan was then taken to determine whether any of the amine had become chemically attached to the fibre surface.

The experiment was then repeated using 200mm sensors made from the high refractive index fibre.

5.3.4 Verification of model validity

The literature in which the models in section 5.2.1 are outlined are in general purely theoretical. None of the papers contain a rigorous comparison of experimental data to the predictions made by the models described. It was thus thought that a significant step would be made by comparing actual results obtained from an optical fibre evanescent absorption sensor, to the model predictions. This comparison consisted of two stages:

i) immersing a sensor in a solution of amine hardener of known, varying concentration. The concentrations used were carefully calculated to simulate those experienced by the sensor during an epoxy cure cycle. This method reduced the refractive index effect on the sensor which has been shown to produce a large signal change. Although the refractive index of the solution did change with increasing concentration the change was several magnitudes smaller than that which occurs during resin cure;

ii) data from the evanescent sensor obtained during actual resin cure were used in conjunction with FTIR data and Abbe refractometer data obtained from similar resin mixtures cured at similar isothermal temperatures with the models to produce an assessment of the models accuracy.

Experiments were carried out to test the validity of the models described above. To do this it was necessary to establish a relationship between the evanescent absorbance and concentration of hexanediamine in a solution. The concentration of hexanediamine hardener in a stoichiometric mixture of resin and hardener can be calculated as 1.33 Mol dm^{-3}. The experiments aimed to determine evanescent absorption of solutions having this concentration and lower to simulate those concentrations observed during cure. A vessel

was constructed from glass tube that would hold a known volume of solvent. The solvent used was chloroform as this had already been shown to have no absorptions over the spectral region of interest that would interfere with the absorption seen by the evanescent sensor. The vessel had an opening in the top into which a known volume of hexanediamine could be introduced using a burette. The length of fibre from which an 18cm sensor had been fabricated was introduced into the vessel that was then filled with solvent. A strong hexanediamine solution (3.38 mol dm^{-3}) was introduced into the vessel 0.5 ml at a time, dispersed throughout the solvent using a magnetic strirrer and the amine absorption peak centred on 1547nm measured using the Bentham spectrometer. A solution of hexanediamine was used instead of the pure hardener since hexanediamine is a solid at room temperature. The absorption peak height was then measured and could be plotted against the calculated hexanediamine solution concentrations. A schematic drawing of the experimental setup can be seen in Figure 5-5.

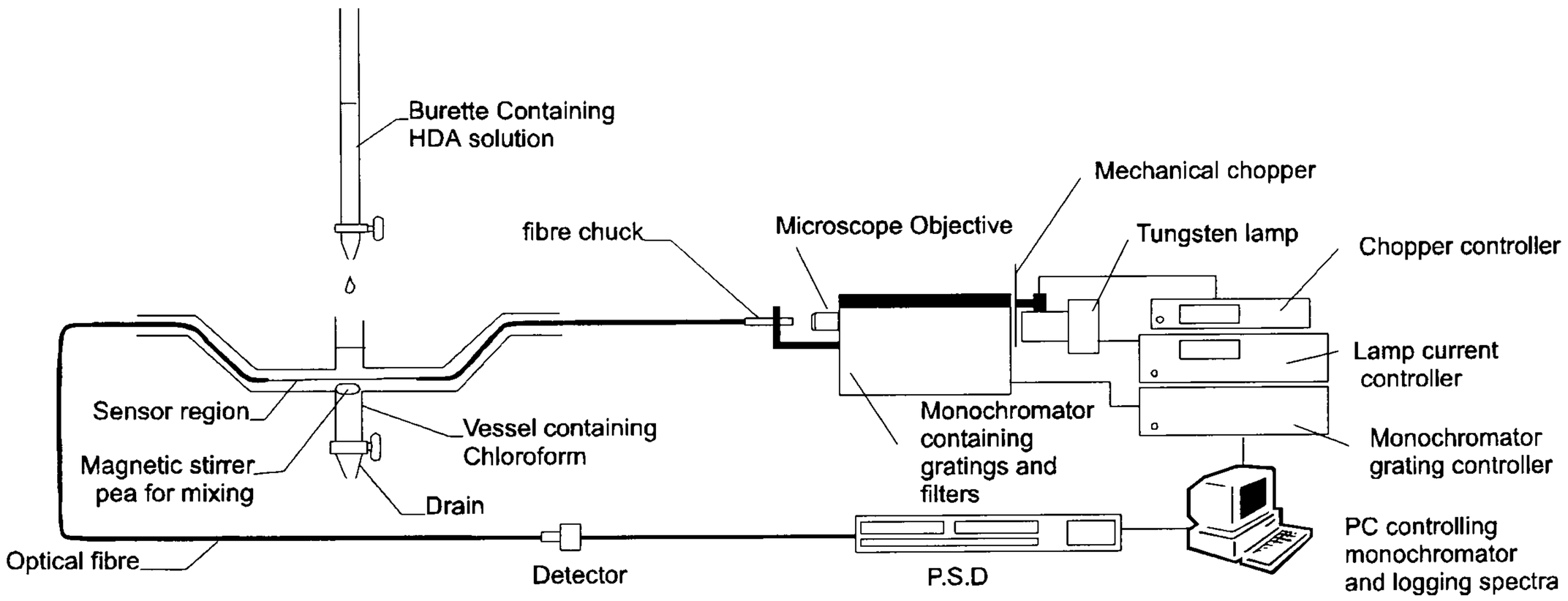

Figure 5-5 layout of arrangement used for measuring evanescent sensor response to changing hexanediamine concentration

Five repeat absorption experiments were performed using the same optical fibre sensor each time. The fibre was thoroughly washed between runs by passing solvent through the apparatus. A baseline spectrum was taken before each experiment to ensure there was no residual hexanediamine solution on the sensor surface.

The measurement of peak heights was taken as the difference between a baseline drawn between the onset and tail of the peak, defined as being at 1500 and 1570nm, and the peak maximum defined as being at 1529nm. This is illustrated in Figure 5-6, which shows from where peak height is measured. This is also the method used to measure successive absorption peak height obtained during the cure monitoring experiments.

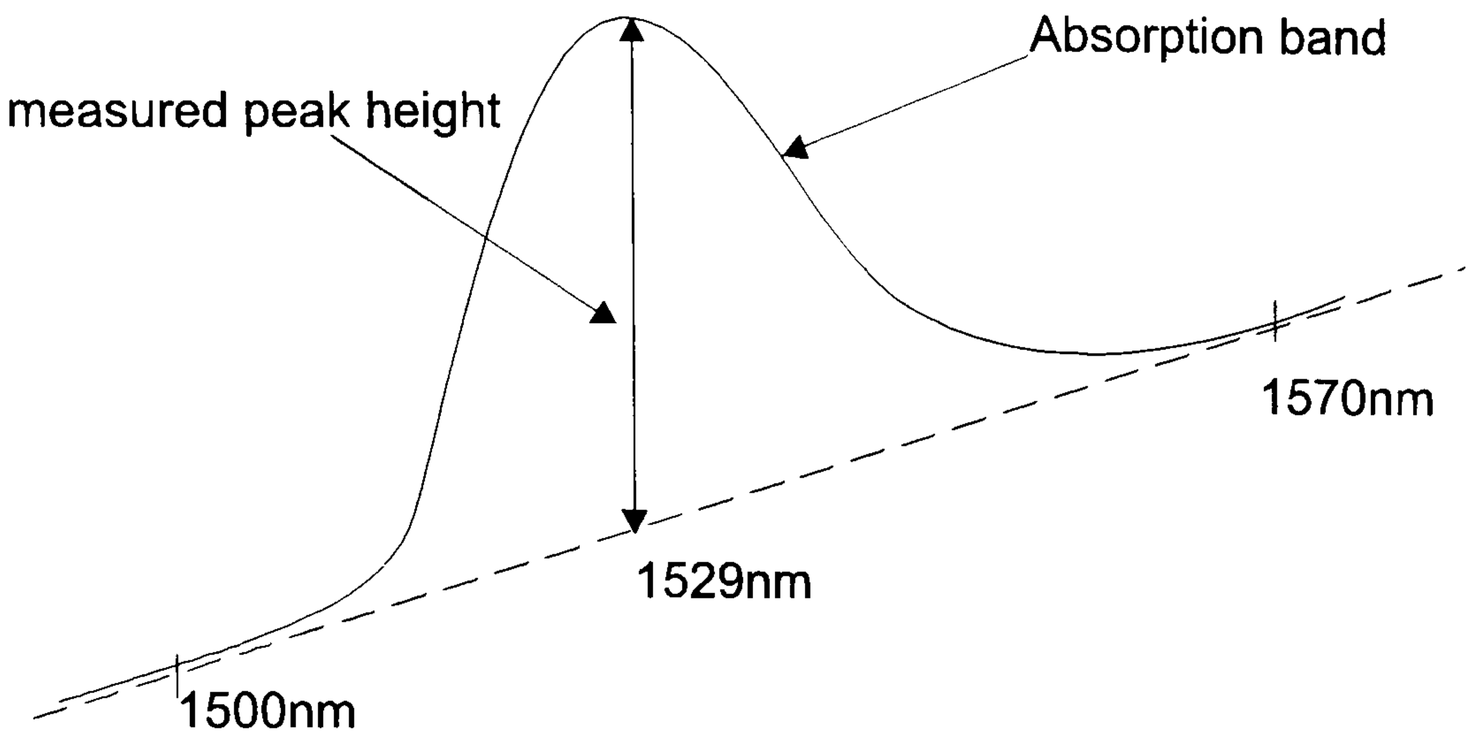

Figure 5-6 Illustration of peak height calculation from raw absorption data

It is more usual practice in the field of spectroscopy to take the peak area as a measure of the strength of absorption. Since the original aim of this project was to utilise single wavelength sources in a cure sensor, peak height was used in the processing of data in these experiments. This is more analogous to sampling of the absorption bands of interest using the monochromatic sources. The validity of this method of analysis was checked by comparing absorbance values calculated using the above method with those obtained using the established technique of baseline corrected absorbance (peak area, see Figure 5-7).

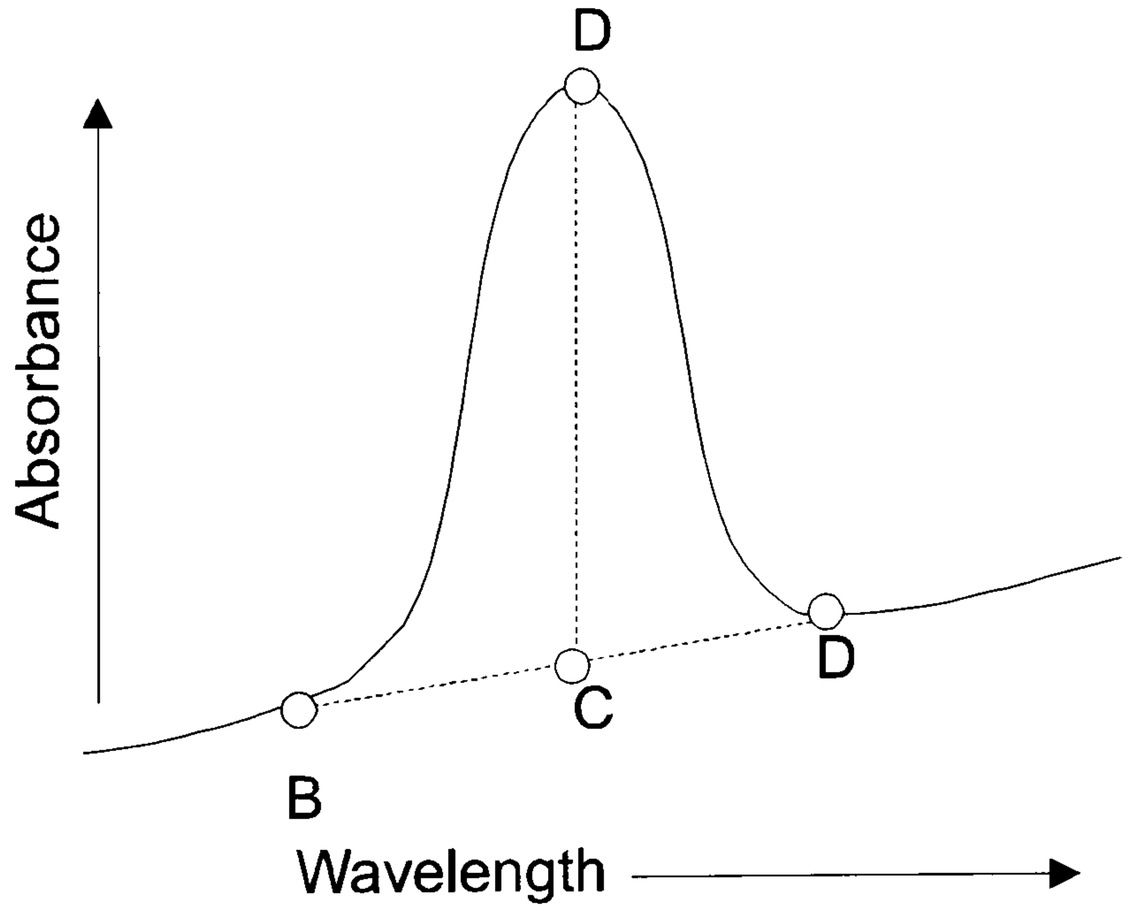

Figure 5-7 Method of calculating baseline corrected peak area from infrared spectrum

Figure 5-8 shows the absorbance values obtained using these two methods plotted on the same graph.

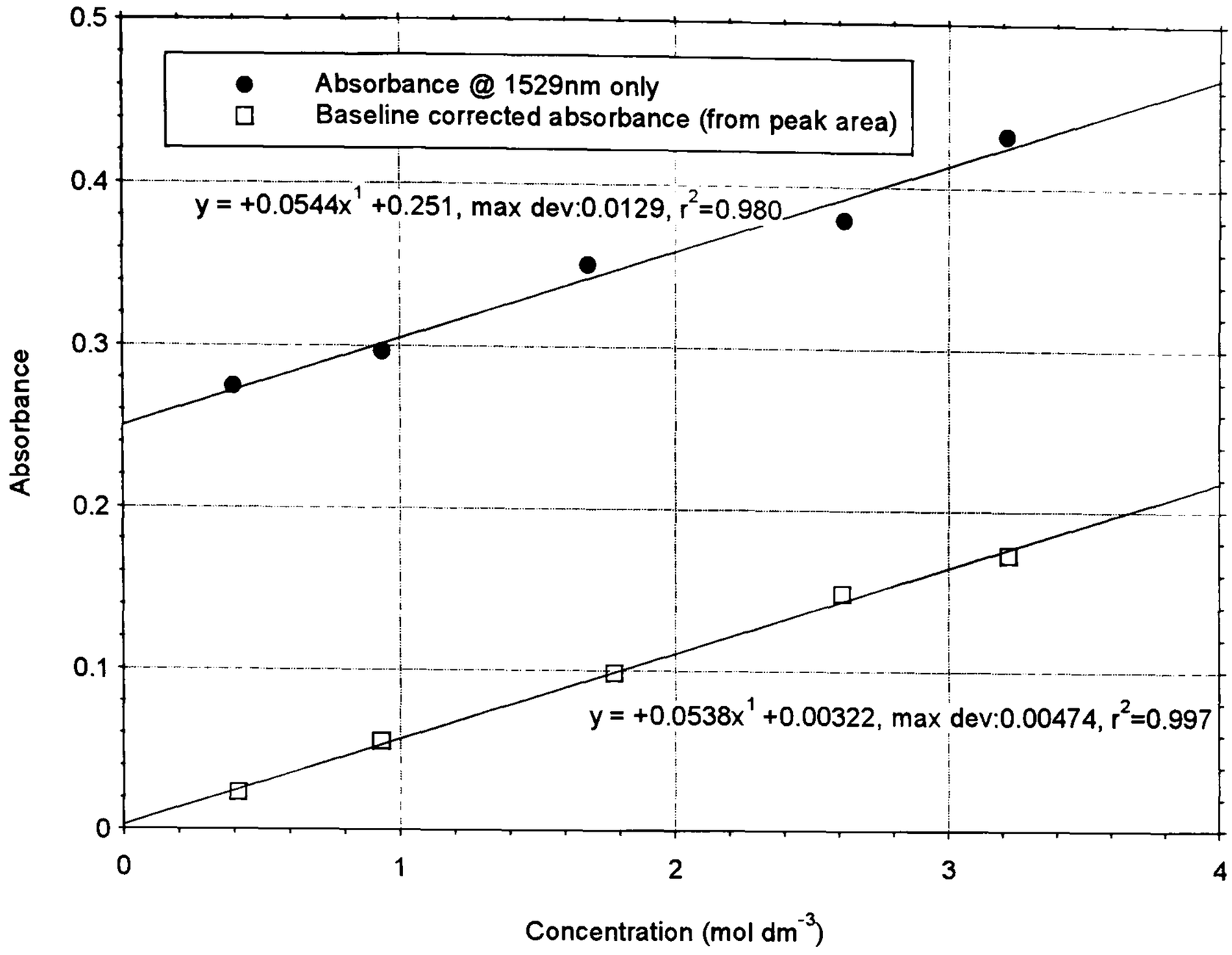

Figure 5-8 Comparison between specific wavelength calculated absorbance and baseline corrected absorbance (based on peak area) for solutions of hexanediamine in chloroform.

It can be seen that although the two methods are offset on the absorbance axis the two are comparable and that the single wavelength method compares well with the established quantitative method of baseline corrected absorbance.

5.3.5 Evanescent absorption cure monitoring of resins

Resin cure monitoring was carried out using the high index optical fibre. The epoxy equivalent weight of the Epikote 828 resin was determined using the ASTM standard D 1652-90 test method B [196]and found to be 187. This method entailed titrating a sample of the resin mixed with a tetraethylammonium bromide solution in acetic acid with a solution of perchloric acid in glacial acetic acid and a crystal violet indicator solution. From the volume of perchloric acid reagent used to titrate the specimen the weight percent of epoxide and the epoxy equivalent weight were calculated. The stoichiometric ratio by weight of resin to hardener was found to be 1 part resin to 0.155 parts hexanediamine. All resin samples used in the cure monitoring samples were made up to this ratio.

Several factors had to be taken into consideration in conducting the resin cure experiments these being:

i) **accurate temperature control**. Experiments were to be carried out at the same four temperatures as FTIR and DSC experiments, namely 30, 40 50 and 60°C. It was thus

necessary to find a way of accurately controlling the resin temperature. This was done in one of two ways. Earlier experiments with shorter sensor lengths were conducted on a temperature controlled hotplate. The sensor was placed on the hotplate on a thin metal sheet and the resin poured on top of it contained by a dam. Monitoring with thermocouples placed at various positions within the resin showed that the temperature stability of this setup was to within ±0.3°C of the temperature controller setpoint. Temperature control in experiments carried out with longer sensor lengths was performed by threading the sensor through gently curving glass tube which, after addition of the resin, was sealed and partially immersed in a temperature controlled water bath. The temperature stability of this method was seen to be much improved at ±0.1°C. This method also had the added advantage of ensuring the fibre had the same curvature and position for each experiment.

ii) **launch conditions**. The evanescent absorption effect depends on the absorption of the evanescent wave. In a multimode fibre the higher order modes make the biggest contribution to the evanescent wave and so ideally these modes should be excited preferentially. This is explored in Section 5.4.8; "Sensor enhancement". Since only a short length of fibre (typically 2-3m) was to be used for each sensor the modes excited on launching light into the fibre should be preserved up to the sensor region[191]. It was thus necessary to ensure that for a set of evanescent cure experiments the launch conditions should be identical for each sensor. Light was launched into the fibre using a microscope objective having a numerical aperture slightly greater than that of the fibre to ensure all of its guiding modes were excited. The launch conditions were optimised for each sensor using the micropositioners present on the output of the monochromator. The sensor fibre was placed into the fibre chuck before the resin was applied to the sensor region. The chuck was then placed at the focus of the monochromator launch objective, which was at the output slit of the monochromator. The other end of the fibre was attached to a photodetector, which was in turn connected electrically to the phase-sensitive detector. Light was launched into the fibre at 1550nm and the micropositioners were then adjusted until the signal reaching the phase-sensitive detector was at a maximum;

iii) **sensor construction.** Great care was taken to ensure that all sensors were constructed from a similar length of high refractive index fibre. The fibre ends were cleaved using a commercial optical fibre cleaver and inspected under x10 magnification to ensure

that the fibre end faces were perpendicular to the fibre and there were no splinters or cladding residues to obscure light being launched into the fibre.

Previous work by other researchers utilising optical fibre evanescent absorption sensing had shown that sensor lengths of the order of at least 10cm were needed in order to obtain a reasonable evanescent absorbance signal (see for example DeGrandpre and Burgess[100]). Several sensor lengths were tried in this investigation, during preliminary experiments, ranging from 2 to 25cm. Short sensor lengths were tried since for an *in-situ* technique desirable to try and localise the sensing area to obtain better spatial information. Sensor lengths of smaller than 10cm were observed to produce little evanescent signal. A sensor length of 18cm was found to produce a good evanescent signal and was of a length compatible with the scale of the experimental apparatus and volumes of resin being used.

Data were obtained using the evanescent sensor at four isothermal temperatures; 30, 40, 50 and 60°C, ten repeat experiments being performed at each temperature. The sensor was fabricated from high index fibre (core index 1.65, core radius 60μm and sensor stripped length 180mm). Isothermal temperature was maintained using a water bath into which a sealed vessel containing the resin and sensor was immersed. This kept the temperature constant to ±0.5°C throughout the cure period.

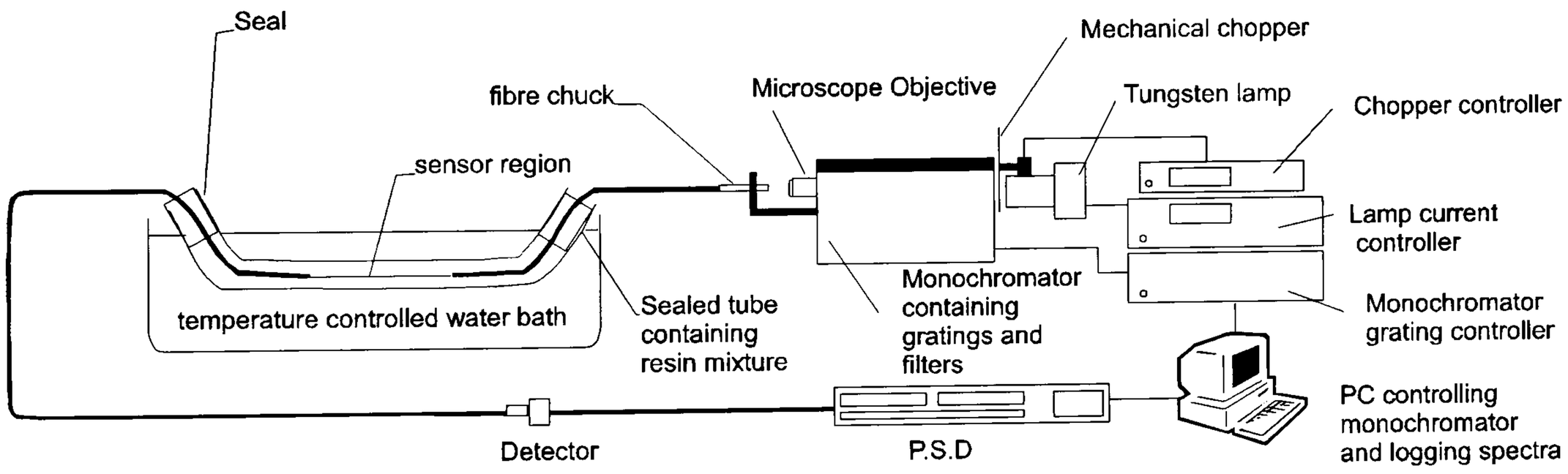

Figure 5-9 Schematic diagram of experimental setup for monitoring of resin cure

This minimised temperature fluctuations throughout the time frame of the experiments. A schematic diagram of the experimental setup can be seen in Figure 5-9.

Spectral scans were made in the wavelength region 1470-1590nm to cover the amine hardener absorption band. The transmission spectra were converted to absorption spectra by ratioing to a baseline taken before the sensor was immersed in the resin using the standard spectroscopic equation for absorbance:

$$A = \log\left(\frac{I_0}{I}\right)$$

- 5.28

Where I_o is the measured transmission intensity, at a specific wavelength, in air and I the measured intensity in the resin at time t.

5.3.6 Sensor enhancement

The absorption signal seen with the evanescent sensor during preliminary experiments was small compared to the background. For this reason an investigation was carried out to determine whether it was possible to enhance the sensitivity of the optical fibre sensor by making modifications to its geometry an the geometry of the launch conditions. Sensor enhancement is discussed in the literature review, in section 3.3.3.2. and, following the ideas put forward by a number of the papers in this section, several geometry modifications were tried.

The modifications investigated were:

i) numerical aperture of the launch optics;

ii) masking of the launch optics to preferentially launch higher order propagation modes;

iii) profiling of the sensing region of the fibre.

5.3.6.1 Numerical aperture

The standard ATR penetration depth equation predicts a greater penetration depth of the evanescent wave at angles close to the critical angle of the fibre. This would result in an increased sensitivity to an absorbing cladding. An experiment was carried out to determine whether this effect could be observed with the optical fibre evanescent sensor. The critical angle of an optical fibre is directly related to its numerical aperture since the numerical aperture is equal to the sine of the acceptance angle of the fibre. The high refractive index fibre has a numerical aperture of $\sqrt{(1.65^2-1.41^2)}=0.86$ corresponding to an internal critical angle of 58.7°. Launching light at with launch optics having a numerical aperture smaller than this will result in the light at the sensor interface being incident at angles smaller than the critical angle.

A sensor was fabricated from a 150cm length of high refractive index optical fibre from which the silicone cladding had been removed over 10cm to create a sensing region. The

sensing region was immersed into a solution of ethylenediamine in isopropyl alcohol made up to a ratio of 1:1 by volume. The launch end of the sensing fibre was connected to the fibre monochromator and the output end to the detector as for the cure experiments. Wavelength scans were made over the spectral range 1500-1600nm with each of three launch microscope objectives in turn. The launch objectives had the following numerical apertures:

i) 0.9, overfilling the fibre and ensuring that all propagation modes were excited;

ii) 0.8, slightly under-filling the fibre and making the maximum angle of incidence 53.1°;

iii) 0.7, maximum launch angle 44.4°;

iv) 0.4, maximum launch angle 23.5°;

v) 0.2, maximum launch angle 11.5°.

5.3.6.2 Masking of objectives

In a paper by Ruddy *et al.* [60] an annular mask is used to "filter spatially" the light launched into a fibre to those modes having "substantial power in their evanescent field in the unclad region". The mask is said to remove the lower order modes that make little or no contribution to the power in the evanescent field. However, there is no comparison in this paper between a sensor using launch geometry utilising a mask and one without to provide a quantitative measure of the enhancement afforded by such a mask.

Experiments were conducted into whether masks of this type could increase the sensitivity of the evanescent absorption sensor described here. A fibre sensor was fabricated as before, the sensor region immersed in a 1:1 by volume solution of ethlyenediamine and iso-propyl alcohol and the ends connected between the monochromator and a detector. The diameter of the entrance to the launch objectives was measured as 12mm. Masks were fabricated from 10mm diameter circles of 50μm acetate film. A spectrum of the laminate film was taken before commencing to ensure the film itself had no absorptions in the 1500-1600nm range. The spectrum showed a region free of absorptions between 1400 and 1620nm.

A standard computer drawing package was used to draw black circles of 2, 3, 4, 5 and 6mm in diameter. These were printed onto the acetate film with a laser printer and when

cut out created 12mm masks with central opaque areas of the above diameters. These masks were placed in turn into the open end of 0.9 numerical aperture launch objective in turn and a wavelength scan recorded between 1500 and 1600nm. The scans were then compared. A schematic of the experimental arrangement can be seen in

Figure 5-10.

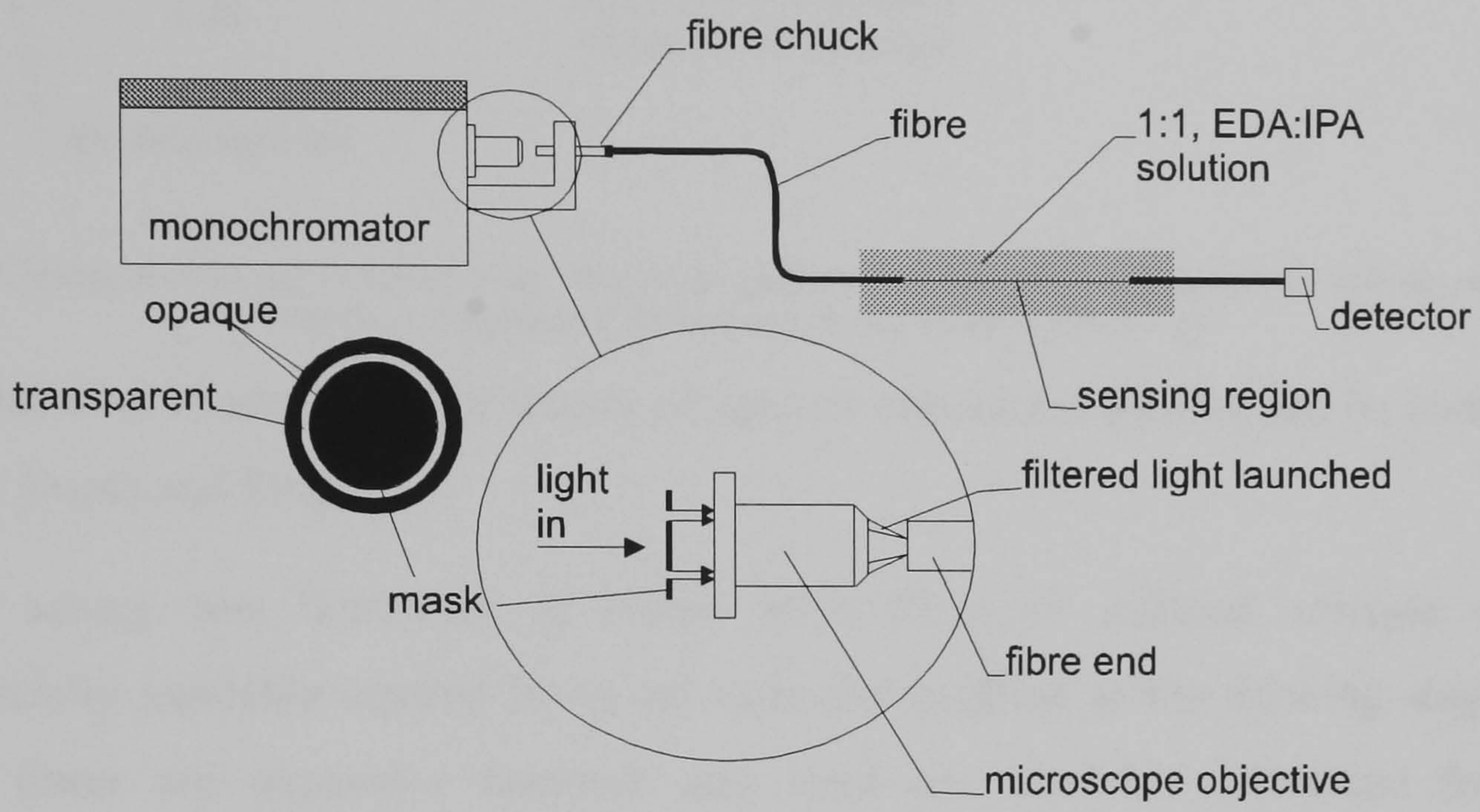

Figure 5-10 Experimental arrangement for masking experiments

5.3.6.3 Tapering of the sensing region.

Another method of evanescent absorption sensor enhancement which has been suggested in the literature is the tapering of the sensing region[65, 94]. The basic idea behind tapering is that if the sensing region is gently tapered then light propagating in the tapered region strikes the core/analyte interface at an angle greater or closer to the critical angle of the fibre. This results in some loss of the higher order modes which are radiated from the tapered region as they strike it at greater than the critical angle. It also results in an increased penetration into the analyte of the evanescent wave belonging to the lower order modes. These would normally contribute little to the energy of the evanescent wave. An illustration of this can be seen in Figure 5-11.

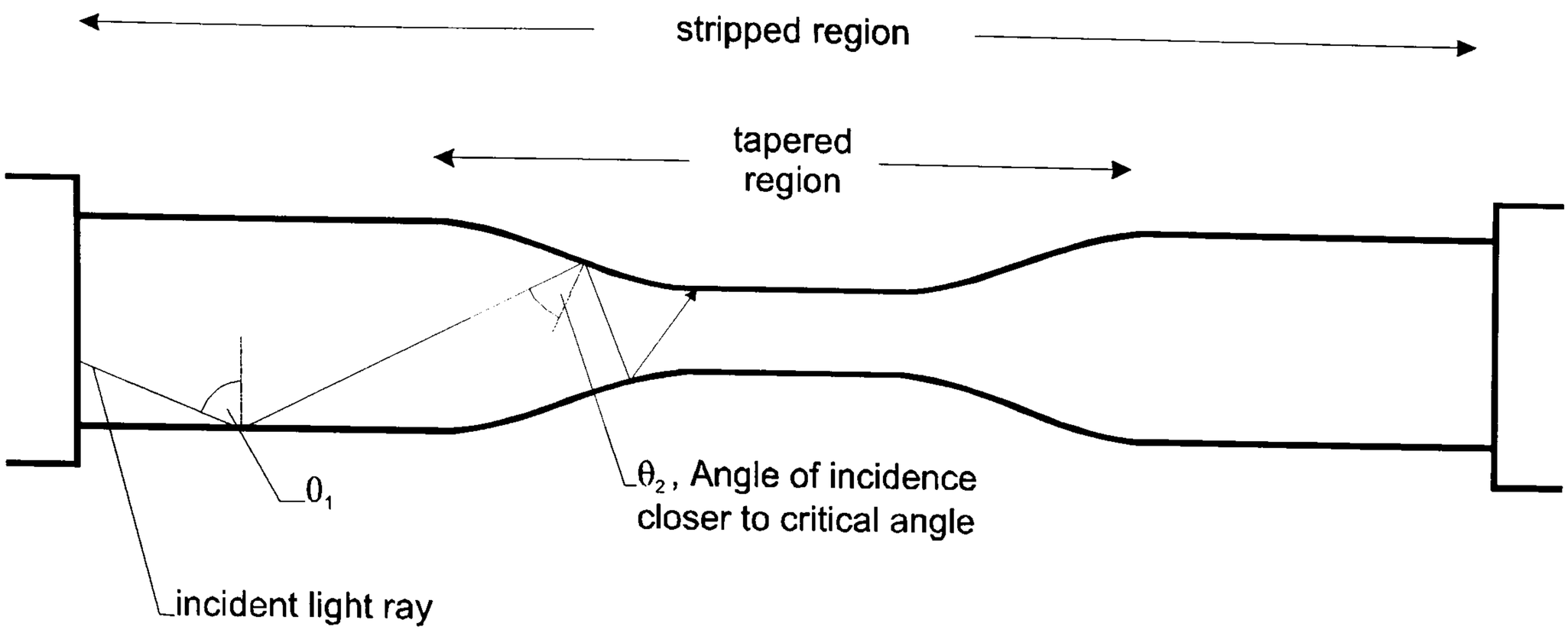

Figure 5-11 Diagram showing the effect of tapering on the angle of incidence of propagating light with the core/analyte interface (longitudinal dimensions greatly reduced for clarity).

A mathematical treatment of the theory of tapered evanescent sensors can be found in the paper by Gupta and Singh[95].

A fibre sensor was fabricated as before with 10cm of stripped silicone cladding. Commercially available tapered fibres are normally profiled at the drawing stage. These tapered fibres are expensive however and were not available fabricated from high refractive index fibre. It was therefore necessary to attempt profiling of the sensing region of the sensors in the lab. To perform this a BIT programmable fusion splicer was used.

A fusion splicer joins or "splices" the ends of two optical fibres together to form a single fibre. This is done by means of an electrical arc that locally heats two aligned fibre ends to a point where the ends become softened. The fibre ends are then pressed or "stuffed" together whereupon the softened fibre ends fuse. The programmable nature of the BIT BFS-60 fusion splicer gave control over the arc current, and the movement distances of the fibres during the fusion process. This meant that by putting the stripped region of a sensing fibre into the splicer it could be made to melt a short portion of the fibre and then apply tension to this region producing a taper.

Some preliminary tests were performed on silica fibre and it was found to be possible to produce repeatable tapers, 5-7mm in length. The fibre core was reduced to half of its unstretched diameter at the centre of these tapers. Applying the same technique to the high index fibre was found to be problematic. The glass from which this fibre was made had a much lower melting point than that of standard silica making it much more liable to degradation and disintegration in the splicer arc. After many tests it was found that with the lowest current setting (20mA) on the splicer and a drawing rate of 0.5mm min^{-1} it was

possible to produce 3mm profiles in the fibre. Several sensors were prepared. The first had a single 3mm profile, the second had three 3mm profiles. A single sensor with a 7mm profile in its sensing region was also produced. The sensors thus prepared were immersed in a solution of ethlyenediamine made to a ration of 1:1 by volume. The ends of the sensing fibre were then connected between the monochromator and detector and, as in the previous experiments, scans made between 1490 and 1600nm.

5.4 Results and discussion

5.4.1 Chemical sensing-proof of concept

The initial experiments aimed to investigate whether an evanescent absorption effect could be observed using the available equipment. The first set of experiments used an LED emitting with a centre wavelength of 830nm and a copper chloride solution which had a broad absorption covering this region. The experiments were performed as described above, an evanescent sensor being transferred from air to methanol to a solution of cuprous chloride in methanol and back, with the sensor output being continuously monitored.

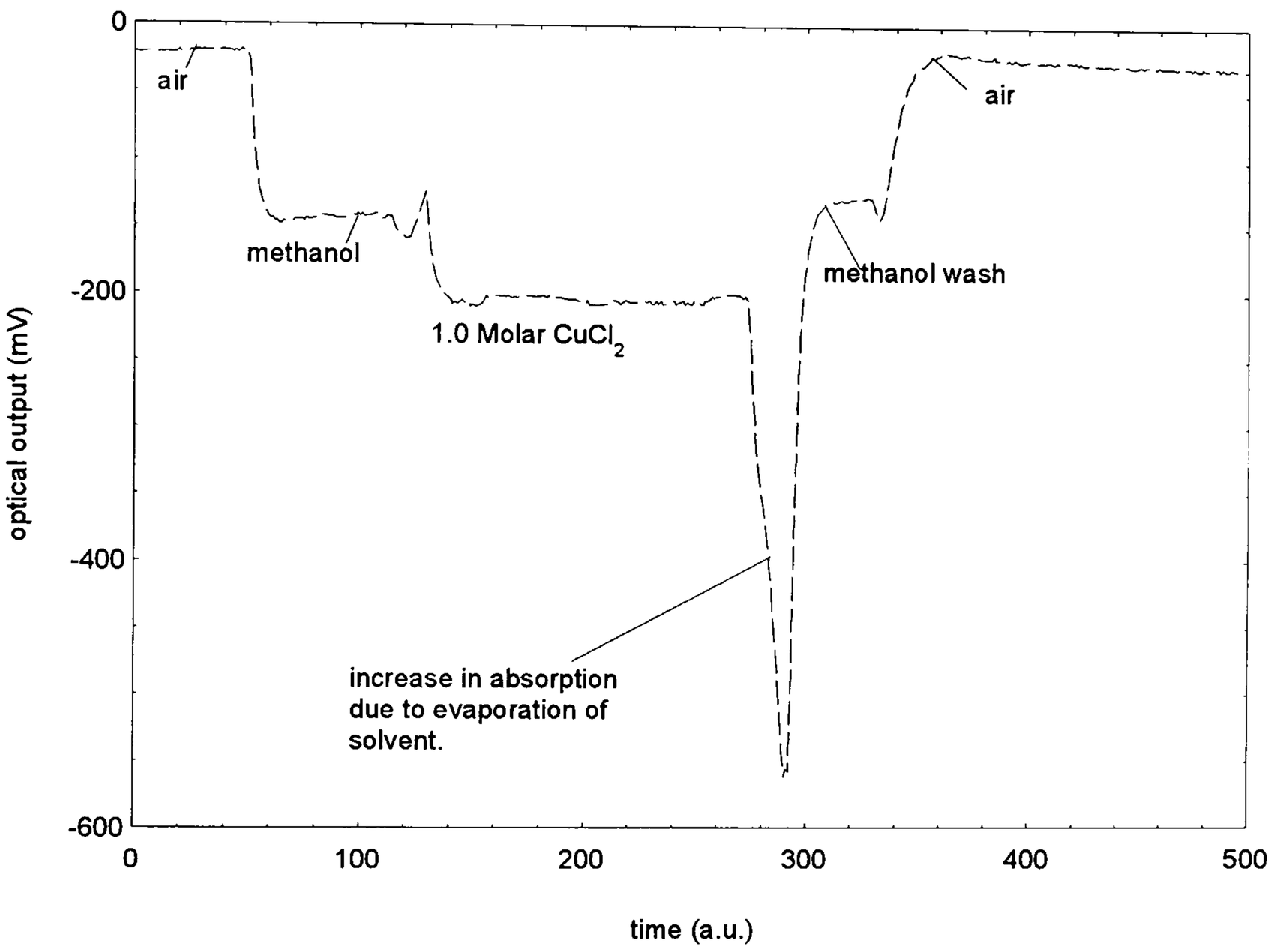

Figure 5-12 Output from evanescent sensor, operating at 830nm in 1.0 molar cuprous chloride solution in IPA

A typical sensor signal can be seen in Figure 5-12. The signal shows a clear decrease when placed in the methanol, this is because of the difference in refractive index and air. Air having a lower refractive index than the methanol actually provides a better cladding and so guiding is stronger. There is another clear decrease on immersion in $CuCl_2$ and this is due to the absorption of the evanescent wave. Upon removal from the solution the concentration of $CuCl_2$ increases greatly as the solvent evaporates and this can be seen as the negative going "spike" on the figure. Figure 5-13 illustrates this. This is a graph of the difference in signal between pure solvent and solutions of various concentrations obtained from immersing the sensor in them, plotted against the concentration.

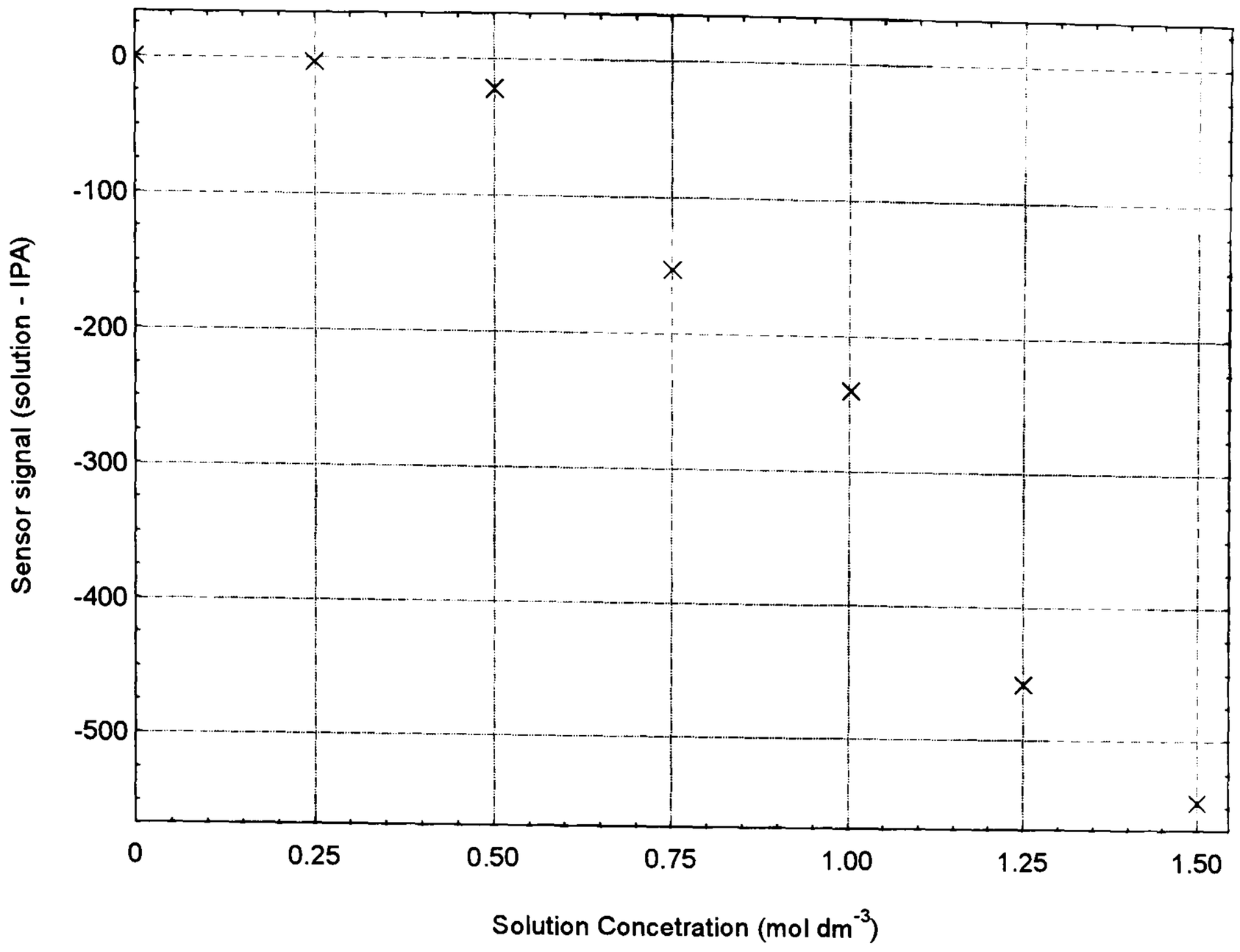

Figure 5-13 Change in sensor signal with increasing concentration of amine in IPA

There can seen to be a clear decrease in signal, *i.e.* an absorption increase, with increasing concentration. It was expected that the increase would be linear, consistent with Beer's law. However, since the length of sensor was very short for these experiments (2mm) it was thought the apparent non-linearity could have been due to the lack of sensitivity and low signal-to-noise ratio at the low solution concentrations. The results obtained using cuprous chloride gave sufficient confidence in the technique to proceed onto the detection of the amine hardeners used in epoxy resin systems. The results from these experiments can be seen in the following section.

5.4.2 Amine sensing

A transmission cell with a pathlength of 3.5mm was used to see if the light emitted by a 1550nm laser was of a wavelength sufficiently close to that at which the amine absorption band occurred to be absorbed. The cell was immersed in solutions of amine of various concentrations and the light transmitted by the optical fibre measured.

The signal was seen to decrease with increasing concentration of amine and this can be seen in Figure 5-14. This is a plot of the signals, converted to absorbances, in the standard way (using $A=\log I_0/I$ where I_0 is the baseline intensity and I the signal in a given solution).

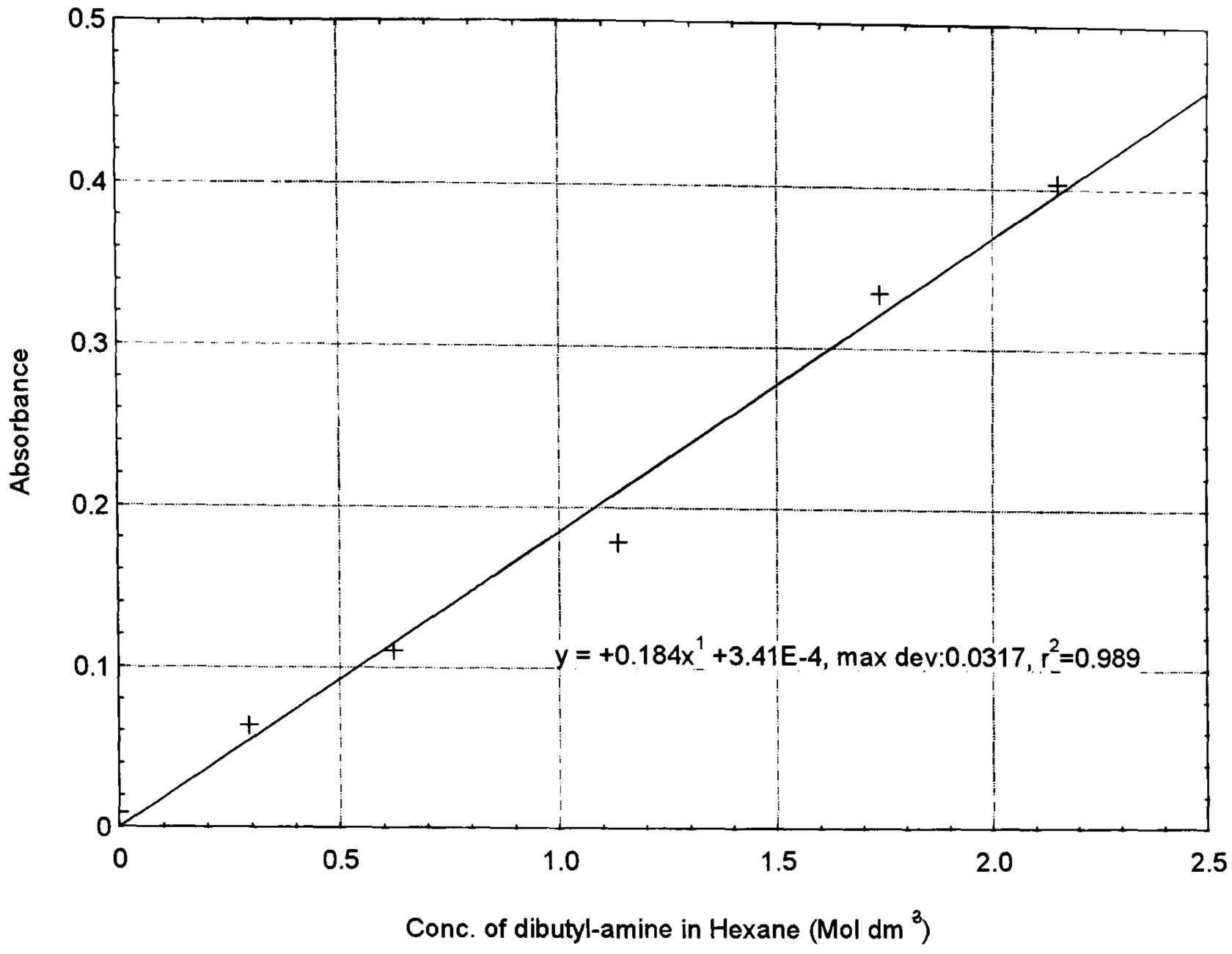

Figure 5-14 Absorbance vs concentration for open path transmission experiment

The absorbances can be seen to be increasing in a linear fashion as predicted by Beer's law with a sensitivity (obtained by using the least squares fit to the data) of 0.181 absorbance units $mol^{-1}dm^{3}$.

The experiment was repeated using solutions of dibutylamine made to the same concentrations but substituting the transmission cell for an evanescent sensor of length 2cm constructed from 200/230 hard clad silica fibre.

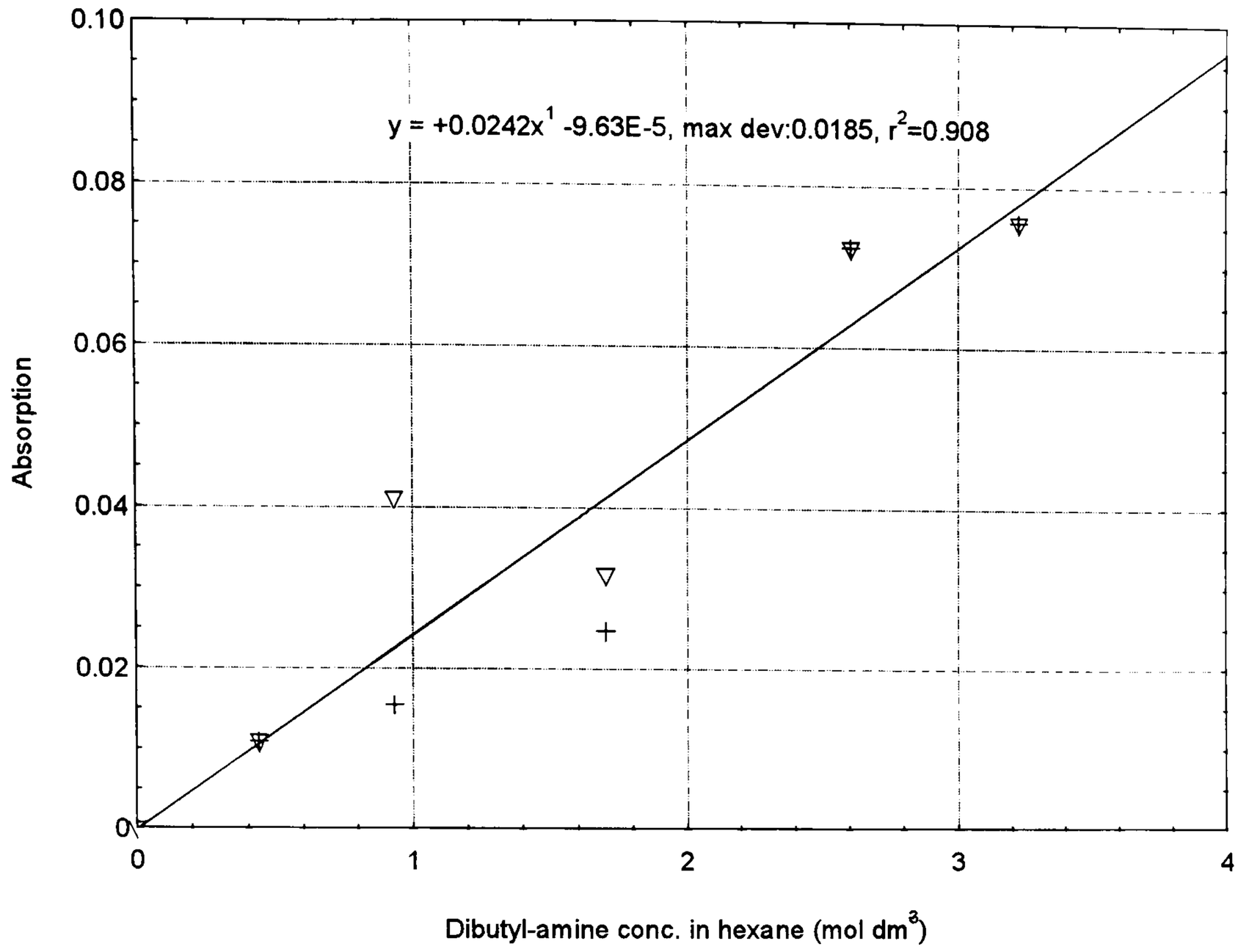

Figure 5-15 Plot of Laser Absorption vs dibutylamine concentration in hexane, 2 repeats, ews

This brief experiment is summarised in Table 5-1

	Transmission cell sensor	Evanescent wave sensor
Pathlength (stripped length) mm	3.5	20
Absorbance *per* mol dm^3	0.181	0.0116
Absorbance $(mol\ dm^3)^{-1}cm^{-1}$	0.517	0.0058

Table 5-1 Summary of amine detection experiment

The main points to be drawn from these results were:

i) the 1550nm lasers were of a wavelength which was sufficiently strongly absorbed by the primary/secondary amine peak centered on 1547nm to allow a moderate concentration change to be detected;

ii) the sensitivity of the evanescent absorbance sensor was smaller by approximately two orders of magnitude to the change in amine concentration used in these experiments;

Further experiments were performed using the apparatus shown in Figure 5-4 in an effort to obtain a more accurate relationship between amine concentration and the observed evanescent absorbance over a wider range of concentrations.

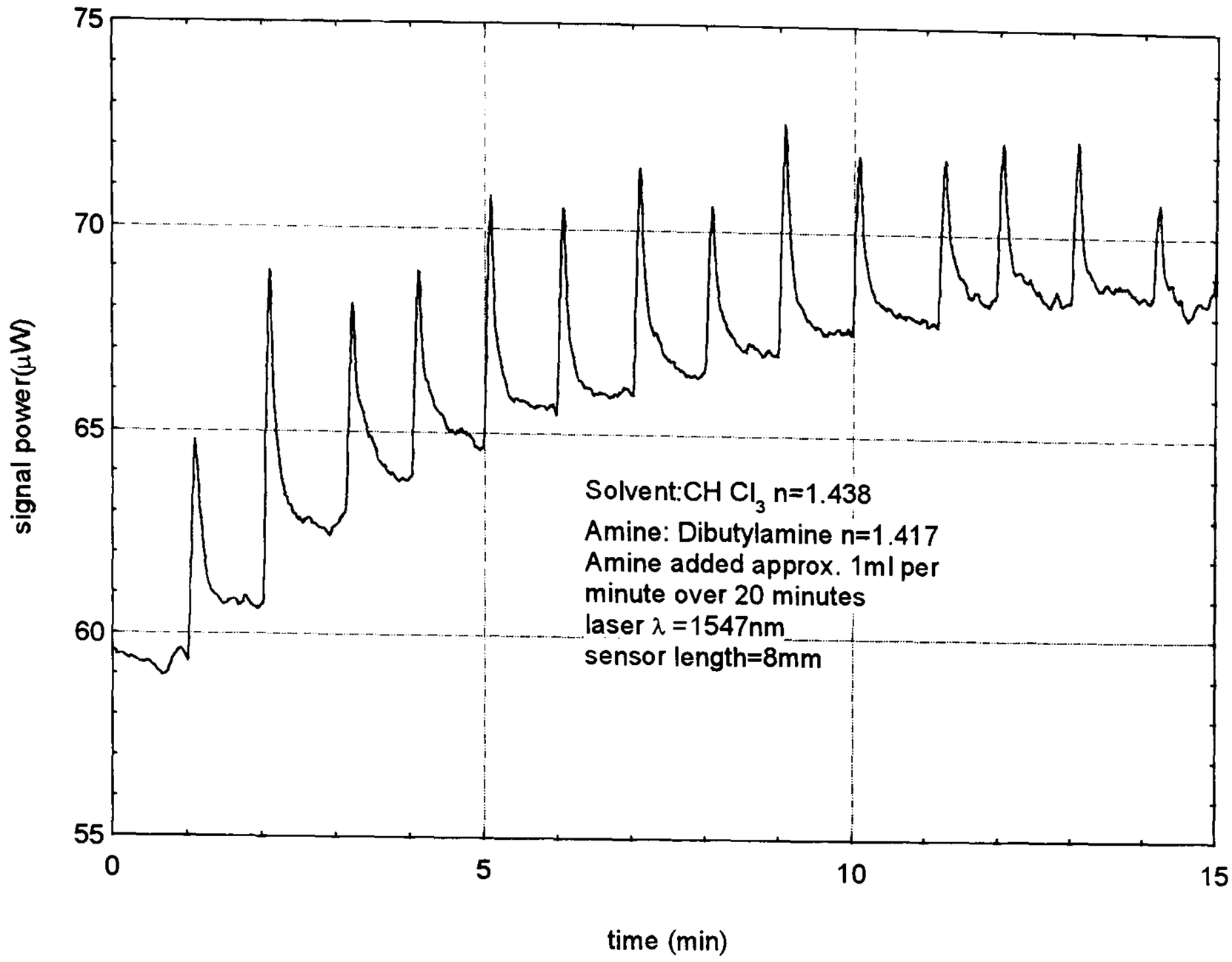

Figure 5-16 Sensor out put vs time for evanescent sensor addition of dibutylamine to chloroform

A typical signal is seen in Figure 5-16. The "spikes" in this curve correspond to the addition of an additional millilitre of amine to the chloroform present in the vessel. The spike decays to a steady value of absorbance as the amine becomes mixed into the solvent with the magnetic stirrer. Interestingly the signal was seen to increase by 25% with increasing concentration of amine over this range of concentration. This was opposed to what was expected and also to the results obtained using discrete solutions where an increase in absorption was seen with increasing concentration. It took a while before it was realised that since the solutions used in this experiment were of a greater concentration than in the previous experiments, there would be a significant change in the refractive index of the solution as increasing amounts of amine were added to the solution. This, in changing the guiding properties of the sensing region, could be responsible for the unexpected signal change. To confirm this the refractive index of the solution as the concentration increased was calculated from the proportions of solvent and amine present. The solutions refractive index was calculated to vary from 1.446 (the refractive index of chloroform) to 1.4434. These refractive index values were substituted into a simple geometrical optics model predicting the signal change due to a refractive index change in a medium surrounding an optical fibre core of refractive index 1.458. This model is outlined in detail in Chapter 6; (Optical Fibre sensor for Refractive index cure monitoring eq^{n} - 6.8)

and is based on the numerical aperture change of the sensing region with changing cladding index.

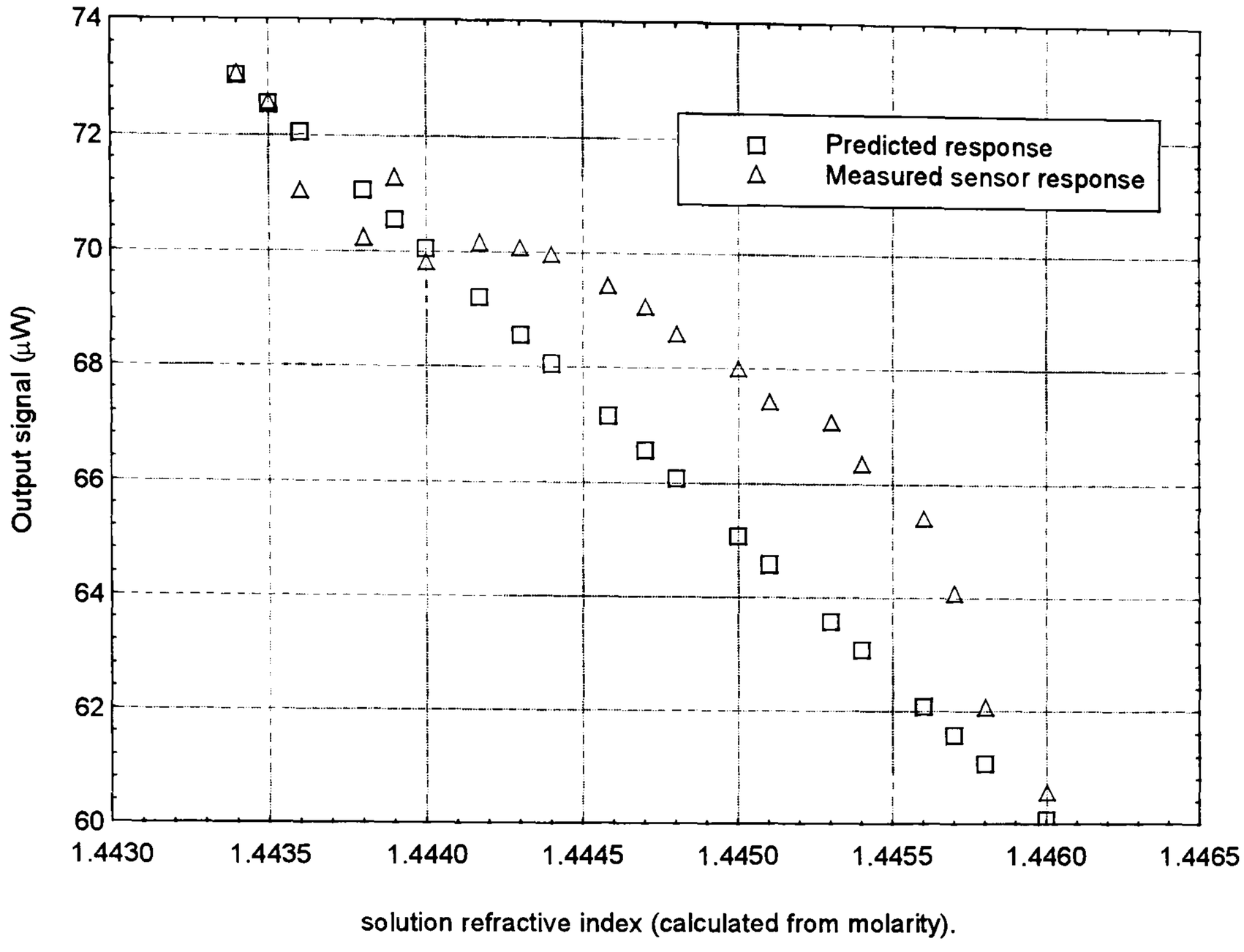

Figure 5-17 Comparison of model and sensor data made from data in Figure 5-16

A comparison of the prediction made by the model and the signal change seen can be seen in Figure 5-17. The agreement can be seen to be sufficiently close to confirm the signal change was due, at least in part, to the refractive index change of the amine solution. The response of the sensor to as refractive index change was utilised as an alternative method of cure monitoring and the experiments performed to investigate this can be seen in chapter 6.

5.4.3 Fibre surface effects

Experiments were conducted to determine whether amine molecules were being preferentially adsorbed onto the cores of the fibres being used to fabricate the sensors. The experimental procedure is detailed in section 5.3.3.

Figure 5-18 is an example of the spectra seen by a hard clad silica fibre sensor over a period of 20 hours.

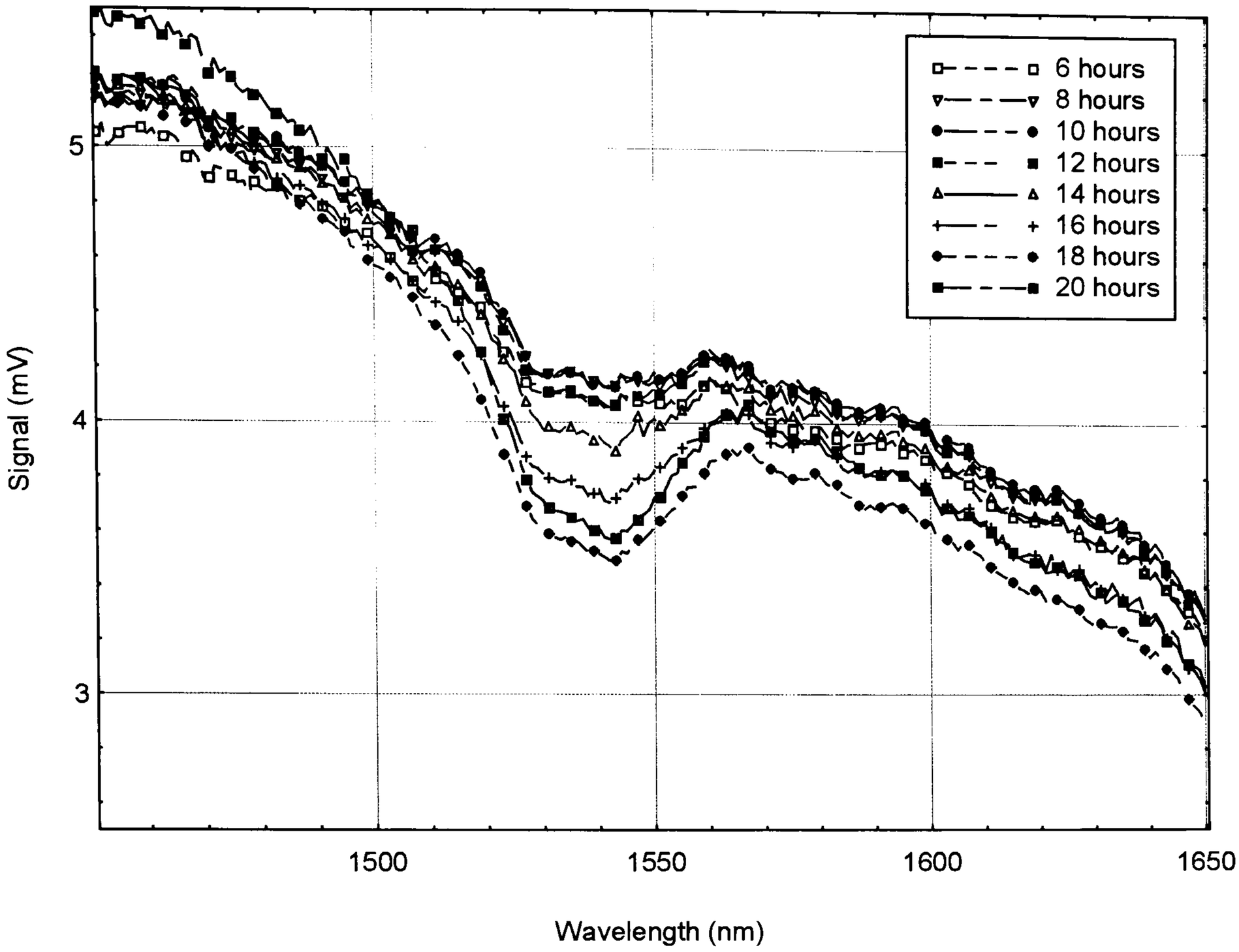

Figure 5-18 Increase in amine absorption peak depth with exposure time to amine solution (hard clad silica fibre)

It can be seen that over this time that the amount of light absorbed by the amine increases steadily. After twenty hours of exposure the absorption can be seen to be more than 2½ times deeper than after six hours exposure. The absorption of final curve was also approximately twice as strong as those seen previously using the hard clad silica fibre sensor. The first, flattest curve on this figure was taken after 10 minutes. Between this time and five hours there was a small increase in absorption between scans However, these scans have been omitted from the plot for the sake of clarity. This set of results suggested that there was some reaction occurring at the fibre/solution interface.

Figure 5-19 shows the spectrum obtained from the same sensor used to obtain the data above. This sensor was rinsed thoroughly in IPA following the acquisition of the data in Figure 5-19 and then immersed in a bath of this solvent for 24 hours. Following this the sensor was dried and a further scan made.

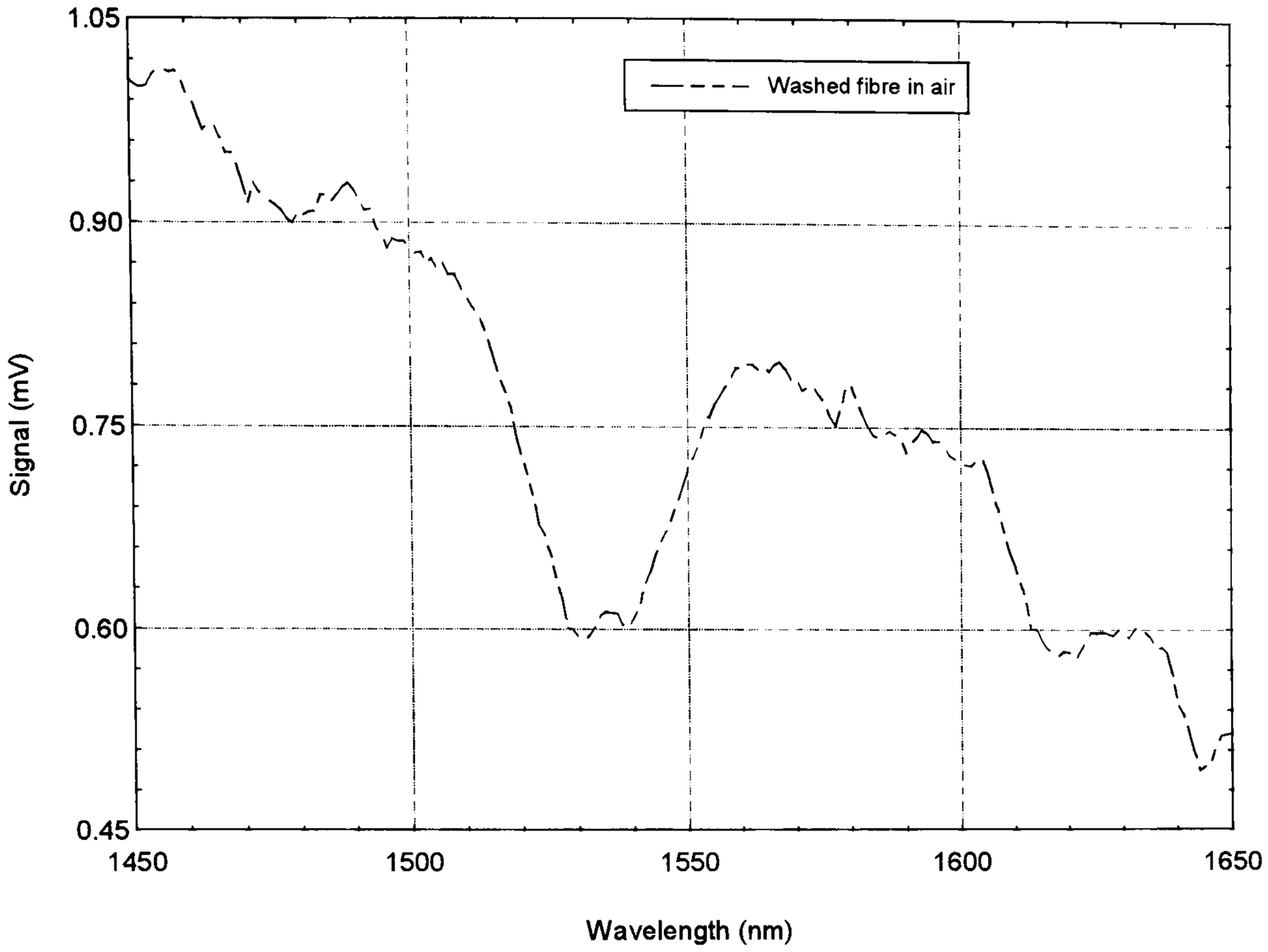

Figure 5-19 Signal obtained from same sensor used for data in Figure 5-19 after soaking in IPA for 24 hours

It can be seen that even after this thorough cleaning process the sensor could still see a strong amine absorption. This effect was seen in the case of all five fibre sensors with which the experiment was performed. This suggests that amine had indeed in some way become adsorbed onto the surface of the hard clad silica fibre. It was thought that possibly a fibre "sensitised" in this way may have been useful as a sensor in itself. It was thought that if a fibre which had been soaked in amine was embedded in a resin/hardener mixture or composite pre-preg which was then cured, the surface-adsorbed amine might be consumed in the cure reaction. The depletion of this amine could then be monitored since the initial absorption seen by these sensors was stronger than those seen previously the signal-to-noise ratio and hence the sensitivity would be improved.

The experiment was repeated with the high refractive index fibre using an identical method. The data obtained from a single repeat of this experiment can be seen in Figure 5-20.

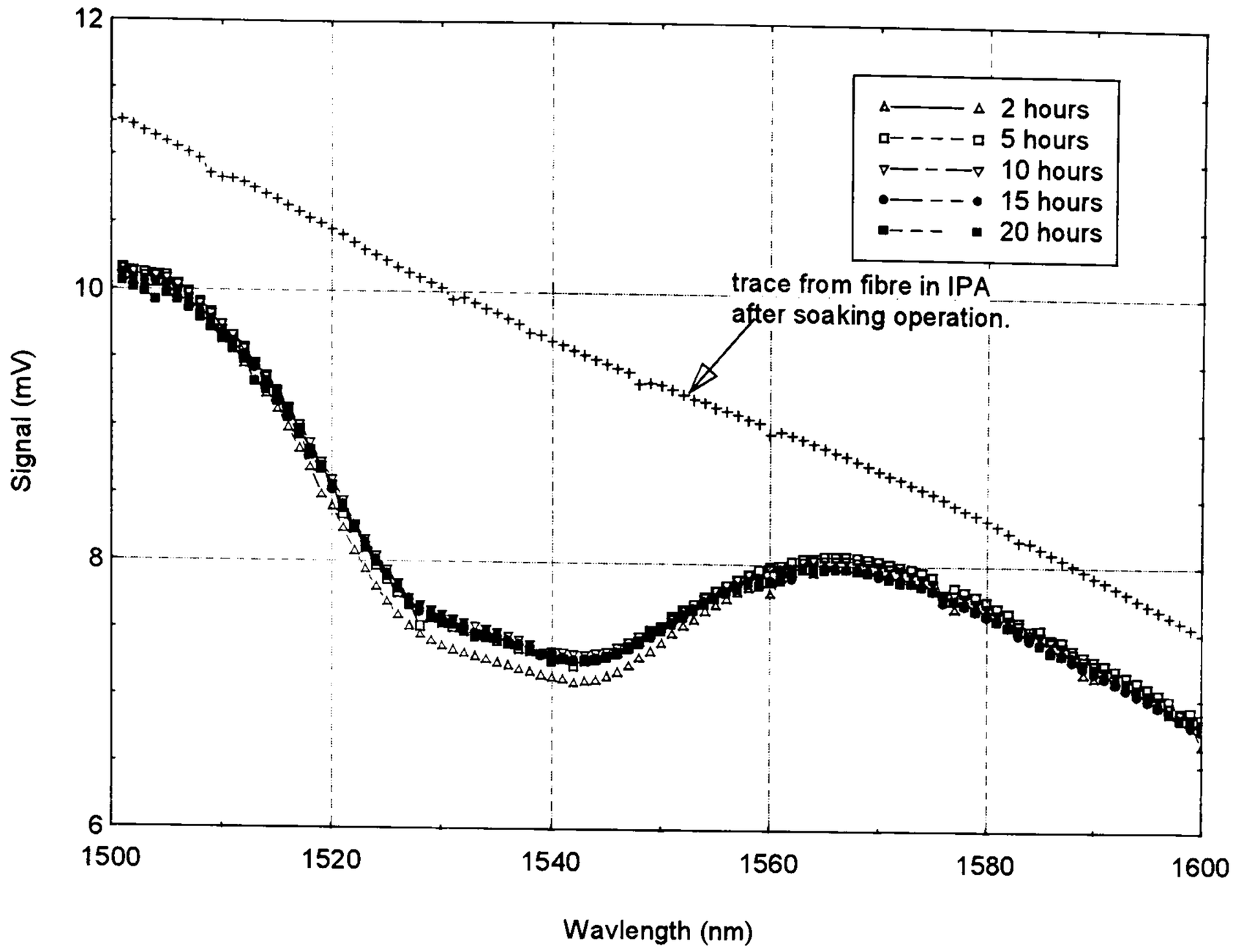

Figure 5-20 Change in amine sensitivity of high refractive index ews with soaking in amine solution.

It can be seen that there is very little change in the absorption band over the time where each fibre was immersed in the amine solution (twenty hours shown on this graph). Again the fibres were washed after the immersion process and a spectrum taken in air. The uppermost curve in Figure 5-20 shows this trace and it can be seen that there is no residual effect from the amine soaking.

These experiments showed that although the amine hardener being used in the investigations was in some way adsorbed onto the core surface of a standard silica optical fibre this was not the case for the high refractive index fibre and so this fibre was suitable for the cure monitoring of resin systems using such hardeners.

5.4.4 Verification of validity of evanescent absorbance models

Experiments to compare the predictions of models from the literature and an original model were performed. An 18cm sensor was immersed in chloroform and known quantities of a hexanediamine solution were introduced. The evanescent absorption spectrum at each concentration was recorded and compared to the absorbance predicted by the models at the same concentration. The experimental method is described in section 5.3.4

An example data set obtained from the Bentham spectrometer setup can be seen in Figure 5-21 for increasing concentrations of hexanediamine in chloroform.

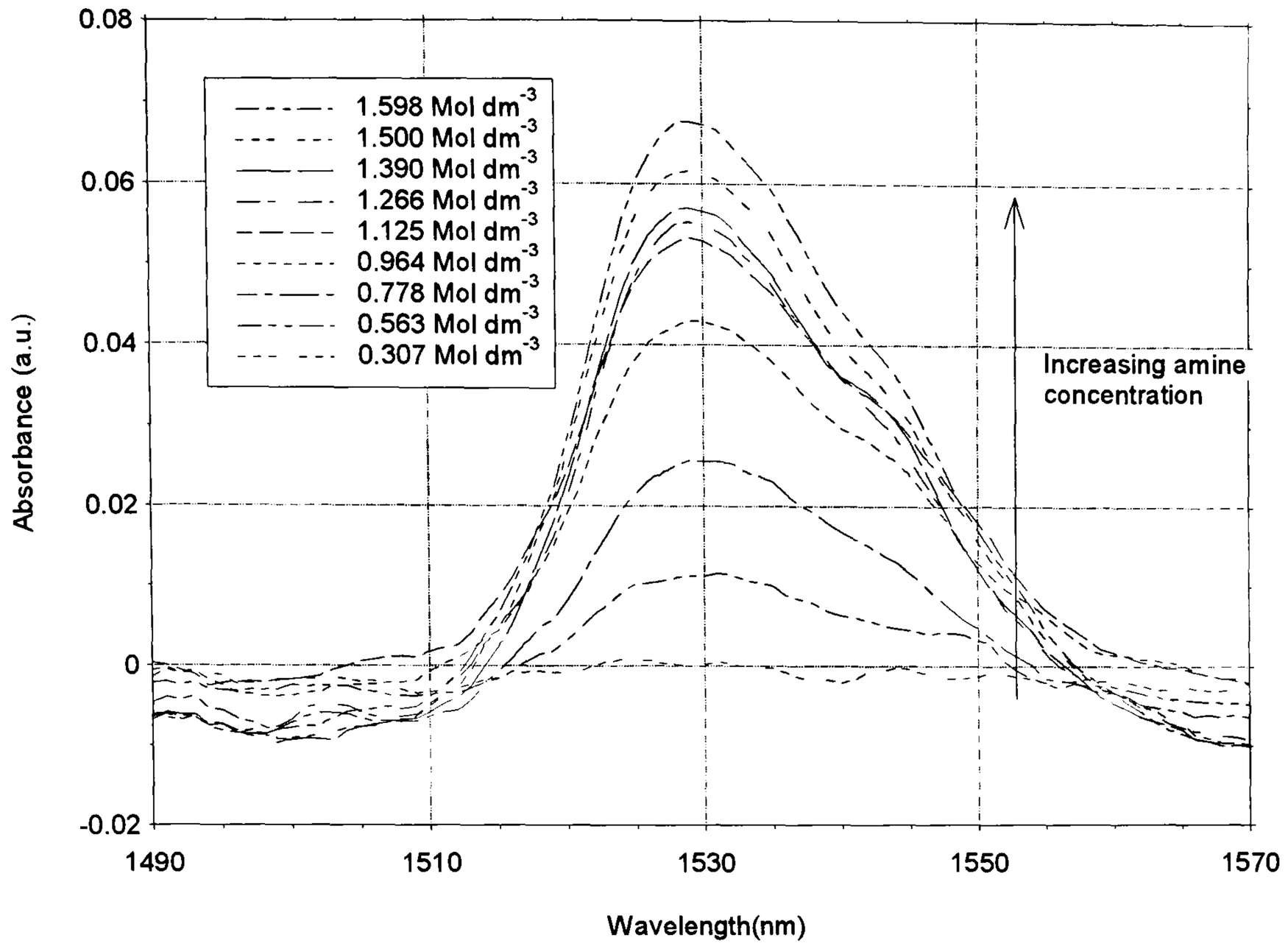

Figure 5-21 Evanescent absorbance data. hexanediamine in $CHCl_4$

This figure demonstrates the increasing absorption peak height with increase in amine concentration. It can also be seen that the absorption baseline remains relatively constant (*i.e.* there is little baseline effect due to refractive index change of the solution). The peak height from five repeats of the experiment was measured using the single wavelength method outlined above and using a centre wavelength of 1529nm. The peaks heights plotted against solution concentration can be seen in Figure 5-22.

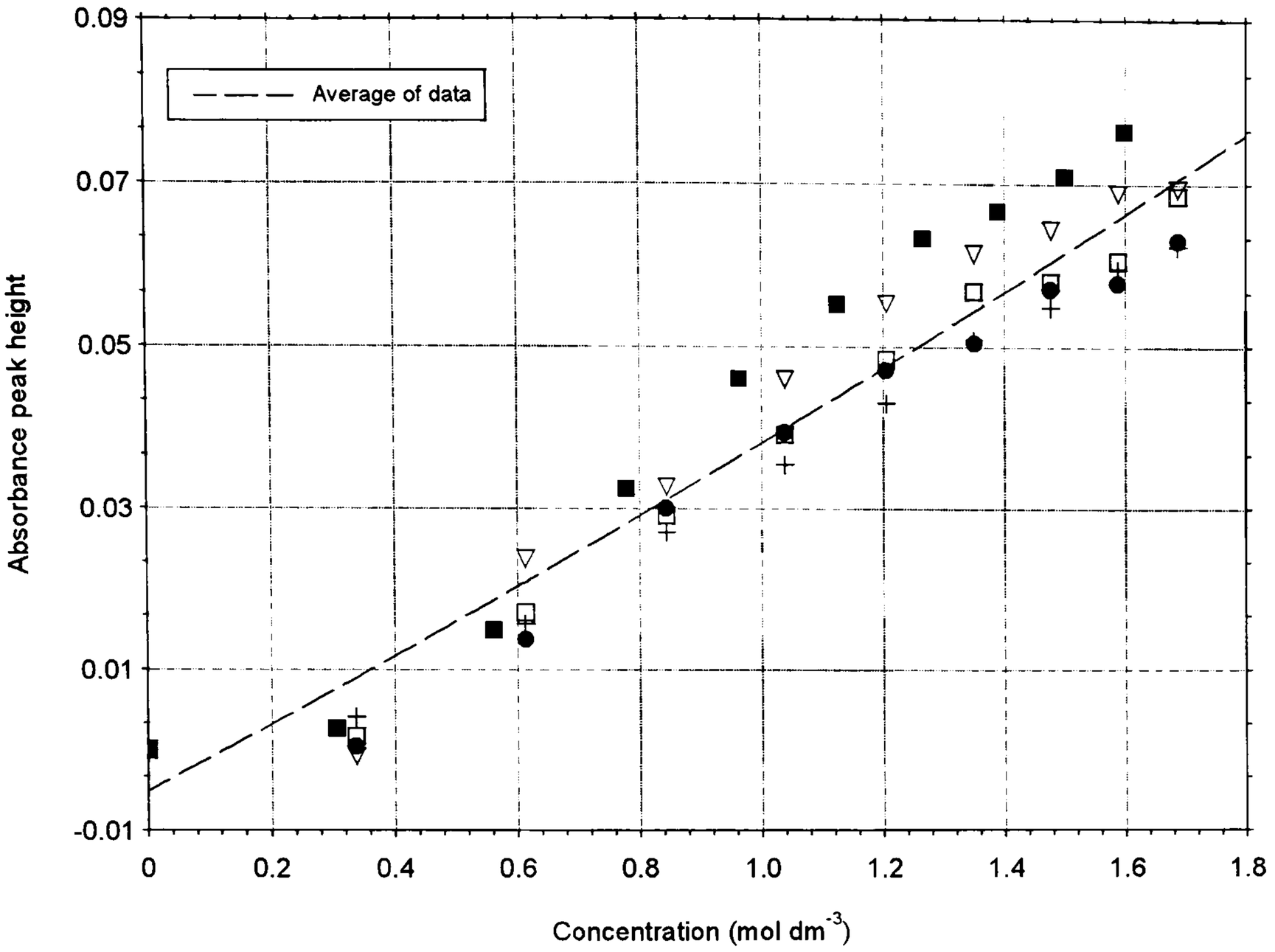

Figure 5-22 plot of absorbance peak height vs solution concentration of hexanediamine in $CHCl_4$ (five repeats)

Also plotted on this graph is the mean value of all the datasets. There can be seen to be a reasonable level of repeatability in these data. The maximum standard deviation was calculated as being 0.008 absorbance units and the maximum error on the mean value 0.004 units.

To compare these data with the models from the literature and also the author's penetration depth model, the model equations were entered as worksheets into the Mathcad mathematical program. The values for the optical fibre properties, the solution refractive indices and the solution concentrations were incorporated into the worksheets and the resulting model predictions plotted alongside the experimental data. The Mathcad worksheets used in these calculations are reproduced in Appendix 2.

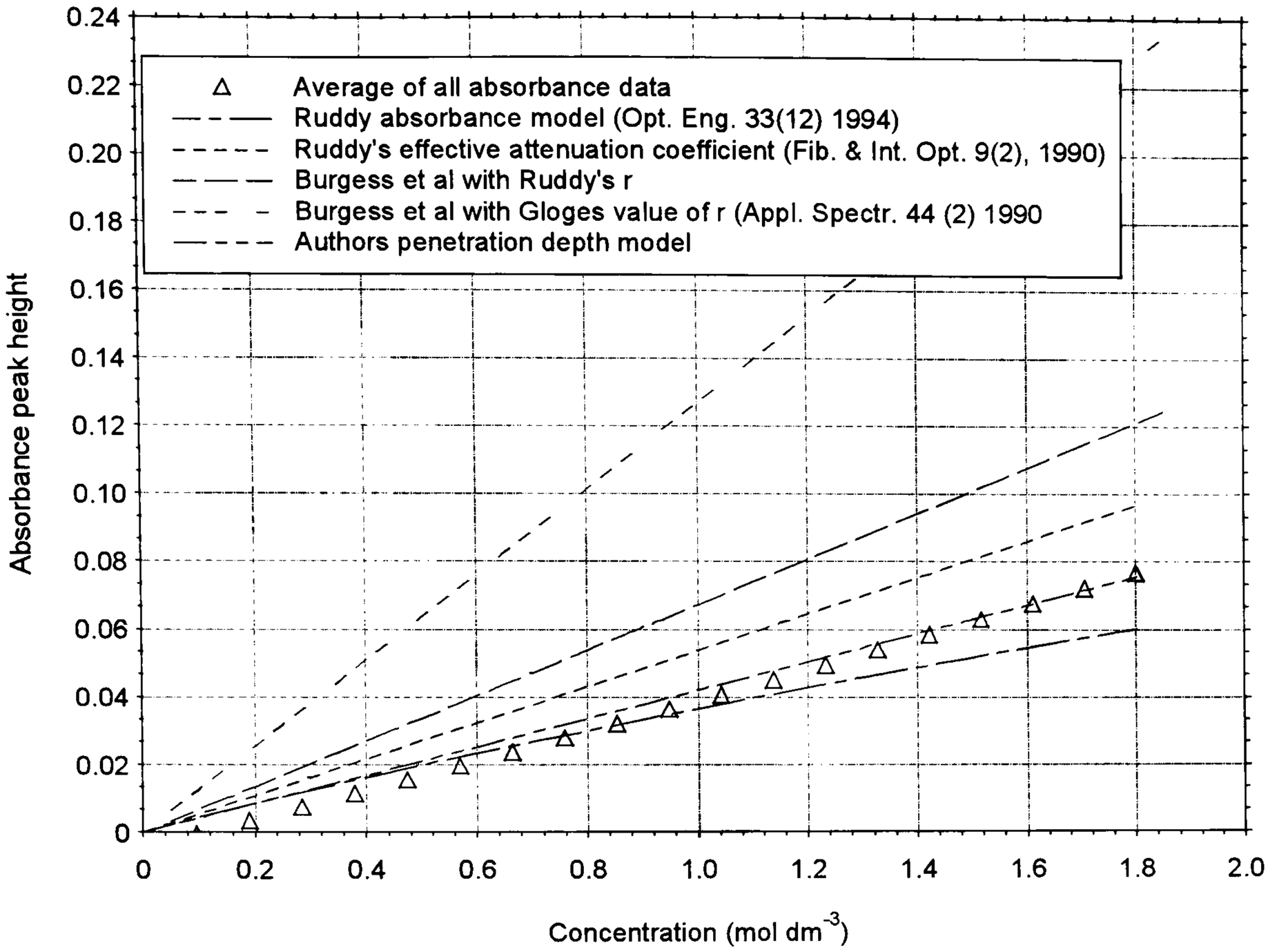

Figure 5-23 Experimental evanescent absorbance data compared to several models from the literature and also author's penetration depth model. n_{co}*=1.65,* n_{cl}*=1.41,* n_{med}*=1.446,* α*=146.37*

These value of the constants put into these models were as follows. The core index n_{co}=1.65, cladding index, n_{cl} =1.41, the medium index n_{med} =1.446 and the absorptivity coefficient of the amine, α=146.37mol $dm^{-3}m^{-1}$. α was calculated from FTIR spectra collected from a 1.22mol dm^{-3} solution of hexanediamine in chloroform. The solution was placed in a 2mm cuvette and three spectra taken. A spectra of the empty cuvette was used as the baseline. The mean absorbance peak height from these three spectra was calculated at 1529nm (=6539cm^{-1}) as 0.357. Since absorbance is the product of the absorptivity coefficient of a solution, its concentration and the pathlength the absorbtivity coefficient of hexanediamine could be calculated as the above value.

The following points can be made about how well these models fit to the experimental data.

All model predictions can be seen to be essentially linear in nature. The only prediction showing a deviation from this is the most recent model by Ruddy. The predicted rate of change of Absorbance with concentration can be seen to decrease with increasing concentration.

Two fits of Degrandpre and Burgess' model have been included in Figure 5-23. The first uses the value of r, the proportion of power in the evanescent wave calculated by Gloge[13]. The second uses the value calculated by Ruddy in his "effective attenuation coefficient" paper [184].

The prediction made using Gloge's r valus can be seen to be a very poor fit to the experimental data. This has been attributed to the simple nature of the model overall and the approximations made in Gloge's r estimate. This takes no account of the angular distribution of light in the fibre and assumes that there each propagation mode contributes an equal amount to the power in the fibre.

Ruddy's r (equation- 5.16) produces a slightly more accurate prediction. This value of r is derived from a triple polar integration of an electric field at the core surface of the form:

$$E(r,\theta) = E_0 \exp\left[\frac{-2(r-\rho)}{d_p}\right]$$

- 5.29

where d_p is, as before, the penetration depth at an incident angle θ and ρ is the radius of the fibre. Ruddy states that for plastic clad silica fibre "r has a maximum at the critical angle" with a value "approximately 17% lower than Gloge" He attributes this discrepancy to the analysis being based on TE modes which penetrate less deeply than TM modes. In both cases it can be seen the Degrandpre and Burgess model shows unacceptable deviation from the experimental data.

The use of Ruddy's effective attenuation coefficient [184] produces a prediction which is closer still to the experimental data (to within 20% worst case deviation). This model is a well thought out and rigorous treatment of the fibre problem, However, the paper contains a few errors, not least in the penetration depth equation. The final equation (- 5.8) for the attenuation coefficient is based around the approximation for small absorption and equal power in each ray reaching the sensing region.

The more recent Ruddy model from reference [195] matches the experimental data to within 5-10% at lower concentrations and 15% as the concentration increases. The use of this model is simplified in that it predicts a value for transmittance which can easily be converted to absorbance since $A=-logT$. Ruddy states in this paper that step index fibre waveguides obey a Beer-Lambert type law only for low concentration values unless the

fibre mode volume is completely filled in the sensor region. Since the numerical aperture of the sensor region with the sensor used in these experiments is smaller than that of the lead-in region (0.795 compared to 0.857) this condition should be fulfilled which is a possible reason for the departure of the model from the experimental data at higher concentrations.

The author's penetration depth model appears to fit the experimental data very well over the amine concentrations seen in a curing mixture of Epikote 828 and hexanediamine. The prediction is closer at the higher end of the concentration range than at lower concentrations. This could be due to the accuracy of measurements of the peak height of the experimental data at lower concentrations because the uncertainty of these measurements (of small absorptions) has a greater uncertainty than those at higher concentrations.

Of course the cure monitoring of a curing epoxy introduces and additional level of complexity into the modelling of the evanescent sensor signal. The absorption experiments described in this section were conducted using a solution of amine hardener the refractive index of which remains relatively constant. A curing resin increases its refractive index substantially as cure progresses and so this must be taken into account in the signal model.

The sensor response to hardener concentration and refractive index has been represented as a three dimensional surface, the x and y axes being the concentration and refractive index of the resin respectively and the z-axis the absorbance seen by the sensor. During the cure of a resin system the absorbance will follow a locus traversing this surface. This surface can be termed a cure surface and an example of such is seen below in Figure 5-24 calculated from Ruddy's model [184]. Superimposed on the cure surface is a typical actual cure profile measured at 50°C which describes a locus across the cure surface. Such a surface could be useful for predicting sensor response at a given refractive index and concentration of hardener.

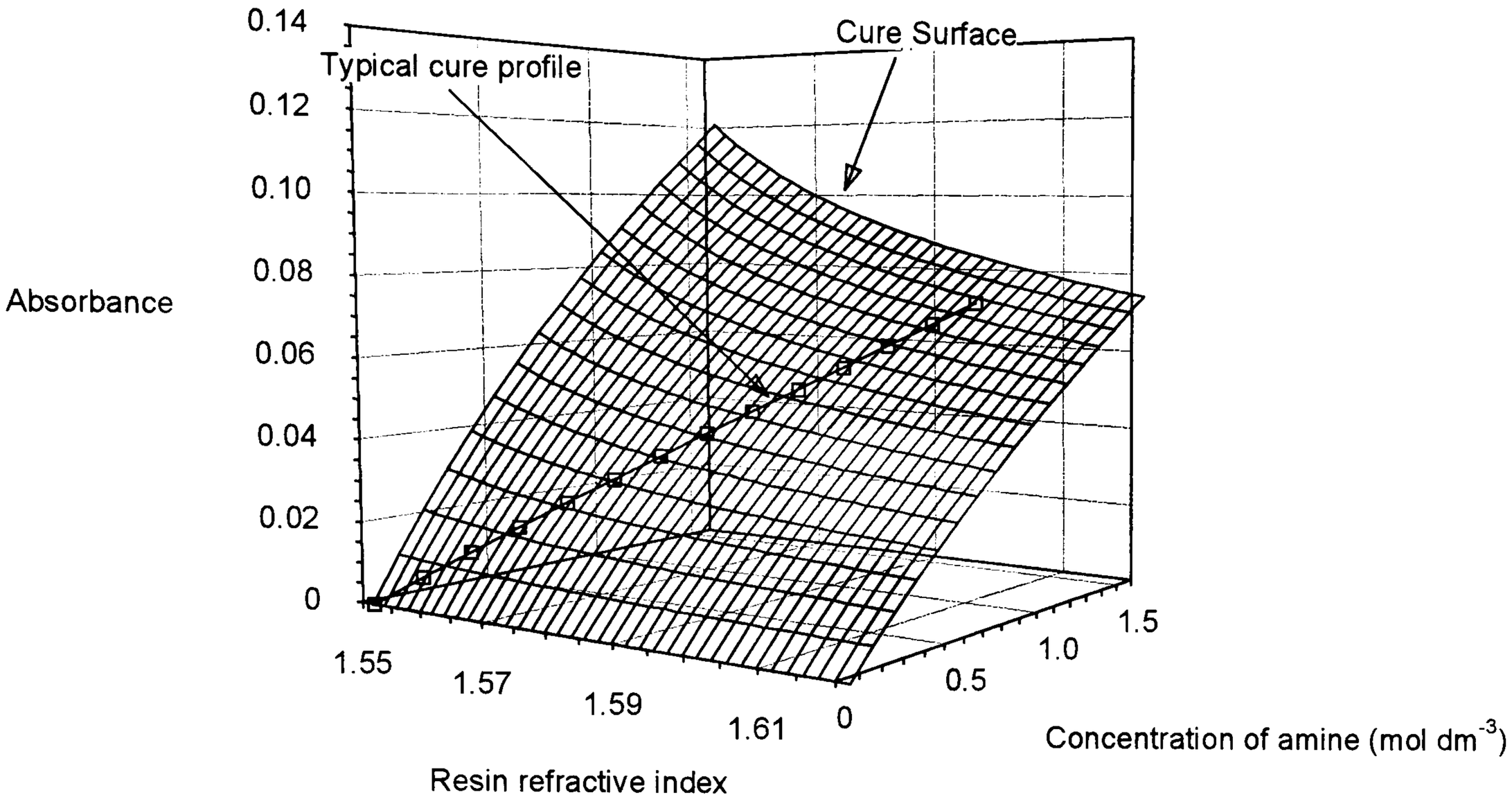

Figure 5-24 "Cure surface" showing predicted absorbance for a range of resin refractive index and amine concentration. Typical cure profile for 828 resin and hexanediamine shown superimposed. Demonstrates dependence on refractive index and solution concentration

With a sufficiently accurate model, absorbance measurements made using the sensor could be applied to such a surface and since each absorbance value has a unique corresponding value of refractive index and amine concentration absolute values of these could be obtained. This would give an excellent indication of the cure state of the resin. The cure surface could also be constructed using an empirical model obtained by calibrating the sensor response in terms of analytes of known refractive index and concentration. A surface constructed in this way would be of a similar value in predicting the cure state of a resin system containing a cure sensor.

5.4.5 Cure monitoring using evanescent cure sensor

Evanescent sensors were embedded into curing stoichiometric mixtures of Epikote 828 and Hexanediamine at isothermal temperatures of 30, 40, 50 and 60°C. The spectral region from 1470-1590 nm was monitored throughout the cure of the resin. This allowed the depletion of the amine absorbance to be monitored as cure progressed. This gave information about the state of cure of the resin system. The experimental layout used for these experiments can be seen in section 5.3.5.

An example dataset from a single cure run at 50°C, converted to absorbance can be seen in Figure 5-25.

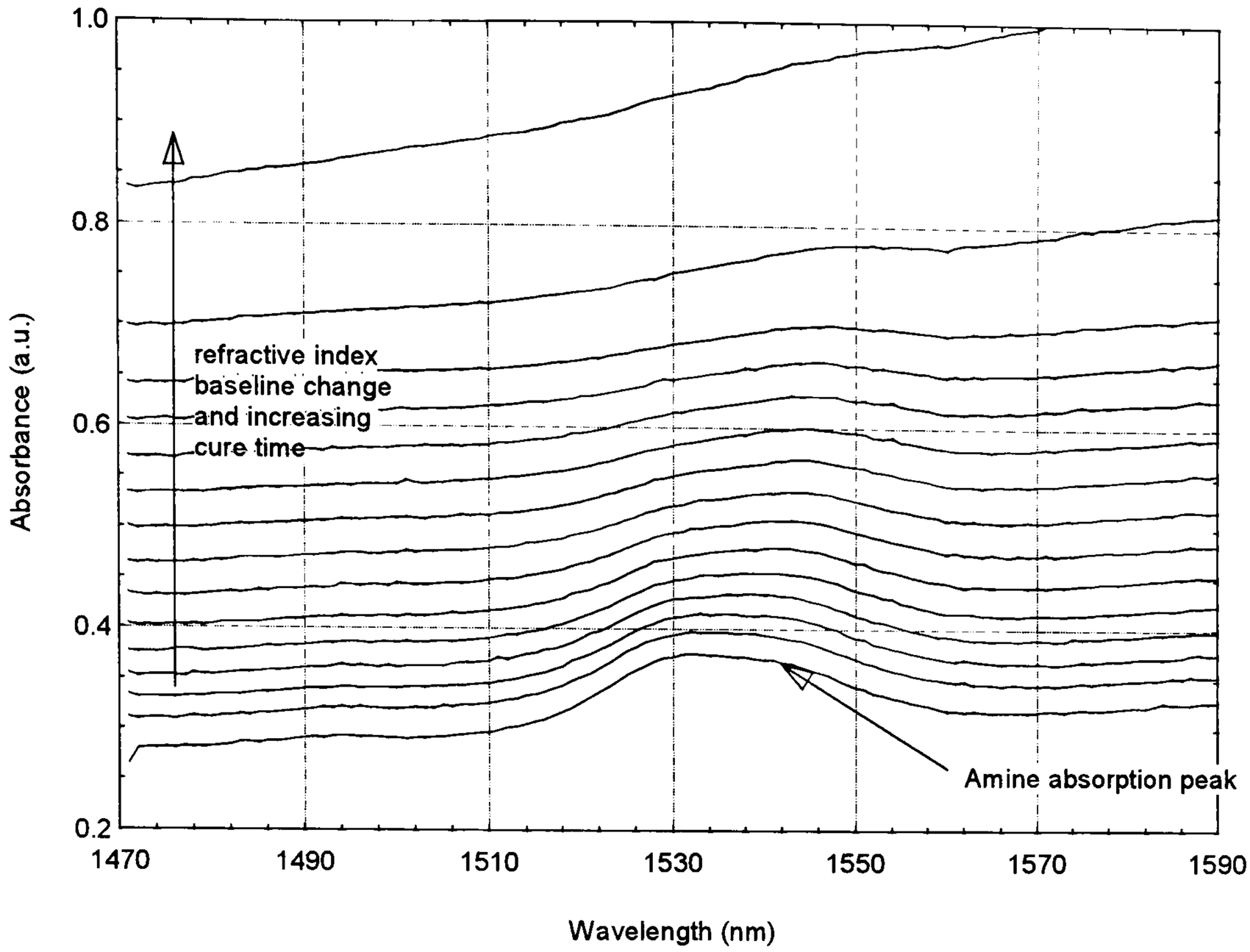

Figure 5-25 Example evanescent sensor data during the first 8 minutes of cure converted to absorbance by ratioing to background taken in air .

The two main features of these data are a rising baseline between traces and the hardener absorption band in each trace which can be seen to decrease in magnitude, as cure time increases.

The rising baseline is due to the refractive index change that occurs in the resin during the cross-linking process. This is the component of the overall absorption described by the second term in equation - 5.14. It can be seen that this effect is several times larger in magnitude than the signal change due to the absorption of the hardener. For comparison of the sensor absorption data to the absorption predicted by the above models it was necessary to measure the absorption peak heights. The above equations all predict the absorption depth at a specific wavelength. Thus, the peak heights were used rather than the peak areas which is the more conventional method used in spectroscopy. The use of peak heights is also more analogous to using a single wavelength telecommunications source to sample the depth of absorption which was the ultimate aim of the project. A program was written as a Microsoft Excel macro to perform the batch processing of all spectra to obtain the peak height from each curve and listing of this can be seen in Appendix 1. Figure 5-26, Figure 5-27, Figure 5-28 and Figure 5-29 show the peak height data for each of 5 representative repeats conducted at the four temperatures.

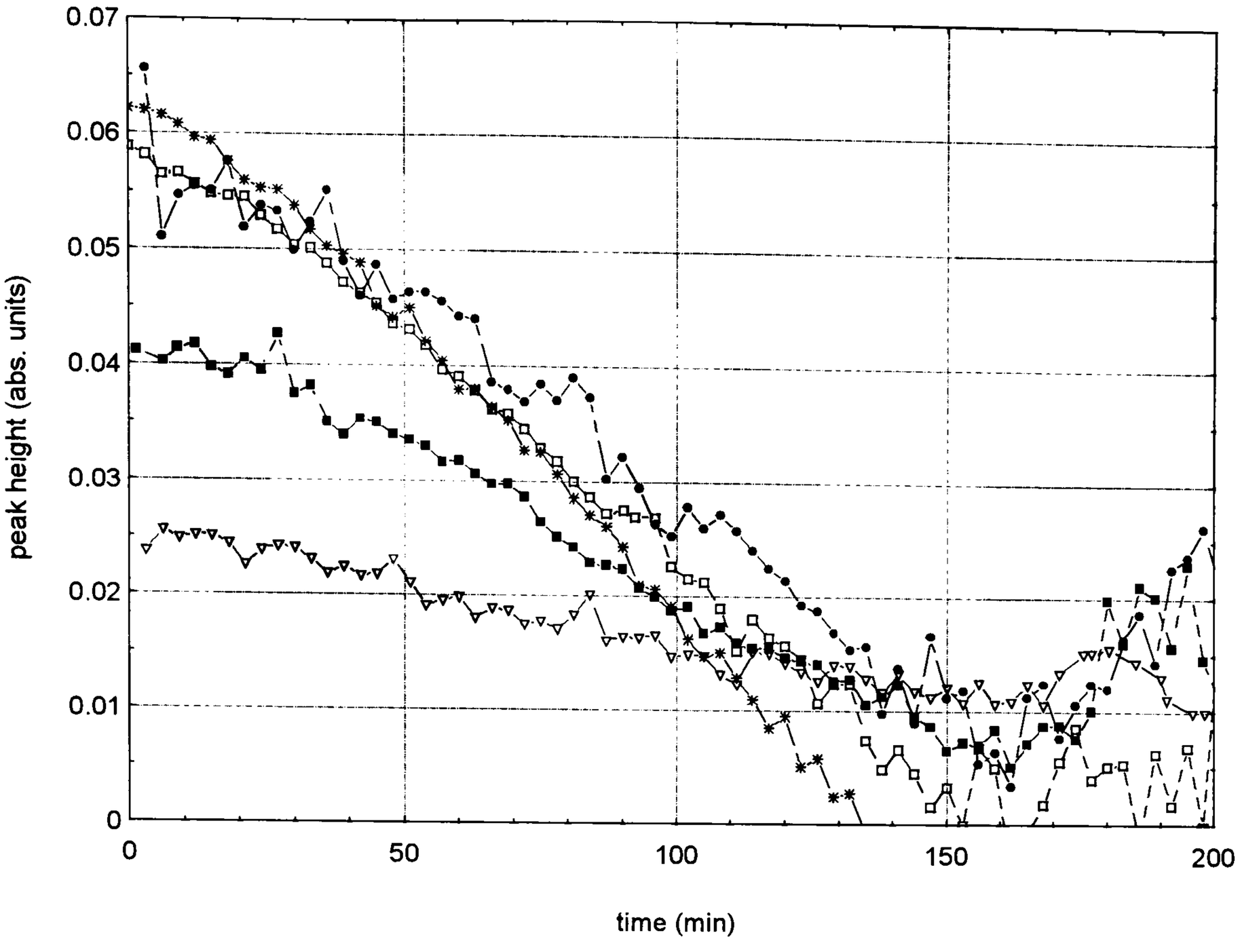

Figure 5-26 Hardener absorbance peak height vs. time @ 30°C in a stoichiometric epoxy/amine resin system (five repeats)

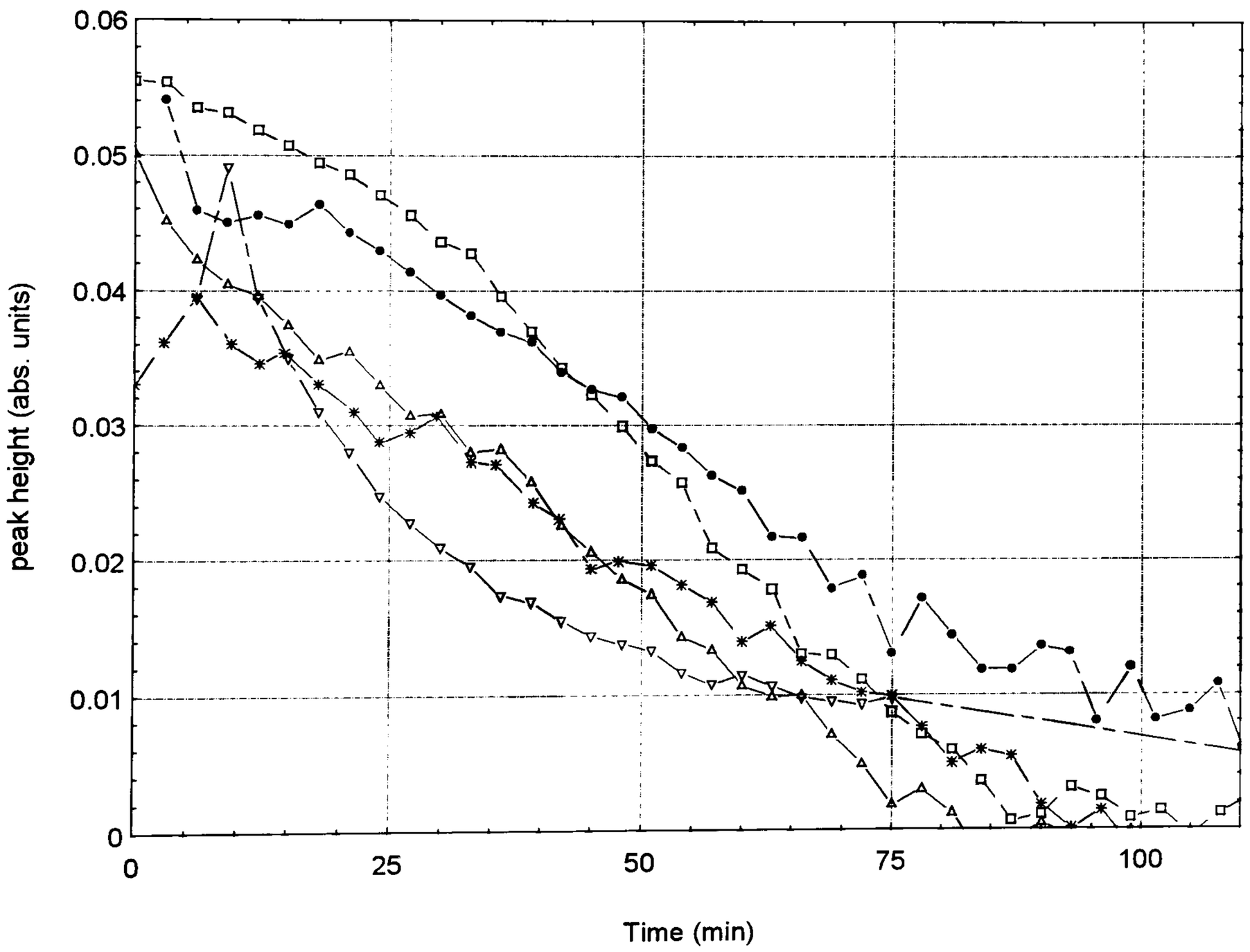

Figure 5-27 Hardener absorbance peak height vs. time @ 40°C in a stoichiometric epoxy/amine resin system (five repeats)

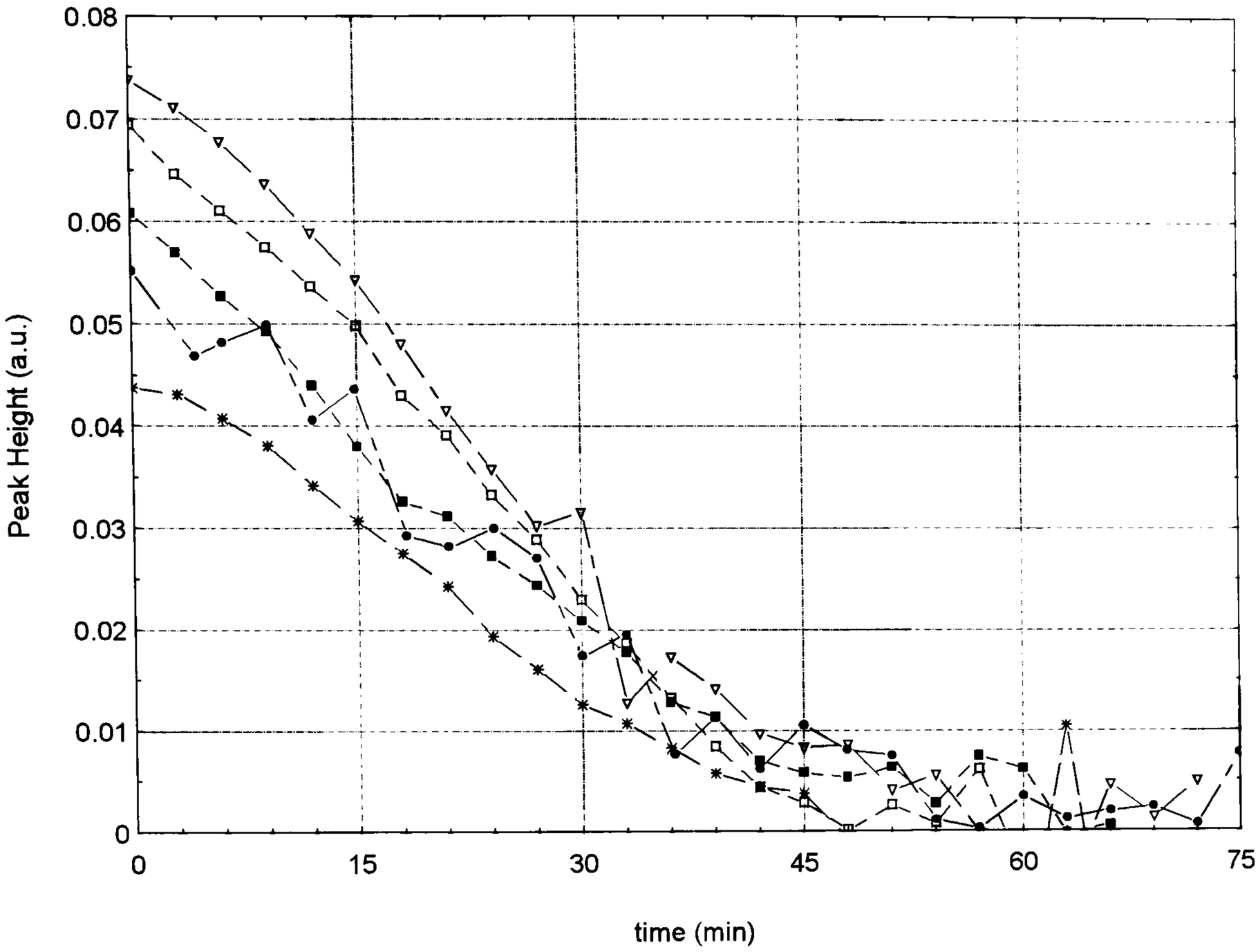

Figure 5-28 Hardener absorbance peak height vs. time @ 50°C in a stoichiometric epoxy/amine resin system (five repeats)

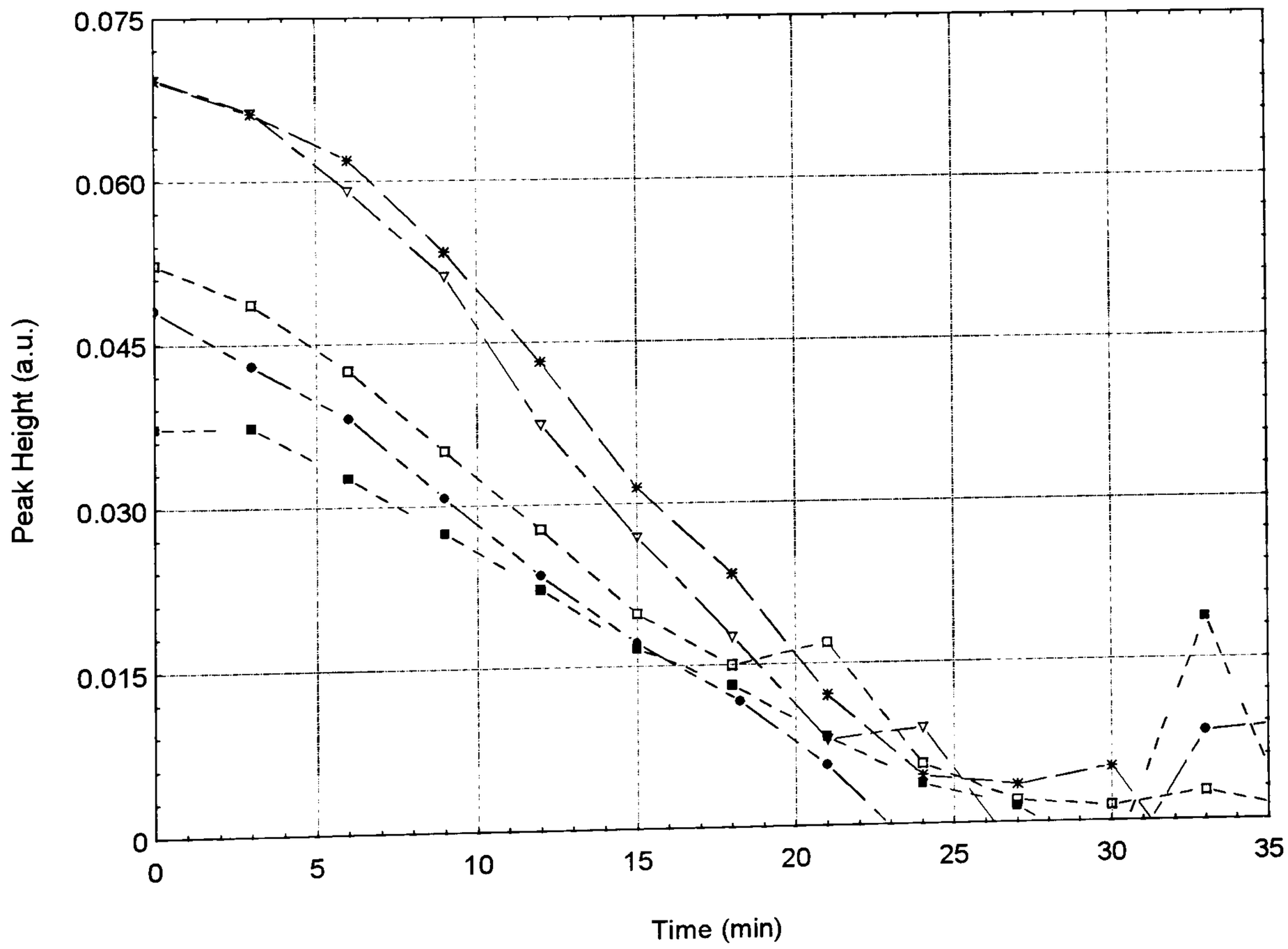

Figure 5-29 Hardener absorbance peak height vs. time @ 60°C in a stoichiometric epoxy/amine resin system (five repeats)

The first thing to be said about these data is that the repeatability is extremely poor. This is despite the efforts made, which have already been discussed, to isolate possible sources of variation between cure runs. The variation in the signals at the beginning of the cure cycles is due to differences in the measured absorbance. Towards the end of the cure time the scatter is of a more random nature and this can be attributed to the signal-to-noise ratio on the absorption peak measurement decreasing as the peak height approaches zero. The spread of these datasets must mainly be attributable to small variations in parameters such as the launch conditions, fibre curvature, fibre position, sensor length and the clad/unclad transition region. Even tiny variations in any of these factors will affect the amount of energy in the evanescent wave, in turn affecting the observed absorption depth.

It was found that an improved comparison between the traces can be made and an idea of the repeatability of the experiment can be obtained if the peak height data is normalised. This is done by dividing each curve on the graphs by their initial value in a similar way to the calculation of percentage conversion, α, is calculated from FTIR absorbance data. The normalisation of the data takes into account the variations in the optical fibre sensor start signal due to slight differences in fibre configuration and losses at the fibre splices. The normalised data can be seen in Figure 5-30, Figure 5-31, Figure 5-32 and Figure 5-33.

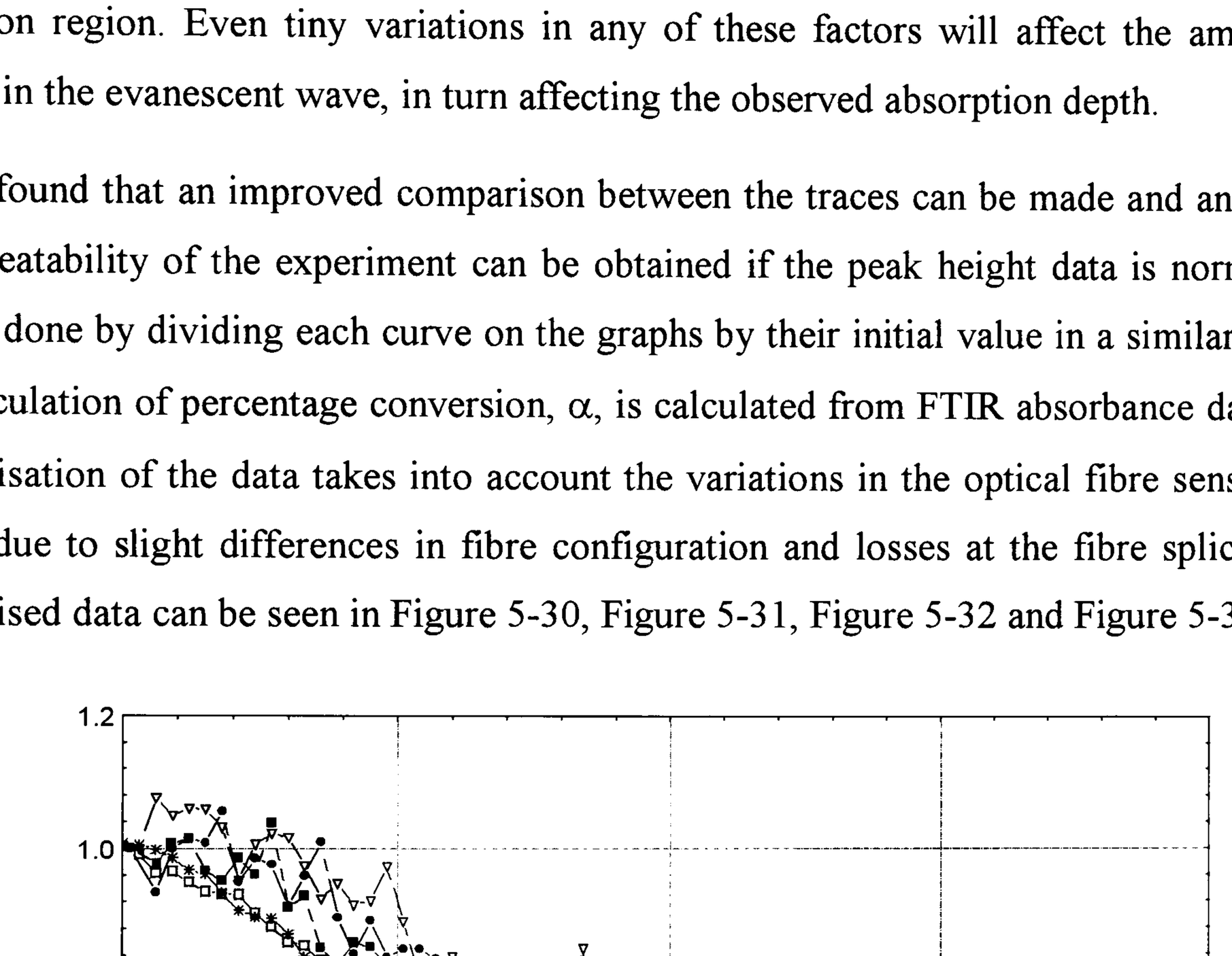

Figure 5-30 Normalised hardener absorbance peak height vs. time @ 30°C in a stoichiometric epoxy/amine resin system

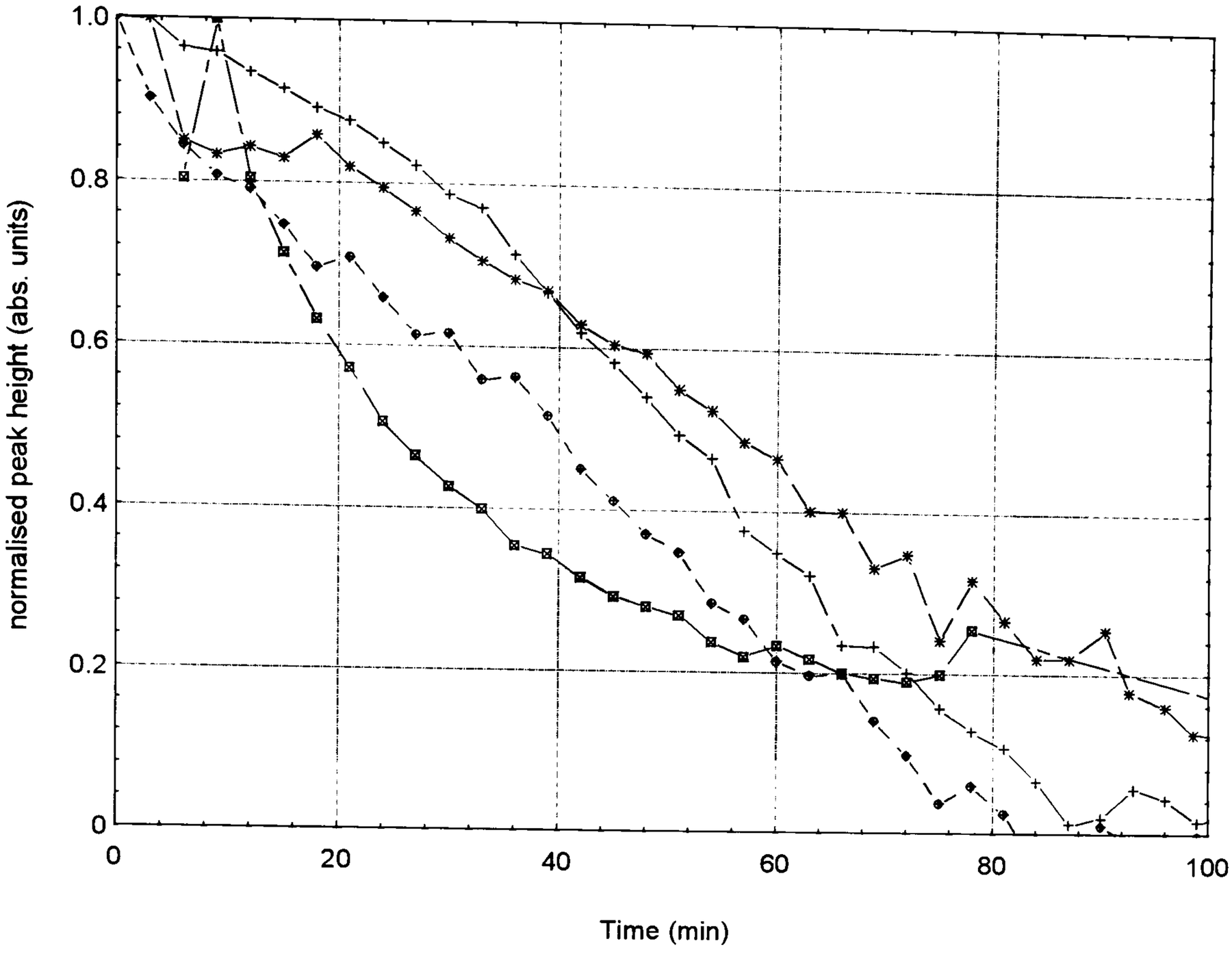

Figure 5-31 Normalised hardener absorbance peak height vs. time @ 40°C in a stoichiometric epoxy/amine resin system

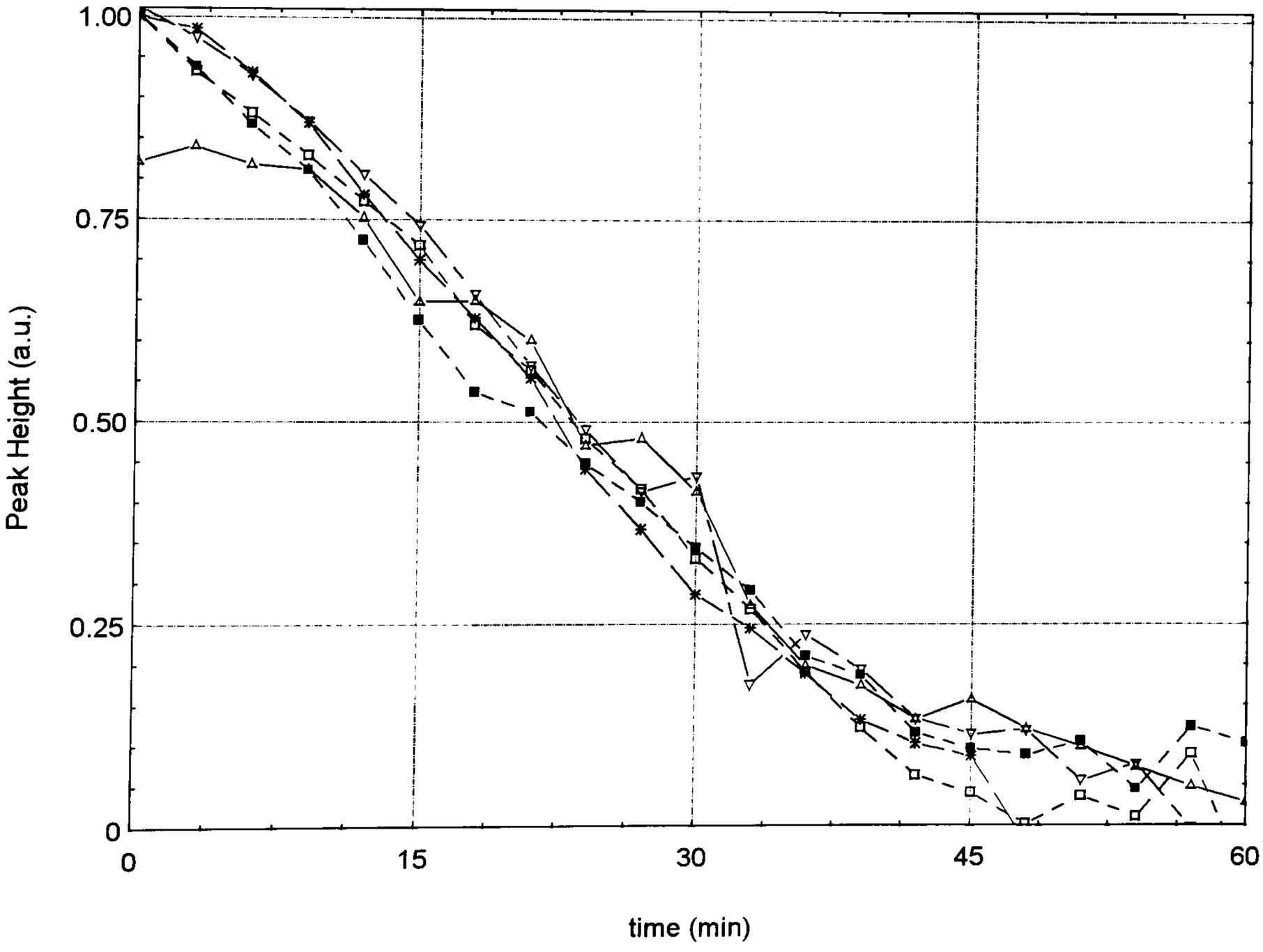

Figure 5-32 Normalised hardener absorbance peak height vs. time @ 50°C in a stoichiometric epoxy/amine resin system

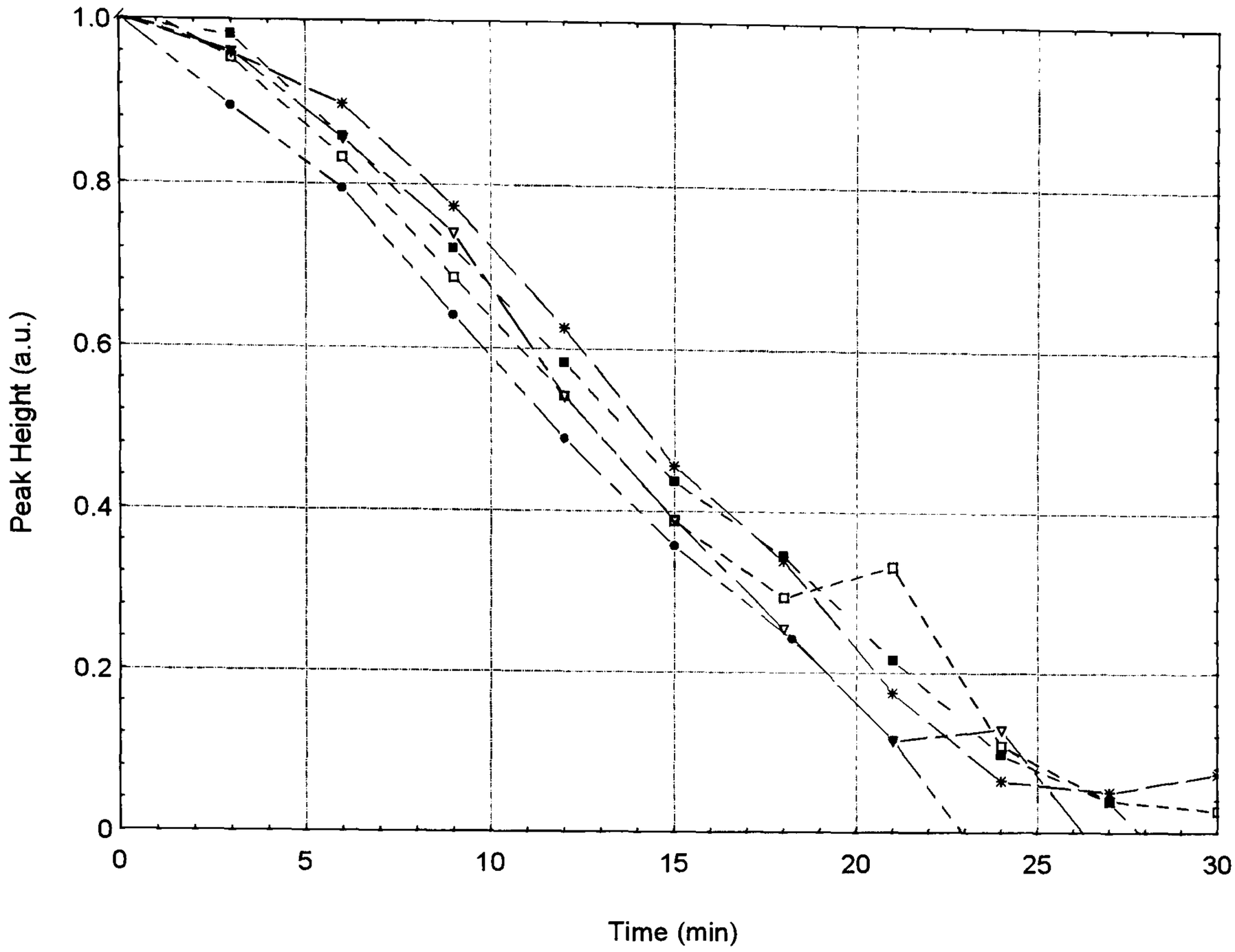

Figure 5-33 Normalised hardener absorbance peak height vs. time @ 60°C in a stoichiometric epoxy/amine resin system

The repeatability of the normalised curves can be seen to be generally poor for the data taken from cure runs at 30 and 40°C. In contrast the 50 and 60°C data have a much better level of repeatability, all results agreeing to within 10%. The superiority of the data at these temperatures can be attributed to the mobility of the resin system which is greater at these temperatures. Because of this the resin wets the sensor surface better at these temperatures and the sensor signal is much improved. Also with increase mobility the resin is better mixed and so variability between cure runs will be less. Table 5-2 is a list of the times at which important cure features appear on the evanescent cure data. This information was obtained by fitting a fifth order polynomial to all the cure data. The expected acceleration of the cure rates with increasing temperature can be seen from the table.

Temperature (℃)	*Cure onset time (mins)*	*Cure termination time (mins)*	*Peak cure rate time (mins)*
30	10	150	60
40	1	115	26
50	0.5	53	18
60	0.3	33	11

Table 5-2 Times of cure features taken from evanescent cure data

In addition to the resin mobility reason the spread between the experimental results can be attributed to the following factors:

i) variation in fibre configuration; although every effort was made to arrange the fibre in a similar manner at every experiment there were inevitably slight variations in the path the fibre took. This would not have been referenced out by the referencing method used to account for source drift and so may have appeared as a signal change in the output of the sensor;

ii) uncertainty in the properties of the transition region between stripped and unstripped regions of the fibre. The chemical stripping process leaves a small length of damaged cladding (≈1mm) which could affect the sensor signal;

iii) other potential reasons include possible moisture contamination of the reactants, differing actual resin temperatures and inadequate mixing of reactants and/or slight differences in the starting stoichiometry of the epoxy amine mixture.

A similar variation between results was seen with the refractive index sensor (section 6.3.2) although not to the same degree and many of the same factors are thought to be responsible.

The referencing of the light source intensity was attempted by inserting a fibre y-coupler to create a reference arm connected directly to a photodiode (see section 6.3.2). It was hoped that this would enable any fluctuation in the source intensity to be monitored enabling them to referenced out from the final signal. However, the introduction of the y-coupler reduced the light reaching the sensor making the sensor signal unusable. This meant that any changes in source intensity could not be accounted for in these data.

The data could be improved by referencing to an internal standard refererence peak such as the C-H peak at 1647nm. Since this peak is invariant during cure it could be used to remove any fluctuations in peak intensity due to factors not related to the cure process. Restrictions in the wavelength range of the fibre monochromator prevented this. Improved data could also be obtained by use of the epoxy peak at 2207nm (Figure 4.8 and Table 4.1) since this is a much stronger band and would give an improved signal in relation to the refractive index change. This again was prevented by source and detector wavelength restrictions but the technique would increase in its usefulness if this higher wavelength were to be used.

In summary, from the above discussion the requirements for improved data collection from this technique are as follows:

i) faster acquisition of spectra, at the moment each wavelength scan take approximately 70 seconds due to the scanning speed of the grating monochromator. This limits the number of data points which can be obtained during a cure cycle. An *in-situ* cure monitoring system will require data processing in real time and to perform this will also require a faster sampling rate;

ii) an extended wavelength range to allow referencing of the hardener absorption band to a cure invariant band (such as the 1647nm C-H band) and the possibility of using the stronger epoxy band at 2207nm for improved signal.

At the time of writing solid state grating spectrometers are just reaching the market which are capable of operating in the near-IR. It is thought that these could be ideal candidates for this application since they allow fast, reasonable high resolution acquisition of spectra over a wide wavelength range. It is also anticipated that, as laser diode technology develops, a wider range of wavelengths will become available as well as tuneable sources (which are also just reaching the market at telecommunication wavelengths) which will enable the technique to be developed to be more in line with the original project proposal, *i.e.* single wavelengths being used to monitor individual absorptions.

5.4.6 Comparison of evanescent and other cure monitoring techniques

To determine whether the evanescent absorption cure sensor results were in any way valid the results obtained using this sensor were compared with those obtained using the Abbe

refractometer, the refractive index sensor (Chapter 6) and FTIR data obtained by the author's co-researcher.

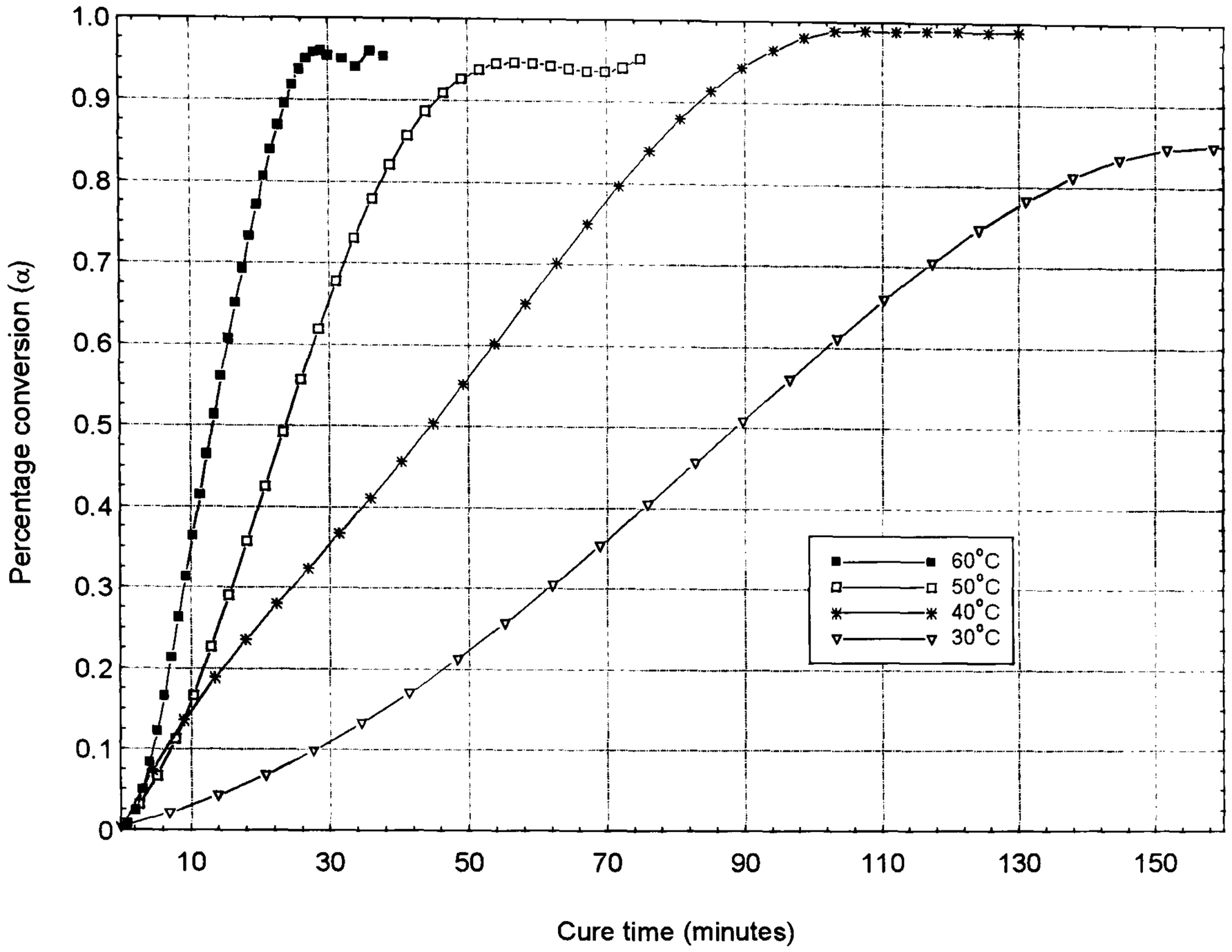

Figure 5-34 values for α (percentage conversion) as a function of cure time calculated derived from evanescent data at four different temperatures

Figure 5-34 shows the values of α calculated from the evanescent sensor data. These data were obtained by fitting a fifth order curve to the normalised peak height data shown in the previous section. These data was then converted to an extent of cure measure using the equation:

$$\alpha = 1 - \frac{(height_{a\min e@1529nm})_{time=t}}{(height_{a\min e@1529nm})_{time=0}}$$

- 5.30

where $height_{amine@1529nm}$ is the height of the amine absorbance at 1529nm.

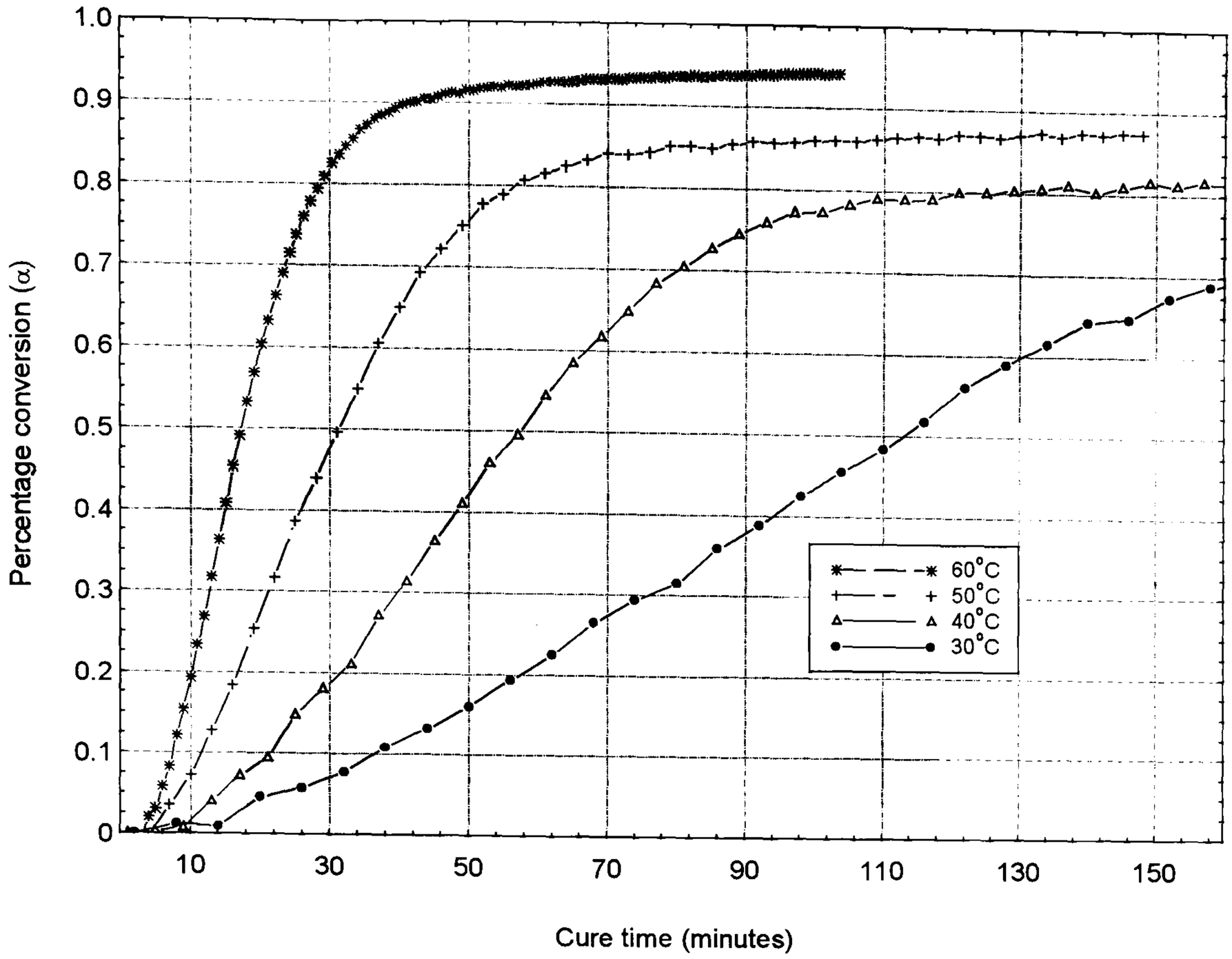

Figure 5-35 values for a (percentage epoxy conversion) as a function of cure time calculated derived from FTIR spectra at four different temperatures

Figure 5-35 represents data for α this time calculated from FTIR transmission spectroscopy measurements made during the cure of Epikote 828 and hexanediamine. These curves were obtained from the ratio of the epoxy peak area at 2.2μm against the C-H peak converted to alpha values using equation - 6.10 in section 6.4. The following comparisons can be drawn:

i) the evanescent data on the whole give a higher value for extent of cure over the FTIR data. This can be attributed to the decrease in sensitivity of the evanescent sensor at high degrees of cure when the concentration of amine hardener is low;

ii) the evanescent data also show the time to completion of cure as being smaller than the FTIR data does. Again this is probably due to the smaller sensitivity of the evanescent sensor as the amine concentration decreases, compared to FTIR transmission spectroscopy which is an extremely sensitive technique.

Figure 5-36 shows the values of alpha from the two techniques, at all four temperatures, plotted against each other.

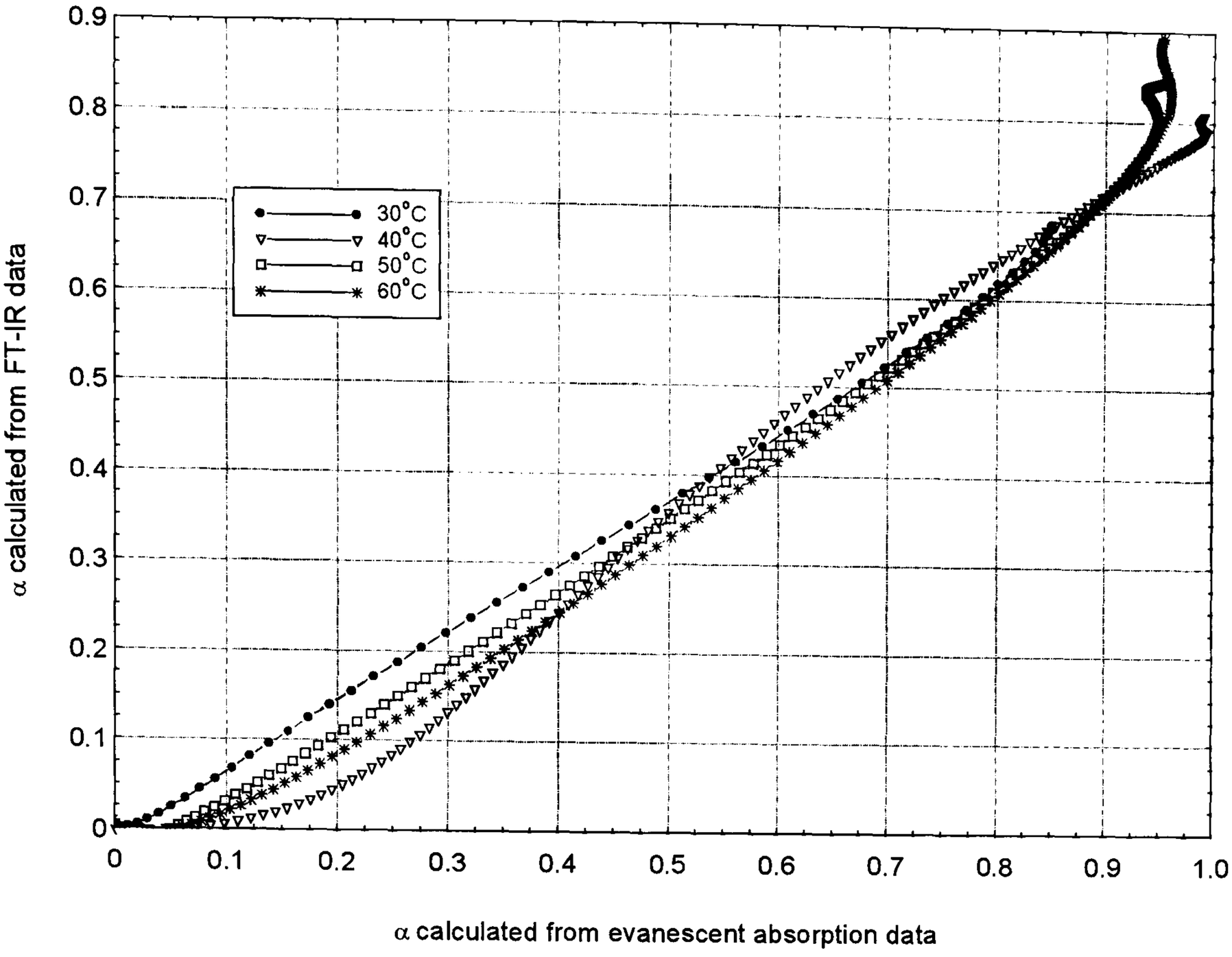

Figure 5-36 Degree of cure calculated from evanescent data plotted against epoxy conversion calculated from FTIR data

It can be seen that the relationship between the two techniques is ostensibly linear except at the higher degrees of cure when the sensitivity of the evanescent technique is low (above $\alpha_{evanescent}$=0.9). The 40°C data show the greatest deviation from a linear relationship and this can be attributed to this dataset showing the greatest degree of spread between experimental repeats. The relationship between the FTIR data and the evanescent cure data was established by fitting by least squares a line to data between $\alpha_{evanescent}$ =0 and 0.9. The fits are summarised in Table 5-3

Isothermal cure temperature (°C)	*Line fit equation*	*Maximum deviation and goodness of fit (r^2)*
30	α_{FTIR} = +0.790 $\alpha_{evanescent}$ -0.0162	max dev=0.0314, r^2=0.998
40	α_{FTIR} = +0.970 $\alpha_{evanescent}$ -0.134	max dev:0.0650, r^2=0.994
50	α_{FTIR} = +0.842 $\alpha_{evanescent}$ -0.0628	max dev:0.0205, r^2=0.999
60	α_{FTIR} = +0.847 $\alpha_{evanescent}$ -0.0782	max dev:0.0809, r^2=0.994

Table 5-3 Summary of relationship between extents of cure deduced from FTIR and evanescent data

The fits show that there can be considered to be a linear relationship between the extents of cure derived from the evanescent and FTIR data. This relationship holds up to an $\alpha_{evanescent}$ of $\approx$0.9 where the amine peak becomes too weak to be detected against the background.

5.4.7 Fitting of evanescent models to cure data.

The literature describing the cure models, discussed in section 5.2, do not contain any comparison of their predictions with actual experimental data obtained using an evanescent sensor. Extensive literature searching has not shown any subsequent literature assessing the validity of these evanescent sensor models. A comparison of this kind could, therefore, be seen as a useful contribution to the field of evanescent sensing. To obtain an indication of the accuracy of the models evanescent absorption data obtained using the sensor was compared to predictions made using these models.

The cure models were used together with cure data obtained from FTIR spectroscopy and Abbe refractive index to predict the magnitude of the absorption seen with the evanescent sensor embedded in a curing resin. The models above all require that the refractive index and the absorbance of the medium in which the evanescent sensor be known at the wavelength of interest. This is trivial for the FTIR spectroscopic data, however, since the Abbe data are measured at a wavelength of 589.3nm it was necessary to in some way find the refractive index values in the NIR. After searching the literature available it became apparent that this information was not widely available for Epikote 828 so a method of measuring the refractive index or calculating it from the n_D values was needed.

Several novel methods for measuring the refractive index in the NIR were tried together with a way of doing this using the Cauchy equation. Cooper's paper[197] on the refractive index measurement of epoxy resins in the spectral region 500-1500nm shows that an epoxy's refractive index varies smoothly over this range. This experimentalist uses a Cauchy formula of the form:

$$n = A + \frac{B}{\lambda^2} + \frac{C}{\lambda^4}$$

- 5.31

to extrapolate the refractive index of several resins up to 1600 nm from measurements made from 589.3 to 1300nm. Here A, B and C are constants specific to the substance and λ is the wavelength at which refractive index, n, is needed. The fit of this equation to the experimental data was seen to be very good ($<2x10^{-4}$) and was said to give the expected monotonically decreasing function.

The Abbe data were used to predict the refractive index of the resin at 1529nm throughout cure by using the data from this paper to calculate equations for A, B and C as a function

of the refractive index at 589nm. The following quadratic equations were calculated fitting a second order polynomial to plots of A, B and C against n_D..

$$A(n_D) = -0.86655n_D^2 + 3.5138n_D - 1.8350$$
$$B(n_D) = 0.52833n_D^2 - 1.5458n_D + 1.1352$$
$$C(n_D) = -0.079009n_D^2 + 0.23372n_D - 0.17294$$

These equations achieved a very good fit with a correlation coefficient smaller than 10^{-5}. Figure 5-37 shows the measured refractive index, at 589.3nm, of the resin/hardener mixture throughout cure at each of the four cure temperatures. Each data point on these curves was transformed using the Cauchy equation with values of A, B and C calculated from the equations above. Figure 5-38 shows the data as they appears after having undergone this transformation. The lower overall refractive indices are seen on these curves which is consistent with normal dispersion in a transparent solid.

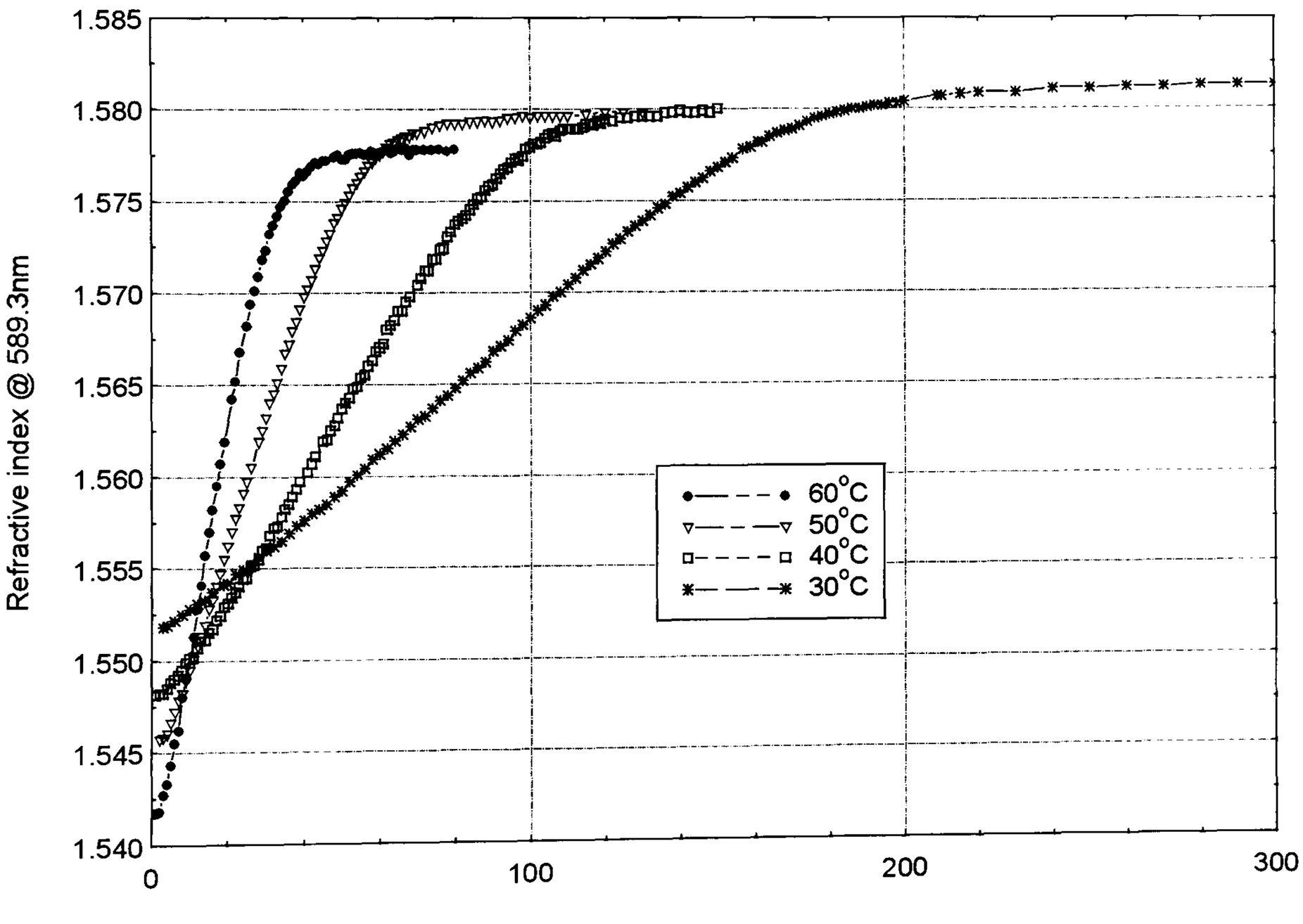

Figure 5-37 Refractive indices with cure time of curing 828 and hexanediamine at 4 cure temperatures@ 589.3nm

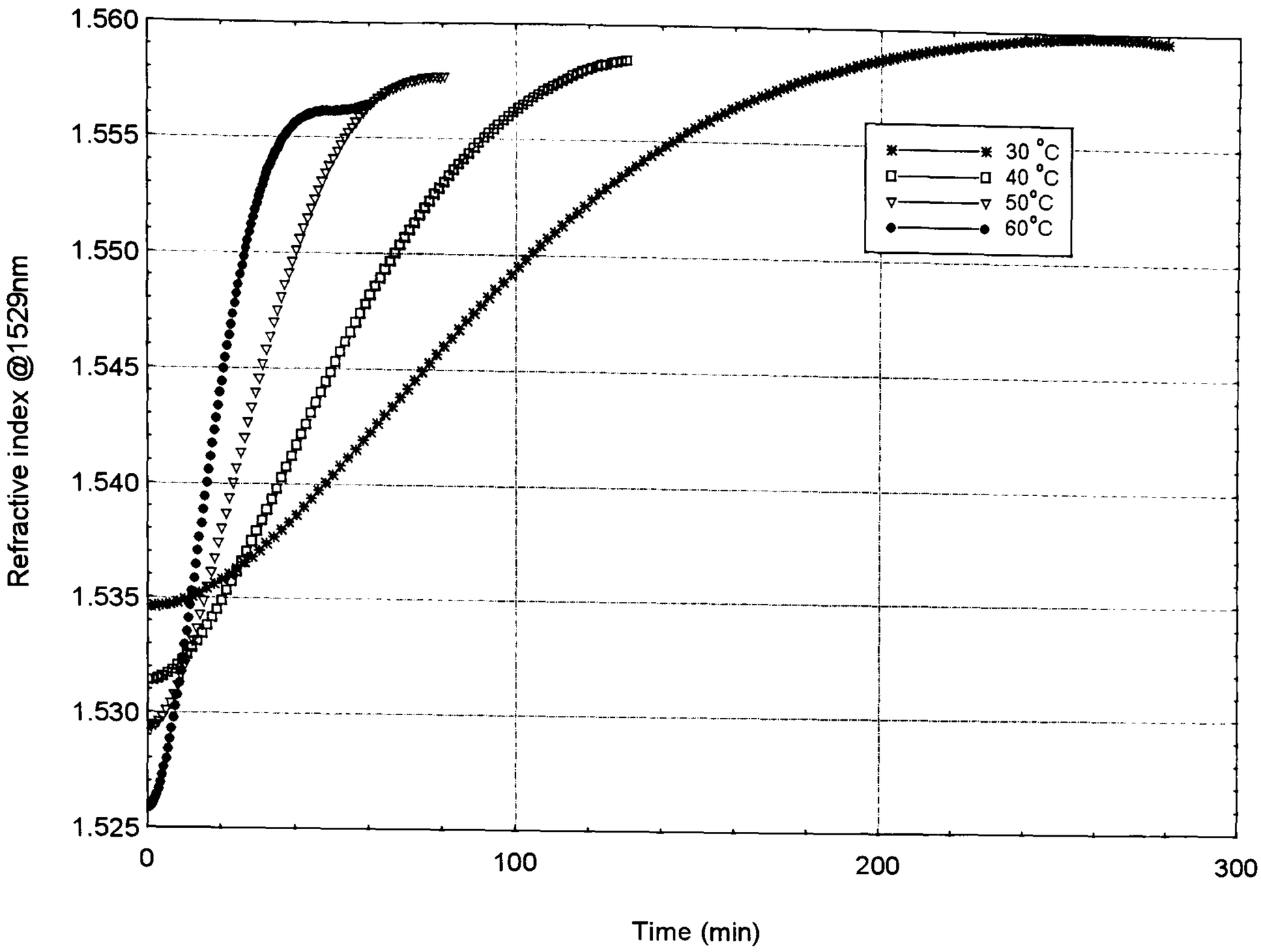

Figure 5-38 Calculated refractive indices with cure time of curing 828 and hexanediamine at 4 cure temperatures @ 1529nm

Amine hardener concentrations were calculated from spectra of curing resin obtained during cure at each of the four isothermal temperatures. This process is involved, and will not be dealt with here but is detailed in the author's co-researcher's thesis[198].

The above refractive index values together with the amine hardener concentration calculated from FTIR data for the four temperatures were substituted into the four models described above. As before, the Degrandpre and Burgess model was used with both Gloge's value for the power in the cladding, r, $(3/\sqrt{2}V)$ and a value for r derived by Ruddy in his paper (equation - 5.16). Ruddy's later absorption coefficient model was also plotted together with the author's penetration depth model. This made five model curves in total.

The signal which results from the resin refractive index change (and the associated fibre numerical aperture change) had been accounted for in the processing of the evanescent data by taking only the evanescent peak height. The components of the Degrandpre and Burgess model which explicitly accounts for this change were thus neglected and only those parts predicting the absorbance change due to changing amine concentration and refractive index change were taken into account in these calculations.

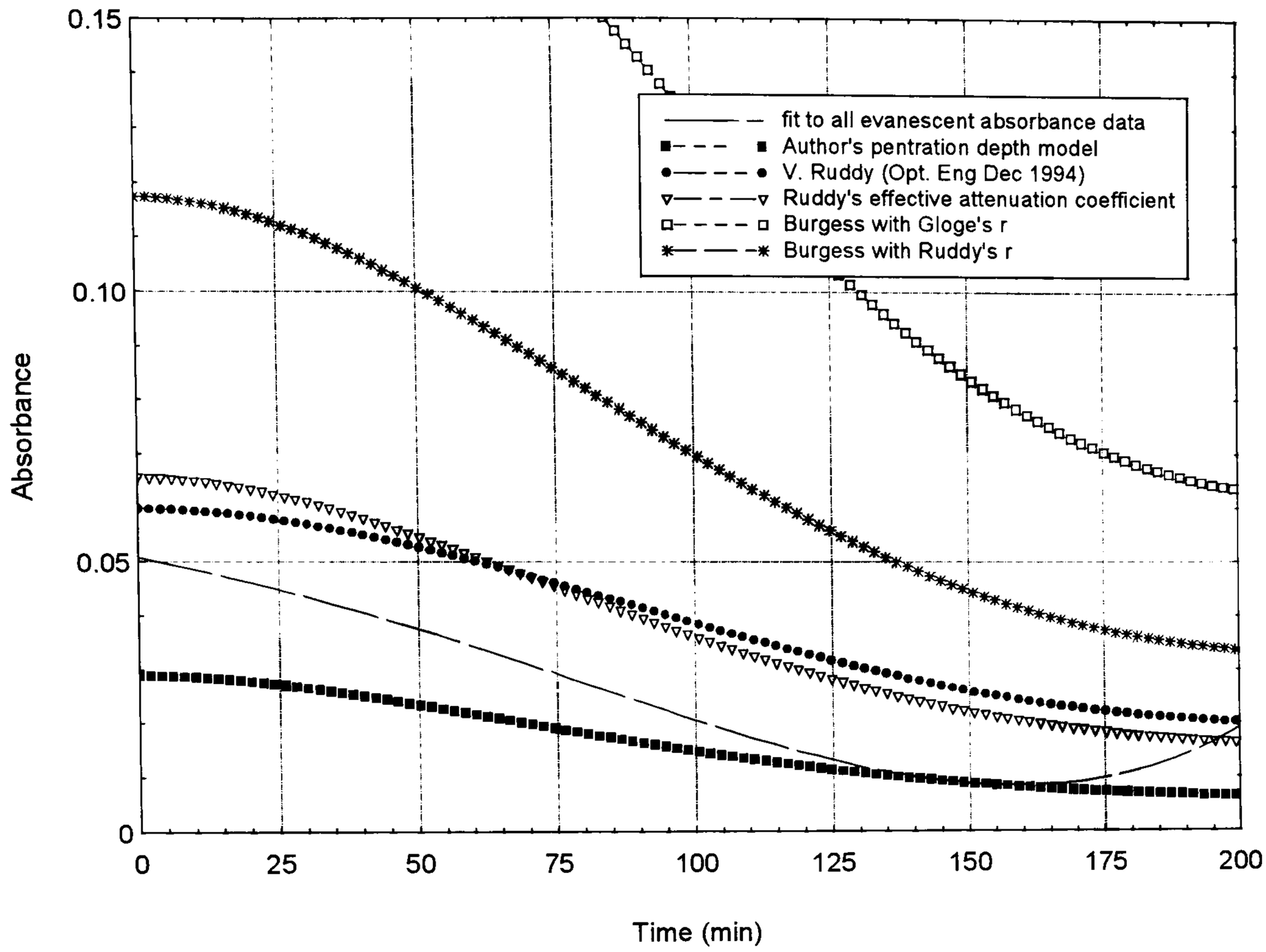

Figure 5-39 Comparison of model predictions and peak height sensor data @ 30°C

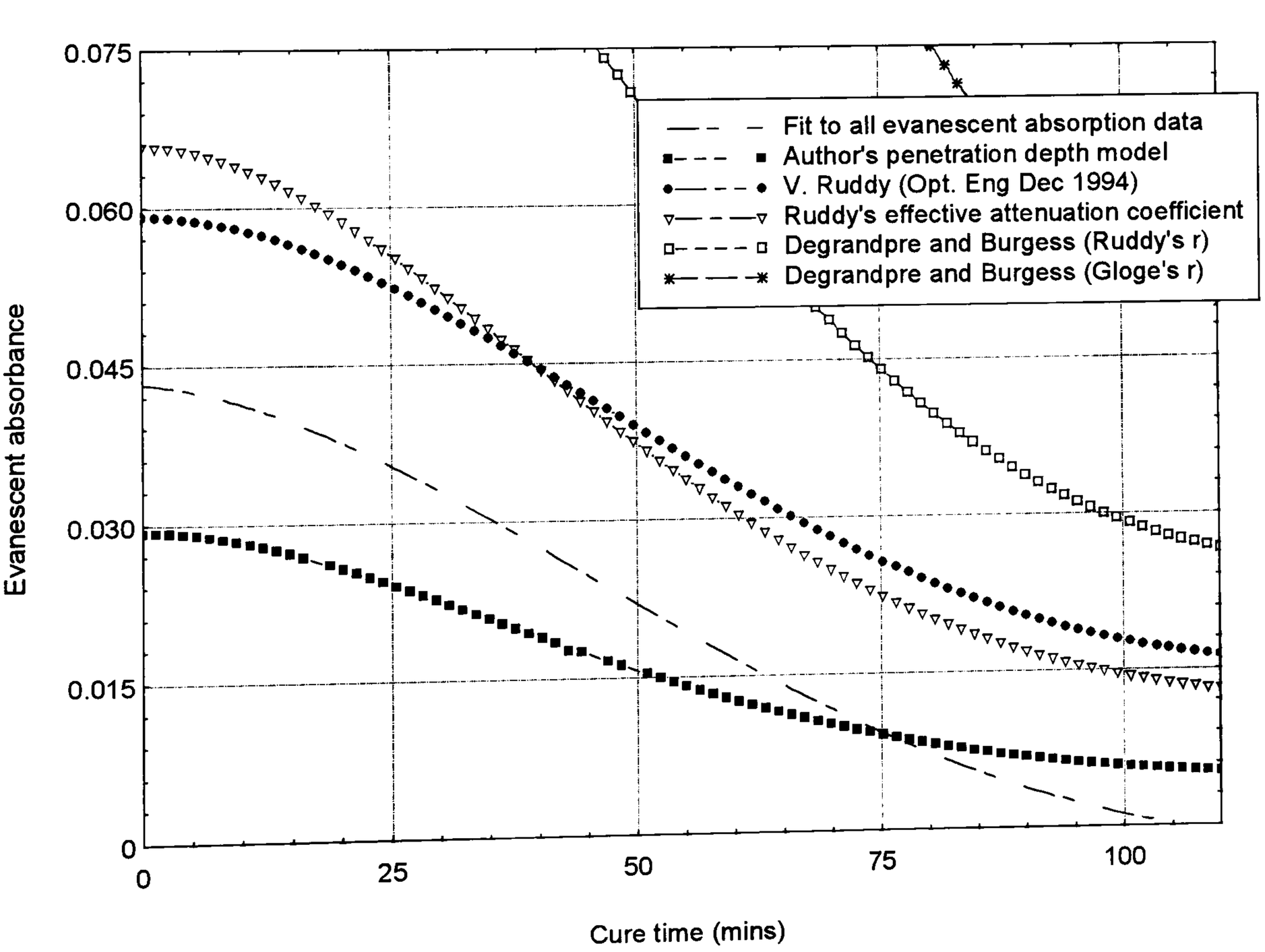

Figure 5-40 Comparison of model predictions and fit to all peak height sensor data @ 40°C

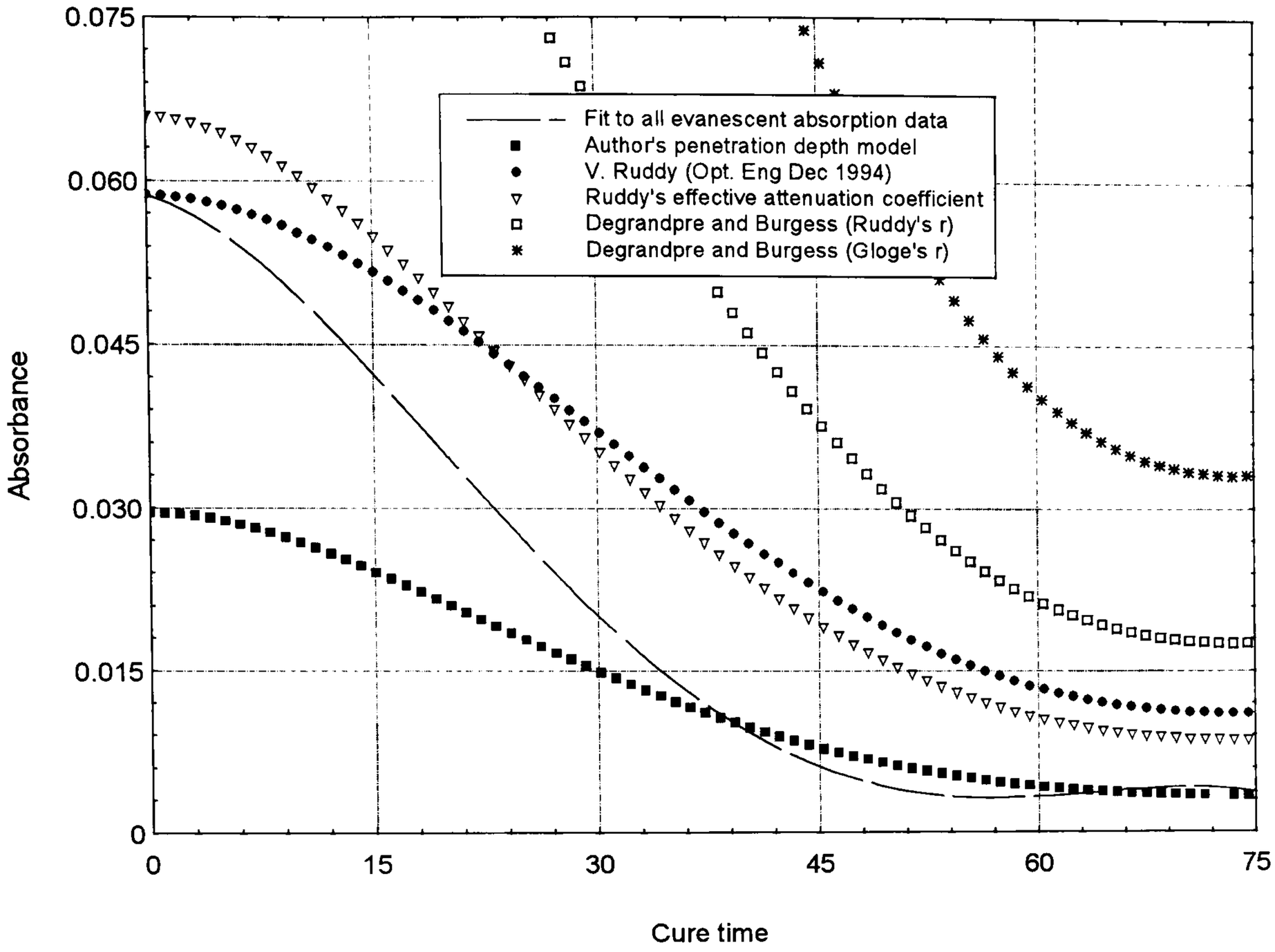

Figure 5-41 Comparison of model predictions and fit to all peak height sensor data @ 50°C

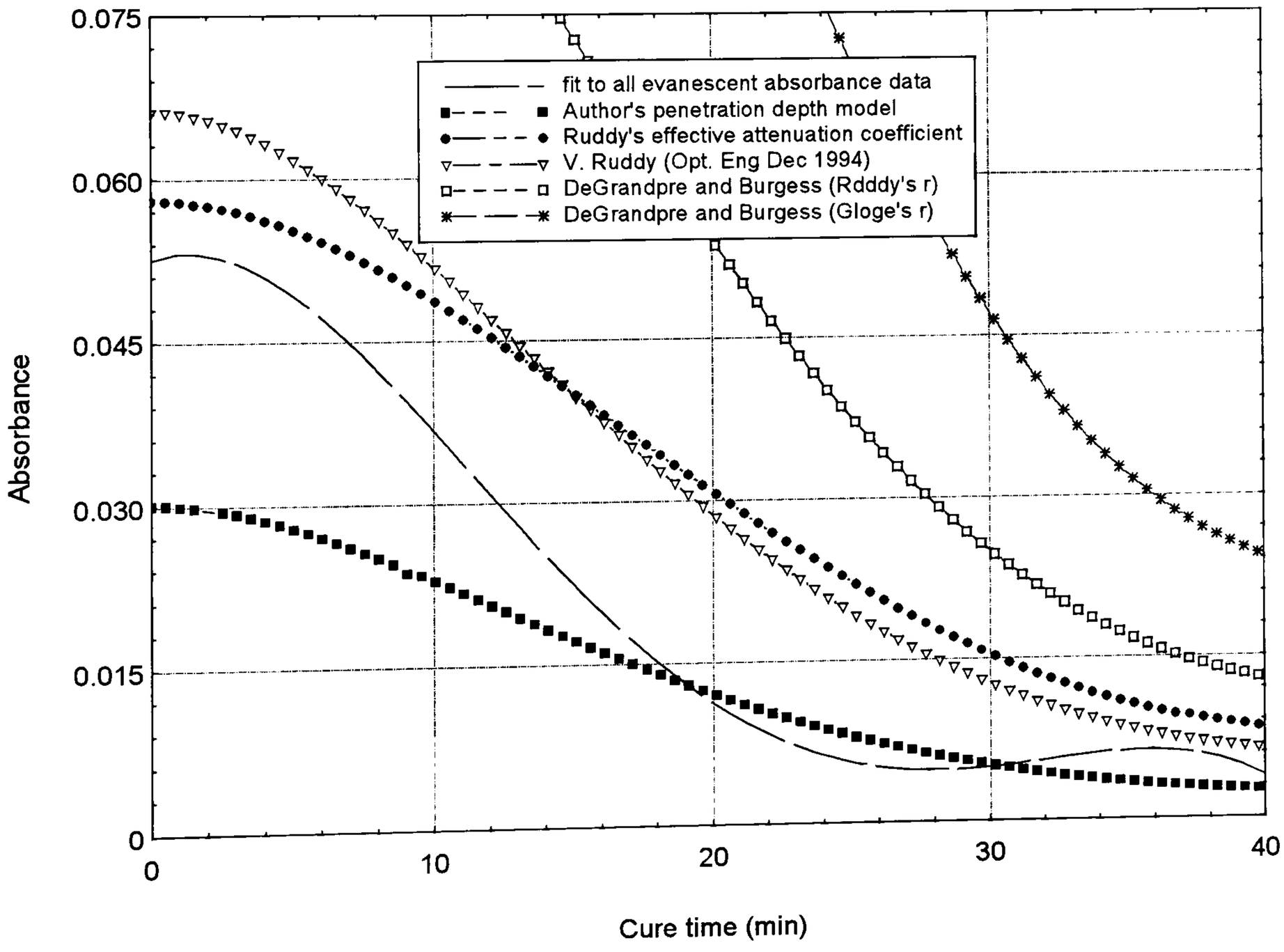

Figure 5-42 Comparison of model predictions and peak height sensor data @ 60°C

Figure 5-39, Figure 5-40, Figure 5-41 and Figure 5-42 show the comparison between an average taken from the non-normalised observed evanescent absorbance data and the predicted data from the five models. Despite the scatter on the evanescent absorbance data being so large this average, is shown on the graphs to aid clarity and make an objective assessment of the accuracy of the models easier. For information, the standard error and maximum deviations of the mean curve from all experimental data are charted in Table 5-4.

Temperature (°C)	Overall absorbance change (measured from mean)	Standard error of mean from data.	Maximum single deviation (absorbance units)
30	0.042	0.00793	0.026
40	0.047	0.00691	0.0194
50	0.056	0.00721	0.0216
60	0.053	0.00858	0.0157

Table 5-4 Standard errors and maximum deviations of data mean from actual experimental data

The model predictions can be seen to follow closely the overall trends seen in the experimental data related to cure start, cure finish and the rate of change of the absorbance band. From these graphs the following assessments were made of the five models as applied to these data.

Degrandpre and Burgess' model[195] with Gloge's r value[194]:

This model can be seen to give a prediction for the absorption approximately four times larger than that seen in the actual data. The predictions made by this model have been truncated from the above graphs for clarity. It is thought that the value for the power in the cladding, r, given by Gloge makes too many approximations to be an accurate enough indication of the true value. The inaccuracy of this model can be attributed to the fact that although Gloge's value of r give an indication of the order of magnitude of the power in the cladding it cannot be considered accurate enough for calculations of this sort.

Degrandpre and Burgess' model using Ruddy's r value[184]

Ruddy's value for the power fraction in the fibre cladding brings Degrandpre and Burgess' model prediction closer to the observed absorption values. The model incorporating this value gives a prediction approximately twice that observed. Overall it is thought that the simplicity of the Degrandpre model does not adequately model the complexities of the evanescent sensor when embedded in a medium having a refractive index change exhibiting the magnitude of refractive index change seen in a curing resin. The model does not take enough account of the change in absorption due to changing penetration depth throughout the cure time.

Ruddy's two models

Both of the Ruddy models [184,195] give predictions for the evanescent absorbance in the epoxy resin system 15-20% than those seen in the experimental data. They do however, on the whole fit the data closely. It is interesting to note that the more recent model of the two predicts a faster change in the observed absorbance than the older model and one that on the whole fits the trend of the experimental data most closely. The accuracy of these models can be attributed to their taking into account many aspects of the evanescent wave along the sensing region. Change in penetration depth, medium absorbance and refractive index are all accounted for.

The penetration depth model

Several of the models from the literature (specifically those quoted by Degrandpre and Burgess) showed deviations from the observed data which were unacceptably large. It was therefore thought that it would be instructive to try and construct a further model which could be applied directly to the problem of resin cure monitoring. This model was formulated with the aim of taking into account all parameters affecting the evanescent contact with the sensing medium while at the same time retaining a simplicity of approach. With reference to the figures above it can be seen that the author's model shows the lowest predicted absorbance of all the models and is generally lower in its predictions than the experimental data. However, its prediction is equal in accuracy to that of Ruddy and as hardener concentrations decreases with increasing cure time approaches the experimental data more closely. The model can therefore be said to be worthy of further consideration in any future studies of the evanescent absorption sensor for cure monitoring.

This work has shown that both the models formulated by Ruddy and the author's model give a good indication of the magnitude of absorbance sensitivity which can be expected

from an evanescent sensor. The Degrandpre and Burgess model would appear to be somewhat naïve in its approach and hence inaccurate in its prediction. To further assess the accuracy of the models it will be necessary to improve the evanescent sensing technique so that the data obtained using it become more repeatable.

5.4.8 Sensor enhancement

Experiments were carried out to determine whether modifications in the geometry of the sensor could enhance sensitivity of the sensor and thus improve the quality of measurements made with it. The experiments were carried out as detailed in section 5.3.6.

5.4.8.1 Numerical aperture

Three spectra of the ethylenediamine absorption peak centered on 1547nm can be seen in Figure 5-43. The three spectra were taken using the 0.9, 0.8 and 0.7 numerical aperture launch objectives. The spectra obtained using the 0.4 and 0.2 numerical aperture objectives displayed negligible evanescent absorption and so have been omitted from this graph.

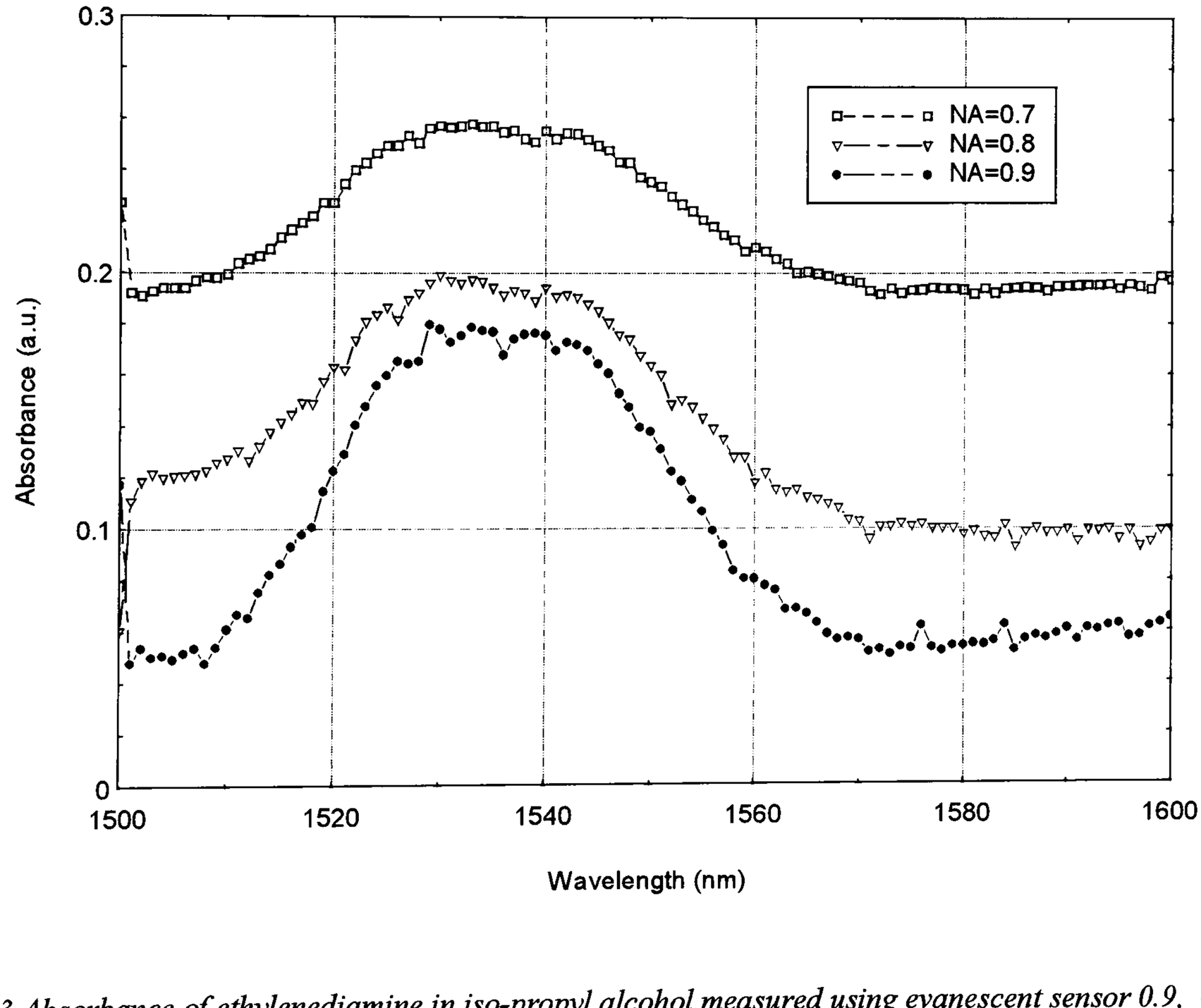

Figure 5-43 Absorbance of ethylenediamine in iso-propyl alcohol measured using evanescent sensor 0.9, 0.8 and 0.7 numerical aperture launch microscope objectives.

Objective Numerical Aperture	Absorption peak height at 1529nm
0.7	0.062
0.8	0.081
0.9	0.127

Table 5-5 Variation in absorption peak height at 1529nm with launch optics numerical aperture

The absorption peak heights taken from Figure 5-43 are given in Table 5-5. The main feature of these data are:

i) the higher numerical aperture launch optics couple light slightly more efficiently into the fibre (resulting in an observed reduction in the baseline absorbance as the launch numerical aperture approaches the fibre numerical aperture);

ii) even underfilling the optical fibre numerical aperture by a small amount results in a substantial reduction in the sensitivity of the optical fibre sensor. (This is 36% in moving from 0.9 numerical aperture objective to a 0.8 numerical aperture objective. This represents a reduction in the maximum launch angle of only 5.6° suggesting 36% of the optical power of the evanescent wave in this sensor is produced by those rays incident at this outer 5.6°);

iii) those rays incident at angles smaller than 23.5° contribute a negligible amount to the power in the evanescent wave (since the spectra taken using the 0.4 and 0.2 numerical aperture launch optics had no absorption peak present).

These results suggested that the strategy of removing those rays which contribute little to the evanescent wave, by masking out the low launch angles, could be a good one for enhancing the sensor sensitivity. By removing these rays the background onto which the absorption peaks are superimposed would be reduced thus increasing the signal to noise ratio.

5.4.8.2 Masking of objectives

Five spectra of ethylenediamine in iso-propyl alcohol can be seen in Figure 5-44 taken over the spectral range 1500-1580nm. Each of these spectra was made using a different size opaque mask placed at the mouth of the 0.9 numerical aperture launch objective to remove those rays which contribute little to the evanescent wave. It was found that masks

with opaque regions greater in diameter than 5mm obscured the launch optics to too great a degree and produced a signal which was too small to measure reliably.

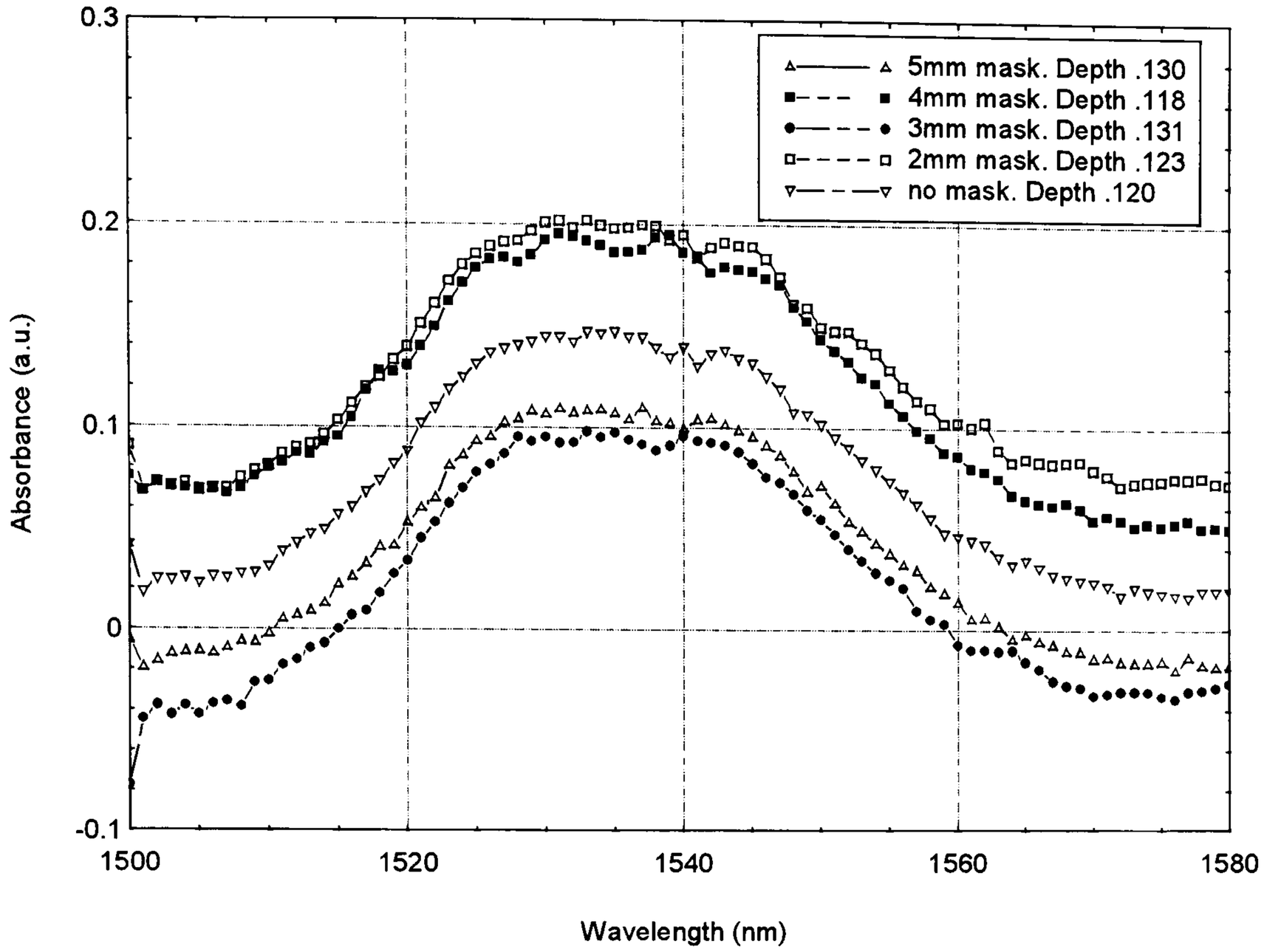

Figure 5-44 Absorbance of ethylenediamine in iso-propyl alcohol as seen by evanescent absorption sensor with opaque masks of several sizes placed on launch objective

It can be seen from these curves that the mask have had little effect on the depth of the evanescent absorption seen by the optical fibre sensor in these experiments. The peak heights at 1529nm the largest and smallest depth being within 10% of each other.

It is difficult to propose a reason for this method of removing the lower order propagation modes having little effect on observed spectral signal. However, it may be that the filtered lower order modes could have been re-excited over the length of fibre between the sensing region and the launch optics. This involves energy being coupled back into the lower order modes from the higher order modes. This phenomenon is discussed by Tateda and Ikeda[199] who use a similar masking technique to that used here to separate modes into groups and observe the mode conversion over lengths of bent, 125μm core, multimode fibre. Mode conversion was observed by these researchers in 5m lengths of fibre so it is possible that a similar effect is occurring over the 2m of fibre between the launch optics and sensing region in these experiments.

5.4.8.3 Profiling of sensor region

Four evanescent absorption spectra of the ethylenediamine/isopropyl alcohol solution taken with sensors having tapered areas in their sensing regions are shown in Figure 5-45. The peak heights measured at 1529nm are stated in Table 5-6.

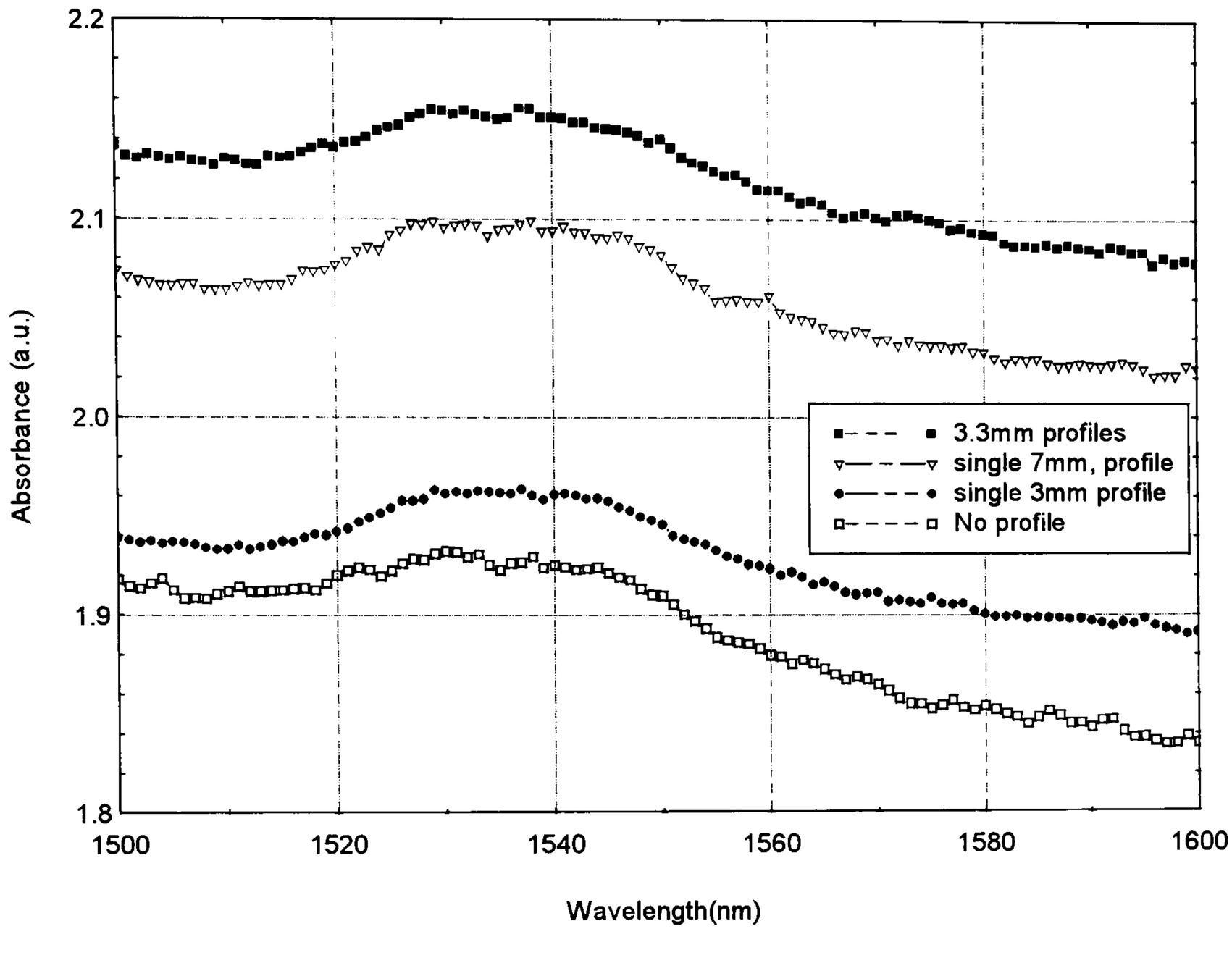

Figure 5-45 Ethylenediamine evanescent absorption variation with several sensor region profiles.

Profile in sensing region	Measured absorption depth
None	0.037
Single 3mm profile	0.045
two 3mm profile	0.042
Single 7mm profile	0.038

Table 5-6 Measured absorption depths of profiled evanescent absorption sensors

As with the masking experiments it can be seen that the sensor region profiles have no appreciable effect on the depth of the absorption observed. There is some change in the baseline but this could be attributed to light incident at the profiles at angles above the fibre core/solution critical angle and being radiated. It is probable that these tapered regions were too short in comparison to the overall sensor length (10cm) to have had much effect on the overall absorbance seen by the sensor but since we had only one way of creating these tapered regions it was not possible to take these experiments any further. Typical

commercially available optical fibre tapers are of the order of 10cm long, However, since these are expensive, and the optical fibre sensor for resins is sacrificial they are not suitable for this application.

It has been demonstrated that the sensitivity of the optical fibre evanescent sensor used in this study is highly affected by the numerical aperture of the light launched into them. The optical fibre from which the sensor is constructed should be slightly overfilled to ensure that the higher order modes which contribute most to the power in the evanescent wave are excited. This is of particular importance with the high refractive index fibre which has a large numerical aperture.

Experiments performed to see if modifications to the sensor and launch geometry have been unsuccessful. For the sensor to become more useful it will be necessary to perform further experiments and try other ways of exciting those modes which contribute most to the power in the evanescent wave.

5.5 Chapter conclusions

An optical fibre evanescent absorption sensor for monitoring the cure of an epoxy resin system has been demonstrated. The sensor is capable of detecting the depletion of the amine absorption band centred at 1547nm as the curing agent reacts with the epoxy groups in the epoxy mixture. The sensor was used to monitor the cure of the model resin system Epikote 828 and hexanediamine. The sensor results could be used qualitatively to predict the time of end of cure. However, quantitative information on the final extent of cure was difficult to obtain due to fluctuations in the sensor signal from cure run to cure run. Further work is required to isolate the sources of experimental fluctuation.

Experiments were carried out to assess the performance of several evanescent absorption models from the literature and an original model formulated by the author, when compared to the observed evanescent absorbance. A model by Ruddy[195] and the author's model showed the closest agreement with the experimental data.

The models were also adapted so that they could be used to predict sensor response during the cure of the model resin system. By incorporating FTIR absorbance data and refractive index data taken during cure at each of the isothermal temperatures and substituting them into the models an expected response could be determined. The same two models produced predictions of the expected sensor response to within the scatter of the experimental data.

The ability of the sensor to detect changes in concentration of the amine hardener has been demonstrated. However, the measurements are still prone to many errors including microbends and connection losses. Many of these errors could be removed if the wavelength range of the instrumentation could be extended and an intensity referencing technique to an invariant absorption was used.

The poor sensor response seen in the cure monitoring experiments prompted an investigation into methods of enhancing its sensitivity. Two methods which were suggested by the literature have been tried and, disappointingly, have been found to produce little or no enhancement of the evanescent absorbance observed. Both of these methods aimed to increase the signal to noise ratio of the measurements by removing some of the large background "noise" signal produced by the modes contained in the fibre which make little or no contribution to the power in the evanescent wave. The enhancement experiments did demonstrate the importance of ensuring that the higher order propagation modes are excited by completely filling or overfilling the optical fibre using a high numerical aperture objective.

6 Optical Fibre sensor for Refractive index cure monitoring

6.1 Introduction

This chapter contains details of experiments carried out to evaluate the refractive index based optical fibre cure sensor. This sensor, being similar in construction to the evanescent absorption sensor detailed in Chapter 5, was fabricated from high refractive index optical fibre (n=1.65). The cladding was removed over a short length (25mm) of the fibre and the sensor was then embedded in a sample of curing Epikote 828 resin. From measuring the amount of light transmitted by the sensor the change in the refractive index of the curing resin could be inferred. Since resin refractive index is directly related to the rate of cross-linking, the cure rate could be determined. The refractive index sensor was also used to follow the cure of a 924resin/glass pre-preg cured using the manufacturers recommended cure schedule. The investigation into the refractive index sensor was a collaborative programme of work with the author's co-investigator.

This chapter covers the following aspects of the refractive index sensor and its use in tracking the cure of resins and composites:

i) theoretical background to the refractive index sensing mechanism;

ii) abbe refractometry cure monitoring;

iii) modelling of Abbe results;

iv) comparison of sensor results and refractive index measurements made simultaneously using an Abbe refractometer to test theory;

v) cure monitoring of Epikote 828 and hexanediamine using the sensor;

vi) use of the refractive index sensor for tracking the cure of a glass/resin composite prepreg.

6.2 Theory of sensor operation.

As explained in section 3 the light guiding properties of an optical fibre are due to the total internal reflection of the light at the interface between the fibre's core and its cladding. One gauge of an optical fibres ability to guide light is its numerical aperture which is defined by the equation:

$$N.A.=\left(n_{co}^{2}\ -n_{cl}\right)^{\frac{1}{2}}=\sin\theta_{a}$$

- 6.1

where n_{co} is the refractive index of the fibre core and n_{cl} is the refractive index of its cladding. The numerical aperture is equal to the sine of the angle over which the fibre will accept light ($sin\ \theta_a$), the acceptance angle. It can be seen that the acceptance angle of the fibre will change if the value of the refractive index of the cladding changes. Thus, the changing n_{cl} will change the amount of light guided by the fibre. This is illustrated in Figure 6-1.

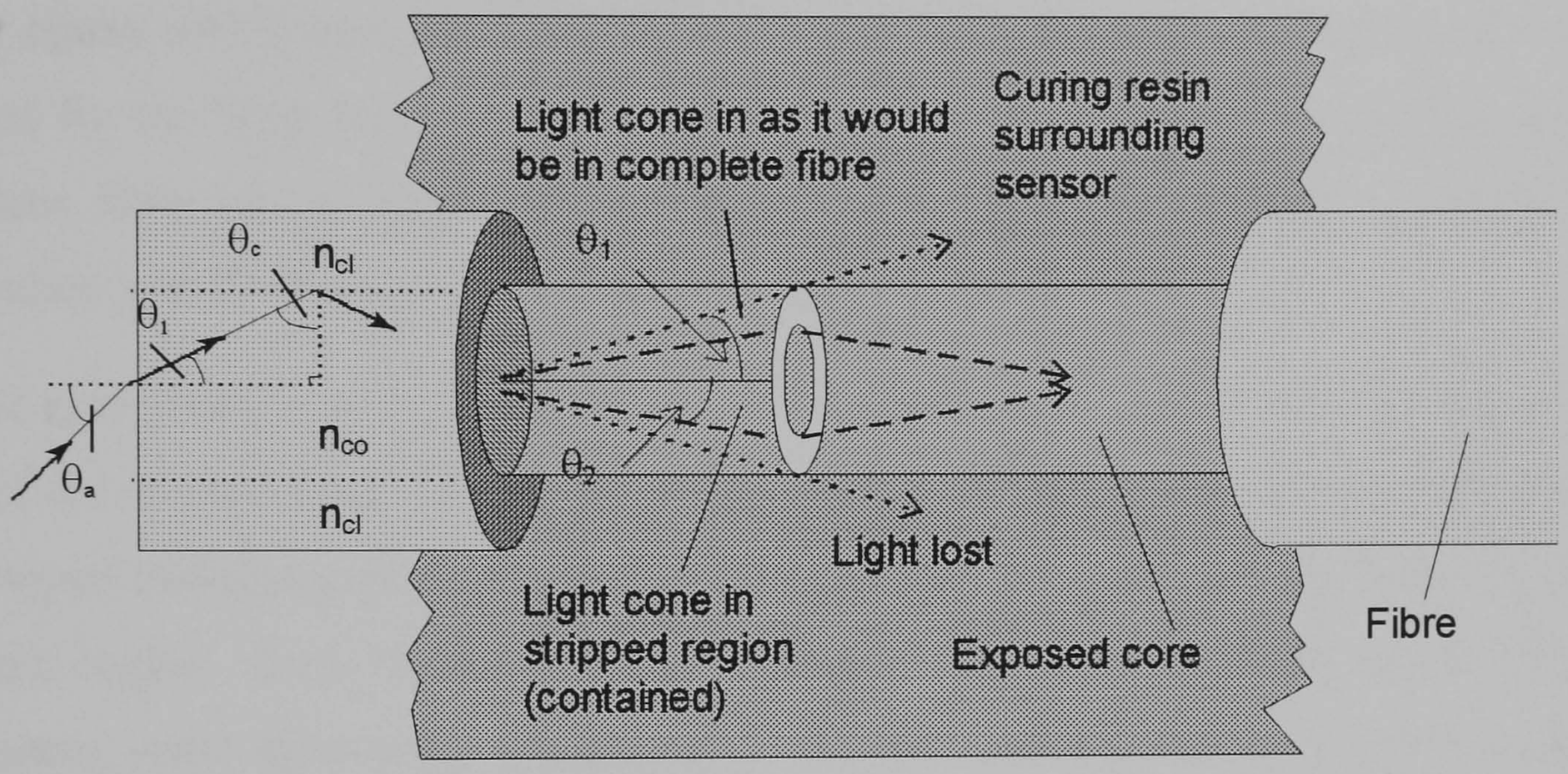

Figure 6-1 Illustration of light cone change for stripped cladding refractive index based sensor.

This figure illustrates light entering an optical fibre from air at an angle θ_a. On entering the fibre, the refracted angle θ_1 is given by:

$$\sin\theta_{1}=n_{co}\sin\theta_{a}$$

- 6.2

where n_{co} is the refractive index of the fibre core. For total internal reflection, the angle at which the ray strikes the core-cladding boundary must be greater than the critical angle θ_c given by:

$$\sin\theta_{c}=\frac{n_{cl}}{n_{co}}$$

- 6.3

where n_{cl} is the refractive index of the cladding. If a portion of the cladding is stripped away and a medium of different refractive index n_3 is placed in contact with the fibre core, different guiding characteristics will apply and the new light cone half angle θ_2 will be given by:

$$\sin\theta_2 = \frac{n_3}{n_{co}}$$

- 6.4

For the case where $n_{co} > n_3 > n_{cl}$, if the refractive index of the medium surrounding the exposed fibre core increases so that it approached the refractive index of the core (*e.g.* a curing epoxy resin) then the value of θ_2 will decrease. This results in some of the light radiated by the fibre core. When the light passes back into the complete fibre since the complete fibre has a larger light cone than in the stripped region, no further light attenuation will be observed.

For the case where $n_{cl} > n_3$, the light cone at the stripped core region is larger that the light cone of the original fibre. Therefore, no light is lost in passing from the complete fibre into the stripped cladding region. However, on returning to the complete fibre from the stripped cladding region, since the guided light will tend to fill up the larger light cone as it propagates, some light will be lost upon returning to the fibre which possesses a smaller cone. A simple geometrical optics approach can be used to predict the amount of light lost from the fibre for given values of n_{co} , n_{cl} and n_3 and indeed for a changing n_3. If it is assumed that light guided by the fibre is evenly distributed over all angles of incidence that the fibre can guide (reasonable for long, very multimode fibre) then the light lost by the fibre can be calculated from the ratios of the areas of the light cones.

The area of the cone (A_1) supported by the unmodified fibre is given by:

$$A_1 = \pi\left(\sin\theta_1\right)^2$$

- 6.5

Similarly for the stripped fibre :

$$A_2 = \pi\left(\sin\theta_2\right)^2$$

- 6.6

therefore the percentage of light remaining after stripping the fibre and surrounding it with a medium with refractive index n_3 is A_2/A_1. Now:

$$\sin\theta_1 = n_{co}\sin\theta_{a1}$$
$$\&$$
$$\sin\theta_2 = n_{co}\sin\theta_{a2}$$

- 6.7

where θ_{a1} and θ_{a2} are the acceptance angles of the unmodified and modified fibres respectively. Substituting the equations from 7 into 5 and 6 we see:

$$\frac{A_2}{A_1} = \frac{\left(\sin\theta_{a2}\right)^2}{\left(\sin\theta_{a1}\right)^2} = \left(\frac{NA_2}{NA_1}\right)^2$$

- 6.8

where NA_1 and NA_2 are the numerical apertures of the unmodified and modified fibres. The values of the numerical apertures are also given by the equation:

$$NA = \sqrt{n_{co}^2 - n_{cl}^2}$$

- 6.9

6.3 Experimental procedure

6.3.1 Abbe refractometry cure monitoring

Refractive index measurements were made using a Bellingham and Stanley Abbe refractometer and a sodium arc light source. This type of lamp emits monochromatic light at 589nm which is a wavelength commonly used for quoting the refractive index of materials. Refractive index measurements made at this wavelength are referred to as n_D and this convention will be followed here. The instrument was calibrated using a silica test piece supplied by the instrument manufacturers.

The refractive index of the curing epoxy/amine mixture was measured using the instrument in transmission mode. Three drops of the mixed system were placed on the lower measurement prism. The upper prism, which had been coated with a thin film of release spray, was placed on the lower prism so as to form a thin resin film between the two. The sodium lamp was positioned so as to pass through the upper prism, the resin film and into the lower prism allowing the refraction angle of the light to be observed using the attached

measurement telescope. From the refraction angle the refractive index of the resin is measured using the calibrated scale on the instrument. A diagram of the prism arrangement can be seen in Figure 6-2.

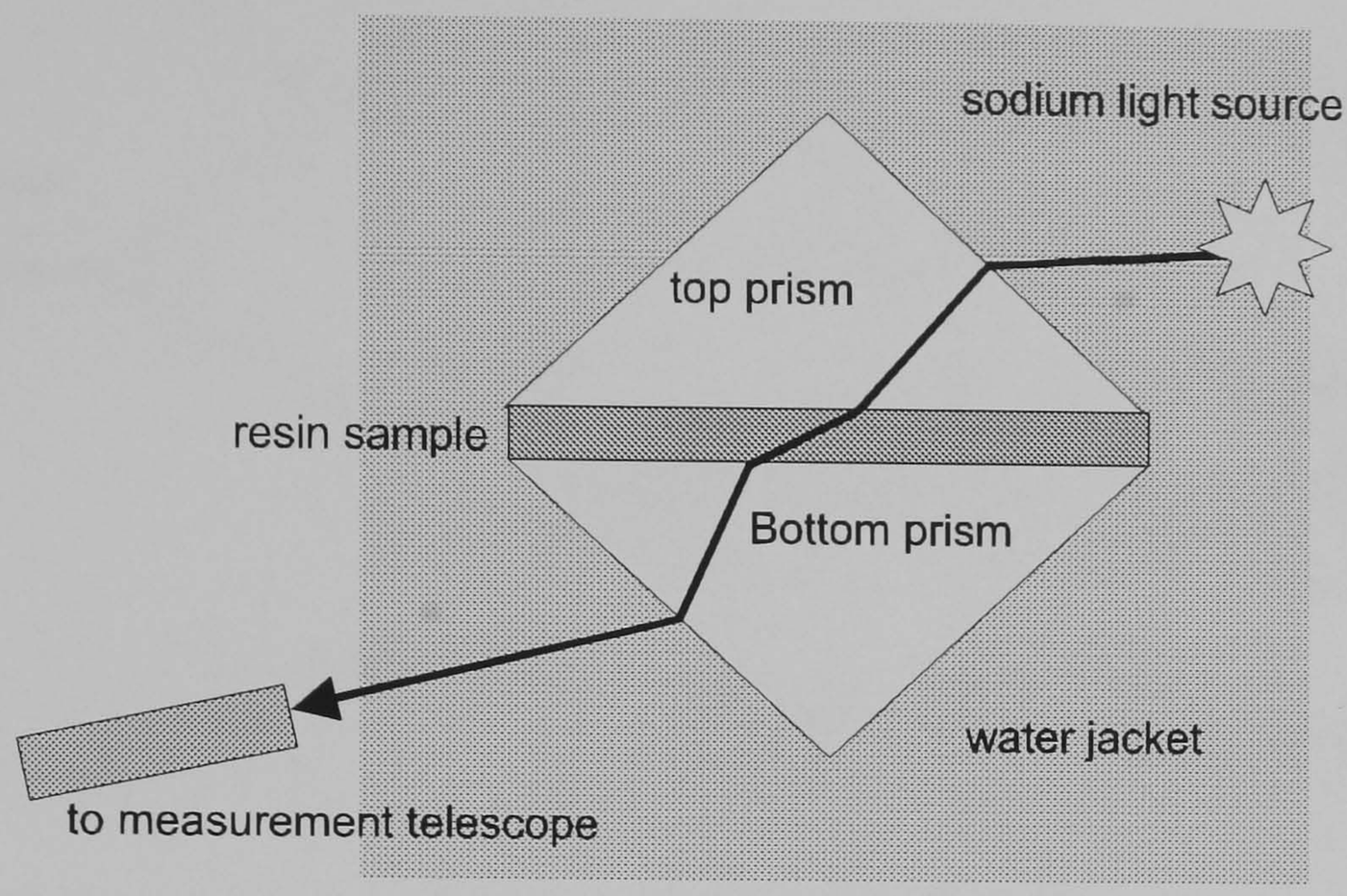

Figure 6-2 Schematic diagram of Abbe refractometer experimental arrangement

Refractive index measurement experiments were carried out on an Epikote 828 and hexanediamine mixture at isothermal temperatures from 30 to 60°C. The isothermal temperatures were maintained by passing water from a heated water bath through a jacket surrounding the prism. This kept the temperature constant to ± 0.5°C.

6.3.2 Cure monitoring using the refractive index sensor.

The prepared sensor was connected to one arm of a 1x2 silica optical fibre coupler. The input of the coupler was connected to a current stabilised, temperature controlled Profile instruments laser diode source operating at 1310 nm. This wavelength was chosen because of the wide availability of stable telecommunications sources at this wavelength and because FTIR measurements of the resin/hardener system had shown there to be no absorption bands at this wavelength which could interfere with the measurements being made. The free end of the sensor fibre and the second arm of the coupler were connected to two InGaAs photodetectors. The purpose of the second arm was to enable the output from the laser to be monitored so that any fluctuation in the source intensity could be referenced out of the sensor signal. The connections between the fibres, detectors and the laser were all made using ST telecommunications connectors which, although producing a certain amount of coupling loss, result in a reproducible connection between the various components. The current from the photodiodes were amplified to a measurable voltage level using Profile instruments photodiode amplifiers and the signals from these were

connected to an analogue-to-digital acquisition card mounted in a PC running acquisition software. A diagram of this set-up can be seen in Figure 6-3.

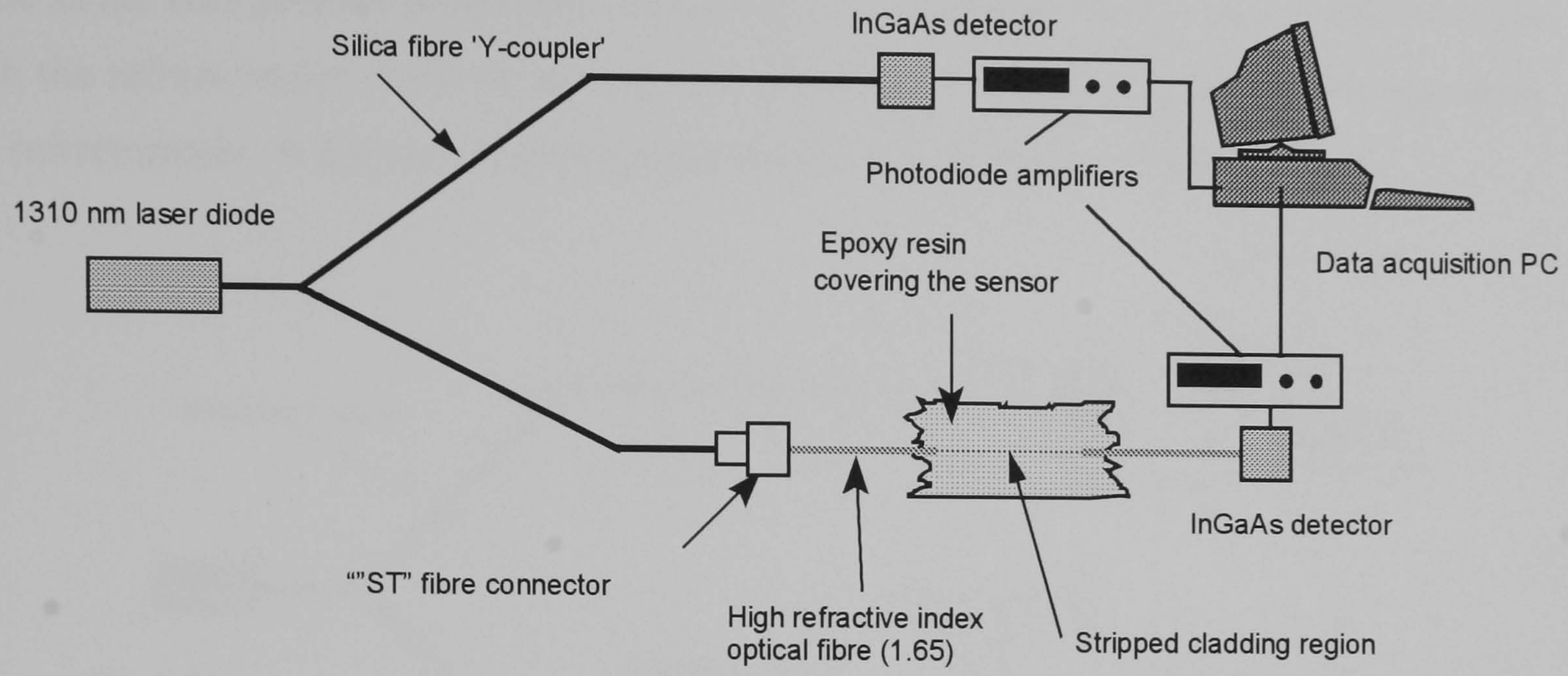

Figure 6-3 Experimental set-up for optical fibre refractive index monitoring experiments

The fibre sensor region was laid in a metal vessel containing a stoichiometric mixture of Epikote 828 (Shell Chemicals) and 1,6-hexanediamine (Aldrich Chemcals).

This resin and hardener stoichiometric mixture was made up immediately before the experiment was to begin and thoroughly mixed before being poured over the sensor region. The vessel was then placed on a hotplate, the temperature of which was controlled using an Omega PID temperature controller accurate to ±1°C. Before the experiment began the hotplate was left to equilibrate at the desired temperature for at least 30 minutes. In addition to the thermocouple used by the temperature controller an additional thermocouple was placed in the resin mixture so that the actual resin temperature could be logged. Data acquisition began immediately the resin was placed onto the hotplate. Cure monitoring experiments were carried out at isothermal temperatures of 30°, 40°, 50° and 60°C.

6.3.3 Simultaneous optical fibre sensor and Abbe refractometry cure monitoring

The results obtained from the optical fibre sensor during cure were compared with actual refractive index measurements made using an Abbe refractometer and a sodium light source which emits at 589nm. The sensor light source used was again a 1310nm laser diode and the experiment was setup in a similar way to the cure experiments except the resin covered sensor region was placed between the two prisms of an Abbe refractometer. The temperature of the prisms was maintained at the isothermal temperature required by

pumping thermostatically controlled water through them. The sodium lamp was used to illuminate the refractometer prisms and measurements of the resin refractive index were made as the cure process progressed. In this way real refractive index measurements made with the refractometer could be directly compared with refractive index data taken using the refractometer. A diagram of the experimental set-up is shown in Figure 6-4.

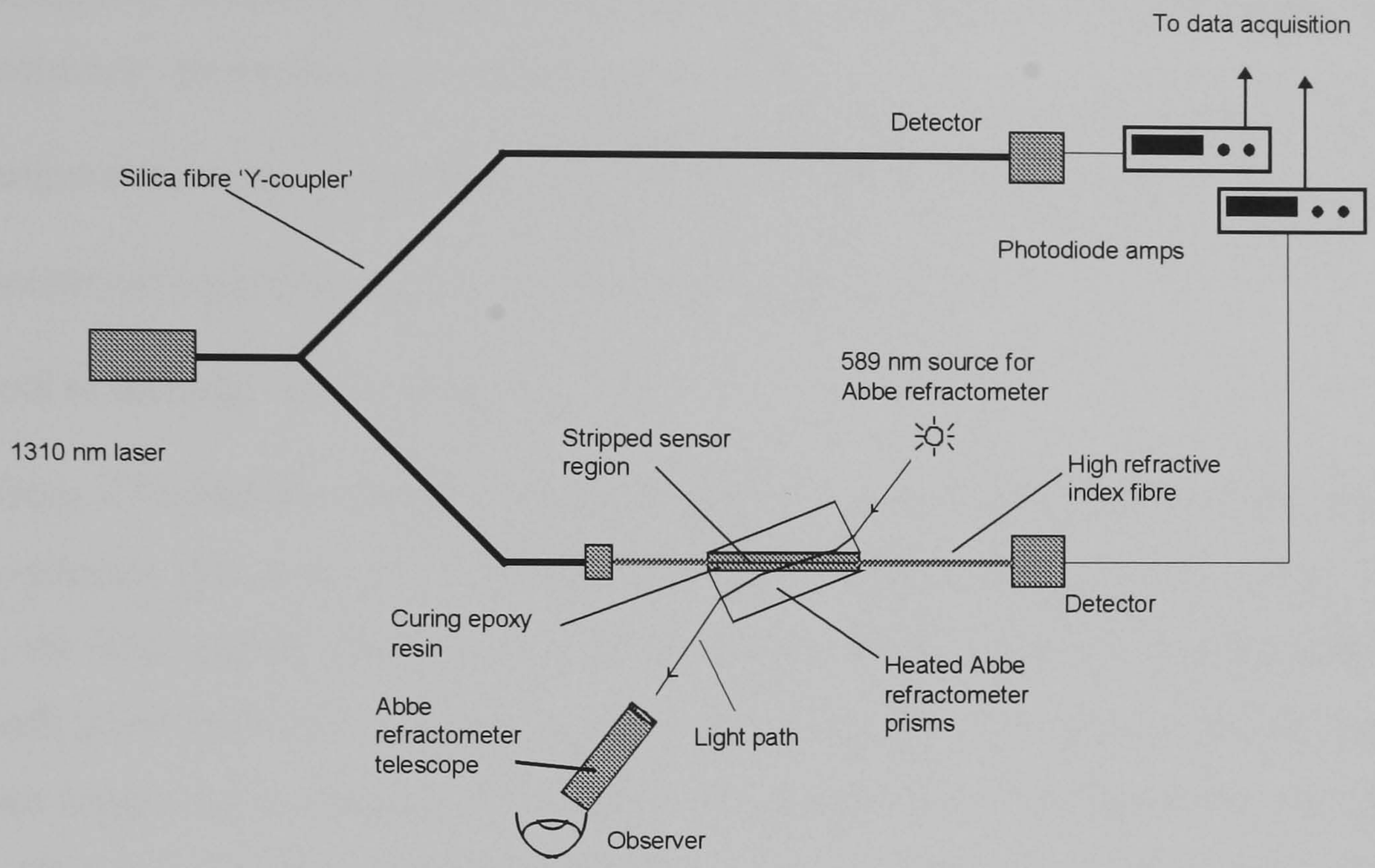

Figure 6-4 *Experimental set-up for simultaneous refractive index and OFS measurements.*

6.3.4 Cure monitoring of a glass/resin composite prepreg.

The refractive index sensor was used to track the cure of an Ciba Geigy 924 epoxy resin /glass fibre composite pre-preg. Sensors were constructed having a stripped length of 7cm and these were embedded between 4 plies of the commercial 924 /glass fibre pre-preg in a single specimen mould custom made for curing single composite coupons. A representation of this mould can be seen in Figure 6-5.

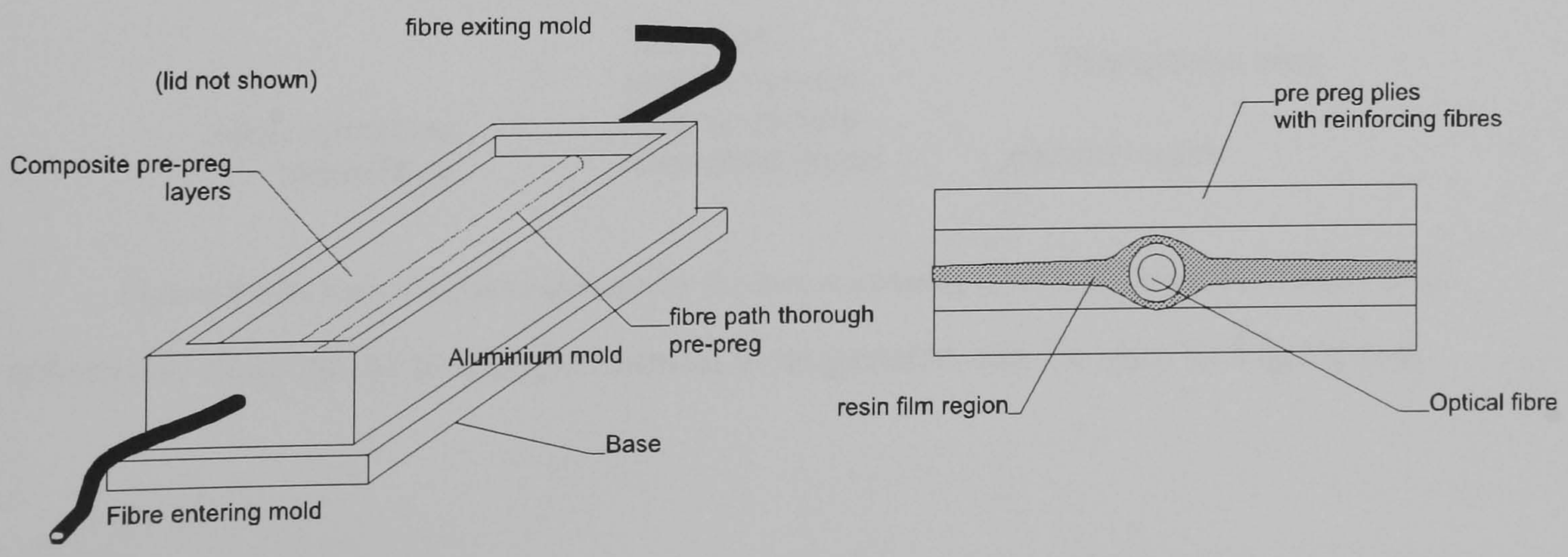

Figure 6-5 Representation of single specimen composite mould and composite/sensor layup

The sensor was passed into the mould *via* the fibre ports at each end and arranged on two plies of the pre-preg. A single layer of 924 resin film was placed either side of the fibre sensor to ensure good contact with the resin in the coupon during cure. A further two plies of pre-preg were then laid on top of the sensor. The base and lid of the mould were then placed around the laid up composite and the whole arrangement placed in a thermostatically controlled heated press. The composite coupon was then cured using the manufacturers' prescribed cure schedule. This was:

i) temperature ramp from ambient to 180°C at a rate of 3K min $^{-1}$;

ii) isothermal temperature hold at 180°C for three hours; and

iii) cool to ambient temperature.

Light from a Profile instruments, stabilised 1310nm laser source was launched into a 1x2 fibre y-coupler one arm of which went straight to a photodiode and the other into the sensor, the other end of which was connected to a second photodiode. The electrical signal from both photodiodes was fed into a photodiode amplifier. The output from the amplifiers was then logged by a computer, at a rate of one sample every two seconds, over the cure period. This arrangement allowed any drift in intensity of the laser source to be referenced from the final sensor data. A thermocouple was also placed within the composite mould so that the actual temperature of the coupon could be monitored throughout the cure cycle.

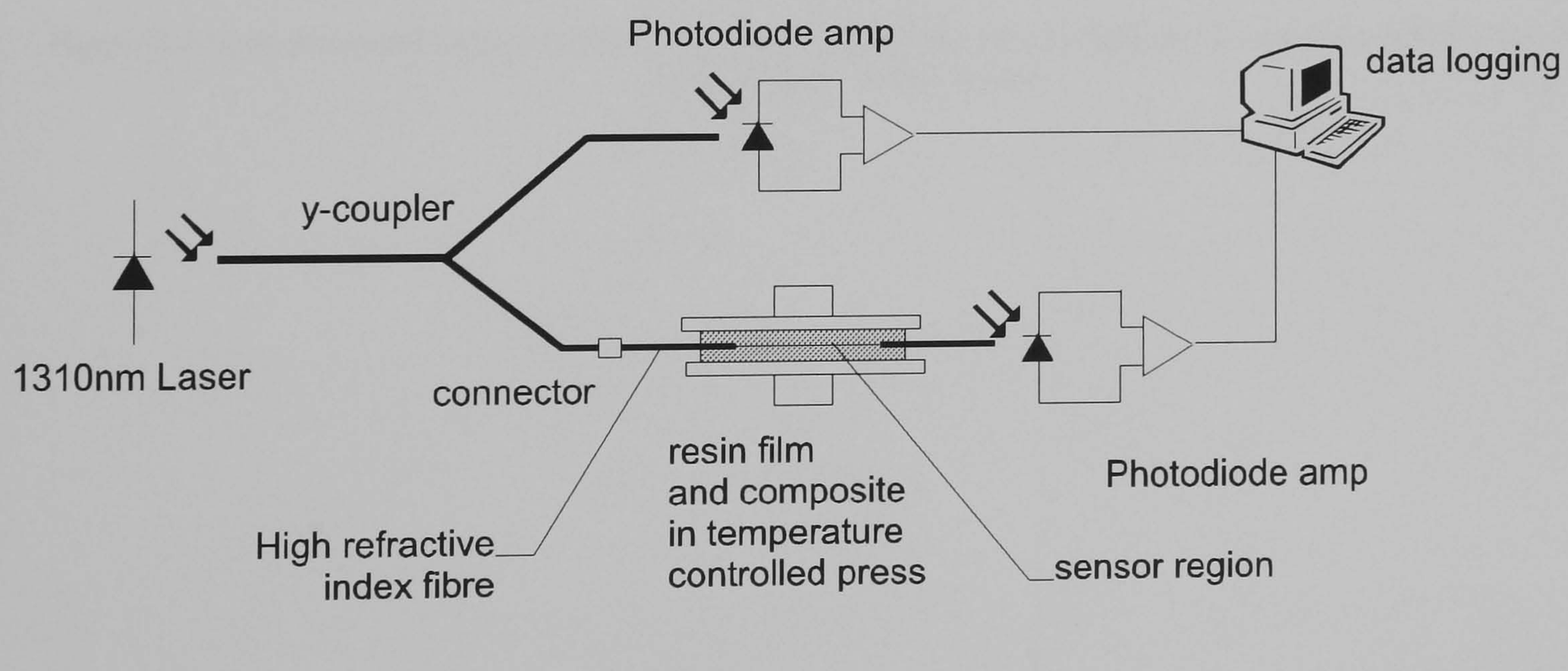

Figure 6-6 Experimental arrangement for the cure monitoring of a glass/resin composite pre-preg.

A schematic diagram of this experimental arrangement can be seen in Figure 6-6.

6.4 Results and discussion.

To determine whether the tracking of refractive index was a suitable method for following the cure of a resin, a series of experiments was performed to determine the refractive index of the curing resin throughout cure at 30, 40, 50 and 60°C. The results from these experiments can be seen in the four figures which follow.

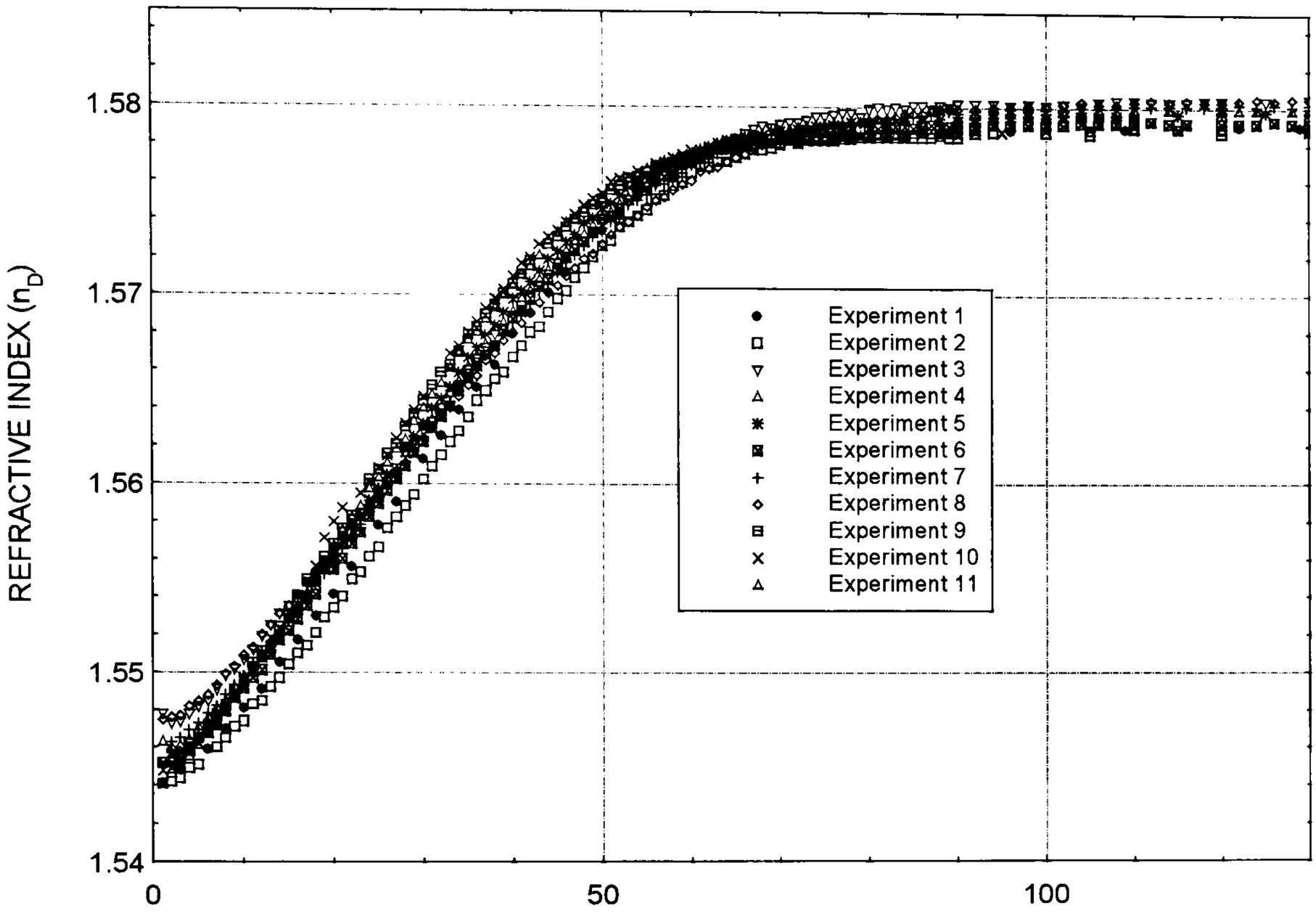

Figure 6-7 Refractive index change at 590nm (n_D) measured during cure of Epikote 828 and hexanediamine at 50°C using an Abbe refractometer

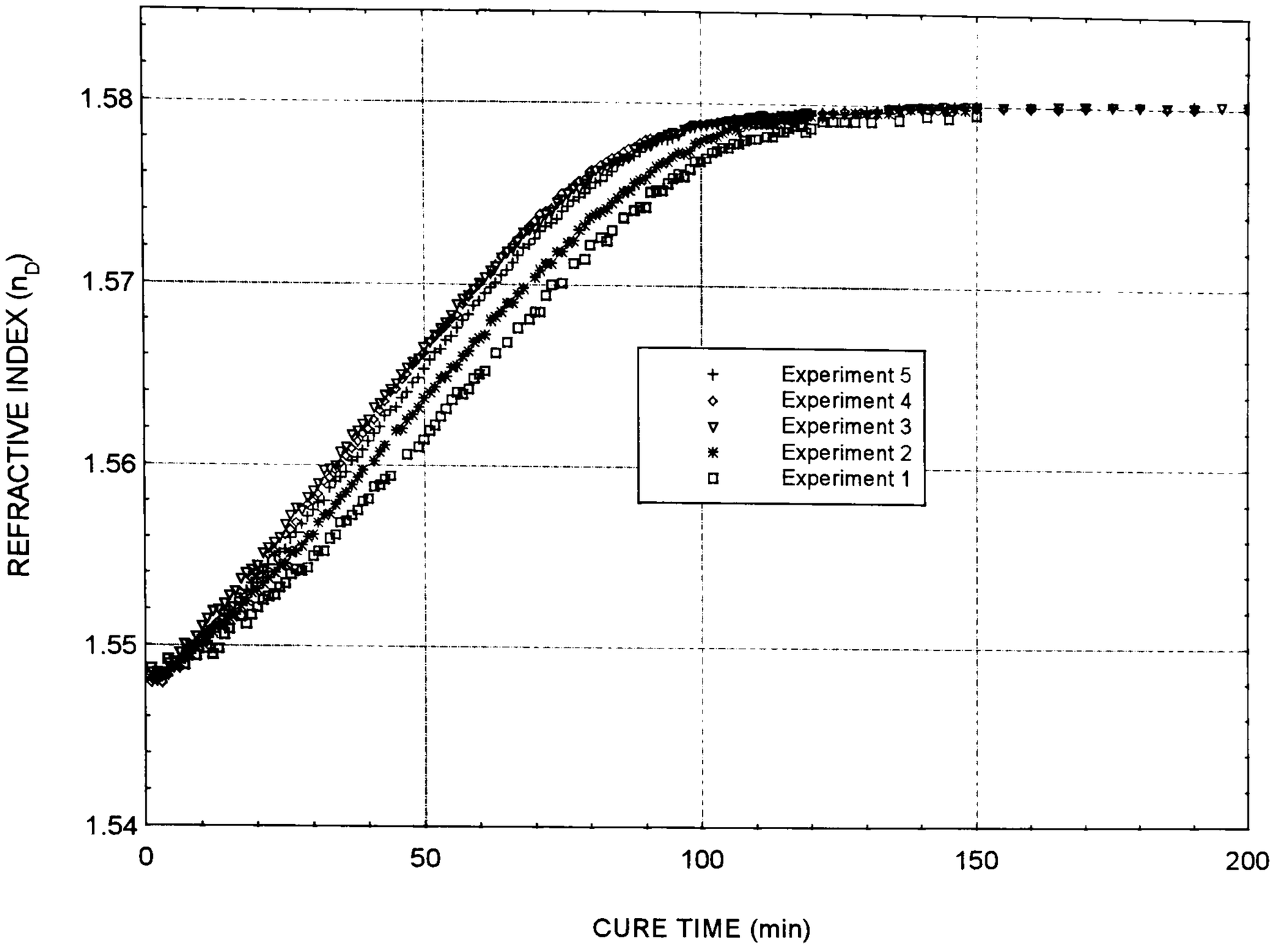

Figure 6-8 Refractive index change at 590nm (n_D) measured during cure of Epikote 828 and hexanediamine at 40°C using an Abbe refractometer

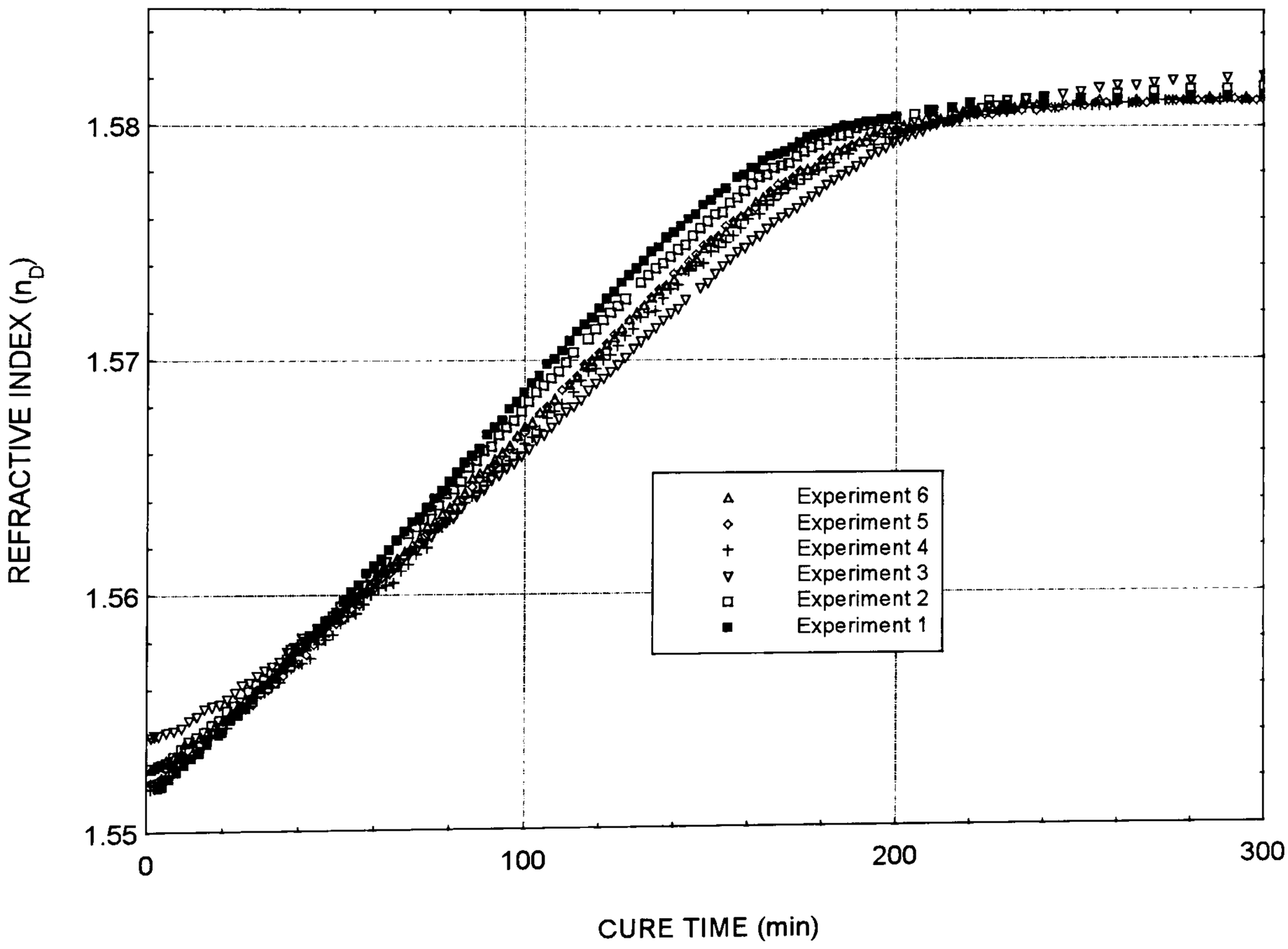

Figure 6-9 Refractive index change at 590nm (n_D) measured during cure of Epikote 828 and hexanediamine at 30°C using an Abbe refractometer

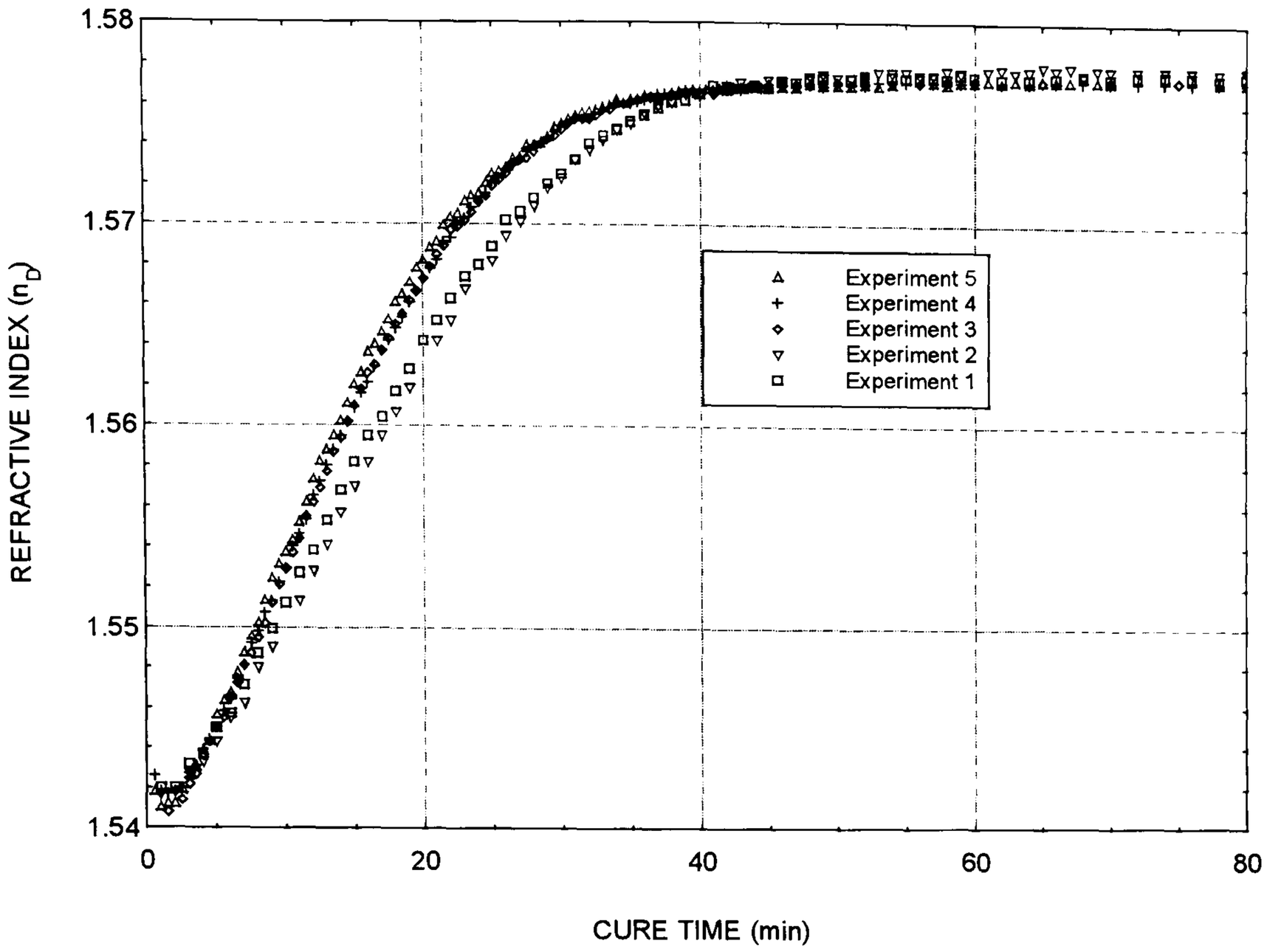

Figure 6-10 Refractive index change at 590nm (nD) measured during cure of Epikote 828 and hexanediamine at 60°C using an Abbe refractometer

Figure 6-7 contains the data from eleven repeat experiments at 50°C. From this particular data the following can be said:

i) the overall change in refractive index at this temperature is about 0.034. This is a sufficiently large change to make the refractive index monitoring of cure a realistic proposition;

ii) the variation of the data between the individual experiments is about 9% of the overall change in refractive index. Possible reasons for this scatter are discussed below.

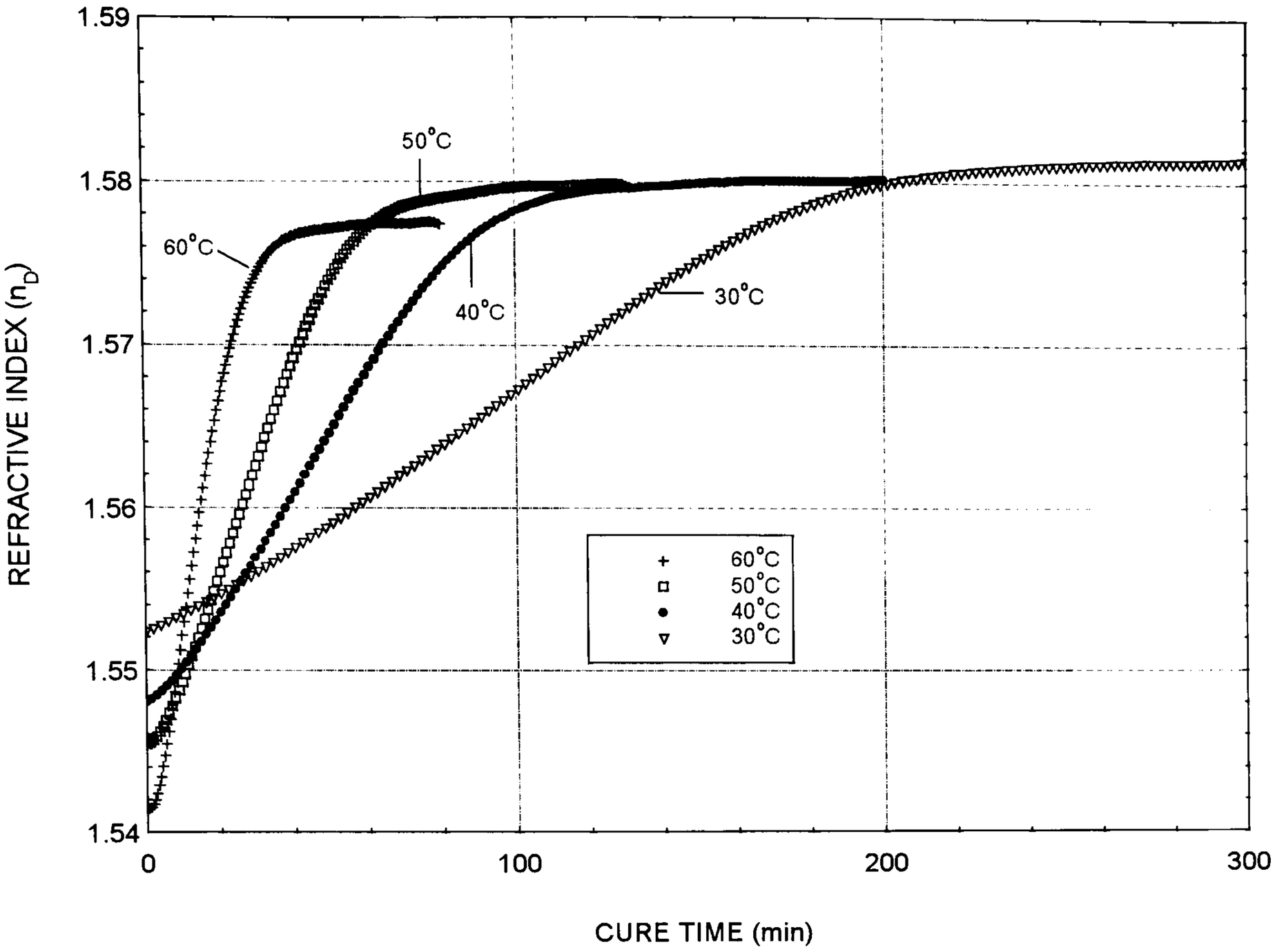

Figure 6-11 Mean of refractive index datasets at each cure temperature summarising refractive index change of resin and amine during cure.

Figure 6-11 summarises the refractive index data, showing the mean of the data at each temperature. The following points are apparent:

i) higher isothermal temperatures result in a faster rate of change in the refractive index of the sample. This can be linked to a faster rate of cure of the resin samples at higher temperatures and agrees with behaviour established using other cure monitoring techniques[198];

ii) the overall change in refractive index of the samples over the cure schedule is greater at higher temperatures (see Table 6-1).

Isothermal Cure temperature (°C)	Overall refractive index Change during cure
30	0.029
40	0.032
50	0.034
60	0.036

Table 6-1 Overall refractive index change of resin mixture during cure

This could be linked to a higher degree of crosslinking being achieved at higher temperatures:

iii) an increase in the extent of cure of a specimen results in an increase in the refractive index this can be seen from the fact that the refractive index at cure end at 30°C is generally higher than that at 60°C;

iv) from the positions of the curves at t=0 it can be seen that there is a temperature dependence of the refractive index also. The refractive index can be seen to decrease with increasing temperature;

v) although all experiments were carried out under similar conditions there is a general variability of the refractive index data between data obtained at each of the four temperatures. Possible explanations for this are:

a) moisture contamination of the reactants;

b) differing actual resin temperatures;

c) contaminated refractometer prisms;

d) inadequate mixing of reactants and/or different starting stoichiometry of the epoxy amine mixture.

Therefore, a model was required relating refractive index, extent of cure and cure temperature.

6.4.1 Relationship between refractive index and cure

In order to use the refractive index of the resin as a method of monitoring its cure it is necessary to relate the change in refractive index during cure to the chemical concentration of reactants. It has been proposed[150] that there is a linear relationship between the concentration of epoxy in the system and refractive index However, little evidence supporting this has been published. Lam and Afromowitz[150] compared fractional conversion data obtained from DSC analysis with refractive index measurements made with a cleaved optical fibre Fresnel reflectometer at several cure temperatures. A linear relationship was found between the two up to the gel point of the resin.

Measurements were made in this work to determine the relationship between refractive index and concentration for the Epikote 828 and hexanediamine mixture being investigated. The work was done using a transmission cell constructed from two optical fibres between which there was a gap of 0.75mm (see Figure 6-12).

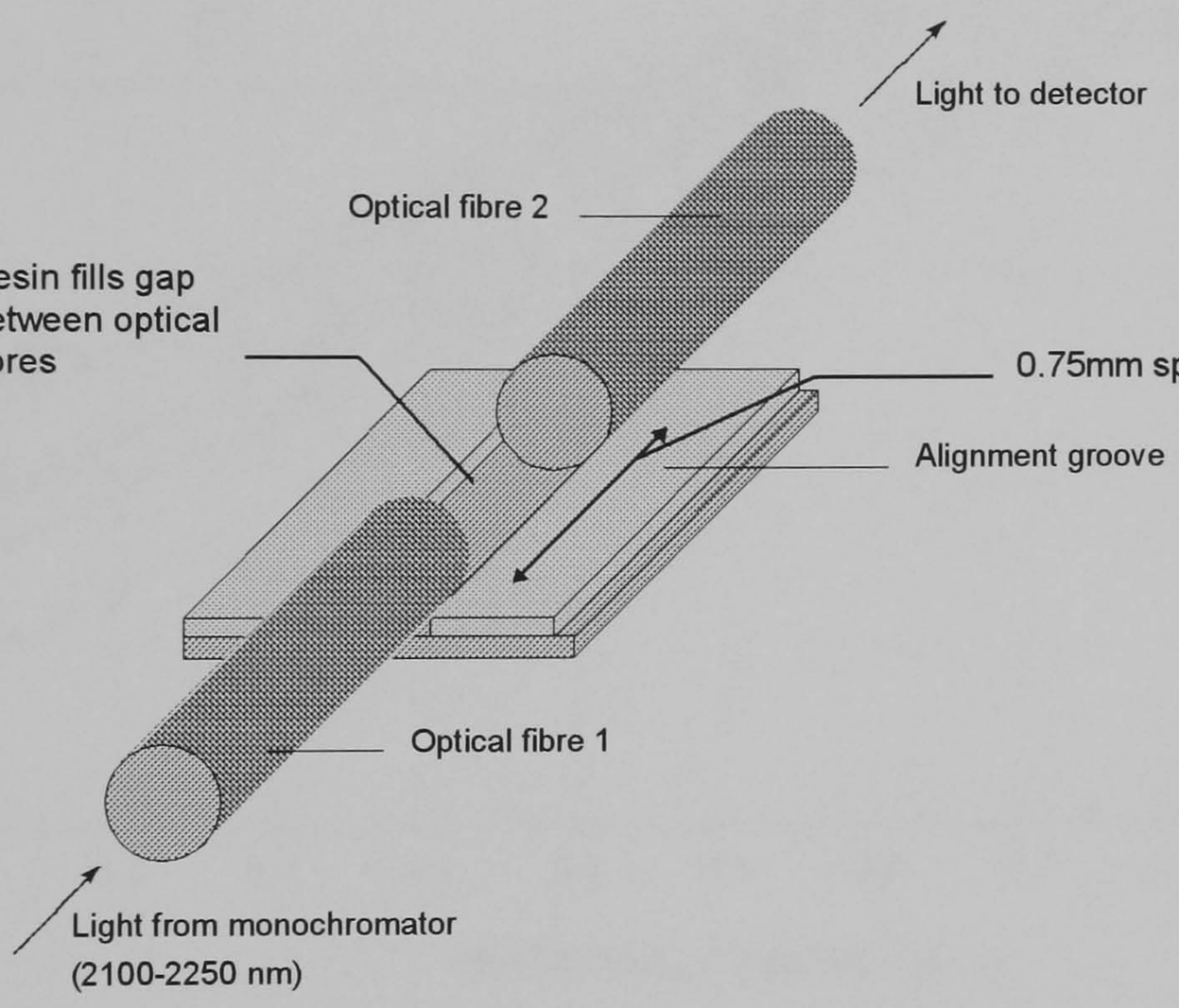

Figure 6-12 Optical fibre transmission sensor

This sensor was placed on the heated prism of an an Abbe refractometer and its free ends connected to the Bentham monochromator and a Peltier cooled lead selenide detector. This type of detector was used since spectra were taken over the wavelength range 2100-2250nm. This allowed observation of the change in intensity of the resin epoxy peak. A sample of the epoxy/amine mixture was placed over the sensor such that it flowed into the gap between the two optical fibres. In this way transmission spectra of the resin could be obtained at the same time as the refractive index at 589nm was measured using the Abbe. Fifty spectra were acquired for each cure experiment.

Following cure the areas of the epoxy peak centred on 2205nm were calculated . This was ratioed against the C-H absorption at 2163nm and this ratio was then used to calculate the degree of epoxy conversion using the equation:

$$\alpha = 1 - \left(\frac{\left(area_{epoxy} / area_{C-H} \right)_{time=t}}{\left(area_{epoxy} / area_{C\_H} \right)_{time=0}} \right)$$

Figure 6-13 shows a summary of the data thus obtained relating refractive index to epoxy conversion.

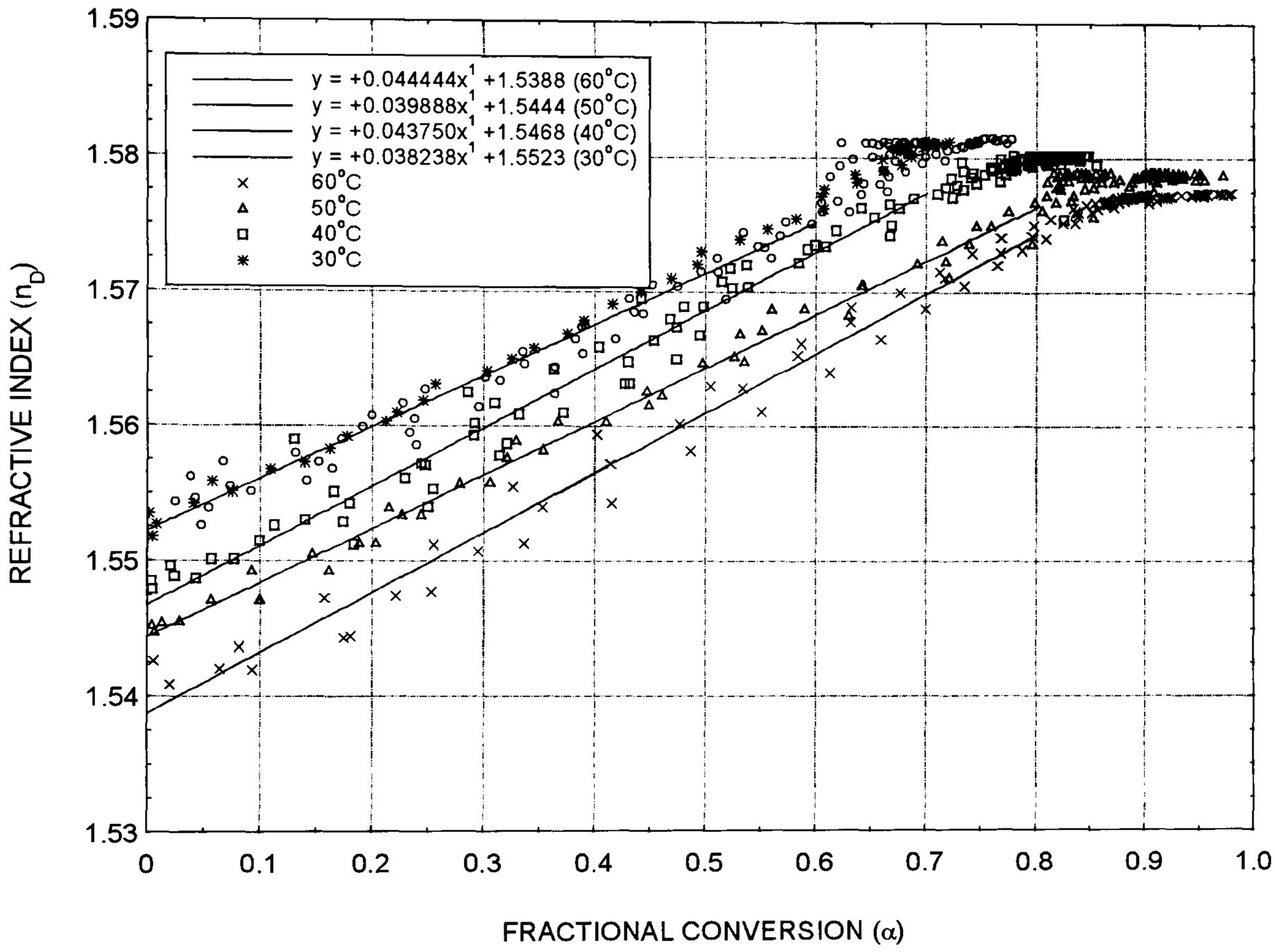

Figure 6-13 Summary of results obtained for relationship between refractive index and extent of cure at four cure temperatures.

It can be seen from this figure that the relationship between refractive index and extent of cure is linear until near to the end of cure corresponding to a fractional conversion of approximately 0.75 which provides experimental verification of the postulate that refractive index is related to degree of cure. At this point the rate of change of refractive index slows although the extent of cure continues to increase. Similar behaviour was observed by Lam and Afromowitz[152] for the cure of a DGEBA epoxy resin. These authors attributed this behaviour to the onset of gelation.

6.4.2 Simultaneous refractive index cure monitoring with sensor and Abbe

To determine whether the numerical aperture model for the optical fibre sensor was valid a number of experiments were conducted. The signal from the fibre sensor was monitored at the same time as the refractive index of the sample into which it was embedded using the Abbe refractometer.

A spectrum of the a sample of the resin mixture was taken using a Perkin Elmer λ19 spectrometer, between 400 and 800nm, before the experiment to determine whether there were any significant absorption bands in this area which could interfere with the results *via* anomalous dispersion. This spectrum indicated that there were no such bands.

Mechanically chopped light was launched from the Bentham Instruments monochromator at a wavelength of 589nm, the same as that provided by the sodium lamp used by the Abbe refractometer, *via* a 0.9 numerical aperture microscope objective. The optical fibre numerical aperture was calculated as 0.86 and so the microscope objective should have filled all available propagation modes in the fibre. Since refractive index does vary with wavelength it was important that both the Abbe measurements and the OFS measurements were made at the same wavelength. The light emerging from the sensor was detected using a silicon photodiode operating in photovoltaic mode, the signal of which was fed into a phase-sensitive detector. The signal from the phase-sensitive detector was logged using a PC.

All sensor results were normalised by dividing all data points by the initial sensor signal.

The mean Abbe data from eleven experiments carried out at 50°C were used to compare calculate a predicted sensor response to compare with the actual sensor signal calculated using the equations shown in Section 6.2. These calculations were performed using Easyplot graphing software, taking the fibre core refractive index to be 1.65 and the cladding index to be 1.41. This comparison can be seen in Figure 6-14.

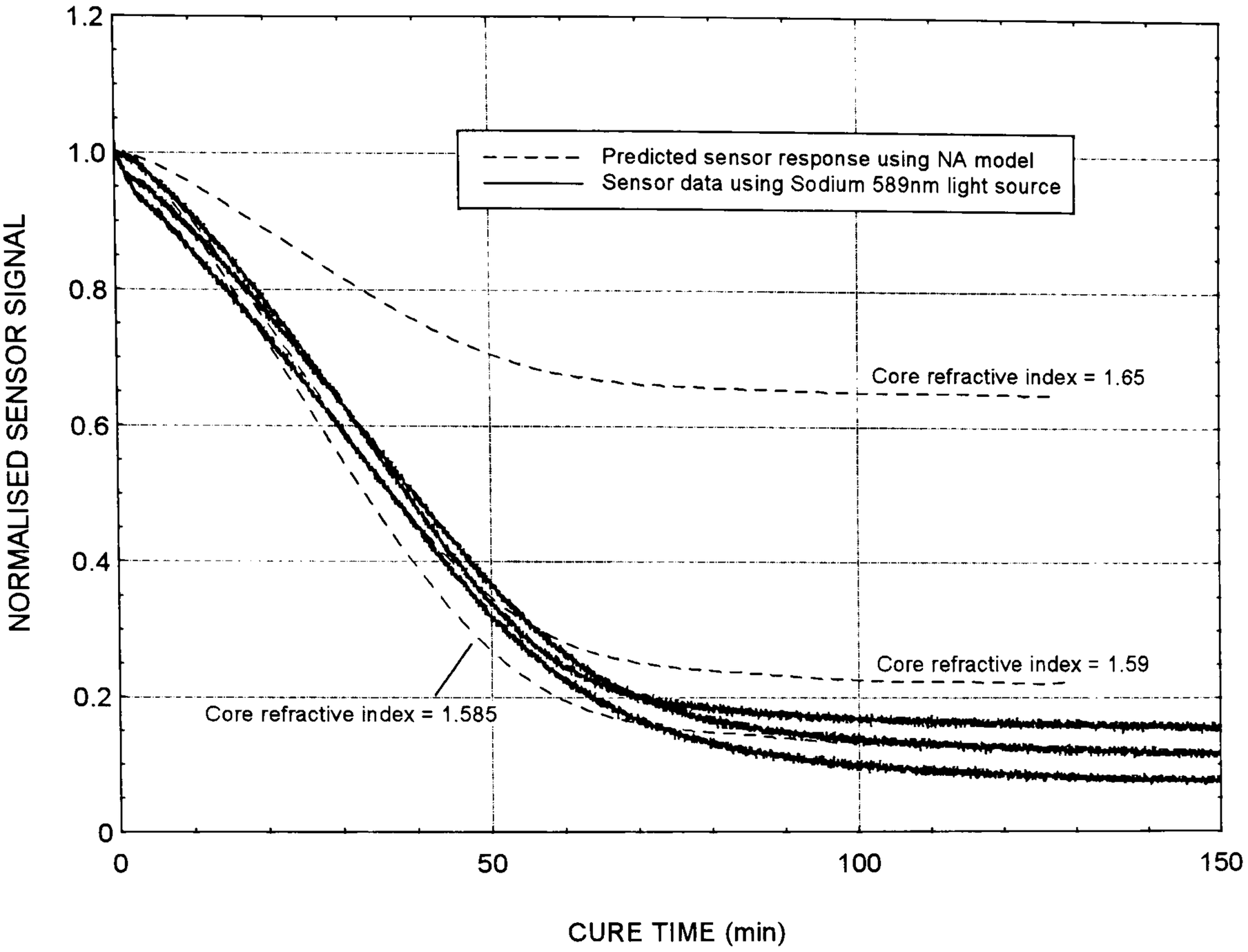

Figure 6-14 Comparison of results obtained using refractive index sensor to predicted sensor response from numerical aperture model

The predicted responses were calculated by substituting the Abbe refractive index values into equations - 6.8 and - 6.9. For example, the resin refractive index can be seen to change from 1.5454 to 1.5799 during the resin cure. The numerical aperture of the unstripped portion of the fibre is:

$$NA_0 = \sqrt{n_{co}^2 - n_{cl}^2} = \sqrt{1.65^2 - 1.41^2} = 0.857$$

-6.11

The numerical aperture of the stripped portion at the start of cure is likewise:

$$NA_{st} = \sqrt{n_{co}^2 - n_{t=0}^2} = \sqrt{1.65^2 - 1.5454^2} = 0.578$$

-6.12

and at the end of cure:

$$NA_{fin} = \sqrt{n_{co}^2 - n_{t=final}^2} = \sqrt{1.65^2 - 1.5799^2} = 0.476$$

- 6.13

The transmission (or light remaining in the fibre) at the start of cure is

$(NA_{st}/NA_0)^2 = 45.5\%$

and at the and of cure

$(NA_{fin}/NA_0)^2 = 30.8\%$

This corresponds to a predicted normalised sensor signal drop of

$$1 - \frac{30.8}{45.5} = 32.3\%$$

A similar calculation was carried out for all refractive index values and these calculations are the predictions plotted in Figure 6-14.

It can be seen that if the manufacturers quoted core index value of 1.65 is used in the model then there is a significant discrepancy between the predicted response and the measured data. The model predicts a fall of about 32% of the original signal level whereas the measured data actually fall to between 8 and 15% of its original value. Possible reasons for the discrepancies are:

i) the model assumes that all the propagation modes of the fibre are have light distributed between them equally. This means that the light in the fibre is distributed evenly across the acceptance angle of the fibre. This assumption is reasonable since the fibre being used contained many thousands of modes. However, it may be possible that the launch conditions of light into the fibre meant that some propagation modes were excited preferentially and the light was confined to those modes having lower internal reflection angles. The experiment did attempt to avoid this by overfilling the fibre using a high numerical aperture launch objective

ii) the model predicts no signal dependence on the length of the sensor region. The results seen in Figure 6-14 show no dependence of this kind. It is possible that the small transition region between clad and unclad regions, which are an artifact of the stripping process may affect the sensor response. Also bubbles attached to the core region may affect sensor response by altering the propagation characteristics;

iii) it can be seen from Figure 6-14 that if the model calculations are performed with a lower value of core refractive index, between 1.585 and 1.59, a much better fit is obtained. It is possible that this is nearer to the actual value of the core index since in

conversation with the fibre suppliers, it appeared that the source of the quoted core index is unreliable. Because the model is based on fairly fundamental optical fibre principles the inaccuracy of the quoted value of core index seems likely. One reel of the fibre, of several used throughout this project, was actually supplied with 1.59 quoted as the core index although this was said, by the supplier to be a labelling error.

To resolve this it will be necessary to obtain an independent assessment of the refractive index of the fibre core using a technique such as ellipsometry to give an accurate measure of its real and complex refractive indices. This would require a bulk sample of the core material which could not be obtained by the fibre supplier. Time constraints on the project prevented this being taken any further.

6.4.3 Cure monitoring of Epikote 828 and hexanediamine using the stripped cladding sensor

Refractive index cure-monitoring utilising the stripped cladding refractive index were carried out in the manner described in section 6.3. A schematic of the experimental arrangement can be seen in Figure 6-3.

Results from ten repeat experiments at 50°C can be seen in Figure 6-15.

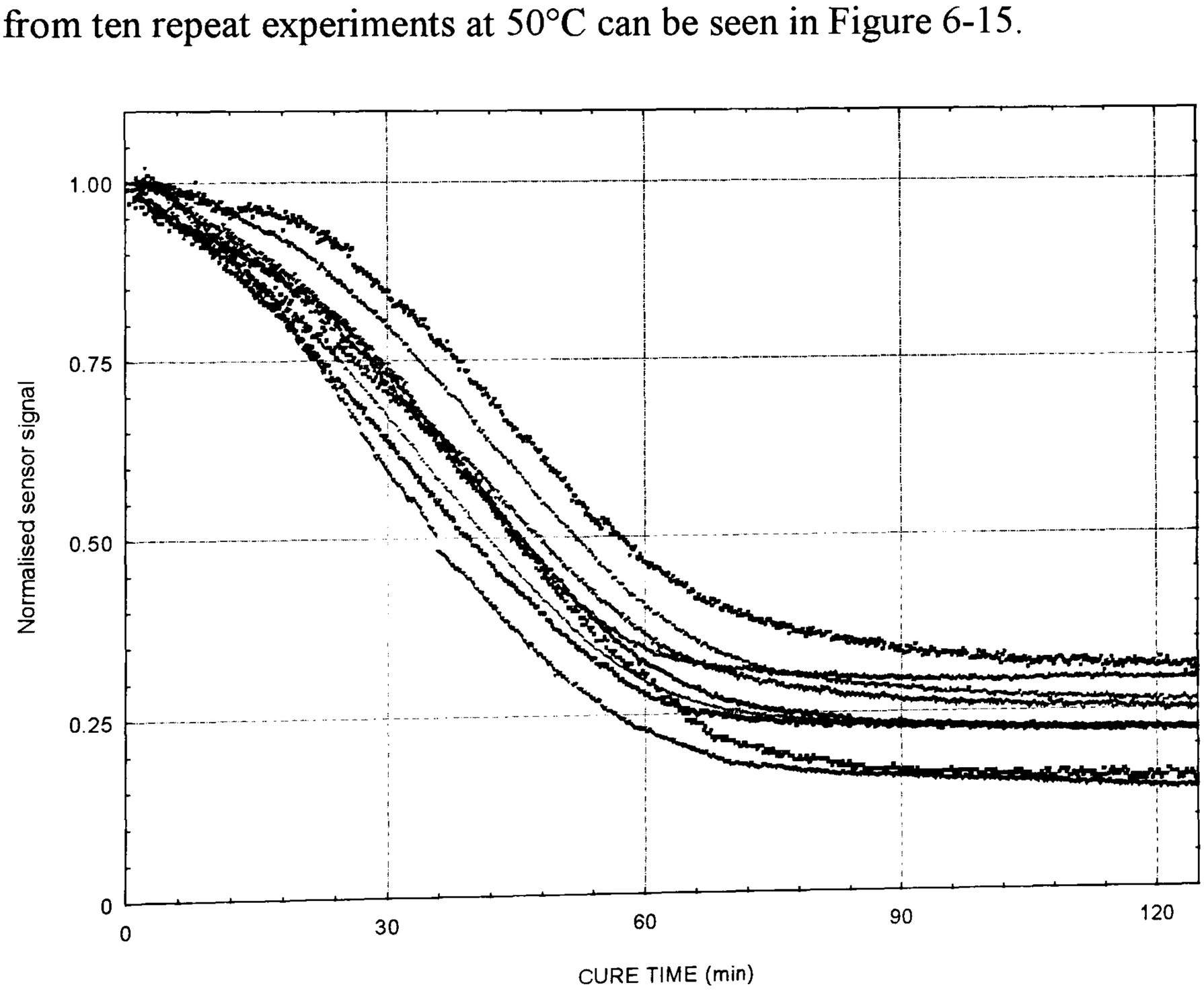

Figure 6-15 Data from stripped cladding refractive index sensor obtained during cure of Epikote 828 and hexanediamine at 50°C. (ten repeats)

As predicted by the sensor model there was no dependence of the signal on sensor length which ranged in these experiments from 20-33mm.

The sensor signal at the end of cure ranged from 0.31 to 0.14 of the original signal although all experiments were carried out under similar conditions. This variability was problematic and possible reasons for it are:

i) uncertainty in the transition region between unstripped and stripped region. Examination of this region with a microscope shows that there is a small length of cladding which has been attacked by the stripping acid but not removed. Since this region is likely to vary between sensors it could be a cause of the variation. In future work it will be important to investigate the effect of this partially clad region of the sensor and to find a way of manufacture sensors which eliminates this region. This effect will have undoubtedly contributed towards the uncertainty in the evanescent sensor also;

ii) bubbles around the sensor formed during cure could also affect the sensor signal.

Although these sensor signals do show a large spread they still possess some characteristics which could be useful.

Differentiating the signals with respect to time produces a set of curves that can be seen in Figure 6-16.

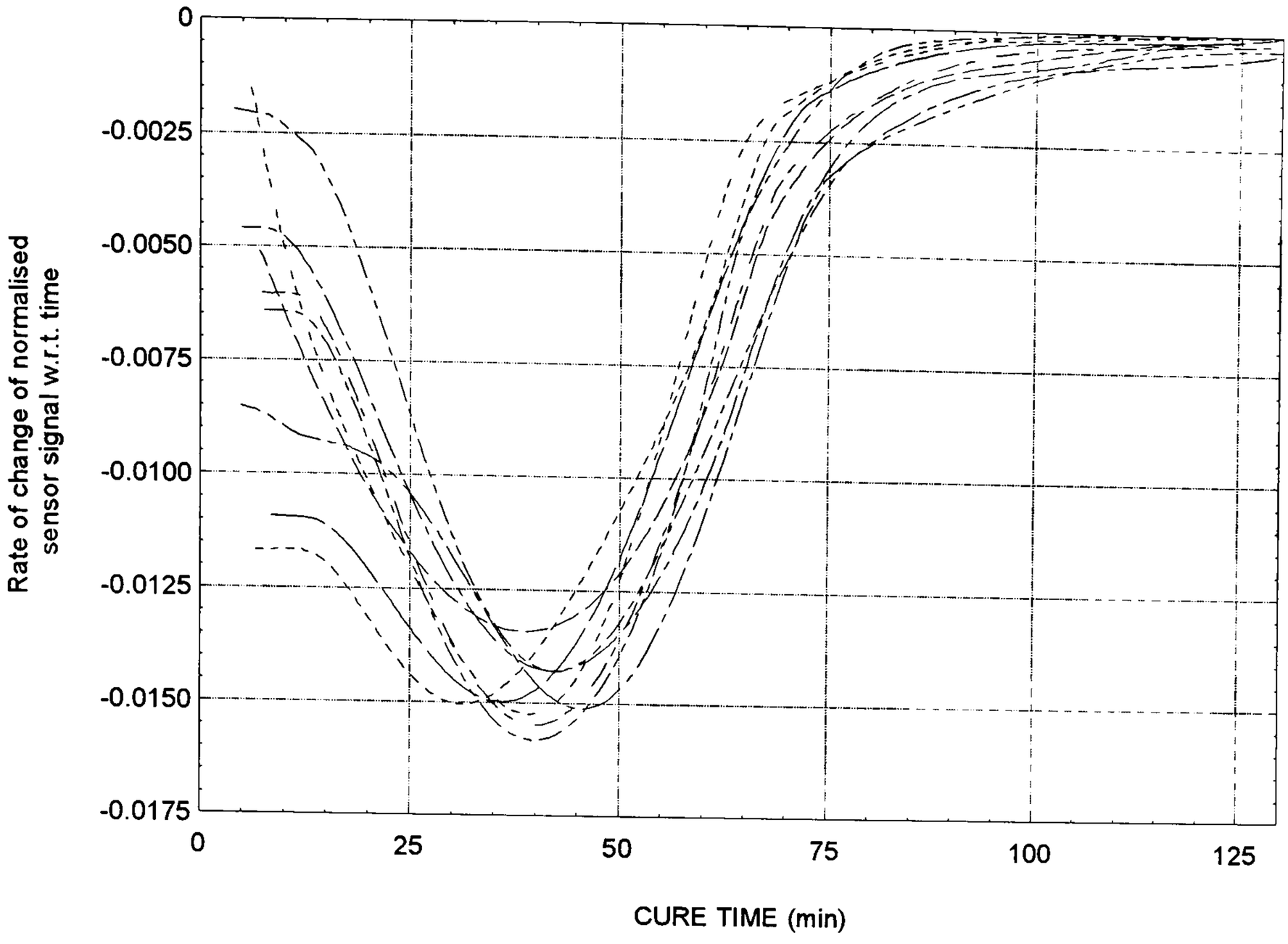

Figure 6-16 Rate of change of refractive index sensor signal with respect to time against cure time for curing Epikote 828 and hexanediamine at 50°C

The data presented in this form gives us two useful pieces of information about the cure process:

i) the minimum value of d[signal]/dt occurs between 35 and 45 minutes for eight of the ten experiments presented above. This point corresponds to the time at which the maximum rate of cure is reached. Over the cure period of two hours this pinpointing of the maximum cure rate to within ten minutes is a reasonable result;

ii) one of the most important pieces of information that is required from a cure sensor is the point in time where the cure reaction ceases. Manufacturers of composite materials made from epoxy resins follow closely the epoxy resin manufacturers cure schedule regardless of the shape or volume of the specimen. Consequently, small or thin parts may be cured for longer than necessary and large parts undercured. Tailoring a cure schedule to a particular part could results in a saving in time and energy for small parts and increased mechanical integrity for larger parts. For the volume of resin used in these experiments at a cure temperature at 50°C it can be seen from Figure 6-16 that the rate of change of cure becomes zero (*i.e.* cure stops) at approximately 120 minutes.

Figure 6-17 shows example data taken from Epikote 828 and hexanediamine cure sensing runs performed at 30, 40 50 and 60°C overlaid on the same plot.

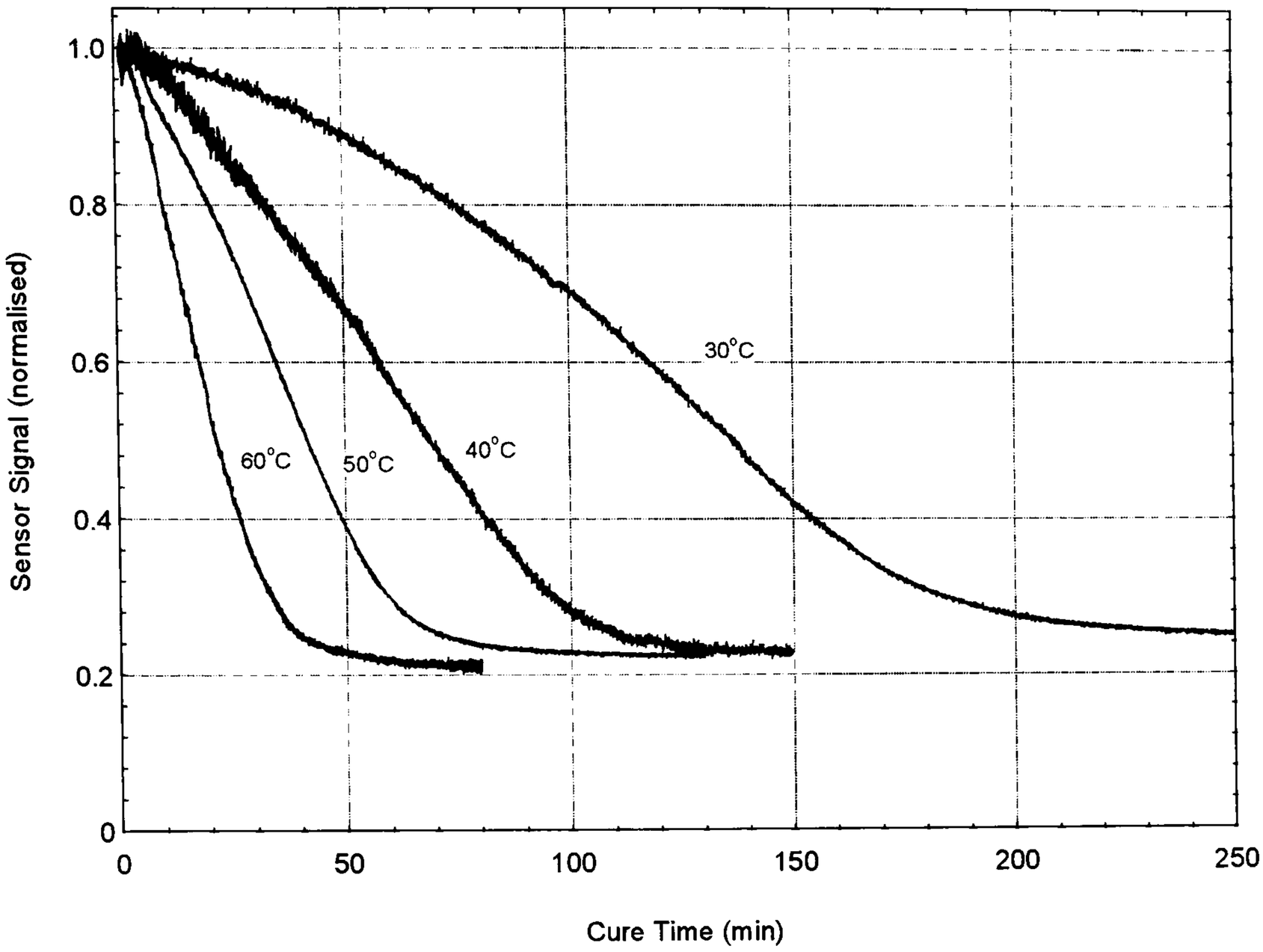

Figure 6-17 Typical results from optical fibre sensor refractive index cure monitoring experiments at 30, 40, 50, and 60°C

It can be seen that, as might be expected, cure progresses at a faster rate at the higher temperatures. Table 6-2 summarises the indicated end time and final sensor signal obtained at the four temperatures using the cure sensor.

Cure temperature (°C)	Final fraction of start sensor signal at cure end	Cure end time (mins)
30	0.16	300
30	0.17	
30	0.21	
40	0.17	150
40	0.25	
50	0.14	120
50	0.16	
50	0.22	
50	0.22	
50	0.22	
50	0.24	
50	0.25	
50	0.26	
50	0.29	
50	0.31	
60	0.21	80
60	0.23	

Table 6-2 Summary of cure sensor data at four temperatures

6.4.4 Cure monitoring of a glass/resin composite pre-preg.

The optical fibre refractive index cure sensor was used to monitor the cure of a Ciba Geigy, Fibredux 924 resin/glass fibre composite. A stripped high index fibre sensor was embedded in four plies of composite pre-preg which was then cured to the manufacturers recommended cure schedule whilst the signal from the sensor was monitored.

Since these experiments were carried out at a higher temperature (180°C) than those using Epikote 828 resin and hexanediamine an initial check was performed to ensure that the high refractive index core optical fibre would not degrade at these temperatures. The signal from an optical fibre was monitored as its temperature was ramped from ambient to 180°C at 3K minute^{-1} and held for 30 minutes. The trace from the fibre was seen to remain constant to within ±0.5% of the signal at 30°C showing no degradation of the fibre's guiding properties at this temperature.

Optical fibre sensor results from three composite cure runs can be seen in Figure 6-18 to Figure 6-20. The sensor and reference signals in these traces have been normalised to their initial values.

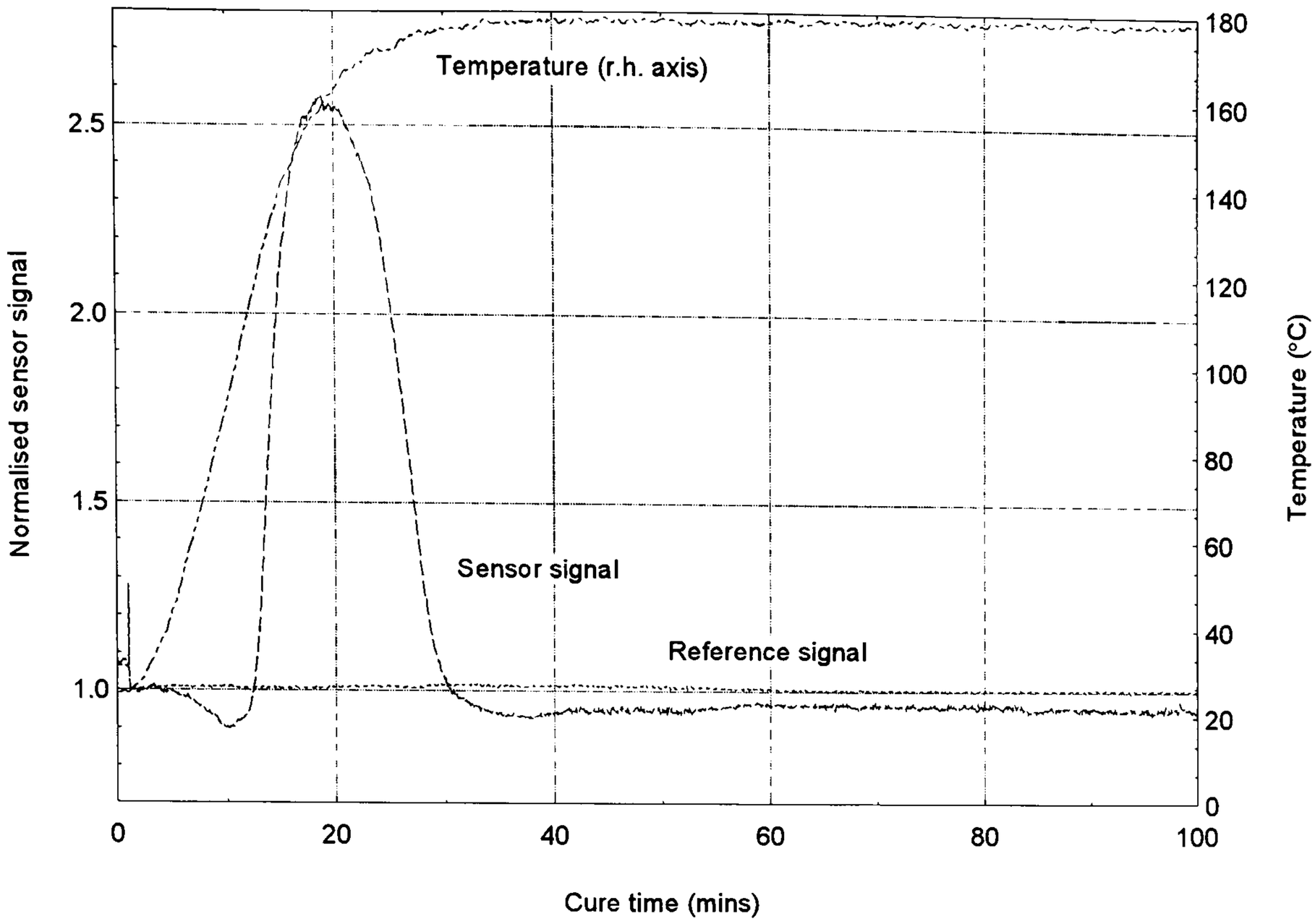

Figure 6-18 Results from optical fibre sensor embedded in curing 924 pre-preg

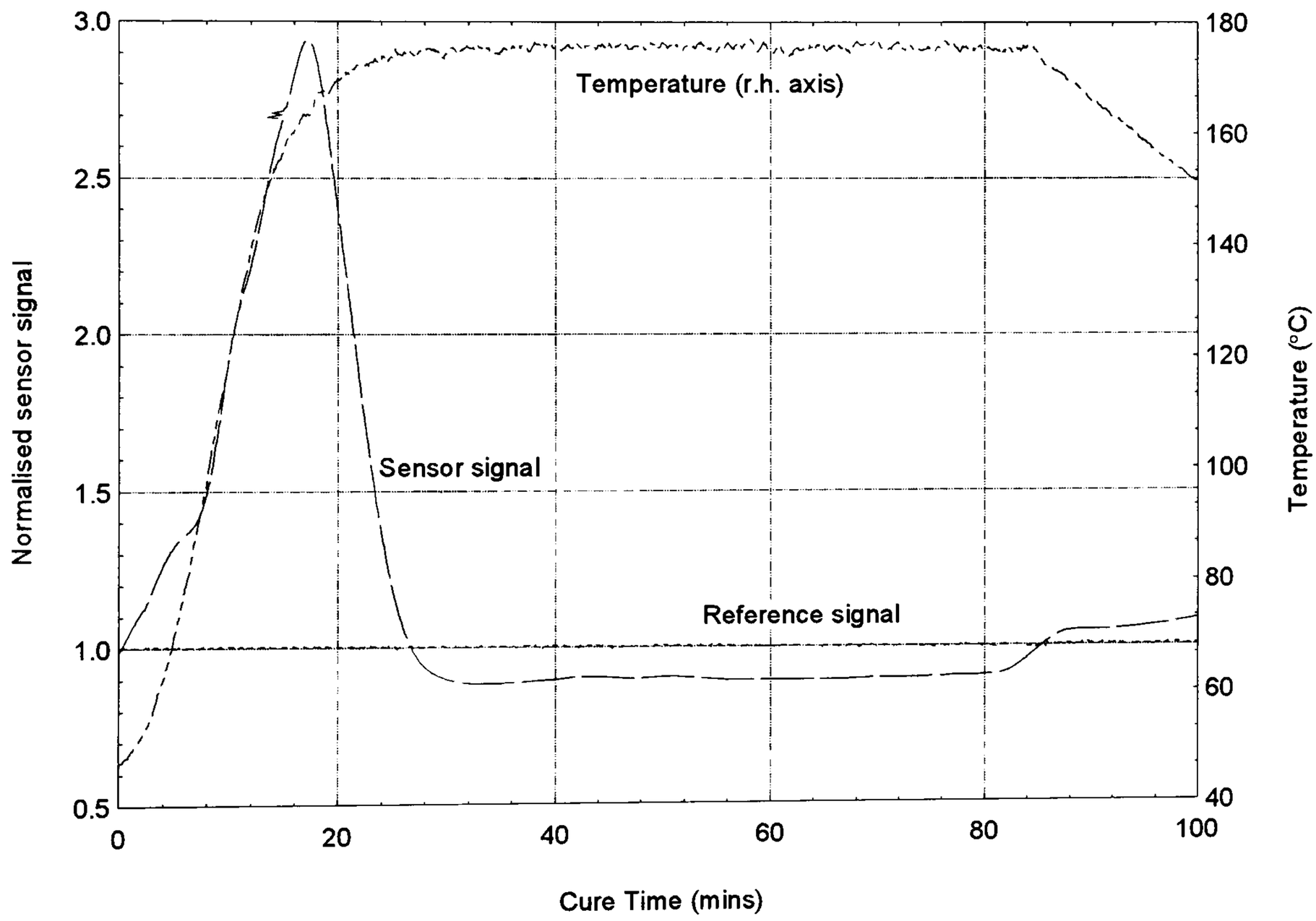

Figure 6-19 Results from optical fibre sensor embedded in curing 924 pre-preg (85 minute hold time)

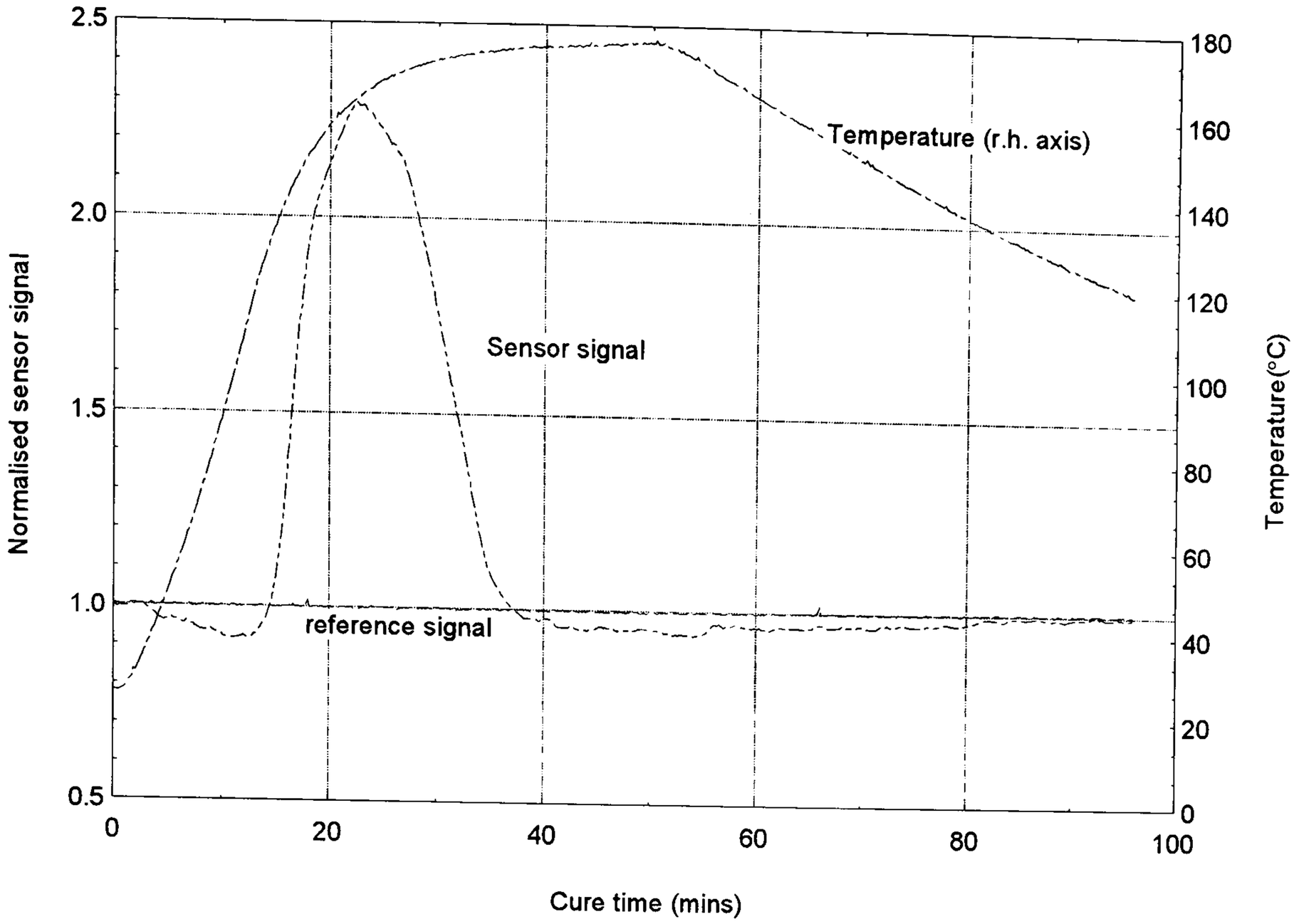

Figure 6-20 Results from optical fibre sensor embedded in curing 924 pre-preg (50 minute temperature hold)

The reference signal was seen to be stable to smaller than 0.5% in all three cases and so was not used in the processing of the data. The main features of the sensor signal are as follows:

i) an initial steep rise in sensor signal starting approximately ten minutes after the temperature ramp began, when the temperature reaches 100°C, and reaching a maximum when the temperature was 160°C. This is thought to be due to the drop in refractive index of the resin brought about by its increase in temperature. At 100°C the resin in the pre-preg begins to melt, wetting the sensor thoroughly and as the temperature increases the mobility of the resin increases and its refractive index drops. The drop in refractive index of the resin slows as the resin begins to crosslink and the signal from the sensor reaches its maximum;

ii) the sensor signal then starts to fall. The signal displays the characteristic 's' shaped curve characteristic of all the cure monitoring curve seen in this work. This fall in signal is due to the rise in the resin refractive index as the crosslinking process proceeds.

In the experiments above the signal can be seen to have reached a final steady state value (*i.e.* cure has finished) at between 31 and 39 minutes after the temperature ramp began. This would suggest that for specimens of this size the three hours temperature hold specified by the manufacturers is excessive. Curing for the time indicated by these

experiments on parts of this size would represent a significant time and energy saving over the manufacturers recommended cure schedule. Of course thicker samples would require a longer cure time but is has been demonstrated that the sensor could be useful in tailoring a cure schedule to a specific sample by determining when the interior of the sample had reached it final cure state.

The maximum rate of cure and the termination of the cure was determined from the differential of the sensor traces. A summary of these from the six cure runs performed can be seen in Table 6-3.

Cure run	**Time maximum cure rate reached (d[signal]/dt=min)**	**Time of completion of cure.**
1	30.1 mins	35 mins
2	25 .2 mins	36.1 mins
3	22.4 mins	31.5 mins
4	29.6 mins	39 mins
5	27.4 mins	36.4mins
6	23.4 mins	32.2mins

Table 6-3 Summary of composite cure monitoring results

It can be seen that there is quite a spread in these results. It is suggested that these differences in cure times and maximum rate time are real and due to small differences in the press heating rates and the lay-up. For example from the temperature traces in Figure 6-18 and Figure 6-19 can be seen that the isothermal temperature is reached 5 minutes earlier in the second of these than in the first. This would have resulted in the difference in the overall cure time of these two runs (2 and 3 in Table 6-3).

6.5 Chapter Conclusions

A refractive index sensor has been demonstrated and is capable of monitoring the refractive index of a medium in contact with a fibre core when the cladding has been stripped away.

The sensor was used to track the cure of a stoichiometric mixture of Epikote 828 resin and hexanediamine hardener mixture curing at 30, 40, 50 and 60°C. The signals obtained could be used to determine the time of maximum cure rate and time of cure finish. However, uncertainty in the sensor signal meant that the final extent of cure measurement was uncertain. Further work is needed to isolate the source of these fluctuations. Possible causes for them include short partially stripped areas between the stripped and unstripped regions and voids nucleating around the sensor.

Comparisons were made between results for the refractive index of the resin mixture during cure made using an Abbe refractometer and the optical fibre sensor. The existence of a relationship between refractive index and degree of cure was established by simultaneous monitoring of the resin spectra and the resin refractive index using an optical fibre transmission cell.

A simple model based on the change in the numerical aperture of the sensor with refractive index change of the measurand predicted a smaller signal change than was actually observed (35% predicted to 85% measured.) This is almost certainly due to the fibre core refractive index being smaller than the value quoted by the suppliers who seemed to be in some confusion over the actual value. The author would venture a core index value of 1.59 which in fact was actually quoted on one reel of fibre (of several) which was purchased. For future work it is imperative that a source of fully characterised high refractive index fibre is found or an independent assessment of the core index is made.

The sensor was also used to monitor the cure of a commercial glass fibre/928 resin pre-preg. A characteristic cure curve for each cure run was seen and from the sensor data it was possible to determine the maximum rate of cure and the cure finish time. The data showed that for the size of sample used, that the manufacturers recommended cure schedule was too long. This demonstrates the sensor's usefulness in tailoring a cure schedule to particular specimen shape and thickness.

In summary, the ability of the stripped fibre sensor to monitor cure has been demonstrated. At the moment the method is subject to the intensity fluctuations, in the same way as most intensity based measurements, due to microbends and differences in connections. Further work is needed to isolate the refractive index measurements from this noise and increase the measurements' accuracy.

7 Summary, conclusions and suggestions for future work

This thesis has described the work that was carried out to investigate two optical fibre sensors for the monitoring of cure of an epoxy resin system.

Experiments were carried out using a model resin system of a type similar to those commonly found in composite matrices. The system chosen for analysis was Shell Chemicals Epikote 828, a diglycidyl ether of bisphenol-A epoxy resin and 1,6-hexanediamine (Aldrich chemicals). The cure mechanism and characteristics of the resin was characterised by the author's co-worker using FTIR spectroscopy and DSC.

The optical fibre sensors used in this study used two parameters to monitor the cure process. These two parameters were evanescent wave absorption and refractive index.

The evanescent absorption sensor was used to monitor characteristic absorptions of active species within the curing resin system specifically the amine hardener absorption peak centred on 1529nm.

The refractive index sensor was used to track the substantial change in refractive index of the resin system as the cross-linking process progressed.

The work carried out on both sensors has been published widely at several conferences and in the journal, Smart Materials and Structures (see Appendix 3: Publications).

7.1 Evanescent absorption sensor

The evanescent absorption sensor was constructed from high refractive index core fibre from which 180mm of silicone cladding had been removed. Initial experiments confirmed that detection of amine hardener was possible *via* evanescent absorption, although any refractive index change of the medium to be sensed had a serious effect on the sensor signal. It was also found that the laser diode sources with which the sensor was to be excited were not sufficiently tuneable to be of use and so a grating monochromator was used to launch light over the wavelength range of interest into the sensor.

The evanescent absorption predictions of several sensor models from the literature and a model formulated by the author were assessed using the sensor immersed in amine solutions of known concentration. This type of comparison, had not previously appeared in any of the literature in which the models appeared. A recent model by Ruddy and the

author's model were shown to give the closest agreement with observed evanescent absorbance.

The stripped region of the fibre was embedded in the curing resin sample. Light was launched into the sensor from a scanning monochromator that performed a wavelength scan between 1470nm and 1590nm at intervals throughout the cure time. The wavelength dependent intensity data collected at the output end of the sensor contained information about the size of the N-H absorption band centred at 1529nm. This was related to the hardener concentration in the resin mixture. Cure experiments were carried out at 30, 40, 50 and 60°C. The data were processed to extract information on the height of the amine absorption peak. Although great care was taken to ensure a consistent experimental arrangement, the data thus obtained exhibited much variation between cure runs. This was probably due, in the main, to slight variation in parameters such as fibre connections, fibre curvature and launch conditions. However, if the data were normalised to the initial amine hardener peak height it became apparent that the percentage drop in amine peak height was more repeatable than was at first apparent, especially in the higher temperature data (50°C and 60°C). It was possible, using these data, to ascertain the cure onset time, cure termination time (or the point at which all of the amine hardener had been consumed) and the time of maximum rate of cure.

The evanescent data were compared to cure data obtained using FTIR spectroscopy and Abbe refractometry. It was found that the degree of cure data obtained using the evanescent sensor agreed to a good degree with those obtained using FTIR spectroscopy. The agreement was reasonable up to higher degrees of cure, where the sensitivity of the evanescent technique is low (corresponding to a degree of cure of 0.9). The evanescent data were also found to show a reasonable degree of agreement with data obtained using Abbe refractometry.

The unnormalised evanescent absorbance data were compared to the predictions made from the models in the literature and the author's model. Abbe and FTIR data obtained during cure were substituted into the cure models and used to make a prediction, which was compared to the evanescent absorbance observed. Three models gave a prediction close to the observed data. Two models by Ruddy[184,195] and the author's model gave predictions which were within the scatter of the observed data. These three models were sufficiently accurate that they could be used in an *in-situ* monitoring system to infer the

state of cure of a resin from the evanescent sensor signal. The original model formulated in this study has thus been shown to be worthy of consideration in any future study of evanescent sensors applied to the problem of cure monitoring.

The idea of a cure surface was proposed. This surface illustrates the variation in evanescent absorbance with variations in refractive index and analyte concentration and could be determined using one of the models described here or empirically. It is particularly applicable to cure monitoring where there is a large change in analyte refractive index as it cures. The signal obtained from an evanescent absorbance sensor describes a locus across this surface and this allows the unique values of analyte concentration and refractive index, specific to each absorbance, to be determined. This gives a good indication of cure state.

Experiments were performed to determine whether it was possible to enhance the sensitivity of the evanescent sensor. It was demonstrated that to ensure maximum sensitivity it was important that the higher order modes of the optical fibre were excited fully. Experiments to enhance the sensor sensitivity by masking the launch optics and tapering the sensing region produced negative results. It is likely that a more gradual taper, of longer length than those tried here would produce a sensitivity enhancement. However, the means to construct or purchase such a tapered fibre were not available during the course of the project and the investigation of such a taper will have to be left for work in the future.

7.2 Refractive index sensor

To determine whether the tracking of the refractive index of a resin sample was a viable technique an Abbe refractometer was used to measure the refractive index of the model resin system during the cure process. It was shown that a higher isothermal cure temperature resulted in a faster rate of refractive index change of the sample during cure. This could be linked to a faster cure rate. The overall change in refractive index of a resin sample was also found to be higher at higher isothermal cure temperatures. There was shown to be experimental evidence for a linear relationship between the degree of cure of a resin and the refractive index of the sample. This was shown using an optical fibre transmission sensor.

The stripped cladding optical fibre sensor was fabricated in a similar way to the evanescent absorbance sensor, the only difference being the length of silicone cladding (25mm) removed from the optical fibre to form the sensing region.

A number of experiments was conducted to determine whether the numerical aperture model of the refractive index sensor was valid. The model predicted a signal fall to 32% of the initial sensor signal whereas the observed signal fell to between 8 and 15% of its original value. Since the model was based on fairly basic optical fibre principles the most likely explanation for this discrepancy was thought to be an inaccuracy in the fibre suppliers quoted value for the core refractive index. A small change in this value was demonstrated to produce a significant change in the model predictions.

Cure monitoring experiments utilising the stripped cladding refractive index sensor were performed using a laser diode source operating at 1310nm. The sensor was embedded in samples that were cured at isothermal temperatures of 30, 40 50 and 60°C. As for the evanescent sensor, variability was seen between cure runs. Possible reasons for this are proposed to be:

i) uncertainty in the properties of the transition region between clad and unclad regions; and

ii) bubbles nucleating around the sensor.

The differentials of these data with respect to time yielded two useful pieces of information about the cure process. These were the maximum rate of cure and the point at which the cure reaction could be said to have ceased. For the 50°C samples the maximum rate of cure occurred between 35 and 45 minutes and the cure had ceased (*i.e.* the rate of change of refractive index with time had become zero) at 120 minutes.

The sensor was also used monitor the cure of a Ciba Geigy, Fibredux 924, glass/resin composite pre-preg. A cure sensor was embedded in four plies of composite pre-preg which was then cured to the manufactures recommended cure schedule whilst the signal from the sensor was monitored. Since the pre-preg cure schedule incorporated a temperature arm the sensor signal took on a different form to that seen in the resin samples. The sensor signal initially began to rise as the pre-preg resin matrix became more mobile with increasing temperature. The signal then followed the characteristic "s-shaped" curve seen in the resin cure experiments as it cross-linked. The four layer pre-preg sample was seen to have completed cure at times between 31 and 39 minutes, with the maximum cure rate occurring at times between 22 and 30 minutes for the six samples. The cure schedule called for an isothermal temperature hold of three hours, which can be seen to be excessive for a small, thin sample of pre-preg such as that used here. This demonstrated that the

refractive index sensor holds promise for tailoring a cure schedule to specific composite part by determining when the cure of that part had completed.

7.3 Recommendations and Future work

The evanescent absorption sensor and the stripped cladding refractive index sensor have been shown to be potentially useful tools for monitoring the progress of an epoxy/amine cure reaction. The following areas of research are recommended for future work to refine the techniques to a point where they can be commercially useful.

Evanescent absorption sensor

i) A disadvantage of the current evanescent sensor arrangement is that the optical arrangement is based on a scanning grating monochromator. The approximate scan rate of this equipment as it stands is approximately 1nm s^{-1}. This limits the number of data points which can be obtained during a single cure cycle. The new solid state monochromators or equipment to introduce light into the fibre from a benchtop FTIR machine would improve resolution and the data acquisition rate of the technique.

ii) At the time of writing, tuneable diode laser sources are reaching the market with high stability and a wavelength tuneability of some 100nm at telecommunications wavelengths. As these become more established and so less expensive they would make ideal sources for the evanescent sensor. This would enable the original project concept of monitoring specific absorption bands with single wavelengths to become realised.

iii) It is possible that the boundary between stripped and unstripped regions of the fibre sensor affect the repeatability of the sensor signal during cure. Therefore, this issue needs addressing and alternative cladding stripping methods, such as re-cladding a bare fibre core, should be investigated. The optical fibre used in these experiments is in need of a greater level of characterisation and it is imperative that in the future either a better characterised fibre type is found or more data is obtained on the existing fibre.

iv) It is suggested that the quality of the evanescent data could be improved greatly by using a spectral referencing technique. This will require a wavelength range exceeding that of which the equipment is currently capable and fibres with improved transmission capabilities into the NIR. Equipment such as that described in i) and ii) would help realise this.

v) The cure surface idea should be extended. A next good step would be the construction of a detailed empirical model to enable accurate values of refractive index and analyte concentration to be obtained from an evanescent absorbance measurement.

Refractive index sensor

Many of the same areas of research which apply to the evanescent sensor have been identified as important for the refractive index sensor.

i) Again, it is important that that the high refractive index fibre is fully characterised or an alternative fibre is found to enable an absolute measure of the resin refractive index to be inferred from the sensor signal. This measurement could also be improved by an improved referencing system to take into account variables such as fibre connections and fibre curvature.

ii) Improved or alternative methods of cladding removal or sensor fabrication are needed to produce more repeatable results and eliminate the transition region between clad and unclad regions.

Finally, both techniques will have to be extended to commercial composite pre-preg systems. This will also entail a complete companion study of the cure kinetics of each of these systems by conventional techniques as was conducted alongside this work by the author's co-researcher.

8 Appendices

8.1 Appendix 1: Microsoft Excel Macro for calculation of peak heights from evanescent sensor data

```
' Peak height macro

' Macro1 Peak height macro
' Macro recorded 25/04/96 by Graham Powell
'
'
Sub Macro1Peakheightmacro()
    'VARS'
     c2 = 1 'destination column'
    Sheets.Add

    '#####label columns#####'
    Sheets("Sheet2").Select
    Cells(1, 1) = "Time"
    Cells(1, 2) = "abs@1500": Cells(1, 3) = "abs@1529"
    Cells(1, 4) = "abs@1570": Cells(1, 6) = "peak height"
    For w = 1500 To 1570 Step 35
    r1 = 65 'start row'
    r2 = 2 'destination row'
    c2 = c2 + 1 'destination column'
    t = 0 'time'
10          Sheets("Sheet1").Select
15          s = Cells(r1, 2)
          If s = "x-axis" Then GoTo 20 '####if end of column do next wavelength###'
          '###if we're at the right wavelength select adjacent cell else look at next###'
          If s = w Then Cells(r1, 3).Select Else r1 = r1 + 1: GoTo 15
          '###cut and paste###'
          Selection.Copy
          Sheets("Sheet2").Select
          Cells(r2, c2).Select
    ActiveSheet.Paste
    '#####label time column on last pass####'
    If w = 1570 Then Cells(r2, 1) = t
    r2 = r2 + 1: r1 = r1 + 1: t = t + 3: GoTo 10
20  Next

'%%%%%%%calculate absorption depth%%%%%%%%'
 Sheets("Sheet2").Select
    Cells(2, 6).Formula = "=(C2-(B2+((D2-B2)/2)))"
    Cells(2, 6).Select
    Selection.Copy
    y = 3
25  check = Cells(y, 1): If check = "" Then GoTo 30
    Cells(y, 6).Select
    ActiveSheet.Paste
    y = y + 1: GoTo 25
30      End
End Sub
```

8.2 Appendix 2: Mathcad worksheets for model calculations

This appendix contains the mathcad worksheets used in calculating the model predictions for the published models and the authors penetration depth model. The following sheets were used in the absorption model/experimental comparisons detailed in section 5.3.4

Burgess's model (done using matrices and Gloge's r)

$i := 0..36$

$j := 0..1$

$c_i := 0.05 \cdot (i + 1)$

$L := 180 \cdot 10^{-3}$

$n_{co} := 1.65$

$n_m := 1.446$

$n_{cl} := 1.41$

$\theta_c := \operatorname{asin}\left(\frac{n_{cl}}{n_{co}}\right)$

$\alpha_c := 146.37$

$\rho := 60 \cdot 10^{-6}$

$\lambda := 1529 \cdot 10^{-9}$

$\theta := \operatorname{asin}\left(\frac{n_m}{n_{co}}\right)$

$NA := \left(n_{co}^2 - n_m^2\right)^{\frac{1}{2}}$

$NA = 0.795$

$V := 2 \cdot \pi \cdot \frac{\rho}{\lambda} \cdot NA$

$$r := \frac{4 \cdot \sqrt{2}}{3 \cdot V}$$

Gloges r Appl. Opt 10,(10)

$$\alpha_e := \alpha_c \cdot r$$

numerical aperture part of model ignored since no r.i. change

$$A_i := \frac{\alpha_e \cdot L \cdot c_i}{2}$$

$$abs_{i,0} := c_i$$

$$abs_{i,1} := A_i$$

WRITEPRN(BURGgloge) := abs

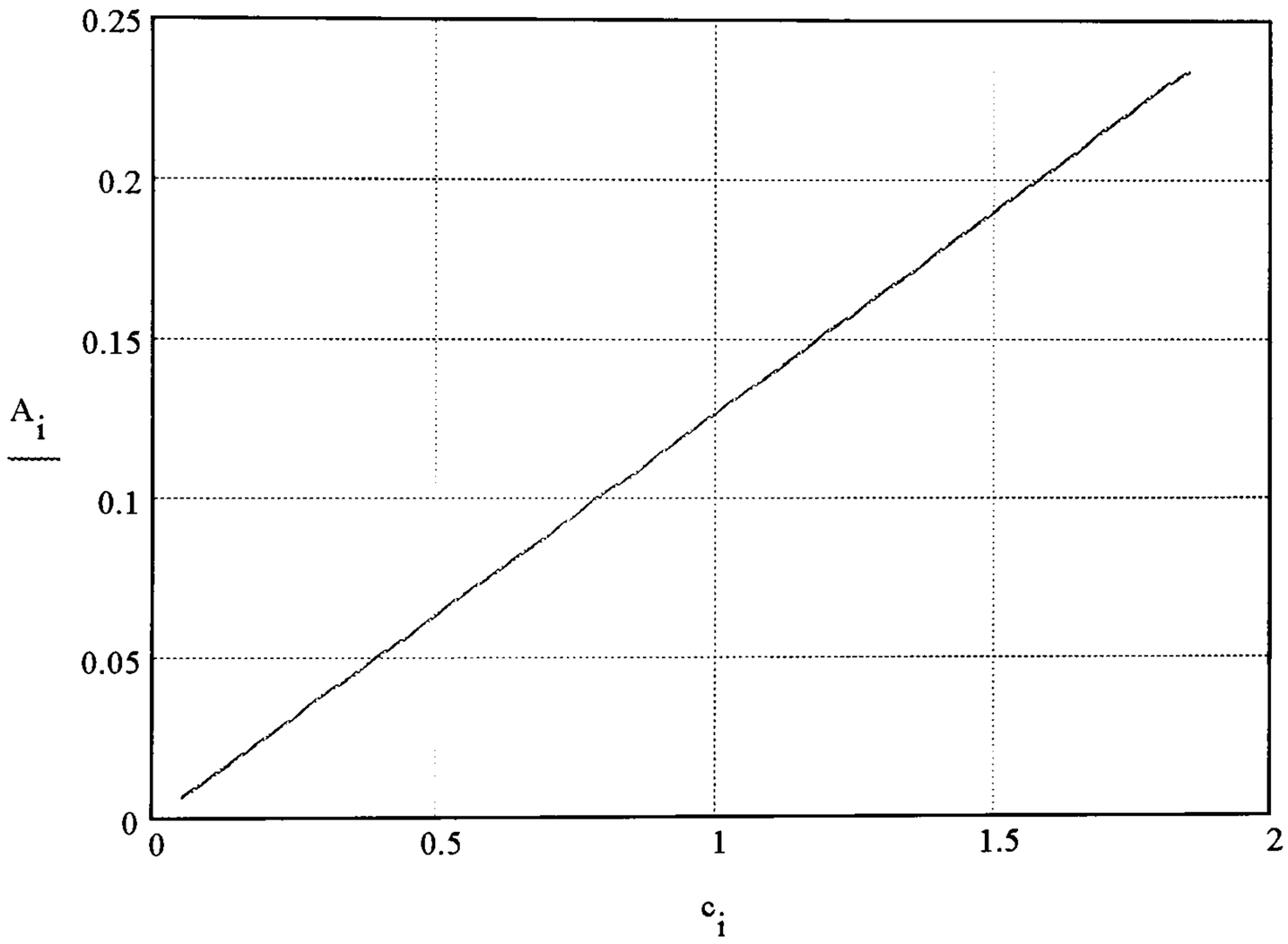

Burgess's model with Ruddy's value for r

$$i := 0 .. 36$$

$$j := 0 .. 1$$

$$c_i := 0.05 \cdot (i + 1)$$

$$L := 180 \cdot 10^{-3}$$

$$n_{co} := 1.65$$

$$n_m := 1.446$$

$$n_{cl} := 1.41$$

$$\theta_c := \operatorname{asin}\left(\frac{n_{cl}}{n_{co}}\right)$$

$$\alpha_c := 146.37$$

$$\rho := 60 \cdot 10^{-6}$$

$$\lambda := 1529 \cdot 10^{-9}$$

$$\theta := \operatorname{asin}\left(\frac{n_m}{n_{co}}\right)$$

$$NA := \left(n_{co}^{2} - n_m^{2}\right)^{\frac{1}{2}}$$

$$V := 2 \cdot \pi \cdot \frac{\rho}{\lambda} \cdot NA$$

$$r := \frac{1}{V} \cdot \frac{\operatorname{asin}\left(\frac{\cos(\theta)}{\cos(\theta_c)} \cdot \sin\left(\frac{\pi}{2} - \theta_c\right)\right)}{\left(\frac{\pi}{2} - \theta\right)}$$

Ruddy's r value

$$\alpha_e := \alpha_c \cdot r$$

$$A_i := \frac{\alpha_e \cdot L \cdot c_i}{2}$$

$$abs_{i,0} := c_i$$

$$abs_{i,1} := A_i$$

WRITEPRN(BURGrud) := abs

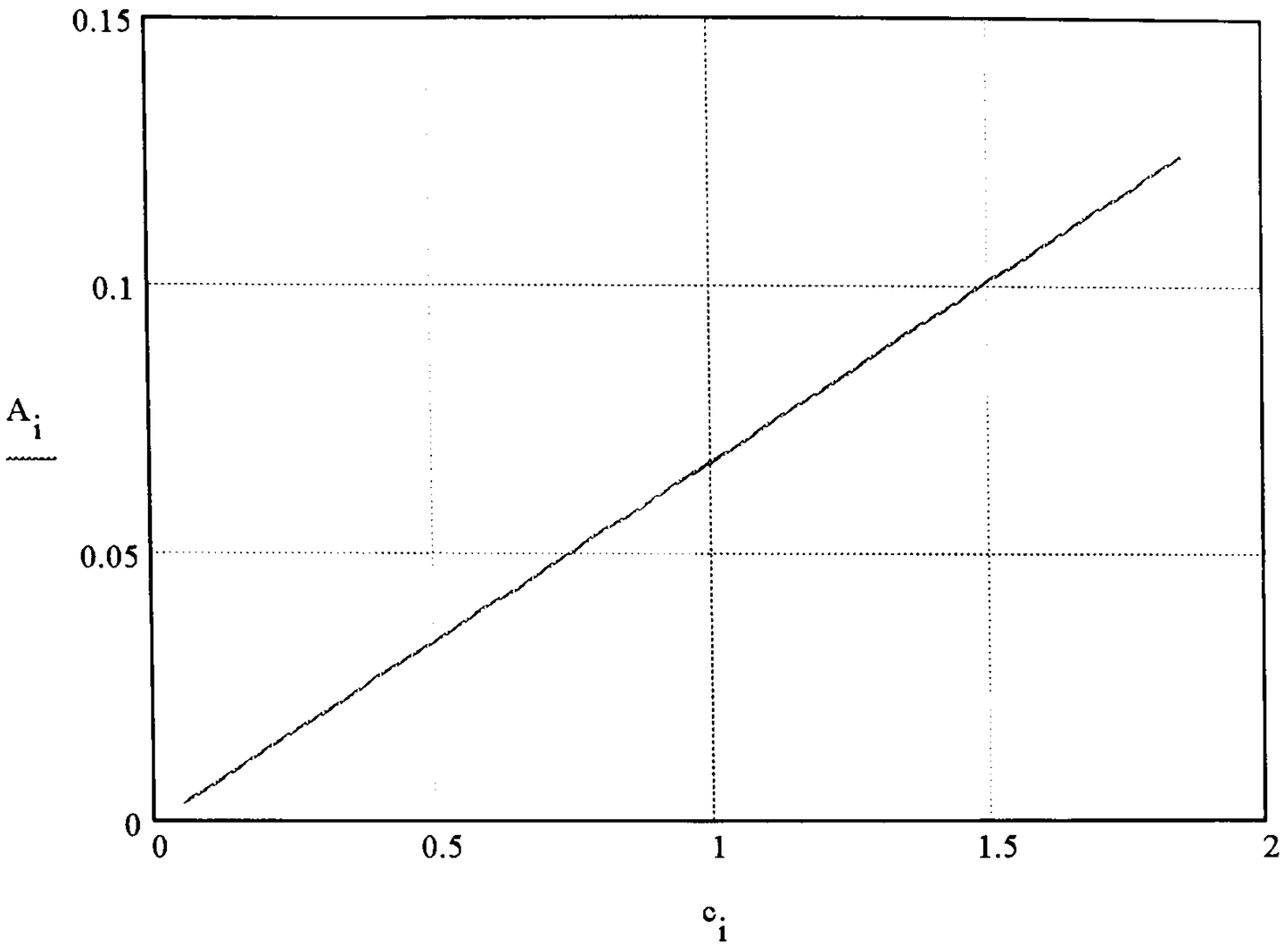

Ruddy's effective attenuation coefficient

$c := 0, .1 .. 1.8$

$\lambda := 1529 \cdot 10^{-9}$

$n_1 := 1.65$

$n_m := 1.446$

$n_{1m} := \frac{n_1}{n_m}$

$n_{m1} := \frac{n_m}{n_1}$

$\theta_2 := \frac{\pi}{2}$

$\theta_1 := \operatorname{asin}\left(\frac{n_m}{n_1}\right)$

$\theta_c := \operatorname{asin}\left(n_{m1}\right)$

$\rho := 60 \cdot 10^{-6}$

$n_2 := 1.41$

$L := 18 \cdot 10^{-2}$

$$\theta_1 = 61.207 \cdot \text{deg}$$

$$\alpha(c) := 146.37 \cdot c$$

$$g(\theta) := -\text{atan}\left(\frac{\cos(\theta)}{\sqrt{n_{1m}^2 \cdot \sin(\theta)^2 - 1}} + n_{m1} \cdot \text{asin}\left(\frac{\cos(\theta)}{\cos(\theta_c)}\right)\right)$$

$$g(\theta_2) = 0$$

$$\gamma(\theta_2, \theta_1, \alpha) := \alpha(c) \cdot \lambda \cdot \frac{n_m}{\pi \cdot \rho \cdot \left(n_1^2 - n_m^2\right) \cdot (\theta_2 - \theta_1)} \cdot \left(g(\theta_2) - g(\theta_1)\right)$$

$$\gamma_{pi}(\theta, \alpha) := \frac{\alpha(c) \cdot \lambda \cdot n_m}{\pi \cdot \rho \cdot \left(n_1^2 - n_m^2\right)} \cdot \left[\text{atan}\left[\frac{\cos(\theta)}{\sqrt{\frac{\sin(\theta)^2}{\sin(\theta_c)^2}}}\right] - \sin(\theta_c) \cdot \text{asin}\left(\frac{\cos(\theta)}{\cos(\theta_c)}\right)\right]$$

$$r(\theta) := \frac{1}{V} \cdot \frac{\text{asin}\left(\frac{\cos(\theta)}{\cos(\theta_c)} \cdot \sin\left(\frac{\pi}{2} - \theta_c\right)\right)}{\left(\frac{\pi}{2} - \theta\right)}$$

$$V := 2 \cdot \frac{\pi \cdot \rho}{\lambda} \cdot \left(n_1^2 - n_m^2\right)^{\frac{1}{2}}$$

$$\gamma_{crit}(\alpha) := \frac{\alpha(c) \cdot \lambda}{2 \cdot \rho \cdot n_m \cdot \left(1 + \sin(\theta_c)\right)}$$

$$A(\gamma) := -\log((\exp(-\gamma \cdot L)))$$

$$\text{WRITEPRN(GAMMA)} := A(\gamma_{crit}(\alpha))$$

$$V = 195.947$$

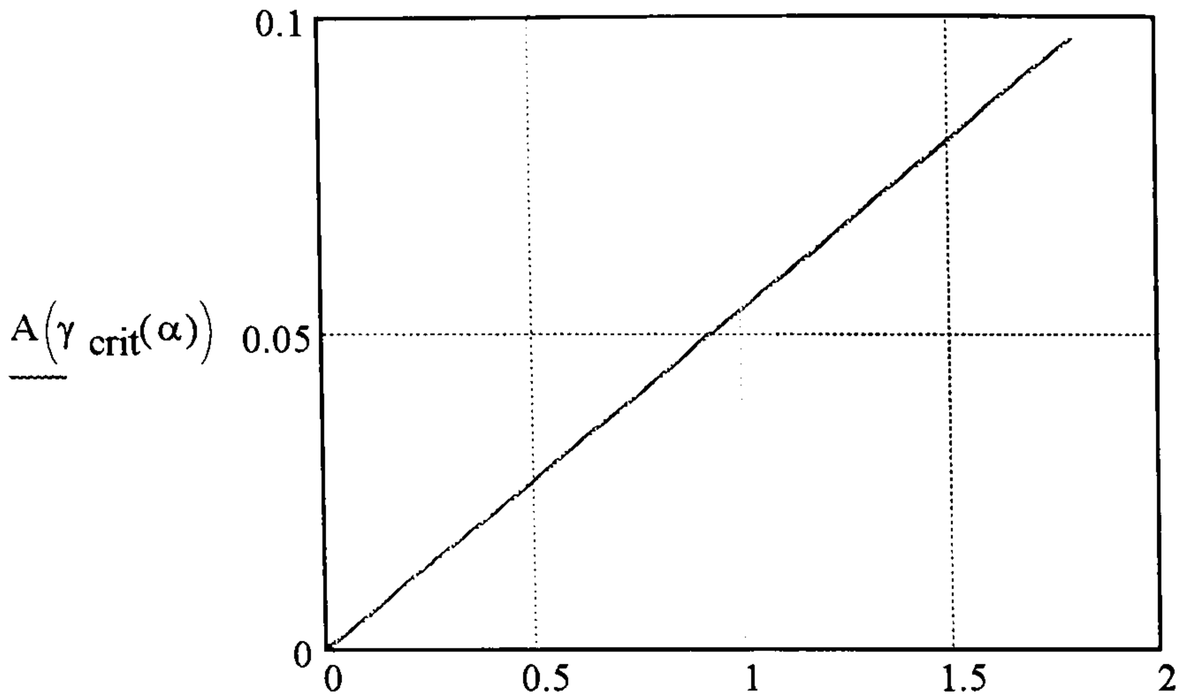

Ruddy's attenuation coefficient from 1994

$c := 0,.1 .. 1.8$

$\alpha := 146.37$

$n_2 := 1.4460$

$L := 18 \cdot 10^{-2}$

$n_1 := 1.65$

$\rho := 60 \cdot 10^{-6}$

$\lambda := 1529 \cdot 10^{-9}$

$$\Delta := \frac{n_1^2 - n_2^2}{2 \cdot n_1^2}$$

$$NA := \left(n_1^2 - n_2^2\right)^{\frac{1}{2}}$$

$$V := 2 \cdot \pi \cdot \frac{\rho}{\lambda} \cdot NA$$

$$T(c) := \left[\int_0^1 \exp\left[\frac{-n_2 \cdot \alpha \cdot c \cdot L}{n_1 \cdot V} \cdot \frac{x^2}{\left[\left(1 - x^2\right) \cdot \left(1 - 2 \cdot \Delta \cdot x^2\right)\right]^{\frac{1}{2}}} \right] dx \right]$$

$A(T) := -\log(T(c))$

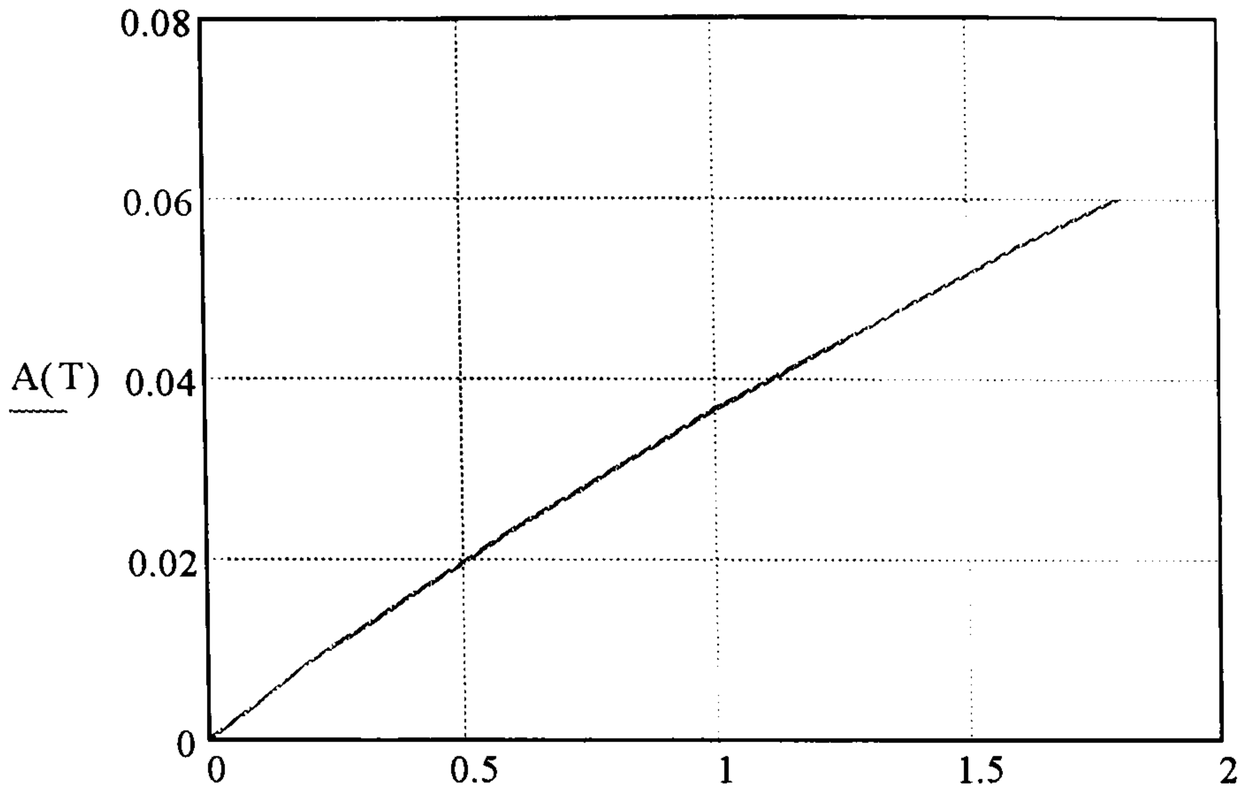

c

WRITEPRN(RUDD) := A(T)

Author's Penetration depth model

$\lambda := 1529 \cdot 10^{-9} \cdot m$

$n_1 := 1.65$

$n_m := 1.446$

$\rho := 60 \cdot 10^{-6} \cdot m$

$L := 18 \cdot 10^{-2} \cdot m$

$\theta_{crit} := \operatorname{asin}\left(\frac{1.446}{1.65}\right)$

$\alpha := 146.37 \cdot liter \cdot m^{-1}$

$c := 0 \cdot liter^{-1}, 0.1 \cdot liter^{-1} .. 1.8 \cdot liter^{-1}$

$\theta_{crit} = 61.207 \cdot deg$

$I_0 := 1$

$E_0 := \sqrt{I_0}$

for a single bounce

$$d_p(\theta) := \frac{\lambda}{2\cdot\pi\cdot\left[(\sin(\theta))^2 - \left(\frac{n_m}{n_1}\right)^2\right]^{\frac{1}{2}}}$$

$$d_e(\theta) := \frac{\frac{n_m}{n_1}\cdot d_p(\theta)\cdot E_0{}^2}{2\cdot\cos(\theta)}$$

$$\cos\left(\frac{\pi}{2}\right) = 0$$

No. of bounces at angle θ

$$N(\theta) := \frac{\cot(\theta)}{2\cdot\rho}$$

$$path(\theta) := \int_0^{\infty} \exp\left(-\frac{2\cdot r}{d_p(\theta)}\right) dr$$

$$d_p\left(\frac{\pi}{2}\right) = 5.052\cdot 10^{-7}\ \cdot m$$

total path

length

$$D_{tot} := \frac{L}{2\cdot\rho}\cdot\int_{\theta_{crit}}^{\frac{\pi}{2}} \cot(\theta)\cdot d_e(\theta)\, d\theta$$

$$D_{tot} = 2.867\cdot 10^{-4}\ \cdot m$$

$$A(c) := \alpha\cdot D_{tot}\cdot c$$

WRITEPRN(GRARM) := A(c)

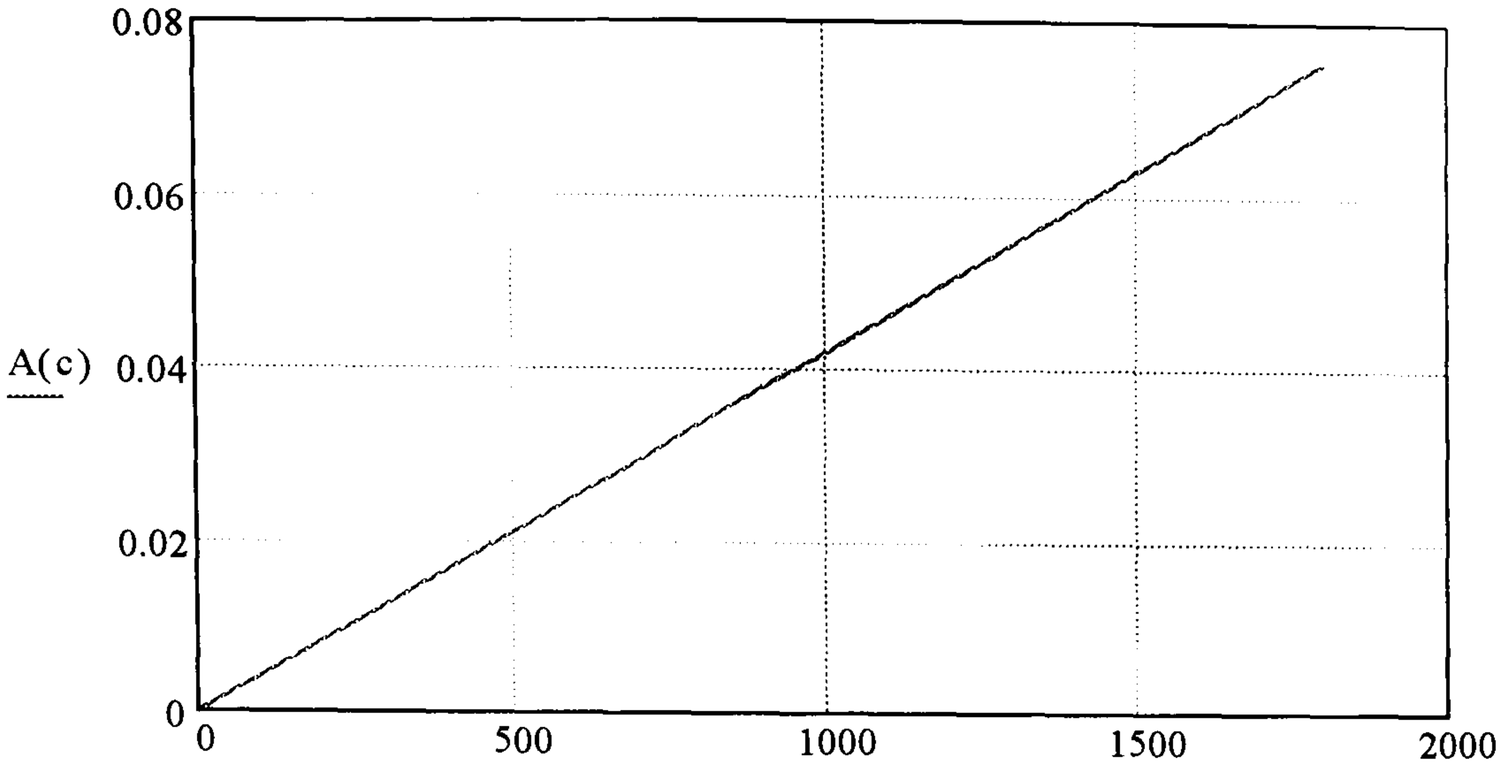

sample volume for ray at angle θ

$$v(\theta) := \pi \cdot \rho^2 \cdot L \cdot d_e(\theta)$$

absorbance of ray @ θ

$$a(\theta, c) := 2 \cdot c \cdot d_e(\theta)$$

total of all bounces at θ

$$a_{tot}(\theta, c) := a(\theta, c) \cdot N(\theta)$$

Total for all θ

$$A(c) := \int_{\theta_{crit}}^{\frac{\pi}{2}} a_{tot}(\theta, c)\, d\theta$$

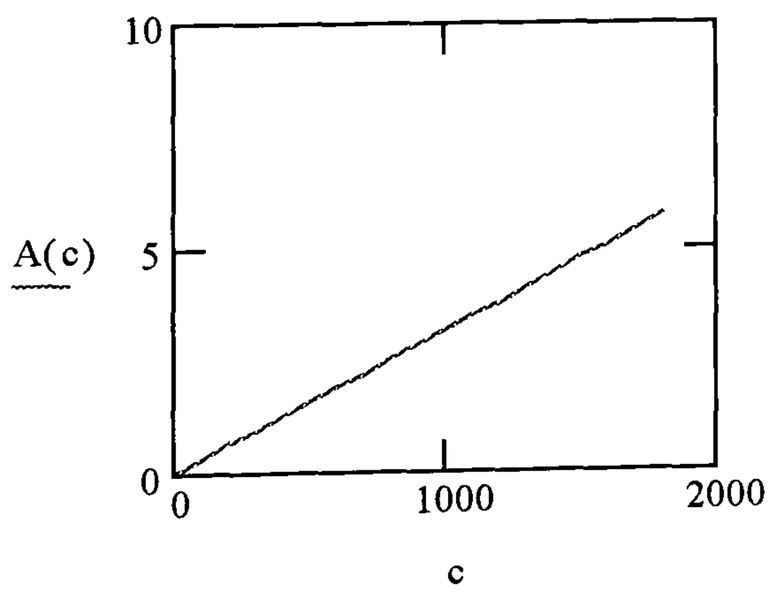

WRITEPRN(GP2) := A(c)

8.3 Appendix 3: Publications

G.R.Powell, P.A.Crosby, D.N. Waters, C.M. France, R.C.Spooncer and G.F. Fernando, "*In-situ* cure monitoring Using Optical Fibre Sensors - A Comparative Study." Accepted for Publication in Smart Materials and Structures, will appear in **August** 1998 issue.

P. A. Crosby, G. R. Powell, G. F. Fernando, D. N. Waters, C. M. France, R. C. Spooncer, "A comparative study of optical fibre cure monitoring methods", *Proceedings of the Society of Photo-optical Instrumentation Engineers (SPIE)*, **3042**, pp.141-153, (1997).

P.A. Crosby, G. R. Powell, T. Liu, X. Wu, G. F. Fernando, "*In-situ* cure monitoring of an epoxy/amine resin system using an optical-fiber transmission sensor, *Proceedings of the Society of Photo-optical Instrumentation Engineers (SPIE)*, **2895**, pp.109-115 (1996).

G.R. Powell, P. A. Crosby, G. F. Fernando, C. M. France, R. C. Spooncer, D. N. Waters, "Optical-fiber evanescent-wave cure monitoring of epoxy-resins", *Proceedings of the Society of Photo-optical Instrumentation Engineers (SPIE)*, **2718A**, pp. 80-92 (1996).

P.A. Crosby, G. R. Powell, G. F. Fernando, C. M. France, R. C. Spooncer, D. N. Waters, "*In-situ* cure monitoring of epoxy-resins using optical-fiber sensors", *Smart Materials & Structures*, 5, No.**4**, 415-428 (1996).

P.A. Crosby, G.R. Powell, G.F. Fernando, C.M. France, D.N, Waters & R.C. Spooncer, " Cure monitoring of epoxy resins using optical fibre sensors." I.O.P. Sensor series Ch. 76 (Dublin) pp. 255-259 (1995)

G.R. Powell, P.A. Crosby, G.F. Fernando, C.M. France, R.C. Spooncer & D.N. Waters. "*In-situ* cure monitoring of advanced fibre reinforced composites" Proc. SPIE **2444** "Smart Structures and Materials" pp. 386-395 (1995)

BLANK IN ORIGINAL

9 References

1 Hull D, *An introduction to composite materials* pp.1-9 Cambridge University Press, Cambridge (1981)

2 Morgan RJ, "Structure-property relations of epoxies used as composite matrices", Advances in Polymer Science, Epoxy resins and composites I, **72**, pp.1-43 (1985)

3 Dealmeida SFM and Neto ZDN Composite structures, **28**(2) pp.139-148, (1994)

4 Lau CH, Hodd KA and Wright WW, British Polymer Journal, **18**(5), pp.316-322 (1986)

5 Bowles KJ, and Frimpong S, "Void effects on the interlaminar shear strength of unidirectional graphite fibre reinforced composites" Journal of Composite Materials, **26**(10) pp.1487-1509, (1992)

6 Lee SY and Springer GS, "Effects of cure on the mechanical-properties of composites", Journal of Composite Materials, **22** (1), pp.15-29 (1988)

7 Taylor MA, Gillham JK, "Effect of anomalous density vs extent of cure on the stresses developed in an epoxy composite specimen", Abstracts of Papers of the American Chemical Society, **198** pp.175-187 (1989)

8 Wenz SM, Mijovic J, "The effect of cure schedule on physical mechanical-properties of graphite epoxy composites", SAMPE Journal-Society for the Advancement of Material and Process Engineering, **22** (2), pp.31-42 (1986)

9 White SR and Hahn HT, "Mechanical property and residual-stress development during cure of a graphite bmi composite", Polymer Engineering and Science, **30** (22), pp.1465-1473 (1990)

10 Ashbee KHG and Wyatt RC "Water damage in glass fibre-resin composites" ProcRSocLondA, **312** (1) pp.553-564 (1969)

11 Yariv A *Optical Electronics*, 4th edition, Saunders College Publishing, London (1991)

12 Snyder AW and Love JD *Optical waveguide Theory* Chapman and Hall, London (1983)

13 Gloge D, "Weakly Guiding Fibres", Appl Opt **10**(10) pp. 2252-2258 (1971)

14 *Optical fibre sensors Volume I: Principles and components* Ed J Dakin and B Culshaw Artech , Boston (1988)

15 *Optical fibre sensors Volume II: Systems and applications* Ed J Dakin and B Culshaw Artech , Boston(1988)

16 Batchellor CR and Edge C "Some recent advences in fibre-optic sensors", Electr and Comms Eng Jn, **Oct**, pp. 175-84 (1990)

17 Dakin JP "Distributed Optical fibre sensors" SPIE Critical reviews **CR44**(10) Fiber Optic Sensors, pp.162-199, (1993)

18 Kersey AD "Multiplexed optical fiber optics sensors" Critical reviews **CR44**(10)Fiber Optic Sensors, pp.161-185, (1993)

19 Udd E "Fiber optic Smart Structures" in "Fiber optic sensors an introduction for engineers and scientists" ed EUdd Wiley & Sons, pp. 2-18, NY(1991)

20 Rozenberg BA, "Kinetics, thermodynamics, and mechanism of reactions of epoxy oligomers with amines", Adv Polymer Sci **75**, pp.113-165 (1985)

21 Shechter L and Wynstra J "Glycidyl ether reactions with amines", Industrial and Engineering Chemistry, **48**, pp. 94-97, (1956)

22 Dusek K, Bleha M and Lunak S, "Curing of epoxide resins: model reactions of curing with amines", Journal of Polymer Science: Polymer Chemistry Edition, **15**, pp. 2393-2400, (1977)

23 Smith I T, "The mechanism of the crosslinking of epoxide resins by amines", Polymer, **2**, pp.95-108 (1961)

24 Mijovic J, Fishbain A, Wijaya, J "Mechanistic modelling of epoxy-amine kinetics Part 1 - model compound study", Macromolecules", **25**, pp.979-985, (1992)

25 Rozenberg B A, "Kinetics and mechanism of epoxy oligomers curing", Makromoleculare Chemie, Macromolecular Symposium, 7, pp.17-26 (1987)

26 Goos F, and Hänchen H, "Ein Neuer and fundamentaler Versuch zur Totalreflexion" Ann Physik, **1**, p333 (1947) quoted in Harrick[33]

27 Sarwate, VV, *Electromagnetic fields and waves*, Wiley, New York, (1993)

28 Hall EE " The Penetration of totally reflected light into the rarer medium" Phys Rev **15** p 73 (1902)

29 Leurgans PJ and Turner AF " Frustrated total internal reflection interference filters" J Opt Soc Am **37**, p 983(A) (1947)

30 Fahrenfort J "Attenuated total reflection - A new principle for production of useful infrared reflection spectra of organic compounds", Spectrochimi Acta, **17,** p698-709, (1961)

31 Harrick N J " Study of Physics of surfaces from Frustrated total internal reflection" Phys Rev Letts **4** p224-226, (1960)

32 Harrick N J "Surface chemistry from spectral analysis of totally internally reflected radiation" J PhysChem **64,** p1110-1116 (1960)

33 Harrick N J *Internal reflection spectroscopy* J Wiley and Sons New York (1979)

34 Fowles GR *Introduction to Modern Optics* pp.152-162 Holt, Rinehart and Winston, London (1976)

35 Harrick NJ and du Pré FK "Effective thickness of Bulk Materials and of thin films for internal reflection spectroscopy" Appl Opt **5**(11) pp.1739-1743 (1966)

36 Müller G, Abraham K and Schaldach M "Quantitative ATR spectroscopy: some basic considerations" Appl Opt, **20**(7) pp.182-1190 (1981)

37 Hawranek JP and Jones RN, "The determination of the optical constants of benzene and chloroform in the ir by thin film transmission" Spectrochimica Acta, **32A, pp.**111-123 (1976)

38 Fahrenfort J and Visser WM "On the determination of optical constants in the infrared by attenuated total reflection" Spectrochim Acta **18,** pp. 1103-1116, (1962)

39 Hirschfield T " Accuracy and optimisation of the two prism technique for calculating the optical constants from ATR data" App Spect **24**(2) pp. 277-282 (1970)

40 Horton JA and Hansen WN "Relationship of internal reflection measurements to bulk optical properties with a transmission comparison" Anal Chem **39** pp. 1098-1190 (1967)

41 Hansen WN "Expanded formulas for attenuated total reflection and the derivation of absorption rules dfor single and multiple ATR spectrometer cells" Spectrochim Acta **21** pp. 815-833 (1965)

42 Hodgson JN *Optical properties of solids* Butler and Tanner, London 1970

43 Golpen TG, Cameron DG and Jones RN "An ATR determination of the optical constants of liquids" Appl Spectrosc **34**, pp. 647-658 (1980)

44 Bertie JE and Eysel HH "Infrared Intensities of liquids I: Determiation of infrared optical and dielectric constants by FT-IR using the CIRCLE ATR cell" Appl Spect **39**(3), pp.392-401 (1985)

45 Huang JB and Urban MW " Evaluation and analysis of Attenuated total reflectance using Kramers-Kronig Transforms" Appl Spect **46**(11), pp.1666-1672, (1992)

46 Dignam MJ and Mamiche-Afara S "Determination of the spectra of the optical constants of bulk pases via fourier transform ATR" Spectrochim Acta, **44A,** pp.1435-1442, (1988)

47 Sperline RP, Muralidharan S and Freiser H "New Quantitative technique for attenuated total reflection (ATR) spectrophotometry; Calibration of the "CIRCLE" ATR device in the infra-red" Appl Spectrosc **40**(7), pp.1019-1022, (1986)

48 Carniglia CK, Mandel L and Drexhage KH "Absorption and emission of evanescent photons" Jn Opt Soc Am **32**(4) pp.479-486 (1972)

49 Blackwell CS, Degen PJ and Osterholtz FD "Internal reflectance spectroscopy of reacted surfaces: Fluorinated polyelethylene and polypropylene" Appl Spectros **32**(5) pp. 480-484 (1978)

50 Lok BK, Cheng Y and Robertson CR " Total internal reflection Fluorescence: A technique for examining interactions of Macromolecules with solid surfaces" Colloid & Interface Sci **91**(1), p 87, (1983)

51 Snyder RW and Fuerniss SJ "ATR/IR spectroscopic method for following photo-polymer Curing" Appl Spectro **46**(7) pp.1113-1116 (1992)

52 Simhony S, Schnitzer I, Katzir A and Kosower EM, "Evanescent wave infrared-spectroscopy of liquids using silver-halide optical fibers", Journal of Applied Physics, 64(7), pp.3732-3734 (1988)

53 Wang A, Wang GZ, Gollapudi S, May RG, Murphy KA and Claus RO, "Advances in sapphire optical-fiber sensors", SPIE **1798** Fiber Optic Smart Structures and Skins V, Ch33, pp.56-65 (1993)

54 Saggese SJ, Shahriari MR and Sigel Jr GH "Fluoride fibers for remote chemical sensing" SPIE **929,** Infrared optical Materials IV, pp.106-114 (1988)

55 Macraith BD, Ruddy V and McCabe S, "The suitability of single-mode Fluoride fibres for evanescent wave sensing"SPIE **1587;** Chemical, Biochemical and environmental sensors III, pp.310-317 (1991)

56 Druy MA, Glatkowski PJ, and Stevenson WA, "Evanescent Wave fibre optic remote Fourier Transform Infrared (FTIR) spectroscopy", SPIE **1587;** Chemical Biochemical and environmental sensors III, pp.199-202 (1991)

57 Druy MA, Glatkowski PJ and Stevenson WA " Applications of remote fibre optic spectroscopy using IR fibers and Fourier transform infrared (FTIR) spectrometers" SPIE **1591** Infrared fiberoptics III pp.218-225 (1991)

58 Lennie AR and Kvasnik F, "Near-infrared sensing using the evanescent field", Analytical chimica acta, **281**, pp. 265-70 (1993)

59 Archibald DD, Lin LT and Honigs DE, "Remote near-IR spectroscopy over an optical fibre with a modified FT spectrometer", Appl Spect **42**(3), pp. 468-472 (1988)

60 Ruddy V, Maccraith BD and Murphy JA, "Evanescent wave absorption-spectroscopy using multimode fibers", Jn Appl Phys, **67**(10), pp.6070-6074 (1990)

61 Degrandpre MD and Burgess LW, "Long path fiber-optic sensor for evanescent field absorbance measurements", Anal Chem, **60**(23), pp.2582-2586' (1988)

62 Paul PH, Kychakoff G, "Fiber-optic evanescent field absorption sensor", Appl Phys Lett, **51**(1), pp.12-14 (1987)

63 George GA, Cole Clarke P, St John N and Friend G, "Real-time monitoring of the cure reaction of a TGDDM/DDS epoxy-resin using fiber optic FT-IR", Journal of Applied Polymer Science, **42** (3), pp.643-657 (1991)

64 Schnitzer I, Katzir A, Schiessl U, Riedel WJ and Tacke M, "Fiber-optic-based evanescent field chemical sensor using tunable diode-lasers for the midinfrared spectral region", JnAppl Phys, **66**(11), pp.5667-5670, (1989)

65 Namkung JS, Hoke M, Rogowski RS and Albin S "Detection of aluminium corrosion by evanescent wave spectroscopy with optical fibres" SPIE **2444,** *Smart structures and materials*, pp. 447-458, (1995)

66 Bunimovich D Belotserkovsky and Katzir A, "Fiber-optic evanescent wave spectroscopy of gases in liquids", Review of scientific instruments, **66**(4), pp.2818-2820 (1995)

67 Driver RD, Downing JN and Leskowitz GM, "Evanescent-wave spectroscopy down infrared transmitting optical fibers", SPIE **1591** (30) Infrared Fiber Optics III, pp.168-179 (1992)

68 Archibald DD, Lin LT and Honigs DE, "Remote near-IR spectroscopy over an optical fibre with a modified FT spectrometer", Appl Spect, **42** (3), pp.468-472 (1988)

69 Sanghera JS, Kung FH, Pureza PC, Nguyen VQ, Miklos RE and Aggarwal ID, "Infrared evanescent-absorption spectroscopy with chalcogenide glass fibers", Appl opt, **33**(27), pp. 6315-6322 (1994)

70 Conzen JP, Burck J and Ache HJ, "Characterisation of a fiber-optic evanescent wave absorbance sensor for nonpolar organic compounds", Appl spect, **47**(6), pp.753-763 (1993)

71 Eenink RG, Debruijn HE, Kooyman RPH and Greve J, "Fiber-fluorescence immunosensor based on evanescent wave detection", Analytica Chimica Acta, **238** (2), pp.317-321 (1990)

72 Golden JP, Anderson GP, Ogert RA, Breslin KA and Ligler FS, "An evanescent-wave fiber optic biosensor - challenges for real-world sensing", SPIE **1796** Chemical, Biochemical, and Environmental Fiber Sensors IV, (47), pp.2-8 (1993)

73 Carome EF, Coghlan GA, Sukenik CN and Zull JE, "Fiberoptic evanescent wave sensing of antigen-antibody binding", Sensors and actuators B, **13-14**, pp.732-733 (1993)

74 Starodub NF, Arenkov PY, Rachkov AE and Berezin VA, "Fiber optic immunosensors for the detection of some drugs", Sensors and actuators B, **13-14**, pp.728-731 (1993)

75 Ruddy V, "Spectroscopy of gases using IR fibers", **1591**(30), Infrared Fiber Optics III, pp.180-191 (1992)

76 Klein R and Voges E, "Integrated-optic ammonia sensor", Sensors and actuators B, **11**, pp.221-225 (1993)

77 Blyler LL, Lieberman RA, Cohen LG, Ferrara JA and Macchesney JB, "Optical fiber chemical sensors utilizing dye-doped silicone polymer claddings", Polymer Engineering and Science, **29** (17), pp.1215-1218 (1989)

78 Steiner G and Renschen CP, "Infrared evanescent-wave sensor for measurements in medicine and biotechnology", SPIE **1796** (47), Chemical, Biochemical, and Environmental Fiber Sensors IV, pp.26-33 (1993)

79 Stewart G, Muhammad FA and Culshaw B, "Sensitivity improvement for evanescent-wave gas sensors", Sensors and actuators B, **11**, pp.521-524 (1993)

80 Lin J and Brown CW, "Near-IR Fiber-Optic temperature sensor", Appl spect, **47**(1), pp.62-68 (1994)

81 Zhengfang G, Brown CW Sun L andYang SC, "Fiber-optic pH sensor based on evanescent wave absorption spectroscopy", Anal chem **65**, pp.2335-2338 (1993)

82 Compton DAC, Hill SL, Wright NA, Druy MA, Piche J, Stevenson WA and Vidrine DW, "*In-situ* FT-IR analysis of a composite curing reaction using a mid-infrared transmitting optical fiber", Appl Spect, **42** (6), pp.972-979 (1988)

83 Michie WC, Thursby G, Johnstone W and Culshaw B, "Optical techniques for determination of the state of cure of epoxy-resin based systems", SPIE **1798** 33, Fiber Optic Smart Structures and Skins V, pp.11-18 (1992)

84 Zhengfang GE Brown CW and Brown M, "Monitoring of lamination processes in an autoclave with fiber-optic infrared spectroscopy", Jn Appl Pol Sci, **56**, pp.667-675 (1995)

85 Thompson RB and Ligler FS, "Chemistry and technology of evanescent wave biosensors", *Biosensors with fiberoptics* Eds Wise and Wingard, pp. 4-29 Humana (1991)

86 Hirschfield T "Total reflection fluorescence", Can Jn Spectr **10,** p128 (1965)

87 Harrick NJ and Loeb NJ " Multiple internal reflection fluorescence spectroscopy", Anal Chem, **45**, pp. 687-691 (1973)

88 Kronick MN and Little WA "A new immunoasay based on fluorescence by internal reflection spectroscopy" J Immun Methods, **8**, pp.235-240, (1975)

89 Andrade JD, Van Wagenen RA, Gregonis DA, Newby k and Lin JN "Remote fiber-optic biosensors based on evanescent excited fluorimmunoassay: Concept and progress", IEE Trans Elec Dev **32**, pp.1175-1179 (1985)

90 Yoshida M, Shigemori K, Sugimura M and Matano M, "Sensitivity enhancement of evanescent wave immunoassay", Meas sci & tech, **4**, pp.1077-1079, (1993)

91 Bhatia SK, Shriver-Lake LC, Prior KJ, Georger J, Calvert JM, Bredehorst R and Ligler FS "Use of thiol terminal silanes and heterobifunctional crosslinkers for immobilisation of antibodies on silical surfaces", Anal Biochem, **178**, pp.408-413 (1989)

92 Love WF and Button LJ "Optical characteristics of fiber optic evanescent wave sensors" SPIE **990** Chemical, Biochem And environmental applications of fibers, pp.175-180 (1988)

93 Orvedahl DS, Love WF and Slovacek RE, "Theoretical considerations for evanescent wave immunosensors in biomedical applications", SPIE **1587**, Chemical Biochemical and environmental sensor III, pp.187-198 (1991)

94 Glass TR, Lackie S and Hirschfield T, "Effect of numerical aperture on signal level in cylindrical waveguide evanescent fluorosensors", Appl Opt, **26** (11), pp.2181-2187 (1987)

95 BD Gupta, C D Singh, "Fiber-optic evanescent field absorption sensor: A theoretical evaluation", Fiber and Integrated Optics, **13**, pp. 443-443, 1994

96 Gupta BD and Singh CD, "Evanescent absorption coefficoent for diffuse source illumination: uniform and tapered-fiber sensors", Appl Opt, **33** (13), pp. 2737-2742 (1994)

97 Golden JP, Rabbany SY and Anderson GP, "Ray-tracing determination of evanescent-wave penetration depth in tapered fiber optic probes" , SPIE **1796** (47), Chemical, Biochemical, and Environmental Fiber Sensors IV , pp. 9-13 (1993)

98 Lowry SR, May TE and Bornstein A, "Signal enhancement technique for internal-reflection spectroscopy", Appl Spect, **47** (1), pp. 30-34 (1993)

99 Klunder GL, Burck J, Ache HJ, Silva RJ and Russo RE, "Temperature effects on a fiber-optic evanescent wave absorption sensor", Appl spect **48** (3), pp.387-393 (1994)

100 Degrandpre MD and Burgess LW, "All fiber spectroscopic probe based on evanescent absorption", SPIE **990**, Chem, Biochem and environmental sensors, pp. 170-174 (1988)

101 Takeo Takashi and Hattori H, "Optical fibre sensor for measuring refractive index", Jap Jn of appl phys, **21**(10), pp.1509-1512, (1982)

102 Stewart G, Muhammad FA, Culshaw B, Sensitivity improvement for evanescent-wave gas sensors", Sensors and actuators B, **11**, pp. 521-524 (1993)

103 Dyott RB and Schrank PF "Self locating elliptically cored fibre with an accessible guiding region" Electron Lett **18, pp.** 980-981 (1982)

104 MacCraith BD, "Enhanced evanescent wave sensors based on sol-gel derived porous glass coatings", Sensors and actuators B, **11**, pp.29-34 (1993)

105 Macraith BD, O'Keeffe G, McEvoy AK, McDonagh CM, McGilp JF, O'Kelly B, O'Mahony JD and Cavanagh M, "Light emitting diode based oxygen sensing using evanescent wave excitation of a dye doped sol-gel coating", Opt Eng, **33**(12), pp.3861-3866 (1994)

106 Blyler LL, Lieberman RA, Cohen LG, Ferrara JA and Macchesney JB, "Optical fiber chemical sensors utilizing dye-doped silicone polymer claddings", Polymer Engineering and Science, **29**(17), pp.1215-1218 (1989)

107 Burck J, Conzen, JP, Ache HJ, "A fibre optic evanescent field absorption sensor for monitoring organic contaminants in water", Fresenius J Anal Chem, **342**, pp.394 (1992)

108 Barton JM, Hamerton I, Thomson CP: " A study of the behaviour of N-(4-Phenoxy)-Phenylmaleimide using DSC analysis" Polymer Bulletin, **30**(5), pp.521-527, (1993)

109 Barton JM, Greenfield DCL, " Differential scanning calorimetry cure studies of tetra-n-glycidyldiaminodiphenylmethane epoxy resins 3 reaction with dicyandiamide" British Polymer Journal **18**(3), pp.196-200 (1986)

110 Barton JM, "The application of differential scanning calorimetry (DSC) to the study of epoxy resin curing reactions" Advances in Polymer science **72** pp. 111-154 (1985)

111 Perry MJ,Lee LJ and Lee CW" On-Line Cure Monitoring Of Epoxy/Graphite Composites Using a scaling analysis and a dual heat flux sensor" Jn Composite Materials **26**(2) pp.274-292, (1992)

112 Prime RB and Bidstrup SA " Cure monitoring and cure modelling of thermosets" Polymer engineering and science **29**(5) p 277-278, (1989)

113 Kim JS andLee DG: "On-line cure monitoring and viscosity measurements of carbon fibre epoxy composite materials" Journal of materials Processing technology, **37**, pp.405-416, (1993)

114 Martin BG "Monitoring the composite cure cycle by dielectric analysis" Materials Evaluation, **47,** March, pp.49-54 (1976)

115 Mopsik FI, Chang SS andHunston DL "Dielectric measurements for cure monitoring" Materials Evaluation, **47** April, pp.448-453, (1989)

116 Kranbuehl, DE et al "Dynamic dielectric analysis- Development of techniques for the curing process of laminating polyester resins" Jnof Polymer Sci-Polymer symposia, **74**, pp.71-81, (1986)

117 Ciriscioli,PR and Springer GS "Dielectric Cure monitoring- a Critical review" SAMPE Journal, **25**(3), pp.35-42, (1989)

118 Hauser EA, Sofer GA:" A new tool for determining the stage of polymerisation of thermosetting polymers" JPolymSci **8**(6), pp.611-20, (1952)

119 Lindrose AM "Ultrasonic wave and moduli changes in a curing epoxy resin" ExperMechan, pp.227-232 (1978)

120 Yoon SS, Yu WJ and Kim HC " Phase-transition of epoxy resin during isothermal curing monitored by ultrasonic velocity measurements" Jn of Materials Science Letters **11**(20), pp.1392-1394, (1992)

121 Harrold RT and Sanjana ZN "Non-destructive evaluation of the curing of resin and pre-preg using an acoustic waveguide sensor" Rev of Prog in Quant Non Destevaluation , **6B,** pp.1277-84, (1987)

122 Weyer LG, "Near-infrared spectroscopy of organic substances", Applied Spectroscopy Reviews, **21**, (1&2), pp.1-43 (1985)

123 Stark E, Luchter K and Margoshes M, "Near-infrared analysis (NIRA): a technology for quantitative and qualitative analysis", Applied Spectroscopy Reviews, **22,**(4), pp.335-399 (1986)

124 Whetsel KB, "Near-infrared spectrophotometry", Applied Spectroscopy Reviews, **2**(1), pp.1-67 (1968)

125 Tosi C, Pinto A, "Near-infrared spectroscopy of hydrocarbon functional groups", Spectrochimica Acta, **28A**, pp.585-597 (1972)

126 Scherzer T, "Characterization of diol modified epoxy resins by near- and mid-infrared spectroscopy", Journal of Applied Polymer Science, **51**, pp.491-502 (1994)

127 Dannenberg H, "Determination of functional groups in epoxy resins by near-infrared spectroscopy", SPE Transactions, January, pp.78-88 (1963)

128 Strehmel V and Scherzer T, "Structural investigation of epoxy amine networks by mid- and near-infrared spectroscopy", European Polymer Journal, **30**(3), pp.361-368 (1994)

129 Chike KE, Myrick ML, Lyon RE and Angel SM, "Raman and near-infrared studies of an epoxy resin", Applied Spectroscopy, **47**(10), pp.1631-1635 (1993)

130 Schiering DW, Katon JE, Drzal LT and Gupta VB, "An infrared spectroscopic investigation of curing reactions of the Epon 828/meta-phenylenediamine system", Journal of Applied Polymer Science, **34**, pp.2367-2375 (1987)

131 Min BG, Stachurski ZH, Hodgkin JH, Heath GR, "Quantitative-analysis of the cure reaction of DGEBA/DDS epoxy-resins without and with thermoplastic polysulfone modifier using near-infrared spectroscopy", Polymer, **34**,(17), pp.3620-3627 (1993)

132 St John NA and George GA, "Cure kinetics and mechanisms of a tetraglycidyl -4,4'-diaminodiphenylmethane / diaminodiphenylsulphone epoxy resin using near ir spectroscopy", Polymer, **33**,13, pp.2679-2687 (1992)

133 De Bakker CJ, St John NA and George GA, "Simultaneous differential scanning calorimetry and near-infra-red analysis of the curing of tetraglycidyldiaminodiphenylmethane with diaminodiphenylsulphone", Polymer, **34**(4), pp.716-725 (1993)

134 George GA, Cole-Clarke P, St John N and Friend G, "Real-time monitoring of the cure reaction of a TGDDM/DDS epoxy resin using fibre optic FTIR", Journal of Applied Polymer Science, **42**, pp.643-657 (1991)

135 Debakker CJ, George GA, Stjohn NA, Fredericks PM, "The kinetics of the cure of an advanced epoxy-resin by fourier-transform raman and near-ir spectroscopy", Spectrochimica Acta Part A-Molecular Spectroscopy, **49** (5-6), pp.739-752 (1993)

136 Davis A, Ohn MM, Liu K and Measures RM: "A study of an Opto-ultrasonic technique for cure monitoring" SPIE 1588 Fibre Optic smart structures and skins , pp. 264-274, (1991)

137 Liu K, Ferguson SM, Davis A, McEwen K and Measures RM :" Ultrasonic detection with embedded fibre optic interferometric sensors for composite NDE", Proc SPIE **1398** pp.206-212, (1990)

138 Ohn MM, Davis A, Liu KX, Measures RM, Embedded fiber optic detection of ultrasound and its application to cure monitoring, , Proc SPIE **1798**(33), Fiber Optic Smart Structures and Skins V, pp.134-143 (1993)

139 Dannenberg H "Refractive index method for determining cure rates of epoxy resins" SPIE Journal Oct, pp. 875-880, (1959)

140 Cooper P R, " Refractive index measurements of paraffin, a silicon elastomer, and an epoxy resin over the 500-1500nm spectral range" Applied Optics **21**(19), pp.3413-3415 (1982)

141 Longhurst RS, *Geometrical and Physical optics*, Longmans, London p88 (1963)

142 Jones BE, Medlock RS, and Spooncer RC, "Intensity and wavelength based sensors and optical actuators" In *Optical fibre sensors, systems and applications*, ed Culshaw B and Dakin JP, Artech house , MA USA (1989)

143 Harmer A, Battelle Institute, Geneva, personal communication (1985)

144 Kapany NS and Pike JN "Fibre optics Part IV: a photorefractometer", J Opt Soc America **47**, pp. 1109-1116(1957)

145 Karrer E and Orr RS "A Photoelectric Refractometer", J Opt Soc Am **36**, pp.42-46 (1946)

146 Kapany NS and Pontarelli DA: "Photorefractometer I: extension of sensitivity and range" Appl Opt **2**, pp. 425-430 (1963)

147 Podoleanu A G, Taplin SR, Webb DJ and Jackson DA "Channeled spectrum liquid refractometer" Rev Sci Instrum **64** (10) pp. 3028-3029, (1993)

148 Afromowitz MA, "Fiber optic polymer cure sensor", Journal of Lightwave Technology, **6** (10) pp.1591-1594 (1988)

149 Afromowitz MA and Lam KY, "Fiber optic cure sensor for thermoset composites", SPIE**986** (25), Fiber Optic Smart Structures and Skins, pp.135-139 (1989)

150 Afromowitz MA and Lam KY, "The optical-properties of curing epoxies and applications to the fiberoptic epoxy cure sensor", Sensors and Actuators A-Physical, **23** (1-3), pp.1107-1110 (1990)

151 Lam KY and Afromowitz MA, "Fiber-optic epoxy composite cure sensor I: Dependence of refractive index of an autocatylitic reaction epoxy system at 850nm on temperature and extent of cure", Appl Opt, **34**(25), pp.5635-5638 (1995)

152 Lam KY and Afromowitz MA, "Fiber-optic epoxy composite cure sensor II: Performance characteristics", Appl Opt, **34** (25), pp.5639-5644 (1995)

153 Zimmermann B, Devries M and Claus R, "Resin sensors for composite cure monitoring", Active Materials and Adaptive Structures, **163**, pp.313-316 (1992)

154 Klosterman D A, Saliba T E, "Development of an in situ fiber optic sensor for on-line void detection and control", 38th International SAMPE Symposium, May, pp. 1322-1332, (1993)

155 Powell G R, Crosby P A, Fernando G F, France C M, Spooncer R C, Waters D N, "Optical-fiber evanescent-wave cure monitoring of epoxy-resins", Proceedings of the Society of Photo-optical Instrumentation Engineers (SPIE), **2718**, pp.80-92 (1996)

156 Crosby P A, Powell G R, Fernando G F, France C M, Spooncer R C, Waters D N, "*In-situ* cure monitoring of epoxy-resins using optical-fiber sensors", Smart Materials & Structures, **5** (4), pp.415-428 (1996)

157 Powell G R, Crosby P A, Fernando G F, France C M, Spooncer R C, Waters D N,"*In-situ* cure monitoring of advanced fibre reinforced composites" Proceedings of the Society of Photo-optical Instrumentation Engineers (SPIE), **2444**, pp.386-396, (1995)

158 Crosby P A, Powell G R, Fernando G F, France C M, Spooncer R C, Waters D N, "A comparative study of optical fibre cure monitoring methods", Proceedings of the Society of Photo-optical Instrumentation Engineers (SPIE), **3042**, pp.141-153, (1997)

159 Kassamakov I and Kafedjiev S "Fibre Optic refractive index sensor" Proc of the 6th international school on Quantum electronics; Lasers, Physics and applications, pp.566-570 (1990)

160 Fridman YB and Shchurov AF "On relations between the refractive indices of epoxy polymers and their chemical Structure" Polym Sci USSR, **25** pp.1702-1707(1983)

161 Askadskii AA, Vointseva BB, Mustafayeva VV and Slonimskii GL "Refractometric method of analysis of chemical conversions of macromolecules in solution" Polym Sci USSR **24**, pp.2813-2826, (1982)

162 Mijovic J, Andjelic S, Kenny J M, "In situ real-time monitoring of epoxy-amine kinetics by remote near infrared spectroscopy, Polymers for Advanced Technologies, 7, pp.1-16, (1996)

163 Crosby P A, Powell G R , Liu T, Wu X, Fernando G F, "*In-situ* cure monitoring of an epoxy/amine resin system using an optical-fiber transmission sensor, Proceedings of the Society of Photo-optical Instrumentation Engineers (SPIE), **2895**, pp.109-115 (1996)

164 Fildes JM, Milkovich SM, Altkorn R, Haidle R and Neatrour J, "In situ infrared spectroscopy and neural network analysis for composite cure monitoring," 25th International SAMPE Technical Conference, October, (1993)

165 Calvert P, George G, Rintoul L, "Monitoring of cure and water uptake in a freeformed epoxy resin by an embedded optical fiber", Chemistry in Materials, 8, 1298-1301, (1996)

166 Xu L and Schlup JR, "Application of Near-Infrared Attenuated Total reflectance spectroscopy for monitoring epoxy resin/amine cure reactions", Applied spectroscopy, **50**(1), pp.109-114 (1996)

167 Xu L, Fu H and Schlup JR, "In situ near-infrared spectroscopic investigation of epoxy resin-aromatic amine cure reactions", J Am Chem Soc, **116**, pp.2821-2826 (1994)

168 Zhengfang G, Brown CW, Sun Linfeng and Yang SC, "Fiber-optic pH sensor based on evanescent wave absorption spectroscopy", Analytical chemistry, **65**, pp.2335-2338 (2993)

169 Bunimovich D, Kellner R, Krska R, Mesica A, Paiss I, Schiesl U, Taga K and Katzir A, "A system for monitoring and and control of processes based on IR fibres and tunable diode lasers" Journal of molecular structure **292** pp.125-132 (1993)

170 Cossins S L, Connell M E, Cross W M, Winter R M, Kellar J J, "Evanescent wave spectroscopy for *in-situ* cure monitoring", Proceedings of the Society of Photo-optical Instrumentation Engineers (SPIE), **2836**, pp.147-156, (1995)

171 Cossins S, Connell M, Cross B, Winter R, Kellar J, "*In-situ* near-IR cure monitoring of a model epoxy matrix composite", Applied Spectroscopy, 50, No 7, 900-905, (1996)

172 Druy MA, Glatkowski PJ, Stevenson WA: "Embedded optical fibre sensors for monitoring cure cycles of composites" ADPA/AIAA/ASME/SPIE Conf. on Materials and adaptive structures **session 42,** Ch. 163, pp. 805-808, (1992)

173 Roberts SSJ and Davidson R, "Cure and fabrication monitoring of composite-materials with fiberoptic sensors", Composites Sci and Tech, **49**(3), pp.265-276 (1993)

174 *The long and the short of epoxy resins - an introductory handbook from the makers of Epikote and Epikure resins*, Shell Chemicals Literature, December 1992

175 Jennings DE "Calibration of diode laser spectra using a confocal etalon" Appl Opt **23**(9) pp.1299-1301 (1984)

176 Lohman FH, Nortman WE Jr "Determination of primary and secondary aliphatic amines by near infrared spectrophotometry" Anal Chem **35**(6) pp.707-711 (1963

177 Strehmel V and Scherzer T, "Structural investigation of epoxy amine networks by mid- and near-infrared spectroscopy", European Polymer Journal, **30**(3), pp.361-368 (1994)

178 Chike KE, Myrick ML, Lyon RE and Angel SM, "Raman and near-infrared studies of an epoxy resin", Applied Spectroscopy, **47**(10), pp.1631-1635 (1993)

179 St John NA and George GA, "Cure kinetics and mechanisms of a tetraglycidyl-4,4'-diaminodiphenylmethane/ diaminodiphenylsulphone epoxy resin using near ir spectroscopy", Polymer, **33**,13, pp.2679-2687 (1992)

180 Snitzer E, "Cylindrical Dielectric Waveguide Modes", Jn. Opt. Soc. Am., **51** (5), pp.491-498 (1961)

181 Snyder AW, "Asymptotic expressions for eigenfunctions and eigenvalues of a dielectric or optical waveguide", **MIT 17**(12), *IEEE Transactions on microwave theory and techniques,* pp.1130-1138 (1969)

182 Colin TB, Yang KH, Arnold MA, Small GW and Stwalley WC, "The effect of length and diameter on the signal-to-noise ratio of evanescent field absorption fiberoptic sensors", Appl. Spect., **46**(7), pp.1129-1133, (1992).

183 Radhakrishnan P, Nampoori VPN & Vallabhan CPG, "Fiber optic sensor based on evanescent wave absorption", Opt. Eng., **32** (4), pp.692-694, (1993)

184 Ruddy V, "An effective attenuation coefficient for evanescent wave spectroscopy using multimode fiber", Fiber and Integrated Optics., **9** (2), pp.143-151 (1990)

185 B.D. Gupta, C. D. Singh, "Fiber-optic evanescent field absorption sensor: A theoretical evaluation", Fiber and Integrated Optics, **13**, pp. 443-443, (1994)

186 Dobbs ER *Electromagnetic waves* , Routledge and Kegan Paul, London (1985)

187 Snyder AW and Love JD *Optical waveguide theory*, Chapman and Hall, London, (1983)

188 Hodgson JN, *Optical absorption and dispersion in solids*, Chapman and Hall, London (1970)

189 Gupta BD and Singh CD, "Evanescent absorption coefficoent for diffuse source illumination: uniform and tapered-fiber sensors", Appl. Opt., **33** (13), pp. 2737-2742, (1994)

190 Bobb LC, Krumboldt HD and Davis JP "An optical fiber refractometer" SPIE **990** *Chemical, Biochemical and environmental applications of fibers,* pp.164-169, (1988)

191 Tateda M and Ikeda M, " Mode conversion in bent step index multimode fibres" Appl Opt. **15**(10), pp.2308-2310, (1976)

192 Arie A, Karoubi R, Gur YS and Tur M "Measurement and analysis of light transmission through a modified cladding optical fibre with applications to sensors" Appl. Opt. **25,** pp.1754-1758 (1986)

193 DeGrandpre M. D., Burgess L. W., "Fiber-optic FT-NIR evanescent field absorbance sensor," Appl. Spect., **44** (2), pp. 273-279, (1990).

194 Gloge D, "Weakly guiding fibres," *Appl. Opt.*,**10**(10), pp.2252-2258, (1971).

195 Ruddy V, "Non-linearity of absorbance with sample concentration and path length in evanescent wave spectroscopy using optical fiber sensors", Opt. Eng., **33** (12), pp.3891-3894 (1994).

196 "Standard test methods for epoxy contents of epoxy resins" Annual book of ASTM standards Vol 16 pp. 28-31, (1990)

197 Longhurst R.S. *Geometrical and Physical Optics* Longmans, London, p. 415 (1963)

198 Crosby P "*In-situ* cure monitoring of epoxy resin systems" PhD thesis, Brunel University (1997)

199 Tateda M and Ikeda M, "Mode conversion in bent step index multimode fibers", Applied Optics, **15**(10), pp.2308-2311 (1976).